Approaching conformality in non-Abelian gauge theories

Nunes da Silva, Tiago Jose

university of groningen

Approaching Conformality in non-Abelian Gauge Theories

PhD thesis

to obtain the degree of PhD at the
University of Groningen
on the authority of the
Rector Magnificus Prof. E. Sterken
and in accordance with
the decision by the College of Deans.

This thesis will be defended in public on

Friday 26 February 2016 at 12.45 hours

by

Tiago Jose Nunes da Silva

born on 5 December 1986
in Jaboatão dos Guararapes, Brazil

Supervisor
Prof. E. Pallante

Assessment Committee
Prof. R.G.E. Timmermans
Prof. V. Miransky
Prof. B. Lucini

ISBN 978-90-367-8648-5 (printed)
ISBN 978-90-367-8647-8 (digital)

Aos meus pais e à minha avó Salete, com carinho...

This work is part of the research program of the Foundation for Fundamental Research on Matter (FOM), which is part of the Netherlands Organisation for Scientific Research (NWO).

Printed by Ipskamp Drukkers, Enschede.

Contents

There is a remarkably close parallel between the problems of the physicist and those of the cryptographer. The system on which a message is enciphered corresponds to the laws of the universe, the intercepted messages to the evidence available, the keys for a day or a message to important constants which have to be determined. The correspondence is very close, but the subject matter of cryptography is very easily dealt with by discrete machinery, Physics not so easily.

Alan Turing

0 Introduction

Ancient Greeks and Indians developed the atomist concept[140,228]: that everything in nature consisted of small, immutable and indestructible basic particles of matter. Our understanding of the fundamental structure of matter has come a long way since the ancient days. It is synthesised in the Standard Model of Particle Physics, which amalgamates three of the four fundamental forces of nature, described by gauge theories: the Strong, Electromagnetic and Weak interactions. Matter is constituted by six quarks (up, down, strange, charm, bottom and top), each in three colours, and six leptons (electron, muon, tau and their respective neutrinos). Vector bosons mediate the interactions between the particles: the strong interaction is mediated by eight gluons, weak interactions by the $W^{\pm}$ and Z bosons, and the Electromagnetic interaction by the photon.

The work presented in this thesis is dedicated to further understanding the strong interaction. More specifically, it aims at understanding the phase diagram of strongly interacting matter and the

phenomenon of the emergence of conformality. A large part of the work presented through this book is based on Lattice Gauge Theory methods, which are a nonperturbative way to numerically study gauge theories. This chapter provides the reader with an Introduction to these subjects. It starts with a brief overview of Quantum Chromodynamics (QCD), the theory of strong Interactions. This will be followed by a theoretical overview of the conjectured picture for the phase diagram of strong interactions and the associated phenomena which play a role in its shape. It ends with an introduction to the lattice methods used during the research.

0.1 Quantum Chromodynamics in a nutshell

Quantum Chromodynamics (QCD) describes the fundamental strong interaction between particles that contain a *colour* charge: quarks and gluons. It is a non-Abelian gauge theory with symmetry group $SU(3)$.

Quarks are described in QCD as twelve component fields transforming in the fundamental representation of the colour $SU(3)$ gauge group. They are represented by Dirac 4-spinors

$$\psi^{(f)}(x)_{\alpha,c}, \overline{\psi}^{(f)}(x)_{\alpha,c}, \tag{1}$$

where x denotes the space-time position, $\alpha = 1, 2, 3, 4$ is the Dirac index and $c = 1, 2, 3$ (or, equivalently, c=red, green,blue) is the colour index. Quarks exist in nature in different flavours, with six flavours being observed so far in nature. The index f represents the flavour and in general runs from 1 to the total number of flavours N_f used in the calculations.

Gluons are described in QCD by gauge fields which carry two colour indices

$$A_\mu(x)_{cd},$$

where again x is the space-time coordinate, c and d are the colour indices and μ is a Lorentz index indicating the direction of different components in spacetime.*

*We will work in Euclidean spacetime. Therefore, the index μ is Euclidean and the metric tensor reduces to the identity matrix.

The QCD action can be written as

$$S_{QCD} = \int d^4x \left(\frac{1}{2g^2}\right) \mathrm{Tr}\left[F_{\mu\nu}(x)F_{\mu\nu}(x)\right] + \sum_{f=1}^{N_f} \overline{\psi}^{(f)}(x)\left(\gamma_\mu(\partial_\mu + iA_\mu(x)) + m^{(f)}\right)\psi^{(f)}(x). \tag{2}$$

The first term on the right-hand side of equation 2 is the gluonic part of the action, describing gluon propagation and gluon interaction, and the second term corresponds to the fermionic part, including quark fields and their interaction with the gluons [†].

The quantity g is the strong coupling constant of QCD and $F_{\mu\nu}$ is the gluon field-strength tensor

$$F_{\mu\nu}(x) = -i\left[D_\mu(x), D_\nu(x)\right] = \partial_\mu A_\nu(x) - \partial_\nu A_\mu(x) + i\left[A_\mu(x), A_\nu(x)\right], \tag{3}$$

here defined in terms of the covariant derivative

$$D_\mu(x) = \partial_\mu + iA_\mu(x). \tag{4}$$

The γ-matrices in the action are Euclidean versions of the Minkowski γ-matrices of the Dirac equation. They are 4×4 matrices in Dirac space, obeying the Euclidean anti-commutation relations

$$\left\{\gamma_\mu, \gamma_\nu\right\} = 2\delta_{\mu\nu}\mathbb{I}, \tag{5}$$

and they mix the different Dirac components of the quark fields.

The action in Equation 2 is obtained through a generalisation of the gauge invariance of electrodynamics, by requiring invariance under local rotations among the quarks colour indices, i.e., we require the action to be invariant under the transformation

$$\psi(x) \to \psi'(x) = \Omega(x)\psi(x), \qquad \overline{\psi}'(x) = \overline{\psi}(x)\gamma_0\Omega(x)^\dagger. \tag{6}$$

Here, $\Omega(x)$ are 3×3 independent complex matrices chosen at each spacetime point x acting on the red, green and blue colour components of ψ. They are required to satisfy the unitarity condition $\Omega(x)^\dagger = \Omega(x)^{-1}$ and to have $\det[\Omega(x)] = 1$. These $\Omega(x)$ matrices constitute the defining representation of the special unitary group $SU(3)$, the 3 being related to the matrices dimension. The

[†] Because gluons couple to themselves, relevant couplings arise from non-linear terms in the field strength. This property of QCD is the origin to its several non-trivial features

group operation of $SU(3)$ – matrix multiplication – is not commutative, and in this case the group is said to be non-Abelian. Theories built from non-Abelian gauge theories are usually referred to as Yang-Mills theories, after Yang and Mills, who originally developed this idea[31].

Imposing the invariance requirement Equation 6 on the fermionic part of the QCD action Equation 2 implies transformation properties for the gauge fields and for the covariant derivative:

$$\begin{aligned} A_\mu(x) \to A'_\mu(x) &= \Omega(x) A_\mu(x) \Omega(x)^\dagger + i(\partial_\mu \Omega(x))\Omega(x)^\dagger \\ D_\mu(x) \to D'_\mu(x) &= \partial_\mu + iA'_\mu(x) = \Omega(x) D_\mu(x) \Omega(x)^\dagger. \end{aligned} \tag{7}$$

By construction, the field strength tensor inherits the transformation property of the covariant derivative, i.e.,

$$F_{\mu\nu}(x) \to F'_{\mu\nu}(x) = \Omega(x) F_{\mu\nu}(x) \Omega(x)^\dagger. \tag{8}$$

Given these properties, it is now possible to note that the gauge part of Equation 2 is indeed a generalisation of the action of Electrodynamics, with the trace being taken in the QCD case, since gluon fields are matrix valued. It is possible to decompose the gauge fields in terms of their colour components, so that the action can be written without the trace. The overall factor g^{-2} in the action is just a more convenient way to introduce the coupling in lattice calculations. Alternatively, it is possible to rescale the gauge fields

$$\frac{1}{g} A_\mu(x) \to A_\mu(x) \tag{9}$$

so that the g^{-2} factor in not written explicitly in the action and the covariant derivative assumes the more familiar form

$$D_\mu(x) \to \partial_\mu + igA_\mu(x), \tag{10}$$

in which it is clear that g is the strength of the coupling of the gauge fields to the quarks.

As mentioned before, quarks come in different flavours, and so far six different flavours have been observed in nature: *up, down, strange, charm, bottom and top*. Each quark flavour has a different mass and, depending on the energy scale at which the theory is considered, some flavours are dynamical while the others ma be "integrated out". To the extent that the masses of the three lightest quark flavours (the up, down and strange) might be considered equal, in addition to the exact local $SU(N_c = 3)$ colour symmetry that is gauged, the action of QCD also exhibits an approximate

$SU(N_f = 3)$ flavour symmetry:

$$\begin{pmatrix} u \\ d \\ s \end{pmatrix} \rightarrow U \begin{pmatrix} u \\ d \\ s \end{pmatrix} \tag{11}$$

where $U \in SU(3)$. This was first noted independently by Gell-Mann and Ne'eman[143,144,244] and played a key role in the development of the quark model[145], for which Gell-Mann was awarded the Nobel Prize in 1969.

0.1.1 Chiral Symmetry

Another important property of QCD is chiral symmetry and its spontaneous breaking. It has vast phenomenological implications and, together with confinement, it plays a central role in shaping the phase diagram of QCD-like theories.

Chiral symmetry is related to the invariance of the QCD Lagrangian density under the chiral rotation

$$\psi \rightarrow \psi' = e^{i\alpha\gamma_5}\psi, \qquad \overline{\psi} \rightarrow \overline{\psi'} = \overline{\psi}e^{i\alpha\gamma_5} \tag{12}$$

where γ_5 is the chirality matrix acting in Dirac space and α is a real constant parameter. If we introduce the right- and left-handed projectors

$$P_R = \frac{I + \gamma_5}{2}, \qquad P_L = \frac{I - \gamma_5}{2}, \tag{13}$$

chiral symmetry decouples the action of left- and right-handed massless fermions. If $\mathcal{L}(\psi, \overline{\psi}, A) = \overline{\psi}D\psi$ is the Lagrangian density of a massless fermion in terms of the Dirac operator $D = \gamma_\mu(\partial_\mu + iA_\mu)$, then the Lagrangian can be rewritten as a sum of independent left-handed an right-handed terms

$$\mathcal{L}(\psi, \overline{\psi}, A) = \overline{\psi}_L D\psi_L + \overline{\psi}_R D\psi_R. \tag{14}$$

The different components, however, are mixed by a mass term:

$$m\overline{\psi}\psi = m\left(\overline{\psi}_R\psi_L + \overline{\psi}_L\psi_R\right). \tag{15}$$

That is why, the limit in which the quark masses go to zero is usually referred to as the *chiral limit*.

The reasoning above can be extended to the case of N_f flavours by introducing the mass matrix $M = \text{diag}(m_1, m_2, ..., m_{N_f})$ in the flavour space and rewriting the Dirac operator as $D = \Big(\gamma_\mu(\partial_\mu + iA_\mu) + M\Big)$. Now, consider the N_f^2 vector transformations

$$\psi' = e^{i\alpha T_i}\psi, \qquad \overline{\psi}' = \overline{\psi}e^{-i\alpha T_i}, \qquad \psi' = e^{i\alpha \mathbb{I}}\psi, \qquad \overline{\psi}' = \overline{\psi}e^{-i\alpha \mathbb{I}}. \tag{16}$$

where $\mathbb{I}$ represents the $N_f \times N_f$ unit matrix and the T_i, $i = 1, 2, ...N_f^2 - 1$, are the generators of $SU(N_f)$, that mix the different flavours. The Lagrangian is invariant under the above transformations in Equation 16 for the case $M = 0$ and also for $M = \text{diag}(m, m, ..., m)$. This latter case is the isospin symmetry. The symmetry holds even for non-degenerate masses if we only consider the subset of transformations

$$\psi' = e^{i\alpha \mathbb{I}}\psi, \qquad \overline{\psi}' = \overline{\psi}e^{-i\alpha \mathbb{I}}. \tag{17}$$

The associated conserved quantity in this case is the baryon number.

We can now define the chiral (or axial) rotations as

$$\psi' = e^{i\alpha\gamma_5 T_i}\psi, \qquad \overline{\psi}' = \overline{\psi}e^{-i\alpha\gamma_5 T_i}, \qquad \psi' = e^{i\alpha\gamma_5 \mathbb{I}}\psi, \qquad \overline{\psi}' = \overline{\psi}e^{-i\alpha\gamma_5 \mathbb{I}}, \tag{18}$$

where the last transformation is the $U(1)$ chiral rotation. Similarly to the single flavour case, the action is invariant under these transformations for the case $M = 0$. The massless action, then, exhibits the symmetry

$$SU(N_f)_L \times SU(N_f)_R \times U(1)_V \times U(1)_A. \tag{19}$$

The $U(1)_A$ axial symmetry is broken explicitly in the quantised theory. Due to this axial anomaly, the symmetry for the quantised massless theory is reduced to

$$SU(N_f)_L \times SU(N_f)_R \times U(1)_V. \tag{20}$$

The $SU(N_f)_L \times SU(N_f)_R$ is explicitly broken by the introduction of a mass matrix of the type $M = \text{diag}(m, m, ..., m)$ to its subgroup $SU(N_f)_V$, and the symmetry of the theory is reduced to

$$SU(N_f)_V \times U(1)_V. \tag{21}$$

Explicit breaking due to a mass term is not the only way in which chiral symmetry can be broken in QCD. The low-energy strong dynamics of the theory rearranges the vacuum, causing a scalar condensate of the quark fields

$$\langle \overline{\psi}(x)\psi(x)\rangle \neq 0, \tag{22}$$

to appear. The condensate transforms like a mass term and is not invariant under chiral rotations, breaking the chiral symmetry of the QCD vacuum. In the case when the action of the theory is invariant under some symmetry transformation but its vacuum is not, we say that the symmetry is *spontaneously broken*. In 2008, Yoichiro Nambu was awarded the Nobel Prize in Physics "for the discovery of the mechanism of spontaneous broken symmetry in subatomic Physics"[nob].

The chiral condensate of QCD breaks eight linearly independent global and continuous symmetries, corresponding to eight currents $j^i_{A\mu}$. According to the Goldstone theorem[148,241,149,58], as a consequence, there will be eight low-energy Goldstone bosons (π^i). If the theory has massless quarks, $\partial^\mu j^i_{A\mu} \equiv 0$ and the associated Goldstone bosons are massless. If the quarks in the theory are very light but not massless (i.e., chiral symmetry is spontaneously and explicitly broken), like the up, down and strange quarks found in nature, the corresponding Goldstone bosons are not massless, but light. This explains why pions, the lightest composite states made of quarks, are so light: they are identified as the would-be Goldstone bosons of QCD.

Phases with different symmetry patterns can be distinguished by a physical quantity known as the *order parameter*. It typically has a non-zero value in one of the phases and vanishes identically in the other. The continuity properties of the order parameter and its derivatives at the transition point determine to the order of the transition. The condensate is non-zero in the broken phase of the theory and vanishes in the phase in which chiral symmetry is restored. It serves, then, as an order parameter for the chiral symmetry breaking phase transition.

0.1.2 The QCD Running Coupling and Asymptotic Freedom

The strength of the QCD interaction is regulated by the renormalised coupling constant g of the theory, a quantity which is dependent on the renormalisation scale of the theory. This dependence, defined via the Callan-Symanzik equation[73,298,299], is encoded in the β-function of the theory:

$$\beta(g) \equiv \mu\frac{\partial g}{\partial \mu} = \frac{\partial g}{\partial \log \mu} \tag{23}$$

For small coupling g, a perturbative expansion for the QCD β-function can be written

$$\beta(g) = -\beta_0 \frac{g^3}{(4\pi)^2} - \beta_1 \frac{g^5}{(4\pi)^4} + \ldots \tag{24}$$

where the β_i are the $(i+1)$-loop coefficients of the expansion, which, in general, are dependent on the underlying $SU(N)$ group and fermion representation. The first two coefficients are universal and can be written, for an arbitrary group representation R of the compact Lie Group G as

$$\begin{aligned} \beta_0 &= \frac{11}{3} C_2(G) - \frac{4}{3} T(R) N_f, \\ \beta_1 &= \frac{34}{3} C_2(G)^2 - \frac{20}{3} C_2(G) T(R) N_f - 4 C_2(R) T(R) N_f, \end{aligned} \tag{25}$$

where $C_2(G)$ and $C_2(R)$ are the quadratic Casimir operators of the adjoint and fermion representations and $T(R)$ is the trace of R. In the case of a $SU(3)$ theory with N_f flavours in the fundamental representation, these become

$$\beta_0 = \frac{1}{16\pi^2}\left(11 - 2\frac{N_f}{3}\right), \qquad \beta_1 = \frac{1}{(16\pi^2)^2}\left(102 - 38\frac{N_f}{3}\right). \tag{26}$$

The value of β_0 was firstly calculated by Politzer[267], Gross and Wilczek[155,156] and 't Hooft[‡]. The result implies that the beta function of QCD is always negative and its coupling runs towards zero for higher energy scales. This concept is known as Asymptotic Freedom and, in 2004, Politzer, Gross and Wilczek received the Nobel Prize in Physics for the discovery of Asymptotic Freedom in QCD. This discovery changed the previous concept that all gauge theories should have a beta function similar to QED, opening the doors for trustworthy perturbative calculations in strong interactions at high energy, and QCD became generally accepted as the theory of strong interactions.

At the one-loop level, the scale dependence of the running coupling constant of QCD α_s is given from the renormalisation group equation by

$$\alpha_s(\mu) = \frac{g^2(\mu)}{4\pi} = \frac{2\pi}{\beta_0 ln(\mu/\Lambda_{QCD})}. \tag{27}$$

It goes to 0 in the momentum scale $\mu \to \infty$ limit or equivalently the distance approaching zero, a theoretical result that has been verified in high-energy experiments to very high precision: the current

[‡]'t Hooft's result was announced at a conference in Marseilles in 1972, but never published

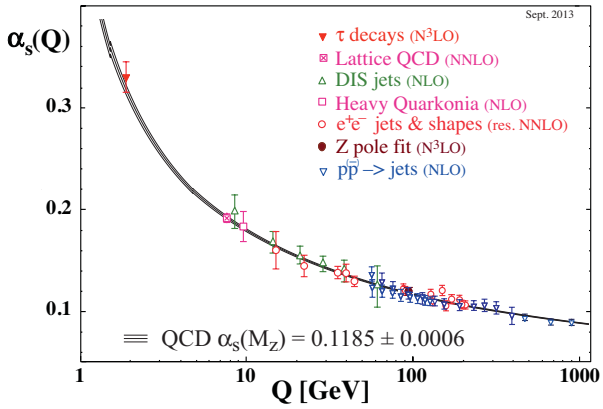

Figure 1: The logarithmic decrease of the strong interaction coupling as energy is increased, as predicted by asymptotic freedom in QCD. The figure illustrates the current agreement between QCD and many experiments. Figure by the Particle Data Group [255].

global average of the running coupling at the mass of the Z-boson, calculated by the Particle Data Group, is $\alpha_s(M_Z) = 0.1184 \pm 0.0006$, with an uncertainty well below the 1% (see Figure 1).

In Equation 27 we have introduced the renormalisation group invariant integration constant Λ_{QCD}. This is the only dimensionful quantity of QCD, and can be experimentally determined. It replaces the dimensionless parameter g through dimensional transmutation and marks the renormalisation scale at which the coupling diverges and is the characteristic scale of QCD processes, such as colour confinement, which will be discussed below. For $\mu >> \Lambda_{QCD}$ we have that $g(\mu) << 1$, i.e, the theory is weakly coupled and perturbative; $\mu << \Lambda_{QCD}$ implies $g(\mu) >> 1$, i.e, the theory is strongly coupled and Physics becomes non-perturbative.

0.1.3 Colour Confinement

The other side of asymptotic freedom is colour confinement, which is the most prominent feature of QCD: at zero temperature and density, in strongly interacting system, only colour singlet states can exist as free particles at distances scales larger than $1/\Lambda_{QCD}$. Colour singlet states are to be understood as colourless combinations (i.e., with zero colour quantum number) invariant under $SU(3)$ colour transformations. Such combinations are not allowed to have arbitrarily small energy, but rather their energy is bounded from below by a scale which is referred to as the mass gap and confinement is also commonly defined as *the existence of a mass gap in quenched QCD* (QCD without dynamical quarks). Due to the existence of a mass gap, the spectrum of this theory consists of massive bound

states of gluons called glueballs. Calculations of the glueball spectrum on the lattice require a huge computational effort in order to satisfy the large amount of statistics required. Because of that, the spectrum is typically calculated in the quenched approximation. The first lattice calculation was performed by Morningstar and Peardon [238] and the main results are in agreement with subsequent works [230,78]. Glueball spectroscopy with dynamical quarks is a more difficult task and constitutes an active area of research within the lattice community. More recently, it was realised that it is possible to formulate the quenched approximation in the framework of the 't Hooft large-N limit, providing a controlled interpolation from QCD to $SU(3)$ Yang-Mills. For a recent overview on the status of glueball studies, the reader is referred to a recent review by Ochs [252]. For a lattice review, the reader is referred to the works by McNeile [229] and by Lucini [211,212] and for recents lattice developments to the work by Gregory et al. [153].

It is important to note that it is still an open challenge to provide a rigorous proof for colour confinement, which remains a conjecture consistent with experimental facts. In particular, a rigorous proof of the existence of a Yang-Mills theory with a mass gap for any compact single gauge group is one the Millennium Problems listed by the Clay Institute [mil].

The colour confinement phenomenon is usually understood through the flux tube picture: the gluons that mediate the strong interaction self-interact and the electric colour field of the interaction is squeezed by the vacuum to a minimal geometrical configuration: a narrow tube with constant energy density. The energy stored in the tube, therefore, increases linearly with the tube length. If one tries to pull a quark-antiquark pair apart, a new quark-antiquark pair will be created. Numerical simulations have observed the flux tube from the plot of energy density in space and confirmed the linear growth of the quark potential [303].

At high temperatures, finite temperature effects become non-negligible and the picture is modified. In the very early universe, for example, for times of order of 10^{-4} seconds after the Big Bang, thermal energy fluctuations were of the order of 100 MeV, which is the order of the mass of the π-meson. In such regimes, the large entropy of infinite length strings will cause them to condensate, leading to a phase of deconfined free quarks, called quark-gluon plasma (QGP). Here, it is important to make clear the meaning of *free* in the previous sentence: it refers to the fact that isolated quarks can propagate freely in the QGP phase, without being bound within hadrons, since the phase is deconfined; it does not mean that the quarks are free from strong interaction. In fact, the small shear viscosity to entropy ratio observed in heavy ions experiments at the Relativistic Heavy Ion Collider

(RHIC)[6,37,7,41] imply that the QGP is strongly coupled[291]. The phase transition associated with deconfinement was first pointed out by Polyakov[268] and Susskind[296]§.

Polyakov also proposed a criterion for confinement at finite temperature[268] based on the quantity known as the Polyakov loop, which is the trace of the time-ordered exponential

$$L(\vec{x}) = \mathrm{Tr}\ \mathcal{P}\, e^{i\int_0^{1/T} dtA(\vec{x},t)}, \tag{28}$$

i.e., it is the Wilson thermal loop going along the temporal direction of length $1/T$, where T represents the temperature. It is possible to imagine that the time variable t is compactified, so that the Polyakov loop winds around the temporal direction

The expectation value of this quantity is related to the free energy $F_0(\vec{x})$ of a single quark (minus the free energy of the vacuum) located at the point $\vec{x}$ of space by

$$\langle L(\vec{x})\rangle = e^{-F_0/T}. \tag{29}$$

Confinement of quarks requires an infinite F_0, i.e., $\langle L(\vec{x})\rangle = 0$. On the other hand, the existence of isolated quarks requires a finite F_0, i.e., $\langle L(\vec{x})\rangle \neq 0$.

In pure Yang-Mills theory, the deconfinement transition can also be understood in terms of the global $Z(3)$ symmetry, which is the centre symmetry of $SU(3)$. The transformation of all temporal link variables on a given time slice $i_4 = t_0$ with the same element $z \in Z(3)$

$$U_4(i,t_0) \to zU_4(i,t_0) \tag{30}$$

produces gauge configurations with the same statistical weight as the original ones. For $SU(3)$, the centre elements are the cubic roots $(\mathbb{I}, \mathbb{I}e^{2\pi i/3}, \mathbb{I}e^{-2\pi i/3})$. Under the action of the $Z(3)$ centre symmetry group, the Polyakov loop transforms as

$$L \to z\,L, \tag{31}$$

§Those interested on the cosmological consequences of the deconfining phase transition can refer to[87,292]

and its expectation value can be written as

$$\langle L \rangle = \frac{1}{3}\langle L + z\,L + z^2\,L \rangle = \frac{1}{3}\left(1 + e^{i2\pi/3} + e^{-i2\pi/3}\right)\langle L \rangle = 0. \tag{32}$$

Thus, exact centre symmetry is associated with $\langle L \rangle = 0$, i.e., with confinement. When centre symmetry is broken, the relation in Equation 32 is not verified, and broken centre symmetry is then associated with $\langle L \rangle \neq 0$, i.e., with deconfinement. Spontaneous breaking of centre symmetry is linked to the finite temperature transition of quenched QCD[301]. Dynamical fermions in the fundamental representation explicitly break the $Z(3)$ symmetry and in this case the centre symmetry argument presented above works in an approximate way and the Polyakov Loop is no longer an order parameter.

A finite volume lattice has a finite number of degrees of freedom, making it impossible for spontaneous breaking of $Z(3)$ symmetry. It is usual then to consider a modified version of the confinement criterion given by the correlator of two Polyakov loops separated by a distance R along a spatial direction[297]. It is connected to the free energy $F(R)$ of separation R between a quark and antiquark via

$$\langle L(\vec{x})L^\dagger(\vec{y})\rangle_{\text{conn}} = e^{-F(R)/T}, \tag{33}$$

with $R = |\vec{x} - \vec{y}|$. At leading order in a strong coupling approximation this is calculated, and yields, for large R,

$$F(R) \sim log(2g^2)R. \tag{34}$$

A zero expectation value of $\langle L(\vec{x})L^\dagger(\vec{y})\rangle_{\text{conn}}$ in Equation 33 is now obtained at infinite separation $R \to 0$. We interpret this as a signal of confinement. The theory deconfines at high temperature, where the free energy of the separation is asymptotically constant.

0.2 The Phase Diagram

The main objective of the work presented in this thesis is to understand the phase diagram of non-Abelian gauge theories and the role played by the emergence of conformality at a high number of flavours in its shape. Now that we have briefly overviewed the basic properties of QCD, we can proceed to introduce these matters and the partly conjectured phase diagram that is shown in Figure 2.

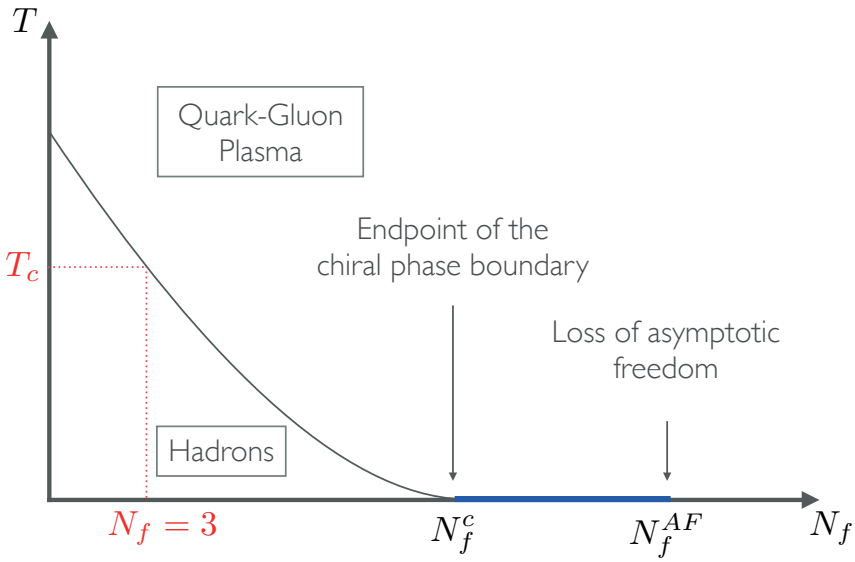

Figure 2: The conjectured phase diagram of QCD-like theories projected in the $T \times N_f$ plane, where T is the temperature and N_f the number of flavours.

Let us consider a $SU(N = 3)$ theory with N_f flavours in the fundamental representation. At small values of N_f, the picture resembles the case of QCD: the beta function of the theory is everywhere negative; at low (and zero) temperatures chiral symmetry is broken and the system is confined, what characterises the hadronic phase of QCD. At high temperatures the system deconfines and chiral symmetry is restored. This is the quark-gluon plasma.

As the number of flavours is enlarged, the beta function acquires a non-trivial zero and the theory develops a second zero at some value $N_f = N_f^c$. Further increasing the number of flavours will cause the beta function to become everywhere positive and asymptotic freedom will be lost at $N_f = N_f^{AF}$ (see Figure 3). Here, we refer to asymptotic freedom in the sense of Section 0.1.2, i.e., the vanishing of the coupling at infinite energy.

The non-trivial fixed point described above is the so called Banks-Zaks infrared fixed point (IRFP), which is an attractor in the infrared and was first described in two seminal papers in the late seventies and early eighties[75,43]. At the 2-loop level, the emergence of such a fixed point is a result of the sign inversion in the coefficient β_1 in Equation 26. For the $SU(3)$ theory with fermions in the fundamen-

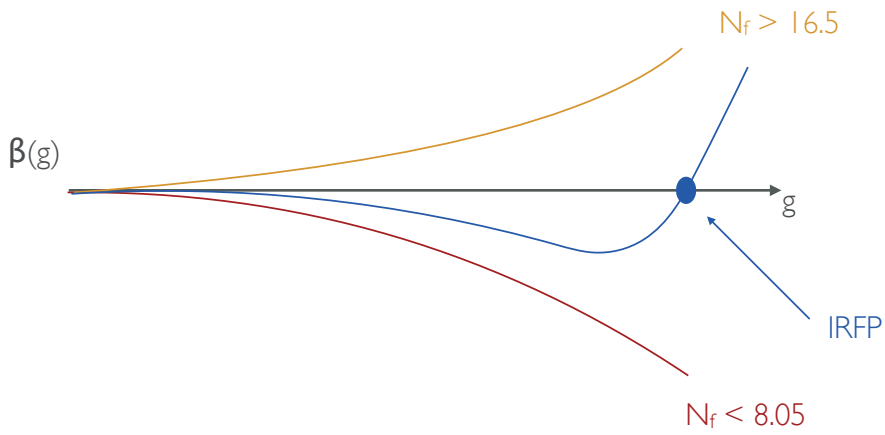

Figure 3: Possible shapes of the perturbative beta function of the $SU(3)$ gauge theory with N_f fundamental flavours as N_f is increased. It is always negative for small N_f and always positive for large N_f. For intermediate values of N_f the theory develops a non-trivial fixed point.

tal representation, again at the 2-loop perturbative level, the IRFP exists for $N_f^c = 8.05 < N_f < N_f^{AF} = 16.5$. The exact value of N_f^c, however, may suffer from nonperturbative corrections and a non-perturbative approach is required to properly study this phenomenon.

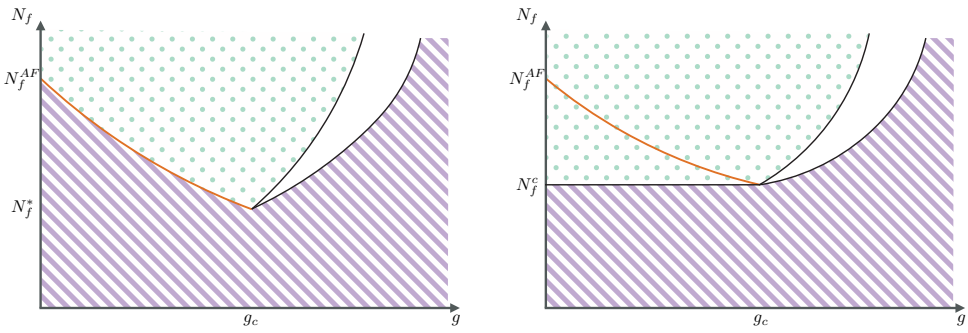

Figure 4: Projection of the phase diagram on the $g - N_f$ plane depicting the Banks-Zaks scenario (left) and the Miransky-Yamawaki scenario (right). The purple stripes fill indicates a phase in which chiral symmetry is broken, while the green polka dots indicate a phase in which chiral symmetry is restored. The red line represents a line of IR fixed points associated to each value of N_f. The horizontal line at N_f^c on the figure in the right is the conformal phase transition (CPT) that opens the conformal window. The figure represents the possibility that the bulk deconfining transition and the bulk chiral symmetry breaking transitions on the strong coupling side are not coinciding. In this scenario, the unfilled area is delimited by a bulk chiral symmetry breaking transition at weaker coupling and by a bulk confinement transition at stronger coupling, so that it would be chirally broken, but not confining. Both lines plausibly coalesce at g_c.

The Banks-Zaks scenario is depicted in Figure 4 (left) through a projection of its phase diagram

onto the zero-temperature plane $g - N_f$: the red line at strong coupling going from N_f^* to N_f^{AF} represents the location of the IRFPs associated with the zeroes of the perturbative beta function for each value of N_f. Chiral symmetry is exact on the area filled with green polka dots, and the theory is deconfined. Chiral symmetry is broken in the area filled with the purple stripes. It was then inferred by Banks and Zaks[43] that a deconfinement transition would be coupled to the emergence of the IRFP, together with the chiral symmetry breaking transition. It would, however, lead to a highly non-intuitive scenario, in which, at a given number of flavours, a phase transition from a chirally broken to a chirally symmetric theory occurs as the coupling grows!

The Banks-Zaks scenario embeds also the possibility that for couplings even stronger than the IRFP coupling, an additional non-trivial fixed point may emerge, being an attractor in the ultraviolet (UVFP). Such a fixed point would then correspond to a new theory in the continuum associated to a second order confining phase transition. If the theory has fundamental fermions, centre symmetry is explicitly broken and the only true order parameter is the chiral condensate. In fact, in this case it is not entirely accurate to talk about a deconfinement transition line and a second order phase transition can only happen at the chiral symmetry breaking line of transitions. In practice, lattice results so far favour the conclusion that the signals for confinement and chiral symmetry breaking approximately coincide for fundamental fermions[190,47]. A crossover is also possible at finite quark mass, and in this case each observable will be allowed to signal a different pseudo-critical coupling. For fermions in the adjoint representation, both the chiral condensate and the Polyakov Loop are true order parameters and they can lead to two phase transition lines. In fact, lattice results have shown that the thermal scale of deconfinement is actually lower than the chiral symmetry restoration scale for adjoint fermions[189] below the conformal window.

In addition to the possibility of a UVFP at strong coupling, where a new theory in the continuum exists, there is another possibility to explain the line of chiral symmetry breaking transitions in the phase diagram in Figure 4. The strong coupling limit of lattice regularised theories is expected to be chirally broken. This means that a chirally symmetric theory on the lattice will undergo a chiral symmetry breaking transition at some sufficiently strong coupling. Such a transition is known as a bulk transition. As will be shown in Chapter 1 of this work, this scenario is indeed realised in the case of QCD-like theories: no UVFP emerges at strong coupling and the transition is a genuine lattice phenomenon for which no continuum limit exists.

A Distinction must be made on the lattice between a scenario with a strong coupling UVFP in

the continuum theory (and thus accompanied by second order phase transitions), and a scenario with a lattice bulk transition to a phase with no continuum limit.

An important contribution to the understanding of conformal symmetry restoration was provided by the studies of Appelquist and collaborators, who have investigated, in a series of works, the N_f dependence of the chiral phase transition in different gauge theories [24,26,155,243,25,30,29,27]. They argued that, as the number of flavours N_f is varied, QCD-like theories in four dimensions undergo a chiral phase transition at a critical value N_f^c, such that chiral symmetries are spontaneously broken below N_f^c and are unbroken above N_f^c [29,27]. They have studied the nature of this transition using a ladder gap equation, considering that the value N_f^c is large enough, so that the infrared fixed point reliably exists and governs the transition.

Miransky and Yamawaki further studied this class of transitions [234] and introduced the concept of conformal phase transition (CPT), which are nothing but the Berezinskii-Kosterlitz-Thouless (BKT) phase transitions observed for finite temperature classical spin systems [199]. The name was given due to their link to the breaking of conformal symmetry. They have modified the Banks-Zaks scenario depicted above by adding the horizontal line seen in Figure 4 (right) and thus avoiding that the chiral symmetry breaking transition takes place along the line of IRFPs. There is one exception at the endpoint of the line. Their key observation, by solving the Schwinger-Dyson gap equation, was that there is a critical coupling above which chiral symmetry must be broken. This critical coupling is linked to the critical number of flavours N_f^c that signals a transition from a chirally symmetric to a chirally broken phase. This is the conformal phase transition: it is continuous in the chiral order parameter and has an abrupt change in the spectrum of the theory. In such transitions, the chiral order parameter vanishes continuously as $N_f \to N_f^c$ from below, so that the transition is not conventionally of first order. Moreover, the correlation length does not diverge as the critical point is approached, so that the transition is not conventionally of second order either.

The conformal transition at N_f^c marks the opening of the *conformal window*, which ends when the beta function becomes everywhere positive and asymptotic freedom is lost at N_f^{AF} flavours. Theories living inside the conformal window have a conformal IRFP at zero temperature, and exhibit restored chiral symmetry and deconfined quarks. Note that, in this scenario, the red line of IRFPs is not a critical line and separates two chirally symmetric phases of the theory, the one at weak coupling being asymptotically free and the already mentioned QED-like or Coulomb phase on the strong coupling side. Note, also, that in the Miransky-Yamawaki scenario the lower endpoint of the new phase occurs

at N_f^c, which can be a priori different from the N_f^* value predicted by the perturbative beta function.

We also stress the point here that, as a result of the discussion above, the existence of an IRFP does not imply *per se* the existence of the conformal window. This important observation must be taken into consideration when devising strategies for the exploration of the phase diagram. In this sense, studying the running coupling of the theory might make it possible to determine the existence or absence of an IRFP for a given theory, but does not make it possible to establish or reject the existence of the conformal window.

It is possible to note that there are many pieces to the puzzle of understanding the phase diagram of gauge theories. A deep comprehension of all of these facets requires combining knowledge extracted with different methods. Analytical perturbative calculations of the beta function for up to four loops have allowed for a perturbative estimation of the anomalous dimension of the fermion mass operator for theories that are, at that order of perturbation theory, located inside the conformal window[302,203,304,274]. An attempt at understanding the shape of the chiral phase boundary below the opening of the window has been presented, using Functional Renormalisation Group methods[66,67,65].

Some important developments were provided by a series of recent papers by Bochicchio[61,60,62]. The author derived the exact beta function of large-N Yang-Mills[59], and large-N QCD in the Veneziano limit[62] $N_c, N_f \to \infty$ with N_f/N_c constant, and identified the lower edge of the conformal window as the threshold for the quantum instability of the glueball kinetic term $N_f/N = 5/2$[59,61]. This result is in agreement with the numerical determination of the lower edge we will present in Chapter 3. One important feature of the derived beta function is that the absence of supersymmetry results in the appearance of an additional anomalous dimension term in the running of the canonical 't Hooft coupling and renormalisation scheme dependence, contrary to what happens in supersymmetric Yang-Mills. Using a topological string model underlying the large-N limit of pure Yang Mills, the author predicted the glueball spectrum of large-N Yang-Mills[60] and found accurate agreement with lattice results. The asymptotic behaviour of the scalar glueball two-point function in the 't Hooft limit of large-N QCD implies a more restrictive definition of asymptotic freedom, in which the approach to zero has powers of logarithms in the two-point correlator that are specific to QCD. Using this as definition of asymptotic freedom implies that it only exists below the conformal window, and inside the conformal window the continuum theory lives at the IRFP. In the latter case, it remains possible to device a flow to the UV by applying relevant perturbations to the IRFP. Theories,

then, can be free in the UV without being asymptotically free as usually understood in QCD. We will return to these results on Chapter , when we discuss the behaviour of the anomalous dimension of the scalar glueball operator.

Still on the analytic side, a beta function was conjectured [273] for $SU(N)$ gauge theories inspired by the Novikov-Shifman-Vainshtein-Zakharov (NSVZ) supersymmetric beta function [251,287]. The authors have then used a unitarity bound to estimate a lower bound on the lower edge of the conformal window $N_f^c \geq 8.25$. It was pointed out [257], however, that supersymmetry guarantees the cancellation of non-zero modes and renormalisation theorems, which in turn fix the anomalous dimension of the gluons in the NSVZ calculation. Without the constraints from supersymmetry, a closed beta function like NSVZ is in general not expected to exist and one has to rely on truncations of the perturbative expansion, on particular simplifying limits such as the large-N limit, or conjectures. In fact, the authors did not account for the extra anomalous dimension term resulting from the lack of supersymmetry calculated in the above mentioned work by Bochicchio [59], hampering the constraint on the lower edge of the conformal window.

Since non-perturbative approaches to the problem are required in order to establish the nonperturbative contributions to the relevant observables and yield a reliable picture of the phase diagram, lattice gauge theory methods emerged as an important tool in studying this subject.

The very first lattice studies of theories with a large number of quark flavours date back to the mid 1980's and beginning of the 1990's, with the works by Kogut et al. [197,198], Fukugita et al. [139], Ohta et al. [253], Brown et al. [68] and Iwasaki et al. [179,178]. These works, however, were hampered by the technical limitations of the time and led to contradictory results then. Finite volume systematics, in particular, were unclear. For the sake of brevity, in what follows we will focus on the works produced in the most recent surge of interest on the conformal window, that benefits from the rapid development of computing resources and algorithms in past recent years.

A wide array of different strategies has been employed in lattice studies that aim at understanding the phase diagram. These strategies typically revolve around attempts to directly to studying the running coupling, studies of the spectrum of the Dirac operator, hadron spectroscopy studies and studies of phase transitions.

Attempts to directly study the running coupling aim at reconstructing the renormalisation group flow of the theory on the lattice through a discretised beta function and then recovering the continuum limit. It is necessary to keep in mind the caveat about the limitations of this type of studies

with respect to establishing the existence of the conformal window, as mentioned before. In the Banks-Zaks scenario, for example, there is no conformal window. The proof of the existence of the conformal window is a problem per se and requires specific strategies in order to be properly addressed. Also, the extrapolation to the continuum limit in such studies only makes sense on the weak coupling side of the IRFP, not on the QED-like (Coulomb-like) strong coupling side, where no continuum limit exists. Controlling the correct phase in which the system under study is located is therefore a mandatory step as it can lead to misinterpretation of lattice data.

The usual techniques used in the strategy of searching for a signature of the IRFP are the Schrödinger functional [216,217] and step scaling [221]. Another possibility is to formulate a Monte Carlo renormalisation group flow on the lattice [158,157]. The objective in these types of studies is to map the beta function and its roots: the existence of a stable IRFP is probed by the flattening of the running coupling after an extrapolation to the continuum limit.

The first explorations of the phase diagram to use the Schrödinger functional method were performed by Appelquist et al. [21,22] who studied the $SU(3)$ theories with $N_f = 8$ and 12 flavours in the fundamental representation. Based on the observed flattening of the running coupling for the $N_f = 12$ theory, the authors concluded that this theory has an IRFP, a bound for which was estimated in the Schrödinger functional scheme. In the $N_f = 8$ case, the authors could explore the continuum-extrapolated beta function up to $g^2_{SF} \leq 6.6$. Within this range, they have found a reasonable agreement with two-loop perturbation theory and no evidence of a IRFP. Two factors, however, have limited the strength of the renormalised coupling that could be investigated in this work: computational costs and the need to avoid the strong coupling bulk transition in the lattice. The latter issue was enhanced by the fact that the authors used an unimproved fermion action.

There are some issues with this strategy: first, the flattening of the running coupling is not a sufficient condition to establish that a theory is conformal and lives at a physical fixed point. The nonperturbative beta function can depart from $n-$loop perturbation theory. Also, the distinction between a flat and a slightly increasing beta function, up to numerical uncertainties, remains a qualitative statement. In addition, there is the issue of the renormalisation scheme dependence of the running coupling.

A strategy was devised that avoids the issues with studies of the running coupling mentioned above. In addition, it allows for a true probe of the existence of the conformal window itself. It is based on the Physics of phase transitions and symmetries patterns and was inspired by earlier work

by Brown and Gies utilising Functional Renormalisation Group methods[66,67,65]. Deuzeman et al. performed the first finite temperature study of the $SU(3)$ theory with $N_f = 8$[115] in this framework. The theory was simulated at fixed bare quark mass $am = 0.02$ for lattices with temporal direction of sizes $N_t = 6$ and 12. The results indicated the existence of a chiral symmetry breaking phase transition in the system, which was found to move towards weaker coupling for larger N_t, in agreement with the expected thermal scaling from two-loop perturbation theory. The existence of this scaling and the uncertainty were interpreted as evidence that the theory would lie below the opening of the conformal window. As will be presented in Chapter 3, the small crossovers that exhibit this scaling actually mark the weak coupling edge of an emergent exotic phase in the system on the lattice between the chirally broken phase at strong coupling and the QED-like phase at weaker coupling. The nature of this exotic phase is investigated in Chapter 1.

The $N_f = 8$ theory was also investigated by Jin and Mawhinney, who used the doubly blocked Wilson (DBW2) gauge action and naive staggered fermions to study the chiral condensate, the heavy quark potential and the π and ρ spectrum of the theory. The results obtained supported, in the chiral and continuum limits, a non-zero value for the scale setting quantities r_0 and r_1[293], a non-zero value for the chiral condensate, a massless π and a massive ρ. These results have been interpreted as consistent with a chirally broken theory[180,181]. The authors have also observed a discontinuity in the chiral condensate as a function of the bare quark mass for a fixed lattice coupling, which was argued to correspond to the finite temperature chiral symmetry breaking transition[182]. The simulations, however, were performed for a reduced number of lattice couplings, not allowing for a precise control over the phase in which the spectrum measurements were performed. Also, no asymptotic scaling study has been presented to confirm the thermal nature of the claimed transition.

The results above seemed to indicate that the opening of the conformal window would happen for $N_f > 8$. Together with the superior cost-effectiveness of staggered fermions for the study of the chiral properties of the system, this motivated several groups to investigate of the $SU(3)$ theory with $N_f = 12$.

Deuzeman et al. performed a study of the mass dependence of the chiral condensate and of the spectrum of the $N_f = 12$ theory for the π and ρ channels, providing evidence that the conformal window scenario is realised and that the $N_f = 12$ theory is located inside the window[112]. The authors also observed a true bulk transition in this theory[118], together with the emergence of an exotic phase of the theory on the lattice at strong coupling. These findings have been confirmed by Cheng et al.[81].

A detailed study of both the bulk transition and the exotic phase will be the subject of Chapter 1 of this thesis.

Studies of the spectrum have also been carried out utilising different lattice actions for this theory and the results obtained by most groups agree that this theory is indeed conformal [13,208,79], with one notable divergence [134]. An attempt at a universal description of the lattice finite size scaling data by considering the effects of leading order scaling corrections was presented by Cheng et al. [79]. We will come back to this topic in Chapter 2, where our study of the spectrum of $SU(3)$ with $N_f = 12$ fundamental flavours will be discussed. From our spectrum results, we also obtained an estimate for the fermion mass anomalous dimension of the theory, which is small.

Miura et al. attempted a study of the fate of the chiral phase boundary obtained from finite temperature studies as $N_f \to N_f^c$, i.e., as the opening of the conformal window is approached from below [237]. The authors attempted to obtain directly the value of the critical number of flavours N_f^c from an extrapolation of the chiral phase boundary and found $N_f^c \sim 12$. The results, however, are likely to be modified by the new results presented in Chapter 3 of this work regarding the nature of the $N_f = 8$ theory.

Two groups have attempted a further investigation of the mass anomalous dimension of the theory through the eigenmodes of the Dirac operator [80,177]. Both concluded that the theory is conformal with a small mass anomalous dimension, in agreement with the results from spectroscopy. The small value of the mass anomalous dimension of the $SU(3)$ theory with $N_f = 12$ indicates that it is well inside the conformal window.

Attention has since shifted back to theories with a lower number of flavours. The LatKMI Collaboration presented a work [16] using Highly Improved Staggered Fermions (HISQ) where it is argued that the spectrum of the theory with $N_f = 8$ at lighter masses can be described by chiral perturbation theory, while their heavier range of simulated masses appear to exhibit some remnant of infrared conformality, in spite of the claimed broken chiral symmetry. The authors also claim that the theory has a light flavour-singlet scalar Higgs-like particle [17]. The USBSM Collaboration, however, simulated the same theory with nHYP-smeared staggered fermions at smaller masses and larger volumes (up to $48^3 \times 96$) and could not confirm spontaneous chiral symmetry breaking [278] with fermion masses as light as $am = 0.004$ on a $48^3 \times 96$ lattice volume.

The USBSM collaboration has since initiated a large project to investigate the $SU(3)$ gauge theories with $N_f = 2, 6, 8$ and 10 flavours utilising domain wall fermions [20]. So far, the results for the

$N_f = 8$ theory, obtained in partnership with the Lattice Strong Dynamics (LSD) collaboration, showed no clear evidence of infrared conformality, but were not able to conclusively establish chiral symmetry breaking either. Notably, a linear chiral extrapolation of the pseudoscalar mass squared results yields a large χ^2/d.o.f and a significantly non-zero chiral limit value, indicating tension with leading order chiral perturbation theory. It was also observed that the mass anomalous dimension of the theory seems to be rather large, $\gamma^* \sim 1$, a behaviour which is expected for $N_f \approx N_f^c$.

More recently, step scaling studies have regained traction [159,160,206,131] with the introduction of an alternative to the Schrödinger functional method, based on the gradient flow running coupling [214,215]. The results show no signal of spontaneous chiral symmetry breaking for the range of couplings so far explored. Here, we recall that these types of study alone are not able to rule out the possibility of an IRFP appearing at a stronger coupling. The study by Hasenfratz et al. [159,160], for example, has explored couplings in the range $g_c^2 \leq 14$ in the gradient flow scheme. As noted by the authors, the nonperturbative $\beta_s(g_c \sim 14)$ is comparable to the four-loop $\overline{MS}$ prediction, which has an IRFP at $g^2_{\overline{MS}} \sim 19.5$. This motivated the authors to attempt a finite temperature study of the $N_f = 8$ theory, with $40^3 \times 20$ and $48^3 \times 24$ lattice volumes. The results of this work could not establish spontaneous chiral symmetry breaking [280].

The results listed in this section indicate that indeed the $SU(3)$ theory with $N_f = 8$ fundamental flavours is close to the opening of the conformal window. It has long been believed that this theory exhibits spontaneous chiral symmetry breaking. However, in spite of studies of the running coupling being consistent with the broken symmetry scenario up to the range of couplings studied, spectroscopy, eigenmodes and finite temperature strategies have been unable to definitely establish spontaneous chiral symmetry breaking. In Chapter 3 we will present numerical and analytical evidence that the opening of the conformal window actually happens below $N_f = 8$.

0.3 Higher Dimensional Group Representations and the connection to phenomenology

In the previous section, emphasis was given to results obtained for the phase diagram of $SU(3)$ gauge theories with fundamental fermions. This is pedagogically motivated by the content of the research presented in the remaining chapters of this thesis. It is also useful and instructive to perform similar studies for higher dimensional group representations.

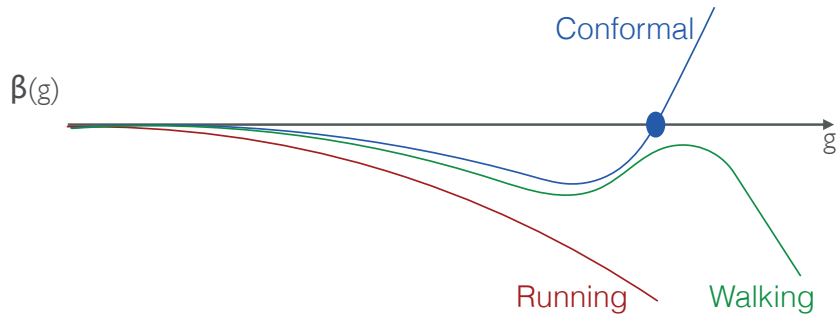

Figure 5: Possible scenarios for the beta function of the theory: in the region immediately before it develops an IRFP, the theory acquires a walking behaviour, in which the beta function turns away from the origin before touching it.

From Equation 25 it is immediate to see that representations which are higher dimensional than the fundamental (larger Casimir) push the roots of the coefficients $\beta_{0,1}$ to lower number of flavours, and therefore are more effective in loosing asymptotic freedom and acquiring an IRFP. For adjoint fermions, the point of loss of asymptotic freedom and the point at which an IRFP appears are $N_f^{AF} = 11/4$ and $N_f^c = 102/96$, respectively. Therefore, restoration of conformal symmetry can be achieved in this representation for slightly flavoured gauge theories, differently from the theory with fundamental fermions, which requires an unnaturally high, from the phenomenological point of view, flavour content. This has made theories with fermions in higher dimensional representations more phenomenologically interesting as extensions of the Standard Model. The results presented in this thesis might change this perspective.

The near-conformal region of the phase diagram might exhibit precursory effects of conformality relevant for phenomenology and model building. If a conformal phase transition takes place at N_f^c, observables in the vicinity of the conformal window, for $N_f \nearrow N_f^c$, realise Miransky/BKT scaling. The inverse correlation length of the system

$$\frac{1}{\xi_{\text{BKT}}} \simeq \Lambda_{\text{UV}}\ \theta(N_f^c - N_f)\ e^{-b'/|N_f - N_f^c|^{1/2}}, \tag{35}$$

has an exponential decrease for $N_f < N_f^c$ and vanishes identically for $N_f > N_f^c$, i.e., inside the conformal window.

In case the Miransky/BKT scaling is realised, the running coupling will slow down as $N_f \nearrow N_f^c$, so that the beta function in the pre-conformal region of the phase diagram might come close to

developing a zero [33], as shown in Figure 5. This will result in a slowly varying, *walking*, gauge coupling as a function of the energy, instead of a *running coupling* as shown in Figure 6. In fact, the Miransky scaling generated by the annihilation mechanism for the disappearance of conformality discussed in the previous section is the simplest way to realise the walking behaviour.

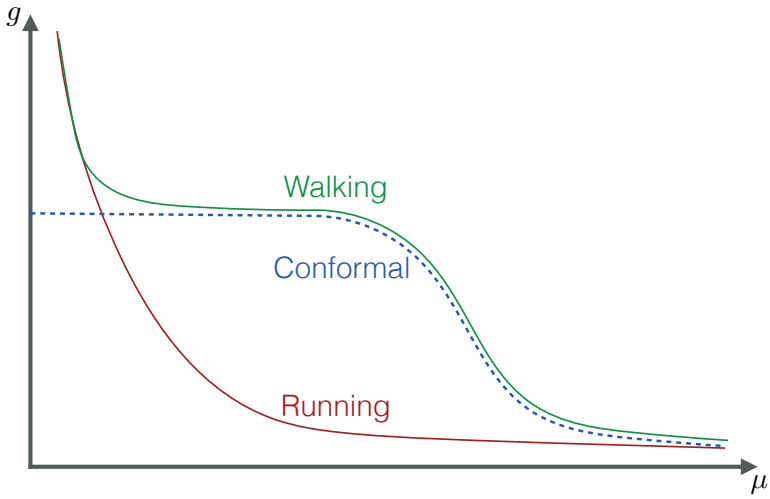

Figure 6: Possible scenarios for the coupling of the theory: in addition to the usual running seen in QCD, if the theory is conformal it reaches an asymptotic value; in the walking scenario the coupling will not run for a large range of energy scales.

The walking behaviour of the gauge coupling is appealing in the formulation of beyond the standard model (BSM) Physics because it provides a framework for a class of dynamical electroweak symmetry breaking (DEWSB) models [121] known as *walking technicolour*.

Models of DEWSB rely on the vacuum expectation value of a fermion bilinear [254] to provide a realisation of the mechanism responsible for breaking the electroweak symmetry down to electromagnetism. In its simplest version, the strong dynamics of a new, asymptotically free, non-abelian gauge theory, called *technicolour*, produces the fermion condensate [306,295]. The new gauge field carrying technicolour (TC) charge is coupled to *technifermions* that transform under some representation of the new gauge group. The coupling α_{TC} becomes strong at the scale Λ_{TC}, which must be of the order of the weak scale. The left-handed components of these technifermions are weak doublets and their condensate breaks the standard model electroweak symmetry. Because the condensate

also breaks the global chiral symmetry of the technicolour theory, the theory has *technipions*, three of which are "Higgsed" and become the longitudinal components of the W and Z bosons, setting the typical scale of the technihadron spectrum.

One serious problem with technicolour is that the Standard Model quarks and leptons are still massless after electroweak symmetry breaking, because no explicit chiral symmetry breaking mechanism is provided to generate their masses. Furthermore, in most TC models there are technipions π_{TC}, which must be given a very large mass in order to have escaped detection. In order to properly describe the flavour sector, technicolour is typically extended by the introduction of additional interactions that break unwanted symmetries, known as *extended technicolour* (ETC)[127,123].

In this scenario, ordinary $SU(3)$ colour, $SU(N_{TC})$ technicolour and flavour symmetries are unified into the ETC gauge group G_{ETC}. Gauge bosons from ETC couple to both the standard model fermions and technifermions. The extended gauge symmetry is broken down to the residual technicolour gauge symmetry at energy scale $\Lambda_{ETC} \sim M_{ETC}/g_{ETC}$, where M_{ETC} is a typical flavour gauge boson mass. The scale Λ_{ETC} is larger than the technicolour scale Λ_{TC}. Interactions between the Standard Model fermions and technifermions will be generated at lower energies.

For the order of magnitude of the technicolour scale Λ_{TC}, the interactions mediated by the ETC can be described by an effective Lagrangian obtained by integrating out the heavy ETC degrees of freedom. For our discussion here, the relevant terms are

$$\begin{aligned} &\frac{1}{M_{ETC}^2}\overline{T}(x)T(x)\overline{\psi}(x)\psi(x) \\ &\frac{1}{M_{ETC}^2}\overline{\psi}(x)\psi(x)\overline{\psi}(x)\psi(x) \end{aligned} \tag{36}$$

where we have denoted the standard model fermions by $\psi(x)$ and the technicolour fermion fields by $T(x)$. Now the Standard Model fermions will receive the contribution of a mass term coming from the technifermion condensate $\langle\overline{T}T\rangle$ and the standard model fermion masses are determined by the value of $\langle\overline{T}T\rangle$ at M_{ETC} in the renormalisation scheme in which the standard model fermion masses are being defined. It is common to follow the convention of the Particle Data Group (PDG) and refer to the standard model masses in the $\overline{MS}$ scheme, but this choice is arbitrary and is is possible to convert between renormalisation schemes. Following the convention of the PDG, in the $\overline{MS}$

scheme, we have

$$m(M_{ETC}) = \frac{1}{\Lambda^2_{ETC}}\langle\overline{T}T\rangle|_{M_{ETC}} = \frac{1}{\Lambda^2_{ETC}}\exp\left[\int_{\Lambda_{TC}}^{M_{ETC}}\frac{d\mu}{\mu}\gamma(\mu)\right]\langle\overline{T}T\rangle|_{\Lambda_{TC}}. \quad (37)$$

Here $\gamma(\mu)$ is the mass anomalous dimension of the technicolour theory in this scheme and the explicit scale dependence of the chiral condensate is shown in the second equality.

Technicolour and extended technicolour have long been challenged by several phenomenological issues. The first issue, and probably the most famous one, is that ETC models are typically expected to have flavour-changing neutral currents (FCNCs) involving quarks and leptons. It was noted long ago that the interactions in the second term in Equation 36 include FCNSc that result in considerable contributions to K and D mixing, so that a lower bound to the ETC scale is implied by the experimental limits on these contributions. The most severe is the constraint coming from possible $|\Delta S| = 2$ interactions that contribute to the $K_L - K_S$ mass difference. The measured mass difference, $\Delta M_K = 3.5 \times 10^{-18} TeV$, gives the limit

$$\frac{M_{ETC}}{g_{ETC}\sqrt{\mathrm{Re}(\theta_{sd})}} > 1300 TeV, \quad (38)$$

where θ_{sd} is a mixing-angle factor, of the order of the Cabibbo angle. Because of this large value of M_{ETC}, it is only possible to generate heavy quark masses if the techniquark condensate obtained from a naive rescaling of QCD is somehow enhanced.

Another famous problem with technicolour comes from electroweak precision measurements. The basic parameters of the electroweak sector are measured so precisely, that they can be effectively used to constrain models of new Physics. Most of the effects on electroweak precision observables can be parametrised by the three parameters S, T, U introduced by Peskin and Takeuchi [260]. Notably, a value of $\mathcal{O}(1)$ for the S parameter is obtained in technicolour by scaling up from QCD, which is much larger than the measured value [40] $S = 0.05 \pm 0.11$.

The final serious problem in (extended) technicolour is the top quark mass. The ETC scale required to produce $m_t = 175\ GeV$ is too close to the TC scale.

The appeal of the walking scenario depicted above to models of DEWSB lies in the fact that such a gauge dynamics can heal most of the problems with (E)TC models. For example, if the anomalous dimension is large, walking theories produce an enhancement of the technifermion condensate [171,172,173,310,10,34,32]: for couplings that vary very little over a wide range of energy scales, a power law

enhancement is the result of the anomalous dimension integral in Equation 37.

$$\langle \overline{T}T \rangle|_{M_{ETC}} = \left(\frac{M_{ETC}}{\Lambda_{TC}} \right)^{\gamma} \langle \overline{T}T \rangle|_{\Lambda_{TC}}, \tag{39}$$

with the anomalous dimension $\gamma(\mu) \sim \gamma$. Using this enhancement of the condensate back on Equation 37, since $M_{ETC} > \Lambda_{TC}$ and if γ is sufficiently large, then quark masses up to a few GeV can be generated. This is still not enough, though, to generate the correct mass of the top quark.

Some alternative models were then proposed in which all [233,235,240,223,167,224,225,207,71,169] or some [168] of electroweak symmetry breaking is due to top condensation $\langle \bar{t}t \rangle \neq 0$. The simplest models were based on a new spontaneously broken but strong gauge interaction that couples preferentially to the third generation of quarks, called *topcolour* [167,224,225,207,71,169], that forms a large large top-quark condensate $\langle \bar{t}t \rangle$ at the energy scale Λ_t. The original topcolour scenario, however, turned out to be highly unnatural, as it would require the topcolour scale to be very high $\Lambda_t \sim 10^{15}\ GeV$ in order for the resulting low-energy theory to simulate the Standard Model. This would imply a fine tuning of couplings of order one part in $\Lambda_t^2/m_t^2 \simeq 10^{25}$. In addition, it implied a top mass that was actually too large. Bardeen et al. [44], estimated that in topcolour models the scale associated with electroweak symmetry breaking, $v = 246\ GeV$, and the top quark mass, are related by the Pagels-Stokar formula [256]

$$v^2 \approx \frac{N_c}{8\pi^2} m_t^2 \ln \frac{\Lambda_t^2}{m_t^2}. \tag{40}$$

As a consequence, topcolour models predict a top mass of about 250 GeV and even for $\Lambda_t \sim M_{\text{Planck}}$, the predicted top quark mass would be of about $m_t = 218\ GeV$.

A possible solution proposed by Hill [168] was to combine the natural mechanism for electroweak symmetry breaking provided by extended walking technicolour with the topcolour explanation to the large top mass in a model that is known the topcolour-assisted technicolour (TC2). A second solution might be provided by the so called "top seesaw" mechanism [85,124,163,69]. In these models, a smaller mass of the top quark is achieved via mixing to an electroweak singlet fermion F that acquires a dynamical mass of several TeV. A more detailed discussion of these models, however, is outside the scope of this thesis and the reader is directed to the references for more information.

Returning to technicolour models, the effect of walking on the S parameter is more delicate and speculative, because some usual assumptions used in its calculation are invalid in a walking theory. Notably, the calculation by Peskin and Takeuchi [260] assumes that the vector and axial current cor-

relation functions that define S are each saturated by a single, narrow resonance. In walking theories, however, one may expect a whole tower of resonances contributing to low-energy observables. Thus, the assumption of saturation of of the correlation functions is unjustified. In spite of these difficulties, it has been argued [28,201,202] that the walking behaviour is accompanied by a near parity doubling of the resonance spectrum, what implicates, from the definition of S, small deviations in the Standard Model electroweak sector.

In standard technicolour models, also known as *Higgsless technicolour*, the scalar boson is too heavy and is then integrated out. As a consequence, these models are very strongly disfavoured by the recent discovery of the Higgs-like scalar boson at the LHC [4,77]. There is, however, an interesting variation that interpolates between Higgsless technicolour models and the Higgs model: a light Higgs boson could emerge as the bound state of a strongly interacting sector, rather than being an elementary field. This composite state would be the pseudo-Goldstone boson associated with the breaking of a global symmetry [186,185].

Some DEWSB models with this feature have been explored in the past decades. These include, but are note limited to, the Minimal composite Higgs model [9], models that interpret the Higgs-like scalar as a dilaton [227,50], models in warped extra-dimensions [270,95,72], and deconstructed dimensions [170,146,36].

A typical feature of composite models is the presence of resonances of different types, in a similar fashion to what happens in QCD [12,84]. The Higgs-like boson discovered in the first run of the LHC, in this sense, could actually be the lightest state of a tower of new resonances and the discovery of new composite states would be a smoking gun evidence of composite dynamics. Such new states, however, have not been observed in the first run of the LHC [91,90,92,3].

This absence of new states suggests the existence of a difference between the electroweak and new physics scale. Pich et al. [266] used a general effective Lagrangian that implements electroweak symmetry breaking to obtain the S and T parameters of electroweak precision tests for a class of models with a light scalar, taking into consideration the Higgs mass measured by CMS and ATLAS in the first run of the LHC, $m_{\text{Higgs}} = 125.09 \pm 0.21 \pm 0.11\ GeV/c^2$ [5].

They have considered a low-energy effective theory containing the Standard Model gauge bosons coupled to electroweak Goldstones, one light scalar scalar state H with mass $m_H = 126\ GeV$ and the lightest vector and axial-vector resonance multiplets $V_{\mu\nu}$ and $A_{\mu\nu}$. They have also assumed the Standard Model pattern of electroweak symmetry breaking, i.e., the theory is symmetric under $SU(2)_L \otimes$

$SU(2)_R$ and becomes spontaneously broken to the diagonal subgroup $SU(2)_{L+R}$. The state H is taken to be a singlet under $SU(2)_{L+R}$, while $V_{\mu\nu}$ and $A_{\mu\nu}$ are triplets. The underlying theory is assumed to preserve parity. To lowest order in derivatives and number of resonance fields, the Lagrangian can be written [265,263,264]

$$\mathcal{L} = \frac{v^2}{4}\,\mathrm{Tr}\left[(D_\mu U)^\dagger D^\mu U\right]\,\left(1+\frac{2\,\omega}{v}\,H\right)+\frac{F_A}{2\sqrt{2}}\,\mathrm{Tr}\left[A_{\mu\nu}f_-^{\mu\nu}\right]+\frac{F_V}{2\sqrt{2}}\,\mathrm{Tr}\left[V_{\mu\nu}f_+^{\mu\nu}\right]+\cdots\,, \quad (41)$$

where the electroweak Goldstone fields $\vec{\phi}(x)$ are parametrised through the matrix $U = u^2 = \exp\left(i\vec{\sigma}\cdot\vec{\phi}/v\right)$, $u^\mu = -i\,u^\dagger\,D^\mu U\,u^\dagger$ and D^μ is the appropriate gauge-covariant derivative. The first term gives the Goldstone Lagrangian plus their interactions with the $SU(2)_{L+R}$ singlet Higgs-like particle. For $\omega = 1$ the $H\phi\phi$ vertex of the Standard Model is recovered. The vector and axial-vector resonance multiplets $V_{\mu\nu}$ and $A_{\mu\nu}$ have masses M_V and M_A, respectively. Their terms are written in tensorial format and defined in the original references [266,263].

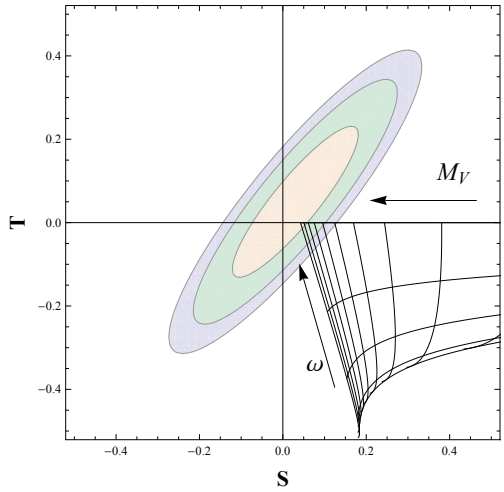

Figure 7: The NLO determination of S and T from Pich et al. [266] compared to experimental bounds [265,263,264]. The grid lines correspond to M_V values from 1.5 to 6.0 TeV, at intervals of 0.5 TeV, and $\omega = 0,\ 0.25, 0.5, 0.75, 1$. The growth directions of M_V and ω is indicated by the arrows. The ellipses give the experimentally allowed regions at 68%, 95% and 99% CL [265].

Figure 7 from Pich et al. [266] presents an interesting comparison of the NLO theoretical determinations of the S and T parameters for different values of $\omega = M_V^2/M_A^2$[¶] (black lines) with the latest experimental bounds [265,263,264] (coloured ellipses). One obtains that the precision electroweak data

[¶] This extra constraint is a result of enforcing two super convergent sum rules known as Weinberg sum rules. [56]

requires at the 68% (95%) confidence level, $\omega \in [0.97, 1]$ ($\omega \in [0.94, 1]$). This result is in agreement with a separate bound derived by the same authors from Higgs signal strengths at the LHC, which requires ω to be within 10% of its Standard Model value[262]. The allowed region also requires the vector and axial-vector states to be very heavy and quite degenerate: $M_A \approx M_V > 5$ TeV (4 TeV) at the 68% (95%) confidence level. Thus, the authors concluded that strongly-coupled electroweak models are allowed by current data provided the resonance mass scale stays above the TeV and the light Higgs-like boson has a gauge coupling close to the Standard Model one.

Models of DEWSB have a long and rich history and it would be a significant triumph of our current understanding of physical phenomena, based on effective-field theories, if they are indeed realised in nature. With the start of the second run of the LHC, more experimental data will be available to confront ideas physicists have been developing in the past three decades. This phenomenological motivation led to several studies of the emergence of conformality for various group representations and of the pre-conformal region of the phase diagram. We now briefly summarise some of these studies.

Lattice studies have been performed for different higher dimensional representations. One of them is the two-index symmetric (2S) representation: $SU(N_c)$ theories with two Dirac flavours in this representation have been studied for $N_c = 2, 3, 4$ as candidates for near-conformal behaviour[284,102,103,104,106,105]. Note that for $SU(2)$ theories there is an identity between the two-index symmetry and the adjoint representations. In this sense, studies of $SU(3)$ sextet theories can been seen as analogue to studies of $SU(2)$ with adjoint fermions. The authors have used the Schrödinger Functional method to calculate the running coupling and its dependence on the scale. They have found evidence that the beta function of the $SU(2)$ theory crosses zero and concluded that this theory has an IRFP[104]. The results obtained for the $SU(3)$[106] and $SU(4)$[105] theory might exhibit an IRFP, but the uncertainties on the results at stronger coupling do not allow this conclusion to be stated with confidence. The possibility that the beta function turns away from zero without crossing it, realising or not the walking scenario, remains. Also, large fluctuations prevent a smooth extrapolation to the continuum limit. Additionally, it is necessary to make sure that simulations have been conducted outside of the Coulomb phase for the continuum extrapolation to make sense.

Another theory that was investigated as being potentially relevant for dynamical electroweak symmetry breaking is the $SU(2)$ gauge theory with two Dirac fermions in the adjoint representation, which is also known under the name of Minimal Walking Technicolour (MWT)[122]. The theory is

believed to have a fixed point[109,166,70]. The spectrum of this theory has been object of several lattice investigations[107,76,109,108,110]. These studies revealed the existence of a low-lying scalar glueball, much lighter than bound states of fermions[109,108,110]. The behaviour in the chiral limit is consistent with the scenario presented by Miransky[232] in which a dynamical Yang-Mills scale is generated in the vicinity a weakly coupled IRFP and exponentially suppressed as a function of the renormalised fermion mass. As shown by Miransky, this feature is a signature for theories that have an IRFP if the value of the IRFP coupling is not too large[232]. The anomalous dimension of the chiral condensate has been studied through different methods, that include finite size scaling[210,109,108], the the Schrödinger functional method[104,70], Monte Carlo Renormalisation Group[76] and Dirac Mode Number scaling[259,110]. The results indicate that the anomalous dimension is much smaller than one. These characteristics severely harm the phenomenological interest in the theory. It continues to be actively studied, however, as it can still provide valuable insight into (near) infrared conformal systems.

More recently, other models have been studied as candidates for realising DEWSB. The interest in such models has risen in recent years, given that the results coming from the LHC are still unable to determine whether the Higgs is a composite particle. These include, but are not limited to, the $SU(2)$ theory with two fundamental fermions[164,38], the $SO(4)$ MWT model[165], the $SU(2)$ theory with eight fundamental flavours[271], a gauge theory with a fermion doublet in the two-index symmetric (sextet) representation of the $SU(3)$ group[133,135,130,132,193,194] The readers are referred to the original references for more details on specific results for the several models.

0.4 Lattice Methods

Lattice gauge theory consists of a set of algorithms and numerical strategies for simulating QCD and other BSM theories numerically. A number of pedagogical introduction articles to the subject can be found in the literature[277,204]. The main idea is to discretise spacetime, i.e., to replace the continuum of spacetime with a discrete four-dimensional lattice of points (three spatial dimensions plus time) and to replace derivatives with finite differences. The discretised action of the theory is written in terms of fields which live on the sites of the lattice or in the links between them. More precisely, gluon fields live on the lattice between lattice sites and are represented, for the case of QCD and the BSM theories we will study throughout this thesis, by $N \times N$ matrices that belong to the special unitary $SU(N)$ group; quark fields live on the sites of the lattice and can transform in different

representations of $SU(N)$.

Monte Carlo methods are used to calculate the evolution of the fields, generating new configurations from the previous ones, such that the set of configurations has an appropriate distribution of values. We call a *configuration* the set of all values of fields across the lattice. They can be seen as a snapshot of the system at a given Monte Carlo time. Once the Monte Carlo chain has reached equilibrium, or *thermalised*, such that the arbitrary initial configuration has been forgotten, physical observables of interest may be calculated.

Let us now be more mathematical in this introduction. For that, consider a gauge theory with gauge group $SU(N)$ and N_f fermions in a given representation of $SU(N)$. Our goal is to obtain a discretised formulation of this theory on a Euclidean four-dimensional spacetime grid preserving gauge invariance. Let us call a the lattice spacing between sites of an isotropic lattice and $A_\mu(x)$ the vector potential. We name the link variable $U_\mu(i)$ and define it as

$$U_\mu(i) = P \exp\left(ig \int_{ai}^{a(i+\hat{\mu})} A_\mu(x) dx^\mu \right). \tag{42}$$

Here g is the gauge coupling and $\hat{\mu}$ is the versor in the μ direction. In this naming convention, this variable links the lattice point $i = x_i/a \equiv (i_0, ..., i_3)$ to the point $i + \hat{\mu}$. The variable corresponding to the negative direction can be obtained through $U_{-\mu}(i) = (U_\mu(i))^\dagger \equiv U_\mu^\dagger(i)$. The link variable $U_\mu(i)$ transforms under a gauge transformation $G \in SU(N)$ as

$$U_\mu(i) \to G(i) U_\mu(i) G^\dagger(i + \hat{\mu}) \tag{43}$$

and its parallel transport along an elementary square of the lattice, known as the *plaquette*, is given by

$$U_{\mu\nu}(i) = U_\mu(i) U_\nu(i + \hat{\mu}) U_\mu^\dagger(i + \hat{\nu}) U_\nu^\dagger(i). \tag{44}$$

It transforms as the adjoint representation of $SU(N)$:

$$U_{\mu\nu}(i) \to G^\dagger(i) U_{\mu\nu}(i) G(i). \tag{45}$$

On the discretised lattice theory, $U_{\mu\nu}(i)$ plays the role played in the continuum theory by the field tensor $F_{\mu\nu}$ in Equation 3.

We are now ready to write down the simplest lattice action for gauge fields, which is given by the Wilson action

$$S_W = \beta \sum_{i,\nu<\mu} \mathrm{Tr}[1 - \mathcal{R}e(U_{\mu\nu}(i))], \tag{46}$$

where $\beta = 2N/g^2$ is the lattice coupling. This action is written only in terms of the trace of the real part of the plaquette. Because of that, and as a consequence of the plaquette property Equation 45, the action is gauge invariant, as expected.

The next step is to implement the discretisation of the bilinears involving the fermion fields in a gauge-invariant way. The lattice action will contain bilinear terms involving spinors evaluated on nearest-neighbour lattice points, which have the form $\bar{\psi}(i)\psi(i+\hat{\mu})$, where ψ is the lattice spinor corresponding to the continuum spinor multiplied by $a^{3/2}$ so that it becomes dimensionless. For the sake of simplicity, let us start by considering fundamental fermions. The fermion bilinear above is modified in the presence of a gauge field according to

$$\overline{\psi}(i)\psi(i+\hat{\mu}) \rightarrow \overline{\psi}(i)U_\mu\psi(i+\overline{\mu}) \tag{47}$$

i.e., by the insertion of the link variable that joins the relevant sites of the lattice. The continuum action of a free fermion field (take $A_\mu(x) = 0$ in Equation 2)

$$S_f = \iint \overline{\psi}(x)(\gamma_\mu\partial_\mu + m)\psi(x)d^4x \tag{48}$$

can be naively discretised[307] by writing the derivative in terms of finite differences. The resulting lattice Dirac operator is a matrix in the Dirac and spacetime indices and has the form

$$D_{i,j} = \sum_\mu \frac{1}{2a}(\gamma_\mu\delta_{i+\hat{\mu},j} - \gamma_\mu\delta_{i-\hat{\mu},j}) + m\delta_{i,j}, \tag{49}$$

and the naive fermion action reads:

$$S_f = a^4 \left\{ \sum_i \frac{\overline{\psi}(i)}{2a} \left[\sum_{\mu=1}^{4} \gamma_\mu \left(\psi(i+\hat{\mu}) - \psi(i-\hat{\mu})\right) \right] + m\overline{\psi}(i)\psi(i) \right\}. \tag{50}$$

One important consequence of this naive discretisation of fermions is the so-called *fermion doubling*[308] issue. With the naive the naive fermion discretisation described above, the lattice dispersion

relation becomes

$$sinh^2(E(\vec{p})a) = \sum_{i=1}^{3} sin^2(p_i a) + (ma)^2, \tag{51}$$

where $E(\vec{p})$ is the energy of a fermion with spatial momentum $\vec{p}$. This expression recovers the continuum dispersion relation $E(\vec{p})^2 = \vec{p}^2 + m^2$ in the continuum limit $a \to 0$. However, in addition to the case $\vec{p} = 0$, $E(\vec{p})$ also becomes small for other momenta $\vec{p}$ located at the corners of the Brillouin zone where momentum vector components take values $p_i = 0$ or $p_i = \pi/a$ implying $sin(p_i a) = 0$. The lattice dispersion relation acquires additional states in the spectrum with respect to the continuum spectrum at the poles of the lattice fermion propagator. These new states (in four dimensions $d = 4$, there are $2^d = 16$ degenerate states) do not disappear in the continuum are called *doubler fermions*.

A first solution to the doubling problem was given by Wilson, who proposed to add an extra term to the Dirac operator, so that in momentum space it would read

$$\widetilde{D}(p) = m\mathbb{I} + \frac{i}{a}\sum_{\mu=1}^{4} \gamma_\mu sin(p_\mu a) + \mathbb{I}\frac{1}{a}\sum_{\mu=1}^{4}(1 - cos(p_\mu a)). \tag{52}$$

The last term in Equation 52 is the so-called *Wilson term*, which vanishes for components with $p_\mu = 0$ and gives a $2/a$ extra contribution for each component with $p_\mu = \pi/a$. It acts as a mass term, so that the total mass of the doublers is

$$m + \frac{2l}{a}, \tag{53}$$

where l is the number of momentum components with $p_\mu = \pi/a$. In the continuum limit $a \to 0$ the doublers become very heavy and decouple from the theory.

We have so far considered one specific discretisation of the continuum theory, the Wilson formulation. There is a degree of freedom in the choice of discretisation. Details of the Physics at the lattice spacing a scale should be washed out so that different lattice formulations have the same continuum limit. This means that it should be possible to add irrelevant (in the renormalisation group sense) interactions at the lattice spacing scale which will be suppressed by positive powers of a and vanish in the continuum limit. Lattice formulations differing only in this way, and therefore having the same continuum limit, belong to the same universality class. In general, the universality class of

a given lattice action will be defined by its symmetries and dimensionality.

Wilson's result allowed for a working formulation of lattice QCD, *Wilson's formulation*. There is, however, one very serious problem with this formulation of QCD on a lattice: the Wilson term explicitly breaks chiral symmetry! As we have seen, chiral symmetry and its spontaneous breaking play key roles in QCD and have important phenomenological implications. It is desirable, therefore, that a reasonable lattice version of QCD is able to realise chiral symmetry the way it is realised in the continuum theory.

The question then became: is there a lattice discretisation that solves the doubling problem and preserves chiral symmetry on the lattice? The first answer to this question came in the form of a no-go theorem, based on topological arguments, by Nielsen and Ninomya[247] stating that the following four conditions are not allowed to hold simultaneously:

- the Dirac operator is local;
- For $p \ll \pi/a$ the Fourier transformed $\widetilde{D}(p) = i\gamma_\mu p_\mu + O(ap^2)$, i.e., we have one Dirac particle;
- there are no doublers;
- $\gamma_5 D + D\gamma_5 = \{\gamma^5, D\} = 0$ (exact chiral symmetry).

A consequence of the theorem is that in order to preserve locality and get rid of doublers, the only possibility is to give up on exact chiral symmetry on the lattice. In the words of the authors: *"the important consequence of our work is to discourage any attempt to construct chiral invariant lattice models for QCD"*.

Implementing chiral symmetry on the lattice became a formidable challenge. The solution to it started to appear when Ginsparg and Wilson found a way to circumvent the no-go theorem[147] by imposing the following modified constraint to the Dirac operator:

$$D\gamma_5 + \gamma_5 D = aD\gamma_5 D, \tag{54}$$

This is an extension of the chiral symmetry defining anti-commutation relation that makes it possible for chiral symmetry to be defined on the lattice for finite a and recovers the continuum form in the naive continuum limit. A lattice formulation that respects Equation 54, therefore, can implement chiral symmetry in the theory. It proved, however, hard to find such a formulation for the

interacting case and the seminal paper by Ginsparg and Wilson went forgotten for many years before it was realised that two independent approaches, namely *overlap fermions*[245,246] and *fixed point fermions*[161] originate Dirac operators that satisfy the Ginsparg-Wilson relation. A further description of these formulations is outside of the scope of this work, and interested readers are referred to the original references for more detailed accounts.

The problem of implementing chiral symmetry on the lattice inspired much research activity and resulted in a variety of formulations for fermions on the lattice, in addition to the Wilson and overlap formulations mentioned above. Notable ones include domain-wall fermions[184], twisted mass fermions[136,137,138] and Kogut-Susskind (staggered) fermions[195,42,294]. The latter, for reasons that will become clear in the following discussion, is the fermion formulation utilised in the numerical simulations presented in this work. In the remainder of this section, we give a brief overview of it.

In the staggered formulation, a transformation mixes spinor and spacetime indices, distributing the fermionic degrees of freedom on the lattice hypercubes. As a result, it reduces the 16-fold degeneracy of naive fermions to only four quarks (4-fold degeneracy) while preserving a subset of chiral symmetry.

The so-called *staggered transformations* read

$$\begin{aligned} \psi(i) &= \gamma_1^{i_1}\gamma_2^{i_2}\gamma_3^{i_3}\gamma_4^{i_4}\psi(n)' \\ \overline{\psi}(i) &= \overline{\psi}(i)'\gamma_4^{i_4}\gamma_3^{i_3}\gamma_2^{i_2}\gamma_1^{i_1}, \end{aligned} \tag{55}$$

where the i_μ are the components of the site index $i = (i_1, i_2, i_3, i_4)$. The naive fermion Equation 50 becomes:

$$S_f = a^4 \left\{ \sum_i \frac{\overline{\psi}(i)'\mathbb{I}}{2a} \left[\sum_{\mu=1}^{4} \eta_\mu(i) \left(\psi(i+\hat{\mu})' - \psi(i-\hat{\mu})'\right) \right] + m\overline{\psi}(i)'\psi(i)' \right\}, \tag{56}$$

where the staggered sign function $\eta_\mu(i), \mu = 1, \ldots, 4$ plays the role of the matrices γ_μ. They are defined as

$$\eta_1(i) = 1, \qquad \eta_2(i) = (-1)^{n_1}, \qquad , \eta_3(i) = (-1)^{n_1+n_2}, \qquad \eta_4 = (-1)^{n_1+n_2+n_3}. \tag{57}$$

The action in Equation 56 has the same form for all four components of the Dirac spinor. By retaining only one of these four components we obtain the staggered fermion action. Coupling the

gauge fields, we have

$$S_f = a^4 \left\{ \sum_i \frac{\overline{\chi}(i)}{2a} \left[\sum_{\mu=1}^{4} \eta_\mu(i) \left(U_\mu(i)\chi(i+\hat{\mu}) - U_\mu^\dagger(i-\hat{\mu})\chi(i-\hat{\mu}) \right) \right] + m\overline{\chi}(i)\chi(i) \right\}, \quad (58)$$

where the fields $\chi(i)$ and $\overline{\chi}(i)$ are one-component Grassmann functions that only have colour indices. Note also that in the spinor basis defined by Equation 55, γ_5 takes the form

$$\overline{\psi}(i)\,\gamma_5\,\psi(i) = \eta_5(i)\,\overline{\psi}(i)'\,\mathbb{I}\,\psi(i)', \qquad \eta_5(i) = (-1)^{n_1+n_2+n_3+n_4}. \quad (59)$$

For a vanishing mass, the staggered action in Equation 58 is invariant under the continuous transformation

$$\chi(i) \to e^{i\alpha\eta_5(i)}\chi(i), \qquad \overline{\chi}(i) \to \overline{\chi}(i)e^{i\alpha\eta_5(i)}, \quad (60)$$

where α is a real parameter. Equation 60 is the residual chiral symmetry for the lattice staggered formulation, in which the fermionic degrees of freedom are now distributed on the hypercube and η_5 plays the role of γ_5.

Because they have no Dirac structure, staggered fermions provide a computationally cheap way of simulating dynamical fermions on the lattice with a remnant chiral symmetry. Because of that, they have been a popular choice for tackling many problems in lattice field theories. There is, however, one caveat: the fact that the staggered action describes four tastes of quarks. When simulating QCD, one does not want a continuum theory with four degenerate quarks, but a low energy theory with 2+1 or 2+1+1 non-degenerate quarks. This leads to the famous *rooting* issue: in order to obtain QCD, is was proposed to use an effective action with one staggered fermion per flavour and take the fourth-root of the determinant. For QCD with 2+1 flavours, this means

$$e^{-S_{eff}} = e^{-S_{\text{gauge}}} \left\{ \det[D_{\text{stagg}}(m_u)]\det[D_{\text{stagg}}(m_d)]\det[D_{stagg}(m_s)] \right\}^{1/4}, \quad (61)$$

where m_u, m_d and m_s are the masses of the three light flavours up, down and strange quarks, respectively. Since the staggered Dirac operator D_{stagg} is positive definite for any non-zero quark mass, it is always possible to take the positive fourth-root. It is, however, an unusual procedure from a conceptual, raising a debate[126,285,94,200,150] amongst lattice theorists about whether this method constitutes a valid regulator for the continuum theory. The main issue comes from the fact that at

nonzero lattice spacing the rooted theory in nonlocal and not unitary. The question then is if the continuum limit can be taken and if it is in the correct universality class. Moreover, an effective field theory is needed to parametrise the nonlocal effects and provide a framework for the approach to the continuum limit. As of the time of writing of this work, no final resolution to this debate has been achieved. While there is still no definitive nonperturbative proof of the validity of the rooting trick, there is also no valid argument that it fails. Mounting theoretical arguments and numerical evidence indicate that it yields the right continuum limit. The main argument for that was provided by Shamir[283], who studied the approach to the continuum limit using renormalisation group block transformations. Such block transformations can be directly defined for the unrooted local theory, but not for the rooted theory. He showed that it is possible to construct a bridge between the unrooted and rooted theory at each blocking step, tying the validity of the rooted theory very strongly to the uncontested unrooted theory. Moreover, it has been shown that it is actually possible to derive effective field theories that take into account the fourth root procedure, such as rooted staggered perturbation theory (RSχPT)[51,54], which are valid at non-zero lattice spacing. Numerical tests using (RSχPT)[51] have indicated agreement between simulation results and theoretical expectations[53], at least perturbatively. Results obtained from simulations with dynamical staggered fermions are also in good agreement with experimental results[39,99,48,52]. One important result shown by Damgaard et al.[98] was that, while staggered fermions in complex representations at non-zero lattice space still belong to the continuum class of spontaneous chiral symmetry breaking, staggered fermions in real and pseudo-real representations at non-zero lattice spacing belong to incorrect symmetry breaking classes. The authors also suggest some strategies for recovering the correct symmetry breaking class in the continuum[98].

To summarise, staggered fermions have provided a useful tool for researchers working on the lattice, combining a lower computational cost when compared to other formulations and allowing chiral symmetry to be studied on the lattice. But in utilising them, researchers must take the associated caveats into consideration.

Our goal with lattice methods is to measure relevant observables for the theories under study by performing numerical simulations. With $S_F[\psi, \overline{\psi}, U]$ and $S_G[U]$ the fermionic and gauge components of the action of the theory, respectively, its path integral is given by

$$Z = \int \mathcal{D}[\psi, \overline{\psi}]\ \mathcal{D}[U]\ e^{-S_F[\psi,\overline{\psi},U]-S_G[U]}, \tag{62}$$

where $\mathcal{D}[\psi, \overline{\psi}]$ and $\mathcal{D}[U]$ are, respectively, the integral measure of the path integral over the fermionic and link variables. The Euclidean correlators between operators $O_1[\psi, \overline{\psi}, U]$ and $O_2[\psi, \overline{\psi}, U]$ have the form

$$\langle O_2(t) O_1(0) \rangle = \int \mathcal{D}[\psi, \overline{\psi}] \; \mathcal{D}[U] \; e^{-S_F[\psi, \overline{\psi}, U] - S_G[U]} \; O_2[\psi, \overline{\psi}, U](\cdot, t) \; O_1[\psi, \overline{\psi}, U](\cdot, 0). \quad (63)$$

For theories formulated on a finite Euclidean lattice volume, the path integral in Equation 62 is in the form of a Boltzmann weight and is an ordinary finite-dimensional integral. It can then be numerically evaluated through Monte Carlo techniques: a Markov chain process generates configurations which are distributed according to the path integral measure and weighted with the Boltzmann factor $e^{-S_F[\psi, \overline{\psi}, U] - S_G[U]}$, which is interpreted as a probability measure. The observables of interest can then be obtained as simple averages over the Markovian process. It can be proved that the estimate O_N of $\langle O \rangle$ for a Markov chain of length N converges to $\langle O \rangle$ in the limit $N \to \infty$. Moreover, the difference $\langle O \rangle - O_N$ is of order $1/\sqrt{N}$ for finite N and the standard deviation of O over the probability measure gives the confidence interval of the measurement.

The set of steps required in a lattice study is usually called the *production chain*. It starts with the generation of the lattice configurations through the Monte Carlo techniques mentioned above. The set of configuration produced and saved along the Monte Carlo history of the system being simulated is called a *Monte Carlo ensemble*. This is typically the most computationally expensive step in the chain, as it involves numerical inversions of the Dirac operator for the calculation of the quark propagator, being highly non-linear. Because of that, the calculations for this step of the chain are usually carried out on parallel supercomputers with a fast communication network and the field of Lattice QCD has even driven the development of new architectures, such as, for example, the system-on-a-chip of the BlueGene series.

In a first post-Monte Carlo step, measurements on the saved ensembles are conducted. This step is generally much cheaper than the Monte Carlo step, and can typically be performed on clusters. The last step is the data analysis, which can be generally done on a desktop computer.

Recent advances in hardware and algorithms have made it possible, in some cases, to accelerate or even run the simulations completely using Graphics Processing Units (GPUs)[86,309], which are massively parallel devices, much cheaper than the typical supercomputer used for lattice simulations. However, it remains a challenge to efficiently fit the complete production chain of a typical lattice

QCD study in such machines.

A vast part of the work presented in this thesis is the result of lattice simulations done on the BlueGene/P machine which was hosted at the Donald Smits Centre for Information Technology at the University of Groningen. We have also used the FERMI BlueGene/Q supercomputer hosted at CINECA, in Italy. Computational time for our Collaboration was provided at Fermi through the European Partnership for Advanced Computing in Europe (PRACE) initiative. Our group has also conducted simulations at the series of Dutch national supercomputers hosted at SARA, in Amsterdam. These include the former national supercomputer Huygens and the current machine Cartesius. In addition to the above mentioned systems, we have also made extensive usage of the Millipede Cluster at the University of Groningen for our post-Monte Carlo analysis.

0.5 Thesis Outline

In the following chapters, we will discuss the work we have conducted aiming at understanding the phase diagram of non-Abelian gauge theories. Chapter 1 is focused on the strong coupling regime of the $SU(3)$ theory with $N_f = 12$ on the lattice. We study the bulk transition of this theory and the emergence of a new exotic phase of this theory as the coupling is enlarged, before chiral symmetry is broken. We investigate the chiral symmetry breaking order parameter, the chiral condensate, and related quantities. We locate the chiral symmetry breaking phase transition and determine its first order nature. We also show how an emerging exotic phase is related to improvement of the lattice action and the underlying symmetries inside the conformal window.

Chapter 2 is devoted to the study of the would-be hadron spectrum of the $SU(3)$ theory with $N_f = 12$ fundamental flavours. Guided by the pattern of underlying symmetries, chiral and conformal, we analyse the two-point functions theoretically and on the lattice, and determine the finite size scaling and the infinite volume fermion mass dependence of the would-be hadron masses. We show that the spectrum in the Coulomb phase of the system can be described in the context of a universal scaling analysis and we provide a nonperturbative determination of the fermion mass anomalous dimension at the infrared fixed point. The measured value $\gamma* = 0.235(46)$ is small, in agreement with other studies and consistent with a scenario where the theory lives well inside the conformal window.

Chapter 3 is devoted to the study of $SU(3)$ theories with multiple number of flavours across the

lower end of the conformal window. We present a lattice study on the N_f dependence of the zero temperature line of bulk transitions of these theories, consistent with the opening of the conformal window at $6 < N_f < 8$. We also present a theoretical analysis of the anomalous dimension of the scalar glueball operator $G^a_{\mu\nu}G^a_{\mu\nu}$, which is a probe of the deconfinement transition, and its consequences for the UV-IR merging mechanism for the emergence of the conformal window proposed by Kaplan et al.[187].

We will conclude with a critical discussion of the results presented here and an outlook.

Truth is ever to be found in the simplicity, and not in the multiplicity and confusion of things.

Isaac Newton

1

The Strong Coupling Regime of twelve flavour QCD

This chapter is devoted to a thorough study of the strong coupling regime of the $SU(N = 3)$ theory with $N_f = 12$ flavours in the fundamental representation. It is largely based on references[113,114,96]. We are specially interested in the so-called bulk transition that emerges in the lattice phase diagram of the theory at strong bare lattice gauge coupling. The main goal of the lattice studies of such theories is of course to understand the theory in the continuum limit. However, relevant physical information can be extracted from their lattice phase diagram, and recent years have witnessed a growing amount of work devoted to the analysis of the bulk transition, see Fig. 1.1, also supported by theoretical work[234] .

Real world QCD and similar theories with a small number of flavours, exhibit a finite tempera-

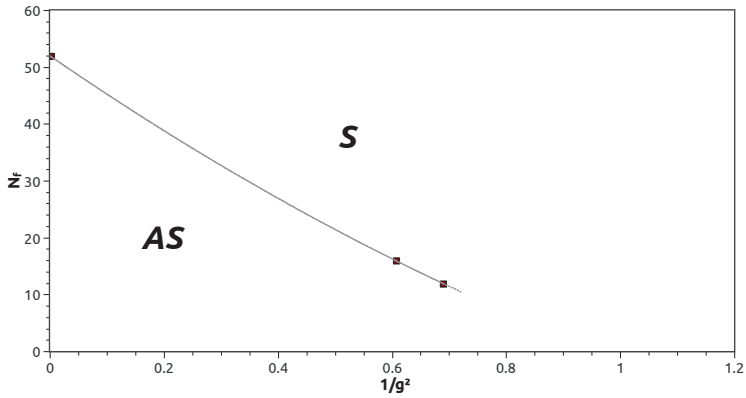

Figure 1.1: The bulk transition line in the N_f-g^2 plane of the phase diagram for SU(3) gauge theories with (unimproved) staggered fermions. The bulk transition separates a QED-like and chirally symmetric, region (S, right side) from a chirally broken phase (AS, left side). The data points are all for a bare lattice fermion mass of 0.025 and should ideally be extrapolated to the chiral limit. Data for $N_f = 16$ agree with Reference [97] after mass rescaling, the point at $g^2 = \infty$ and $N_f \simeq 50$ is from Ref. [100] and the point for $N_f = 12$ is from Reference [114]. The end point of the bulk line is discussed in Chapter 3. References [118,113,82] reported a further bulk transition in the chirally symmetric phase. In this chapter we show that next-to-nearest neighbour interactions in the improved fermion action cause the second transition to occur.

ture transition that separates a chirally broken and confined phase at low temperatures from a chirally symmetric and deconfined sector at high temperatures. This transition has been object of much scrutiny on the lattice — see [46,300] for a review or recent results, especially for the case of QCD. In particular, the order of the phase transition between the hot gas of hadrons and the QGP has be found to be a crossover [15] with a chiral transition temperature $T_c \sim 155$ MeV [18,14,63,49]. It has also been studied in the case of large number of flavours. Notably, this group has presented lattice studies for theories with $N_f = 6$ and $N_f = 8$ flavours [115,236].

A thermal transition is absent for theories that lie inside the conformal window; these theories are already deconfined and chirally symmetry at zero temperature. On the other hand, a new type of transition emerges: early studies based on the strong coupling expansion of QCD have predicted that chiral symmetry is always broken in the strong coupling limit, regardless of the number of flavours. This claim was supported by the work of Damgaard et al. [97], who uncovered a bulk transition for sixteen fundamental fermions. A true bulk transition also appears in QCD with twelve flavours, and the careful scrutiny of the region at its weak coupling side is consistent, within numerical uncertainties, with exact chiral symmetry [112,113].

Interestingly, and amusingly, a second bulk transition was uncovered by us [113,118], between the first observed bulk transition and the weak coupling region, where chiral symmetry and spectrum studies

were carried out. This was an interesting and unexpected observation calling for further analysis. The existence of a second transition at nonzero fermion mass was confirmed by the work in [82,279], where it was observed that the shift symmetry of staggered fermions was broken in the intermediate phase. A recent interesting development re-examined the early strong coupling studies: contrary to previous conclusions, it was observed that, with unimproved fermions, the line of bulk transitions ends for $N_f \simeq 51$. No second transition was observed in this case [100].

A more general line of work involving quantum – or bulk – transitions in a particle physics environment dates back to early studies of QED at strong coupling. The transition in this context has been for a long time investigated in the hope of finding an interacting, non asymptotically free theory in four dimensions. Such a theory requires a second order transition with non-trivial critical exponents. Indeed, the bulk transition for QCD with a large number of flavours can be seen in analogy with the QED transition and in this spirit, inspired by the work by Kaplan et al. [187], this group has proposed [118] to search for an interacting UVFP at the bulk transition itself. One of us has also explored this possibility in the context of AdS/CFT [45]. QED-like lattice systems are also being used for the simulation of strongly coupled graphene. Using an effective field theory description, the system can be modelled by QED in 2+1 dimensions, whose bulk transition can be analysed borrowing early lattice methods and strategies [125].

Bulk transitions are, therefore, interesting for several reasons ranging from a diagnostic of the conformal window to fundamental QFT questions and the physics of condensed matter systems, such as graphene. Lattice methods are mandatory, based on today's knowledge, for studying such strongly coupled phenomena.

This chapter is dedicated to the study of the bulk transition for $N_f = 12$ and the role of improvement. We present our results on the nature of the peculiar intermediate phase that exists between the bulk transitions, referred to as exotic phase in the following, and on the role played by improvement in its emergence.

1.1 The Actions

In order to disentangle the different effects of improvement of the gauge and fermion sectors, we simulated the $SU(3)$ gauge theory with twelve flavours of staggered fermions in the fundamental representation using four different lattice actions, which differ by different choices of improvement.

Action	Gauge Improvement	Fermion Improvement
A	No	No
B	Yes	No
C	No	Yes
D	Yes	Yes

Table 1.1: Actions used in this work: gauge improvement refers to tree-level Symanzik improvement in the gauge action, while fermion improvement refers to tree-level Symanzik improvement of the staggered fermion action, i.e. the addition of the Naik term [239,57].

All considered cases are labeled A to D in Table 1.1.

Many of the comparisons presented here are for a bare lattice fermion mass of 0.025 and a volume $16^3 \times 24$, as in Fig. 1.2. For some of the actions we have explored an extended set of parameters. These will be indicated.

Our choice of action A is explicitly written as:

$$S = -\frac{N_f}{4}\mathrm{Tr}\ln M(am, U) + \beta\,\mathrm{Re}(1 - U(\mathcal{P})) \tag{1.1}$$

where $M(am, U)$ is the fermion matrix for the naive staggered fermion action for a single flavour with mass m, $\beta = 6/g^2$ is the SU(3) lattice coupling and $U(\mathcal{P})$ is the trace of the ordered product of link variables along the single plaquette P divided by the number of colours.

The addition of tree-level Symanzik improvement of the gauge action leads to Action B,

$$S = -\frac{N_f}{4}\mathrm{Tr}\ln M(am, U) + \sum_{i=0,1}\beta_i(g^2)\sum_{\mathcal{C}\in\mathcal{S}_i}\mathrm{Re}(1 - U(\mathcal{C})) \tag{1.2}$$

where $U(\mathcal{C})$ are the traces of the ordered product of link variables along the closed paths $\mathcal{C}$ divided by the number of colours.

The $\mathcal{S}_0$ contains all the 1×1 plaquettes (nearest neighbours), while $\mathcal{S}_1$ contains all the 1×2 and 2×1 rectangles (next-to-nearest neighbours). The couplings are defined as $\beta_0 = (5/3)\beta$ and $\beta_1 = -(1/12)\beta$, where $\beta = 6/g^2$ is the SU(3) lattice coupling of the unimproved gauge action.

Improvement of the staggered fermion action can be realised following the Naik prescription [239,57], which effectively extends the Symanzik improvement to the fermions. The Naik improved fermion

action can then be written as:

$$\begin{aligned} S_F \quad &= a^4 \sum_{x;\mu} \eta_\mu(x)\bar{\chi}(x)\frac{1}{2a}\left\{c_1\left[U_\mu(x)\chi(x+\mu) - U^\dagger(x-\mu)\chi(x-\mu)\right]\right. \\ &+c_2\left[U_\mu(x)U_\mu(x+\mu)U_\mu(x+2\mu)\chi(x+3\mu)\right. \\ &\left.\left.-U^\dagger_\mu(x-\mu)U^\dagger_\mu(x-2\mu)U^\dagger_\mu(x-3\mu)\chi(x-3\mu)\right]\right\} \\ &+a^4 m\sum_x \bar{\chi}(x)\chi(x) \end{aligned} \tag{1.3}$$

where the phase factor $\eta_\mu(x) = (-1)^{(x_0+x_1\ldots+x_{\mu-1})}$ and the action is written in terms of the one component staggered fermion fields $\chi(x)$. The coefficients $c_1 = 1$ and $c_2 = 0$ reproduce the naive staggered fermion action, while the Naik choice $c_1 = 9/8$ and $c_2 = -1/24$ provides $O(a^2)$ accuracy at tree level. Notice that the additional Naik term involves up to third-nearest neighbour interactions.

1.2 The Observables

The chiral condensate, the order parameter for the chiral symmetry breaking transition, for N_f degenerate flavour in lattice units

$$a^3\langle\overline{\psi}\psi\rangle = \frac{N_f}{4N_s^3N_t}\langle\mathrm{Tr}\left[M^{-1}\right]\rangle, \tag{1.4}$$

was determined by using a stochastic estimator with 20 repetitions. Here, N_s and N_t represent, respectively, the spatial and temporal lattice extents. The chiral susceptibility, $\chi = \partial\langle\overline{\psi}\psi\rangle/\partial m$ at a fixed lattice parameter β can be divided into a connected and disconnected components $\chi = \chi_{\mathrm{conn}} + \chi_{\mathrm{disc}}$, which are given in lattice units by

$$\begin{aligned} a^2\chi_{\mathrm{conn}} &= -\frac{N_f}{4N_s^3N_t}\langle\mathrm{Tr}\left[(MM)^{-1}\right]\rangle, \\ a^2\chi_{\mathrm{disc}} &= -\frac{N_f^2}{16N_s^3N_t}\left[\langle\mathrm{Tr}\left[M^{-1}\right]^2\rangle - \langle\mathrm{Tr}\left[M^{-1}\right]\rangle^2\right], \end{aligned} \tag{1.5}$$

respectively. The disconnected chiral susceptibility is a non-local quantity that can be estimated from the variance of the bulk behaviour of the chiral condensate. However, by computing the variance of the condensate with stochastic estimators, part of the connected contributions will automatically

be included through random sources multiplying themselves. We have followed the prescription by Bernard et al.[55], in order to eliminate those contributions by only considering the off-diagonal elements of the covariance matrix of the random sources introduced for the estimation of the chiral condensate.

The chiral susceptibility and the chiral condensate are then used to define two physically relevant quantities, χ_σ and χ_π as

$$\chi_\sigma \equiv \chi = \frac{\partial \langle \overline{\psi}\psi \rangle}{\partial m} = \chi_{\text{conn}} + \chi_{\text{disc}} \tag{1.6}$$

and

$$\chi_\pi = \frac{\langle \overline{\psi}\psi \rangle}{m}. \tag{1.7}$$

Adding together all the above mentioned ingredients, it is then possible to construct the associated chiral cumulant

$$R = \frac{\chi_\sigma}{\chi_\pi}. \tag{1.8}$$

The susceptibilities χ_σ and χ_π are related through Ward identities to the spacetime volume integral of the scalar (σ) and pseudoscalar (π) propagators. Their ratio should tend to zero in the chiral limit in the zero in the spontaneously broken phase and is one in the chiral limit in the chirally symmetric phase due to degeneracy of the chiral partners. Therefore, the cumulant defined in Equation 1.8 is a probe of chiral symmetry[191,115].

1.3 The effect of improvement

The main numerical finding of this chapter is presented on Fig. 1.2, where we show the transition region of the chiral condensate for the fully improved and unimproved actions: two rapid crossovers of the condensate are present with the improved action, while a single chiral symmetry breaking transition is present in the unimproved case.

Figure 1.3(a) shows the rapid crossover for the chiral condensate (left) superimposed on the plaquette (right), at the bare lattice mass $am = 0.025$. No additional structure is observed in the chiral condensate. We corroborate these observations by showing the connected component of the chiral susceptibility χ_{conn} in Figure 1.3(b); its behaviour is as expected and no sign of an intermediate phase at weaker coupling and additional transitions is present.

Given the absence of phase transitions or indications for a crossover, it is plausible to conclude

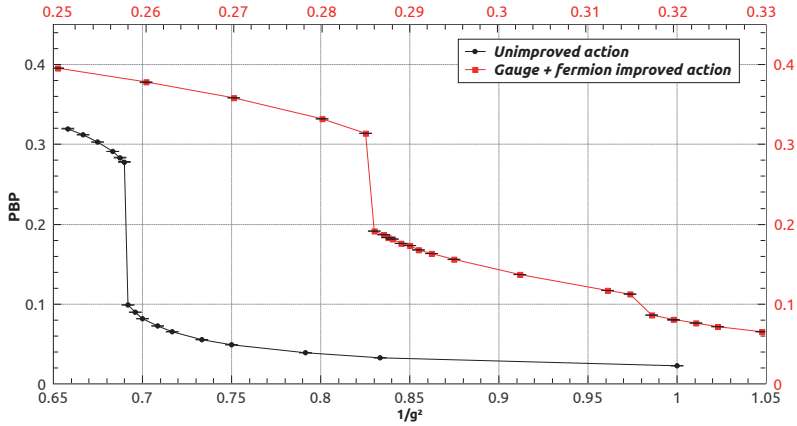

Figure 1.2: The chiral condensate for the SU(3) gauge theory with $N_f = 12$ fundamental flavours as a function of $1/g^2$, with g the lattice bare coupling. We show the results for the unimproved action, Action A (leftmost, black) and for the improved gauge and fermion action, Action D (rightmost, red). Data are for am=0.025 and volume $16^3 \times 24$. The weaker coupling crossover of the improved action disappears in the unimproved case.

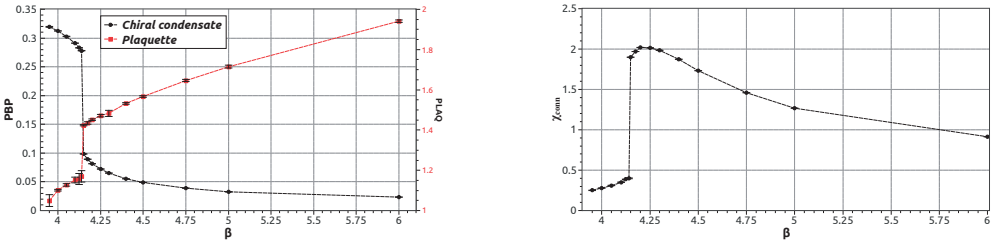

Figure 1.3: (a) Rapid crossover of the chiral condensate (PBP) and the plaquette for $N_f = 12$ flavours with the unimproved action (Action A) as a function of the lattice coupling $\beta = 6/g^2$ in the strong coupling region, for $am = 0.025$ and volume $16^3 \times 24$. (b) The connected susceptibility for the same parameters.

that the weak coupling phase of this theory is continuously connected with the asymptotically free regime that admits a continuum limit. If this is true, its symmetry properties are the same as the ones of the improved action, extensively investigated in our previous work. We then conclude that the rapid crossover observed for Action A in Figure 1.3 should be interpreted as the finite mass remnant of a bulk chiral transition separating the chirally broken phase at strong coupling from the chirally symmetric phase, in complete analogy with the unimproved results obtained by Damgaard et al[97] for $N_f = 16$.

1.3.1 Action D: the improved gauge and fermion action

We now consider Action D, i.e. the case where both fermion and gauge actions are tree-level Symanzik improved. For small enough bare masses ($am \lesssim 0.04$), at the simulated volumes, two rapid crossovers

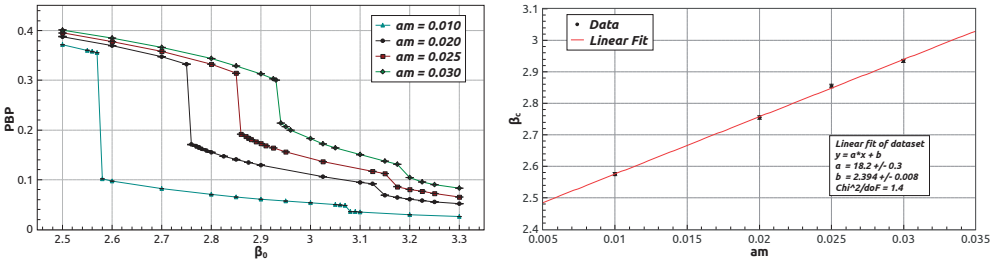

Figure 1.4: (a) Rapid crossovers in the chiral condensate (PBP) with the improved action as a function of the coupling $\beta_0 = 10/g^2$ in the strong coupling region for different bare masses. (b) The mass dependence of the critical β value extracted from the central point of the strong coupling is in agreement with a linear scaling expected for a first order transition.

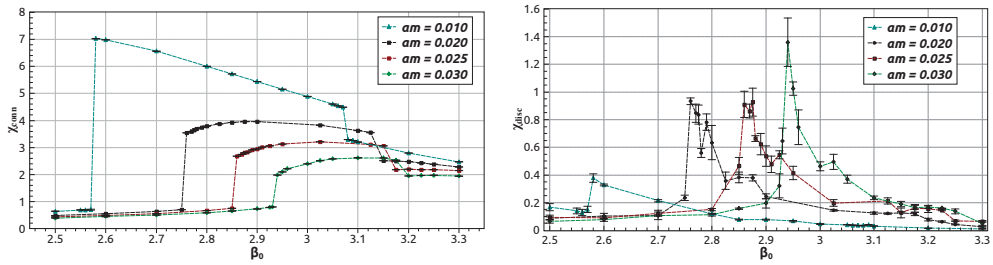

Figure 1.5: Mass dependence of the connected chiral susceptibility (left) and the disconnected chiral susceptibility (right).

are observed in the value of the chiral condensate: a large one at stronger coupling and a smaller one at weaker coupling (see Fig. 1.2). As expected, the transition to the chirally broken phase moves towards stronger couplings when the action is improved. Less expected is the fact that the transition appears to be realised in two steps, leading to one intermediate region. Fig. 1.4(a) shows that the crossover at stronger coupling becomes more pronounced as the bare mass decreases. No dependence on the lattice temporal extent is observed and no perturbative scaling can be realised[118,113]. The mass dependence of the location of the strong coupling rapid crossover in Fig. 1.4(b) is in agreement with a linear scaling expected for a first order transition.

The disconnected component of the chiral susceptibility shows a pronounced peak only in correspondence to the strong coupling rapid crossover, as shown in Fig. 1.5(b). These results indicate that the strong coupling rapid crossover is the one corresponding to chiral symmetry breaking. Consider now the crossover in the chiral condensate at weaker coupling. The hints at a jump become weaker as we approach the chiral limit, see Fig. 1.4(a). On the other hand, the behaviour of the chiral condensate as a function of the mass suggests a discontinuity in its mass derivative, which is best studied by considering the chiral susceptibility.

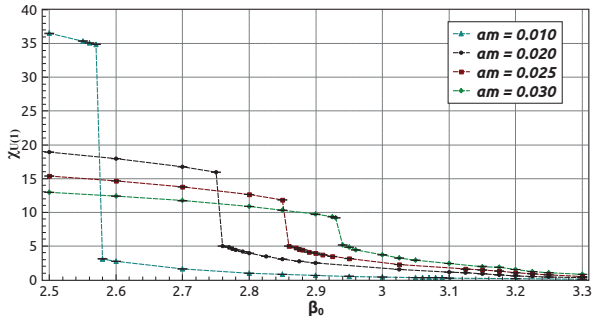

Figure 1.6: Mass dependence of the difference of the pseudoscalar susceptibility $\chi_\pi = \langle\bar{\psi}\psi\rangle/m$ and the connected scalar susceptibility. This order parameter probes $U_A(1)$ (effective) restoration in the continuum theory. Its behaviour would suggest $U_A(1)$ restoration (see caveats in main text) at the chiral transition.

The connected component of the chiral susceptibility exhibits near discontinuities at the condensate crossovers, as shown in Fig. 1.5(a). The magnitude of both discontinuities increases as the bare mass decreases. This suggests that the jump at weaker coupling also corresponds to a genuine phase transition in the chiral limit, as suggested in [118] and confirmed in [113,82]. We conclude that we are observing two distinct phase transitions, one associated with a change of the slope of the chiral condensate at weaker coupling, the other with the chiral condensate itself at stronger coupling.

In the continuum language the observed pattern of the susceptibilities, and of the continuum order parameter shown in Fig. 1.6, suggests $U_A(1)$ (effective) restoration at the strong coupling chiral transition. However, a proper analysis of the axial anomaly is hampered at strong coupling by the absence of a conserved local flavour singlet current. It would be interesting to further analyse the lattice non-local order parameter in the intermediate region in terms of the point-split staggered correlators, analogous to the finite temperature study in [192].

1.3.2 A first look at the spectrum

The next chapter will be devoted to a detailed study of the meson correlators for the $SU(3)$ theory with $N_f = 12$ flavours. Here, we give a first look at some properties of the correlators in the different phases of the system with respect to the coupling. First, let us recall that staggered meson correlators on a lattice with temporal extent T and periodic boundary conditions have the general form

$$C(t) = \sum_i A_i \left(e^{-m_i t} + e^{-m_i (T-t)}\right) + (-1)^t \tilde{A}_i \left(e^{-\tilde{m}_i t} + e^{-\tilde{m}_i (T-t)}\right) . \tag{1.9}$$

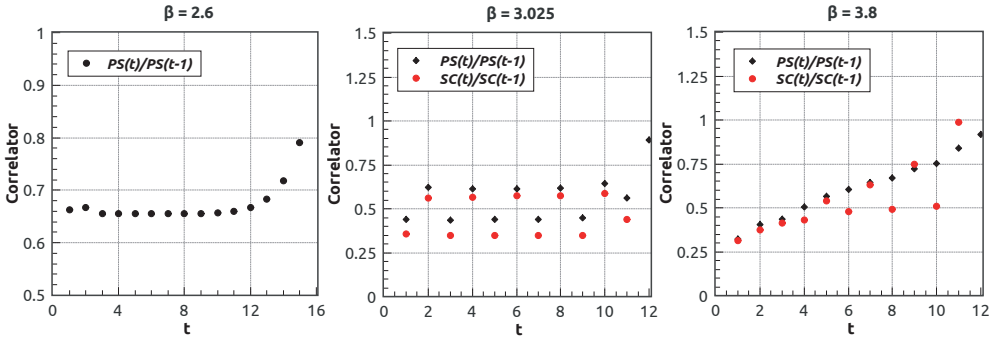

Figure 1.7: Central values of the ratios $C(t)/C(t-1)$ for the pseudoscalar (PS, black circles) and scalar (SC, red squares) two-point correlation functions for coupling values in the three interesting regions. From left to right: the chirally broken phase, the intermediate phase and the weak coupling phase. The coupling in this case corresponds (left to right) to the improved $\beta_0 = 10/g^2 = 2.6, 3.025, 3.8$.

For each state, the parity partner adds a component with alternating sign $(-1)^t$. This is a property of the staggered formulation and it is true for all correlators with the exception of the equal mass Goldstone pseudoscalar correlator. For equal quark and antiquark masses, the parity partner operator for the Goldstone pion is proportional to a charge density operator and thus its vacuum expectation value is zero.

We give an overview of our results in Fig. 1.7. The most salient feature in Fig. 1.7 is an oscillatory component that arises for the pseudoscalar correlator in the intermediate region ($\beta_0 = 10/g^2 = 3.025$). In this region chiral symmetry is exact and the scalar and pseudoscalar correlators should become increasingly degenerate by moving towards the chiral limit.

What we see in Fig. 1.7, moving from weak to strong coupling (right to left), is as follows. In the chirally symmetric region, the pseudoscalar and scalar correlators are close to each other. As expected, the staggered scalar correlator has an oscillating component while the pseudoscalar has not. The non-horizontal shape of the ratios indicates a significant contribution from excited states.

In the intermediate region, a new oscillating component arises in the pseudoscalar correlator, and seems to also arise in the scalar correlator for $\beta_0 = 3.025$. This is consistent with the abrupt change of slope in the mass dependence of the chiral condensate, given that the chiral susceptibility $\langle\bar{\psi}\psi\rangle/m$ equals the volume integral of the pseudoscalar correlator.

At strong coupling ($\beta_0 = 2.6$) chiral symmetry is broken and the pseudoscalar lightest state is the Goldstone boson of the broken symmetry, thus very light and largely non degenerate with the scalar state. We observe that the oscillating component in the pseudoscalar correlator visibly decouples. A

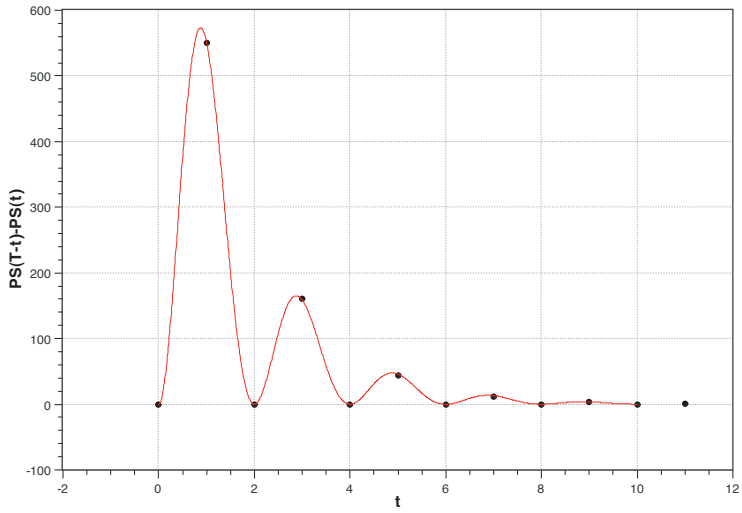

Figure 1.8: The asymmetry of the Goldstone pseudoscalar correlator in the intermediate region ($\beta_0 = 3.025$), with superimposed the result of the fit to eq. (1.11); the fitted parameters are $m \simeq 0.62$ and $C \simeq 1027$.

second observed effect is the presence of an asymmetry under $t \to T - t$ of all studied correlators in the intermediate region, i.e. $\beta_0 = 3.025$. To highlight this asymmetry we have plotted the difference $C(t) - C(T - t)$ for the pseudoscalar correlator in Fig. 1.8. We see that

$$\begin{aligned} C(t) &\neq C(T-t) \qquad \text{for t odd} \\ C(t) &\sim C(T-t) \qquad \text{for t even} \end{aligned} \tag{1.10}$$

In other words there is a violation of staggered-time reversal symmetry. The asymmetry is well fitted, see Fig. 1.8, by the functional form

$$C\left(1-(-1)^t\right)\left(e^{-mt} - e^{-m(T-t)}\right) \tag{1.11}$$

with $C \simeq 1027$ and $m \simeq 0.62$ consistent with the fit of the pseudoscalar correlator on $t \ll T$.
One caveat is in order: it is known that such an asymmetry may typically be present when configurations are not thermalised or statistics is too low. For this reason we have increased thermalisation time and statistics for this point to a few times the ones in the other two regions. The asymmetry persists and does not vary with increasing thermalisation or statistics. Hence, even if the observed asymmetric state is a metastable state, its tunnelling probability to the opposite asymmetry seems to

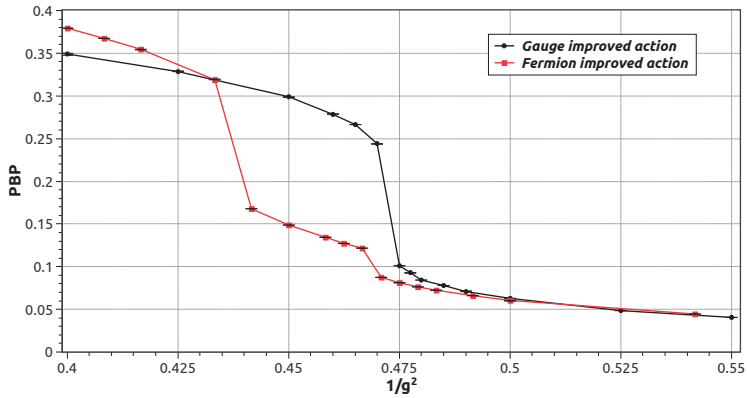

Figure 1.9: Two rapid crossovers are observed for the Naik improved fermion action (red), while one rapid crossover is observed for the Symanzik improved gauge action (black).

be extremely low, suggesting that a seed is indeed stabilising it.

Fermion versus gauge improvement

In order to expose the separate effects of improvement of the fermion action and gauge action, we have performed two additional sets of lattice simulations with one improvement at a time - Action B and C in Table I. In Fig. 1.9 we show the results for the improved fermion action, or the improved gauge action. These results make clear that in the case under study the Naik improvement of the staggered fermion action is mainly responsible for the appearance of an intermediate region in the gauge coupling, and given the underlying symmetries of the system in this phase.

1.3.3 Order of the transition

Another point of interest when studying chiral symmetry breaking bulk transitions in the context of conformality is to determine the order of the transition. If the bulk transition is second order, this would signal the emergence in the continuum of a second non trivial ultraviolet attractor (UVFP), in addition to the non trivial infrared attractor (IRFP), which characterises theories inside the conformal window. If instead the transition is first order, no continuum limit exists. However, a UVFP would emerge at the end-point of a line of first order chiral bulk transitions. A possible scenario for the disappearance of the conformal window could then be realised through the annihilation of a pair of IR and UV fixed points. There are, however, some caveats related to the shape of the beta-function implied by UV-IR annihilation mechanism and the trend of the scalar glueball anomalous

dimension. These will be discussed in detail in Chapter 3.

Figure 1.4 shows a linear mass dependence of the critical inverse coupling obtained using the improved action D. It is also instructive to look at the stability of the Monte Carlo thermalisation curves of the chiral condensate obtained with different initial conditions, as shown in Figure 1.10. The runs

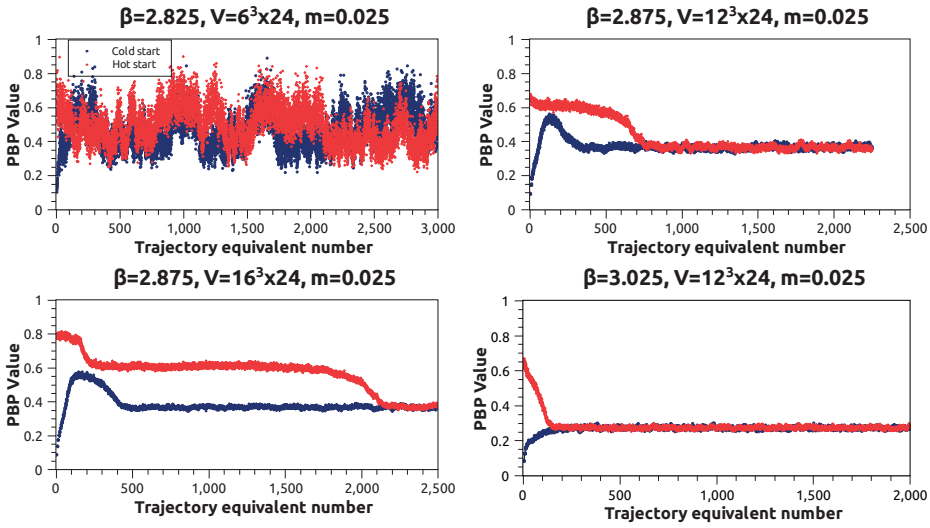

Figure 1.10: Comparison between cold (ordered) and hot (random) starting configurations. As the volume is increased the stability of these metastable states is increased. Away from the transition region (including the intermediate region between the two jumps) no metastability is observed (lower-right)

labeled as *cold* were started from ordered lattice configurations, while the runs labeled as *hot* were started from disordered lattice configurations, in such a way that they should approach thermalisation, respectively, from below and from above. Tunnelling between metastable states is observed around the transition at stronger coupling for small volumes (top-left corner). As the lattice volume is enlarged the occurrence of tunnelling ceases and the stability of metastable states is increased as we approach infinite volume (top-right and lower-left). Around a first order transition the existence of metastable states is expected. As a result, for the different initial conditions, the observable does not thermalise at the same value for a large number of trajectories, giving rise to a hysteresis loop.

We conducted a similar study for the unimproved case and obtained similar results. In Figure 1.11(a) we observe the hysteresis loop obtained from runs with different initial conditions. Again, a linear mass scaling of $\beta_c = 6/g_c^2$ is found. This is shown in Figure 1.11(b). They are consistent with the expected linear scaling and fitting with the functional form $y = Ax+b$, yields $A = 7.8 \pm 0.2$ and

$B = 3.940 \pm 0.005$. This combined evidence points towards a bulk transition of first order, which

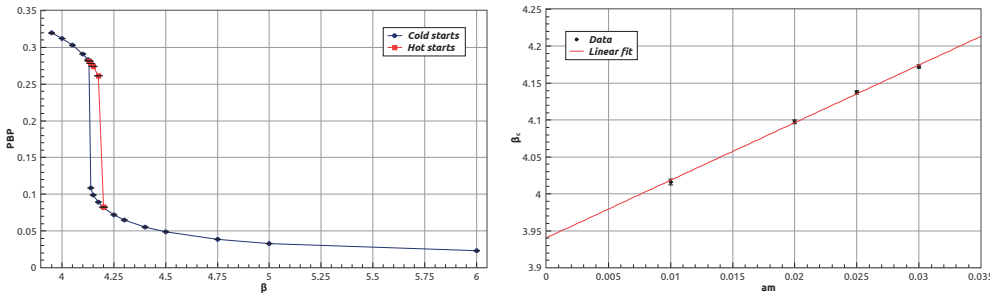

Figure 1.11: (a) Hysteresis loop in the chiral condensate obtained from cold (ordered) and hot (disordered) starting lattice configurations; (b) Linear mass scaling of the critical β at which the bulk transition takes place for different bare masses; (a and b) Both results are consistent with a first order nature of the transition.

is unaffected by improvement. In this scenario, a UV fixed point can only exist at the end-point of a line of first order chiral bulk transitions.

1.4 Discussion

The results presented above suggest that next-to-nearest neighbour terms in the Naik improved fermion action are responsible for the appearance of an intermediate phase.

This is perhaps not unexpected. It is well known that models with competing interactions may give rise to non-homogeneous structures and novel phase transitions. One prototypical example is the axial next-to-nearest neighbour Ising model, known as the ANNNI model [282]. These effects have not been observed at weak coupling, where non-nearest neighbour terms concur to a faster approach to the continuum limit, but might well appear at strong coupling when those terms become relevant, and provided the underlying symmetries allow for it. It is quite possible that quantitative predictions for the appearance and properties of the additional phase could be obtained in the framework of a strong coupling expansion that takes the improvement term into account explicitly – we do not pursue this here.

Here, we provide a plausible argument that accounts for the appearance of such an intermediate phase and its peculiar properties: i) the emergence of an oscillating component of the staggered two-point correlation function in the pseudoscalar channel, and ii) the asymmetry of all two-point correlation functions under $t \to T - t$.

Arisue and Fujiwara have considered the exactly solvable Ising chain (1D) of length L with next-

to-nearest neighbour interactions[35]. This example is extremely instructive. There are two regions of parameters. In one region the eigenvalues of the transfer matrix are real and positive. In the other region, pairs of complex conjugate eigenvalues appear. Intuitively, the first region (region I) is where the nearest neighbour interaction is dominant, while the second region (region II) is where the next-to-nearest neighbour term becomes dominant.

As observed in[35], the two regions will also emerge in a Symanzik improved gauge action where the couplings β_0 and β_1 are fixed as a function of the inverse gauge coupling β. In other words, it is the competition of nearest neighbour and next-to-nearest neighbour interactions at increasingly coarse lattice spacing that causes the system to enter the second region.

The same argument can be repeated for the Naik improved staggered fermion action, with up to third-nearest neighbours. In this case, the emergence of complex eigenvalues of the transfer matrix can be understood by looking at the free lattice fermion propagator for a single flavour, given by

$$S_F(p)^{-1} = \sum_\mu i\gamma_\mu \left(\frac{9}{8} \sin p_\mu - \frac{1}{24} \sin 3p_\mu \right) \tag{1.12}$$

with $-\pi/2 \leq p \leq \pi/2$. The interacting theory at strong coupling can in principle significantly modify the coefficient of each sine contribution. In particular, the change of sign of the second term will induce a pair of imaginary poles (zero tri-momentum) in the massless dressed propagator, i.e. ghosts will appear*. This signals the emergence of region II, likely the intermediate phase we have observed.

It would certainly be interesting to understand more quantitatively the connection between the poles in the quark propagator – as emerging from the non-Hermiticity of the transfer matrix with Symanzik improvement[218] – and the detailed structure of the two-point correlation functions in the intermediate phase. Here, we offer a qualitative explanation as to why a chirally symmetric phase with the observed exotic features can appear in a gauge theory with fermion improvement.

In general, the occurrence of an oscillatory secondary state in the pseudoscalar (Goldstone) correlator with staggered fermions is forbidden by the baryon current conservation. With improvement of the action, the total fermionic current will include additional terms which in turn define a modified form of the baryon number operator at zero chemical potential. For the Naik improved free

*It is known that the dispersion relation for Naik improved staggered fermions always contains complex roots at non-zero tri-momentum. All ghosts generated by the improvement decouple in asymptotically free theories when approaching the continuum limit.

fermion action this construction has been explicitly given by Gavai[142]. In the interacting case, a simple construction that should suffice for our purpose starts with implementing the Kogut-Hasenfratz-Karsch prescription[196,162] $U(x) \to \exp(\mu)U(x)$, $U^\dagger(x) \to \exp(-\mu)U^\dagger(x)$ along the temporal direction. The total baryon number density is then

$$n(\mu) = d/d_\mu log Z(\mu) = n_1(\mu) + n_3(\mu) \tag{1.13}$$

where $n_1(\mu)$ comes from local interactions and $n_3(\mu)$ comes from the third-nearest neighbor term. At vanishing chemical potential the total density $n(\mu = 0)$ must vanish due to baryon number conservation. This can be realised in two ways, either $n_1(\mu = 0) = n_3(\mu = 0) = 0$, or $n_1(\mu = 0) = -n_3(\mu = 0) \neq 0$. When the vanishing baryon number is realised in the second way, a non-zero oscillating component is allowed to appear in the (Goldstone) pseudoscalar channel, as its coefficient is roughly speaking, proportional to n_1. At the same time, n_1 is also a measure of the forward-backward asymmetry. Hence, $n_1 \neq 0$ allows an oscillating term in the pseudoscalar channel and a time asymmetry in all correlators; this is indeed what we observe for the pseudoscalar correlator and the other correlators in the intermediate region.

Putting all the elements together, we would then arrive at this simplified picture: with an improved staggered fermion action the occurrence of imaginary poles of the quark propagator (or equivalently complex eigenvalues of the transfer matrix) opens the possibility of intermediate phases. In the chirally symmetric phase, and for sufficiently weak coupling, the tendency towards degeneracy of the scalar and pseudoscalar propagators is contrasted by the requirement of zero baryon number; the latter forces the amplitude of the oscillating component in the pseudoscalar channel to vanish ($0 = n \simeq n_1$), while the oscillating component in the scalar channel starts appearing. Towards stronger coupling, third-nearest neighbor interactions in the improved fermion action become increasingly relevant. Now, chiral symmetry (i.e. the degeneracy between scalar and pseudoscalar correlators) can still be preserved by allowing $n_3 = -n_1 \neq 0$. In this way the oscillating component appears in the pseudoscalar channel and the temporal asymmetry appears in all channels. This is the intermediate phase. When the coupling grows even larger, chiral symmetry is finally broken, the lightest pseudoscalar is its Goldstone boson, and scalar and pseudoscalar correlators can depart from each other. Our observations in the broken phase (see Fig. 1.7) are consistent with a situation where the conservation of baryon number is again realised in the usual way.

We note that such a characterisation of the intermediate phase is consistent with the breaking of the shift symmetry discussed by Cheng et al.[82]. In fact, the "partial baryon number operators" n_1 and n_3 might well be directly related to the operators measuring the breaking of the shift symmetry. In addition, the presence of ghost poles in the quark propagator of the improved fermion action can be translated into the presence of complex eigenvalues of the improved transfer matrix, and in the case of staggered fermions the (real time) transfer matrix is related to the shift operator as $T = S_4^2$.

1.5 Conclusions

This study shows that the emergence of an exotic intermediate phase in the chirally symmetric SU(3) gauge theory with twelve fundamental (staggered) flavours is due to the improvement of the fermion action, which adds next-to-nearest neighbor interactions that compete with the local terms at strong coupling.

We also have presented evidence of the first order nature of the bulk transition that appear in the strong coupling regime of $N_f = 12$ QCD and of the fact that this nature is not affected by improvement.

These observations might be of interest to model builders, when needing to realise exotic intermediate structures in interacting gauge models with a relatively simple and controlled procedure. It is also amusing to notice that it is possible to mimic features of a dense system and a complex action (time asymmetry) by working with a real action, without the sign problem. These features are of interest, for example, in numerical studies of the graphene.

Of course, from the perspective of the study of the phase diagram for SU(N) gauge theories with many flavours, the observed features remain a peculiar form of lattice artefacts that should be well disentangled from the underlying physics of the system.

Quantum theory provides us with a striking illustration of the fact that we can fully understand a connection though we can only speak of it in images and parables.

Werner Heisenberg

2

On The Particle Spectrum and the Conformal Window

This chapter is devoted to the study of how the particle spectrum of non-Abelian gauge theories changes once they enter the conformal window. Everywhere in the parameter space of such theories, except at the fixed point, the observables will only show remnants of conformality; these remnants and the realisation of exact chiral symmetry determine features of the correlation functions and the spectrum that are quite distinct from those of QCD.

The purpose of this study is twofold: first, to theoretically describe the properties of the spectrum of the continuum theory at a Banks-Zaks IRFP under a small mass perturbation; secondly, to explore the lattice realisation of the theory and identify in this context the universal scaling properties of the IRFP. To this end, we take the $N_f = 12$ system as a prototype of theories inside the conformal

window and study both the fermion mass and volume dependence of the would-be hadron masses in a lattice box, and the fermion mass dependence of the spectrum at infinite volume.

This analysis updates and largely extends this group's first study of this system [117]. Importantly, this is the first study of universal scaling for the complete would-be hadron spectrum — pseudoscalar, scalar, vector, axial mesons and the nucleon. Inspired by [79], it also provides a unified description of all existing lattice spectrum results for this system.

As previously mentioned in this thesis, the existence of an infrared fixed point does not necessarily imply the existence of the conformal window. In this work, we go beyond probing the fixed point and probe the existence of the conformal window and the nature of the symmetry breaking patterns. We also attempt for the first time a study of the fermion mass anomalous dimension of this theory on the lattice. With all due caveats and still sizeable uncertainties, the value we obtain is in good agreement with most of later results.

To summarise, in this chapter we concentrate on the would-be hadron spectrum in the QED-like (or Coulomb-like) phase of the $N_f = 12$ lattice system – which is chirally symmetric but not asymptotically free – as a specific probe of conformal and chiral symmetries. Here we stress the importance of correctly identifying the phase where observables are measured.

2.1 The spectrum: Theoretical premise

Symmetries guide our understanding of physical phenomena, and we should identify the observables sensitive to those symmetries. We are interested in the two-point functions inside the conformal window, and the relevant symmetries are conformal, chiral and, to a certain extent, the $U(1)$ axial symmetry; the latter will be shortly discussed at the end of this chapter. The pattern of phases for a theory inside the conformal window formulated on the lattice is depicted in Figure 2.1.

The picture is as follows: for small values of the bare lattice coupling $g_L < g_L^*$ the theory is in the asymptotically free phase, characterised by a negative β-function. At bare lattice coupling g_L^* the lattice theory then crosses the IRFP and enters a Coulomb, or QED-like. In this phase the β-function is positive. Asymptotic freedom is lost for all $g_L > g_L^*$ and the lattice theory has no continuum limit — the only exception being the possible appearance of a UVFP at stronger coupling.

Chiral symmetry is exact for $g_L < g_L^{**}$ in figure 2.1. At g_L^{**} the lattice theory exhibits a bulk phase transition to a chirally broken phase. There are indications that the line of bulk phase transitions

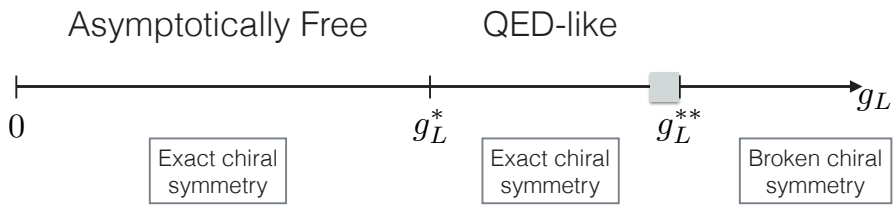

Figure 2.1: Phases of the many-flavour $SU(N)$ gauge theory formulated on the lattice inside the conformal window. As the bare lattice gauge coupling g_L increases from left to right, the lattice theory encounters an asymptotically free phase (negative β-function), it crosses the IRFP at some g_L^* and enters a QED-like phase (positive β-function); chiral symmetry is exact in all these phases. At g_L^{**} a phase transition occurs to a chirally broken phase. It may be preceded by an exotic phase (grey shaded area) due to the improvement of the lattice action [114,83,96].

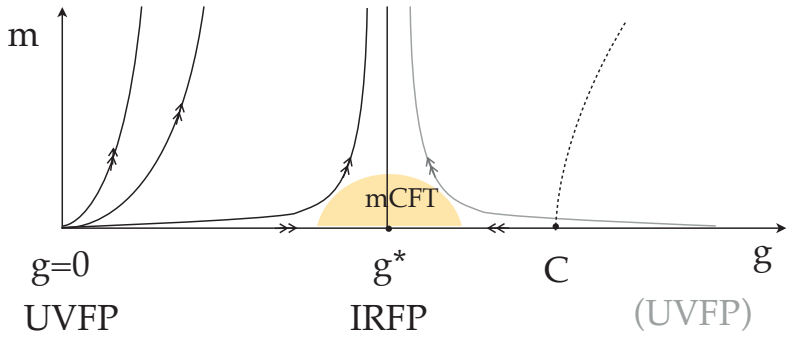

Figure 2.2: Wilson RG flow and fixed points of non-Abelian $SU(N)$ gauge theories in $d = 4$ spacetime inside the conformal window, with fermion mass m and gauge coupling g. For the massless theory ($m = 0$), the trivial UVFP ($g = 0$, asymptotic freedom) becomes unstable towards g perturbations due to quantum corrections and the system flows toward the non-trivial IRFP at g^*, $m = 0$. The fermion mass operator is always relevant and the gauge coupling is irrelevant at the IRFP. Mass deformed conformal field theory (mCFT) for $g \simeq g^*$ and $m \to 0$ provides the universal scaling laws for observables at the IRFP. The dashed line is a line of possible initial values (m, g) for the lattice system, and its critical point C flows into the IRFP. A UVFP at strong coupling may emerge.

ends at a finite $\overline{N}_f \gg N_f^{af}$ [100]. The grey shaded area in figure 2.1 indicates the possible emergence of an exotic phase with exact chiral symmetry due to improvement of the lattice action [114,83,96], which was mentioned in the previous chapter of this work.

In line with recent work [111] and renormalization group (RG) theory *à la* Wilson, figure 2.2 illustrates how the fermion mass term perturbs the RG flow of the continuum massless interacting theory inside the conformal window — we have assumed that no other couplings are present besides the gauge coupling and the mass itself. The mass term is a relevant operator that drives the theory away from the IRFP, while the gauge coupling is irrelevant due to quantum corrections. As discussed in [111], mass deformed conformal field theory (mCFT) can be used within the basin of attraction of the IRFP to uncover the universal scaling properties of the correlation functions at infinite and finite

volume. Away from the IRFP violations of universal scaling will gradually appear, while correlation functions still satisfy all constraints implied by the non spontaneously broken chiral symmetry. A UVFP at strong coupling may emerge, however no indications of it have been found in preliminary lattice studies of the $N_f = 12$ theory[120]. We also note that, at strong coupling, new operators may be promoted from irrelevant to marginal or relevant; if so, the fixed point structure of the theory needs to be reanalyzed in an enlarged space of couplings, possibly complicating the lattice search for new UV/IR fixed points.

2.1.1 Two-point functions

We are interested in the two-point functions made of currents of the type $J_M \sim \bar{q}\Gamma_M q$, with $\Gamma_M = 1, \gamma_5, \gamma_\mu, \gamma_\mu\gamma_5$ for the scalar (S), pseudoscalar (PS), vector (V) and pseudovector (PV) mesons, respectively, and the nucleon correlation function with current $J_N \sim qqq$. In other words, we identify the would-be hadrons of QCD in order to allow for a direct comparison with the spectrum of theories inside the conformal window.

At the IRFP the theory is massless and interacting, and its two-point functions satisfy universal scaling relations with nonzero anomalous dimensions

$$\langle 0|T J_H(x_1) J_H^\dagger(x_2)|0\rangle \sim (x_1 - x_2)^{-\Delta_H} \qquad H = M,\ N \tag{2.1}$$

with $\Delta_H/2$ the scaling dimension of the current J_H. More specifically, we are interested in the Euclidean two-point functions with zero total 3-momentum

$$\begin{aligned} C_H(t) &= \int d^3x \, \langle 0|T J_H(t,\vec{x}) J_H^\dagger(0,0)|0\rangle \sim t^{-\Delta_H+3} \\ &= \int_0^\infty dE \, K(E,t)\, \sigma(E)\,. \end{aligned} \tag{2.2}$$

This is the well-known power-law scaling of the correlations $C_H(t)$ at the IRFP. We have also introduced the representation of $C_H(t)$ in terms of the spectral function $\sigma(E)$ and the kernel $K(E,t)$. Spectral functions are a powerful probe, widely used in the study of the QCD phase diagram at finite temperature and chemical potential; for example, they are a direct probe of the gradual melting of bound states in the quark-gluon plasma close to the critical temperature.

In the presence of a nonzero fermion mass mCFT provides rigorous results inside the IRFP basin

of attraction; these are derived in the next section. Away from the IRFP, known cases, such as QCD at zero temperature or QGP close to its critical temperature, provide a phenomenological insight. QCD is confining in the infrared, and free in the ultraviolet. Its complete spectral function $\sigma(E)$ entails the low-energy resonances and the high-energy continuum. Schematically, it is made of a series of Dirac δ-functions (the propagator poles) and a continuum with a high-energy threshold $\sigma(E) \sim E^{\Delta_H - 4}\left(A_H \delta(E^2 - m_H^2) + C\theta(E - E_0)\right)$, where for simplicity we assumed one resonance (pole) per channel H. If we take in eq. (2.2) the kernel $K(E,t) = \exp(-Et)$, i.e. the Fourier transform of a free boson propagator for infinite temporal extent, the two-point function $C_H(t)$ can be exactly computed in terms of upper incomplete Γ functions

$$C_H(t) = C_H^{pole} + C_H^{cont} \sim \sum_H m_H^{\Delta_H - 3} e^{-m_H t} + \frac{C}{t^{\Delta_H - 3}} \Gamma(\Delta_H - 3, E_0 t) \ . \tag{2.3}$$

At large times $t \to \infty$, using $\Gamma(s,x)/(x^{s-1}\exp(-x)) \to 1$ as $x \to \infty$, one obtains for the high-energy continuum contribution

$$C_H^{cont}(t) \sim \frac{E_0^{\Delta_H - 4}}{t} e^{-E_0 t}, \qquad t \to \infty \, . \tag{2.4}$$

The high-energy continuum generates an exponentially decaying contribution with time dependent coefficients, and leading $1/t$ behaviour at large times, differently from the low-energy poles.

QGP close to its critical temperature is instead an example of a deconfined, though strongly interacting, theory with restored chiral symmetry; it is almost analogous to a theory inside the conformal window, except that there is no IRFP. A realistic description of the QGP two-point functions is a rich subject of study that is beyond our analogy. It is here enough to observe that the system undergoes a gradual melting of the QCD bound states till their disappearance into a continuum. How gradual is the analogous transition inside the conformal window depends on various factors: the nature of the zero temperature phase transition that opens the conformal window at N_f^c, the strength of the interactions at the IRFP, the quantum numbers of the would-be hadrons.

Universal scaling laws at infinite volume

In order to understand the behaviour of the two-point functions $C_H(t)$ and the would-be hadron masses in the surroundings of the IRFP we summarize, partly reformulate and adapt to our case

known aspects of the scaling theory at a conformal fixed point. The scales of the system are the lattice spacing a (that can be thought as the inverse of an ultraviolet momentum cutoff), the characteristic length ξ that will emerge in the scaling analysis, and the spatial length L of the lattice box; we shall consider specific ranges for a, ξ and L. The couplings are the fermion mass m and the gauge coupling g. They have scaling dimensions

$$[m] = 1 + \gamma, \qquad [g] = -\gamma_g \,, \tag{2.5}$$

where the scaling dimension is the sum of the canonical dimension and the anomalous dimension, γ and $-\gamma_g$, respectively. At the IRFP, $g = g^*$ and $m = 0$, the anomalous dimensions have values γ^* and $-\gamma_g^*$, and we introduce the exponent $\delta = (1 + \gamma^*)^{-1}$ for later use. For the interacting theory, the coupling m is always relevant in the RG sense ($0 < \gamma < 2$), while g has $-\gamma_g < 0$ due to perturbative quantum corrections and it is thus irrelevant. We first consider the lattice system in the infinite volume limit $L \to \infty$ and in the continuum limit $a \to 0$[*]. The invariance of the system under a rescaling of coordinates in the presence of a small perturbation of the relevant coupling m at the IRFP provides the universal scaling relations for $C_H(t)$; they are universal in the sense that they do not depend on the microscopic details of the system. Under a rescaling of coordinates $x' = x/b$ — where x indicates both space and time — the form of the correlation is dictated by its scaling dimension s_H

$$C_H(t/b; b^{1/\delta} m) = b^{s_H} C_H(t; m) \,, \tag{2.6}$$

where $s_H = \Delta_H - 3$. Setting $m = 0$, eq. (2.6) yields $C_H(t/b) = b^{s_H} C_H(t)$, hence $C_H(t) \sim t^{-s_H}$, the scaling form already introduced in eq. (2.2). Setting $b = \exp(l)$ gives a better intuition of the approach to large distances. Since eq. (2.6) holds for any l, we can choose $l = l^*$ so that $m \exp(l^*/\delta) = 1$. We can also define a characteristic length $\xi = \exp(l^*)$, so that we obtain

$$C_H(t) = Z_H \, \xi^{-s_H} \, F\left(\frac{t}{\xi}\right) \,. \tag{2.7}$$

The coefficient Z_H accounts for the microscopic details of the system and has zero scaling dimension. The second factor carries the scaling dimension s_H of C_H, while the third factor is the adimensional

[*] The latter limit is realized, in practice, whenever the characteristic length ξ, defined later in eq. (2.7), is much larger than a.

universal scaling function that only depends on the ratio t/ξ, with zero scaling dimension. In the most general case, the scaling function F will depend upon all possible products with zero scaling dimension, made of a scale and a coordinate or a relevant coupling. The function F is universal in the sense that does not depend on the microscopic details of the system. It depends on the scaling dimension of the operators $H = M, N$, their spin and normalisation. For any nonzero m, one can think of ξ as a finite characteristic length $\xi = m^{-\delta}$; eq. (2.7) says that for a change of m, the coordinate t changes at the scale ξ. In the limit $\xi \to \infty$, or equivalently $t \ll \xi$, the system approaches the IRFP and eq. (2.7) should reproduce the form $C_H(t) \sim t^{-s_H}$; this constrains the asymptotic behaviour of the scaling function $F(t/\xi)$. In the opposite limit $t \gg \xi$, the two-point functions decay exponentially, so that

$$\begin{aligned} C_H(t) &\sim t^{-s_H}, & t \ll \xi \\ C_H(t) &\sim \xi^{-s_H} f\left(\frac{t}{\xi}\right) e^{-t/\xi}, & t \gg \xi\,. \end{aligned} \tag{2.8}$$

While the time dependence is dictated by the scaling dimension of C_H, the numerator in the limit $t \ll \xi$ depends on the spin and normalisation of the operators $H = M, N$. In the opposite limit $t \gg \xi$, dimensional reasoning allows for all terms in $f(t/\xi)$ that reproduce the correct scaling at the fixed point, $\xi \to \infty$ or equivalently $t \ll \xi$. Specifically, it allows for all powers $t^{-\alpha}$, with $0 \leq \alpha \leq s_H$ and including $\alpha = 0$. While the limit $t \ll \xi$ is uniquely determined by the conformal fixed point, the details of the limiting behaviour for $t \gg \xi$ depend on the nature of the interactions in the quantum system. Our case is that of composite operators in a deconfined and interacting non-Abelian gauge theory close to a non trivial IRFP; we do not know a priori if the system is weakly or strongly coupled. Without a detailed knowledge of the quantum correlators, we can still infer their most general form close to the fixed point. The presence of a mass threshold, i.e. ξ finite, produces a pole and branch-cuts (i.e., a continuum of critical excitations) in the propagators of the quantum composite operators[†]. Using for the sake of illustration the schematic form in eq. (2.3) for the continuum part, with threshold $E_0 = n/\xi$, for some n, one obtains

$$C_H(t) \sim \xi^{-s_H} e^{-t/\xi} + \frac{C}{t^{s_H}} \Gamma\left(s_H, \frac{nt}{\xi}\right)\,, \tag{2.9}$$

[†]Analogous examples can be found in magnetic systems close to a quantum critical point, where a quasi-particle pole and multiparticle continuum thresholds are present in the system.

for any intermediate time and finite ξ. The first term is generated by the would-be hadron pole with residue ξ^{-s_H}. The second term is a continuum of excitations with energy threshold proportional to ξ^{-1}. The relative position of the pole and thresholds depends on the specific theory and interactions. It is always true, however, that all thresholds and the pole merge at the fixed point, where the residue at the pole vanishes.

Note that the would-be hadron pole, the first term in eq. (2.9), is proper of the deconfined theory close to the IRFP and is not to be identified with the hadron poles of confined QCD. In fact, it vanishes at the fixed point and the theory smoothly flows to pure Yang Mills at infinite fermion mass, i.e. $\xi \to 0$. This description of theories inside the conformal window does not need, but does not exclude, the occurrence of a phase transition at a finite fermion mass between a deconfined and a confined phase, a scenario proposed in [175]; note that confinement is always realized in the limit $m \to \infty$, where fermions decouple.

From the practical viewpoint of a lattice study of the system, it is sufficient to observe that the two-point functions $C_H(t)$ in the presence of a fermion mass $m = \xi^{-1/\delta}$ are dominated by a constant times an exponential, i.e. $\xi^{-s_H} \exp(-t/\xi)$, for $t \gg \xi$ and $\xi \neq 0$, while the time-dependent power-law contributions to $f(t/\xi)$ in eq. (2.8) become increasingly important at smaller times and for decreasing masses. We also observe that the addition of a UV cutoff, i.e. a nonzero lattice spacing a, or a finite temporal extent $t \leq T$, do not qualitatively change any of the properties discussed, nor affect the extraction of the would-be hadron mass from the dominant pole contribution.

The comparison of eq. (2.7) with the large euclidean time behaviour $C_H(t) \sim \exp(-m_H t)$ for a would-be hadron of mass m_H provides the universal scaling form

$$m_H = c_H \, m^{\delta} \,, \tag{2.10}$$

at coupling $g = g^*$ and with coefficient c_H that depends on the spin of the operator $H = M, N$.

Universal scaling laws at finite volume

Keeping $g = g^*$, we now consider the system at finite volume L, with ξ, $L \gg a$, and we trade the characteristic scale ξ for the mass m, using $\xi^{-1} = m^{\delta}$; in this way, the system has effectively one relevant scale L, and we can study the scaling of C_H under a change of L. In full analogy with eq. (2.7),

the correlation is now[‡]

$$C_H(t;m,L) = \tilde{Z}_H\, L^{-s_H}\, F\left(\frac{t}{L}, Lm^{\delta}\right) . \tag{2.11}$$

It is the product of a coefficient $\tilde{Z}_H$, which accounts for the microscopic details, a scaling factor and the universal scaling function F with zero scaling dimension arguments, made of products of the scale L and a coordinate or a coupling. The leading scaling form of the would-be hadron mass in the channel H as a function of the fermion mass and L now reads

$$m_H = \tilde{c}_H \frac{1}{L} f(x), \qquad x = Lm^{\delta}\,, \tag{2.12}$$

where the scaling function $f(x)$ depends on the parameter x with zero scaling dimension. To recover the infinite volume limit of eq. (2.10), one needs $f(x) \sim x$ as $x \to \infty$ and $\tilde{c}_H = c_H$. One has also $f(x) \to const$ as $x \to 0$. The function $f(x)$ a priori depends on the channel $H = M, N$ through the spin of the corresponding operators. However, once the constant c_H is factored out, its $x \to \infty$ limit is H independent. Moreover, the study of section 2.3.3 and figure 2.11 suggests that most of the H dependence is contained in c_H for all x. Eqs. (2.10) and (2.12), important for the scaling analysis of the lattice results, were first derived in [111]. Eq. (2.12) says that finding the universal curve followed by Lm_H/c_H as a function of x, with $1/\delta = 1+\gamma^*$, is a way to determine the mass anomalous dimension γ^* at the IRFP.

New operators and corrections to universal scaling

The emergence of new marginal or relevant operators can occur in the system at sufficiently strong coupling, e.g., the four fermion operator can turn from irrelevant to marginal, or relevant. In this case the fixed point structure has to be reconsidered, together with the RG flow towards the fixed point(s) in the enlarged parameter space. This is hardly the case for the IRFP studied here, but it may play a role in the possible emergence of a new ultraviolet fixed point at stronger coupling.

On the lattice, one can isolate the universal scaling in eq. (2.12) by identifying the perturbative corrections in the volume L and mass m that produce a deviation from the scaling function $f(x)$ and possible nonperturbative scaling violations. We discuss a few aspects below.

- perturbative corrections in L and m: close to the fixed point the irrelevant couplings, i.e.

[‡]The large volume limit of the field theory at the IRFP can be treated analogously to the low-temperature perturbation of a lattice spin system at a zero temperature critical point.

$g \neq g^*$ in our case, generate perturbative corrections made of products of couplings and scales with zero scaling dimension.

- nonperturbative corrections: they should be expected when the scale(s) of the microscopic dynamics becomes comparable to or larger than the characteristic length of the system. Violations of universal scaling in this context can appear with nonuniversal functions that cannot be factored out of $f(x)$. One example is when the box size L becomes small compared to the Compton wavelength of the would-be hadron ξ. Other examples are provided in this context by the occurrence of the bulk phase transition at strong coupling, which changes the underlying symmetries of the system, or the possible appearance of new phases that precede the bulk transition and are induced, e.g., by competing interactions in Symanzik-improved lattice fermion actions on coarse lattices [114].

The first type of corrections, perturbative in L and m, deserves some discussion. They are induced by the irrelevant coupling g, whenever we take $g \neq g^*$. Consider a small variation Δg; the smaller the scaling dimension γ_g^* of g, the slower the system will flow back to the IRFP. The leading perturbative corrections to eqs. (2.7) and (2.11) can be of two types. Firstly, Z_H ($\tilde{Z}_H$) and m (the relevant coupling) should be redefined, in a way that may generically be difficult to compute[§]. Secondly, multiplicative corrections to the scaling function F appear. They can be written in terms of products with zero scaling dimension, made of the coupling Δg and the relevant scale, thus $1 + \Delta g \xi^{-\gamma_g^*}$, or equivalently $1 + \Delta g m^{\delta \gamma_g^*}$, in eqs. (2.7) and (2.11), and $1 + \Delta g L^{-\gamma_g^*}$ in eq. (2.11). The first corrections become increasingly unimportant as $\xi \to \infty$ ($m \to 0$), the second ones as $L \to \infty$. The same perturbative corrections for $g \neq g^*$ will enter m_H as redefinitions of c_H, the fermion mass m itself (equivalently the scaling dimension δ), and multiplicative corrections of the type $1 + \Delta g \xi^{-\gamma_g^*}$ and $1 + \Delta g L^{-\gamma_g^*}$.

- The coefficient Δg, referred to as the fitting parameter b in section 2.3, measures the deviation of the gauge coupling from its value at the fixed point, or, on the lattice, the deviation from g^* along the line of lattice parameters that flows to the IRFP in the continuum limit. It is a nonuniversal parameter that vanishes at the IRFP, possibly changing its sign. In particular, when symmetries allow for a linear dependence on $g - g^*$, we can expect Δg (or the parameter b) to change sign at the boundary between the two phases of the lattice system, indicating if

[§]However, a perturbative treatment of the RG equations in the case of an IRFP at weak coupling may provide the leading contributions to these corrections.

the latter is located on the strong coupling side of the IRFP, i.e. the QED-like phase on the lattice, or the weak coupling side of the fixed point, i.e. the asymptotically free phase on the lattice. We also expect Δg to flow to zero in the continuum, i.e. $\beta_L \to \infty$, where the lattice system reaches the IRFP.

- The exponent $\delta\gamma_g^*$, entering the perturbative corrections to scaling, is universal and it is given by the anomalous dimension of the fermion mass γ^* and the anomalous dimension of the gauge coupling at the fixed point $-\gamma_g^*$; this tells that the universal scaling function as well as its perturbative corrections contain information on γ^*.

We will encounter realizations of the perturbative corrections in m and nonperturbative corrections in L in section 2.3. As a final note, the mixing of the couplings m and g under the RG flow cannot generate in this system a new fixed point *à la* Wilson-Fischer at $m^* \neq 0$ due to the chirality protection of the fermion mass term, i.e., $dm/d\mu \propto m$ with renormalization scale μ. We study eq. (2.12) on the lattice in section 2.3.3 and eq. (2.10) in section 2.3.5.

2.1.2 The fermion mass anomalous dimension at the IRFP

One aim of this study is to measure γ^* nonperturbatively on the lattice, by identifying universal scaling and the pattern of scaling violations in the would-be hadron spectrum. Numerous lattice studies have recently reported over a wide variety of evidences that the $N_f = 12$ theory is inside the conformal window, supporting the first results in [23], based on the flattening of the running gauge coupling, and [117] that probed the very existence of the conformal window. While the phenomenological interest mainly resides in theories just below the conformal window, it remains important to determine the pattern and sizes of observables inside the window, since they are directly, and in some cases smoothly, related to their value below the window lower endpoint; one such quantity is the fermion mass anomalous dimension γ^* along the IRFP line. Its value determines if the theory is strongly or weakly interacting at the IRFP. It is null in the free theory, at $N_f = N_f^{af}$, and it is bounded to be $\gamma^* < 2$ by the unitarity of the conformal theory [222,128]. An appealing conjecture suggests $\gamma^* = 1$ at the lower endpoint of the conformal window, $N_f = N_f^c$, so that chiral symmetry breaking is triggered [31] — for $\gamma^* = 1$ the four-fermion operator becomes relevant. The theoretical question if $\gamma^* = 1$ holds exactly at N_f^c is still open; it is however appealing to think that the exactness is realized [88], and some consequences of this scenario are discussed in section 2.3.5.

The value of γ^* can be determined nonperturbatively on the lattice[¶] and it has been computed in perturbation theory at two-loops [75], three and four loops [304,305], see also [151,174] for studies in the large-N_f limit, [290,275] for analyses of renormalization scheme transformations and [261] for a recent fixed point analysis of classes of gauge theories. It is thus mandatory to compare the genuinely nonperturbative lattice determination with perturbation theory, and in this spirit we analyze the lattice results in section 2.3. Here, we discuss a few relevant aspects that can be inferred from [304,305] and we compute the gauge coupling anomalous dimension $-\gamma_g^*$ to four loops. By inspection of the four-loop β-function and the mass anomalous dimension γ in [304,305] one observes that:

- The $N_f = 12$ IRFP coupling in the $\overline{\text{MS}}$ scheme moves from $g^2/(4\pi^2) \simeq 0.24$ at two loops to $g^2/(4\pi^2) \simeq 0.15$ at four loops, and the mass anomalous dimension at the IRFP — a renormalization scheme independent quantity — moves from $\gamma^* \simeq 0.77$ to $\gamma^* \simeq 0.25$. The latter value provides $\delta \simeq 0.8$; this value will turn out to be in good agreement with our lattice determination.

- The IRFP coupling moves towards the origin when going from two to four loops, while the lower endpoint of the conformal window stays around $N_f = 8$.

- The N_f dependence of the coefficients β_i and γ_i, $i = 0, 1, 2, 3$, of the four-loop β-function and γ, respectively, deserves some discussion. The four-loop coefficient β_3 grows rapidly with N_f and it is responsible for the appearance of a new zero for $N_f \geq 17$, just above the conformal window. Analogously, the four-loop coefficient γ_3 grows rapidly with N_f and causes a change of sign of the running anomalous dimension at some g for $N_f \geq 8$; importantly, this happens at a coupling $g \gg g^*$ for $N_f = 12$, suggesting that perturbation theory may still be reliable for $N_f = 12$ at $g = g^*$. This is no longer true for $N_f \sim 8$, where g^* is larger and the change of sign occurs for $g < g^*$. We do not further address the problem of the reliability of perturbation theory for $N_f \sim 8$, with or without a truncation to a given order in the loop expansion. We only note that this is the region where nonperturbative contributions can play a significant role in the disappearance of the conformal window. An instructive comparison between perturbation theory and nonperturbative results can be carried out in the Veneziano limit, see [290] for studies in this limit, or with a large-N_f resummation as initially

[¶] It is worth noting that other field-theoretical techniques, such as conformal bootstrap and variations thereof, are becoming increasingly useful in constraining correlators and anomalous dimensions of operators in strongly coupled field theories.

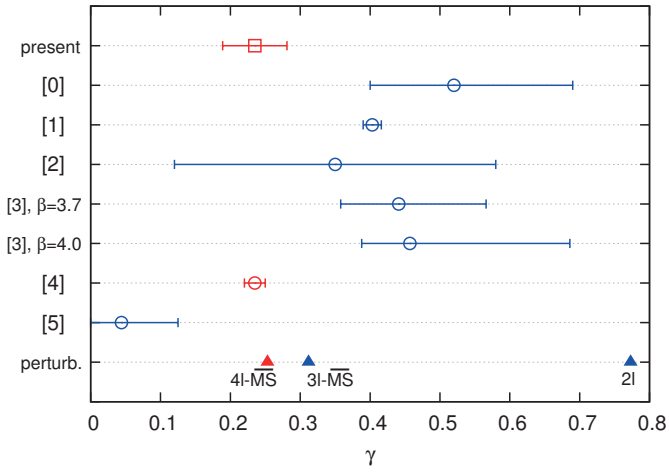

Figure 2.3: Collection of recent lattice determinations of the mass anomalous dimension γ for the $N_f = 12$ system, and the perturbative prediction of its value at the IRFP to 2, 3 and 4 loops. From top to bottom, the value from this work, [0] from [117], [1] from [19], [2] from [101], [3] from [13], [4] from [79], [5] from [176], and the perturbative determinations from [304,305].

proposed in [151]. Recent progress in constraining by field-theoretical techniques the correlators of large-N QCD and $\mathcal{N} = 1$ SQCD [62,60] should help in the task of identifying the role of nonperturbative contributions.

- Finally, we derived the value of the gauge coupling anomalous dimension at the IRFP to two and four loops from [304] as $-\gamma_g^* = \partial\beta(g)/\partial g|_{g=g^*}$. As all other critical exponents, this is a renormalization group invariant quantity. A straightforward calculation gives $\gamma_g^*|_{2-loop} \simeq 0.360$ and $\gamma_g^*|_{4-loop} \simeq 0.283$, consistently with the fact that the IRFP moves towards weaker coupling from two to four loops.

To summarize, four-loop perturbation theory predicts $\gamma^* \simeq 0.25$, i.e. $\delta \simeq 0.8$, and the universal exponent $\delta\gamma^* \simeq 0.23$ for the $N_f = 12$ system at the IRFP. This prediction misses the nonperturbative contribution, and some renormalization scheme dependence can be induced by the truncation of the perturbative expansion. A comparison with the nonperturbative lattice determination of γ^* is therefore instructive. Figure 2.3 collects recent lattice determinations of γ^* and the predictions of perturbation theory, anticipating the result of this chapter later discussed in section 2.3. The most salient feature of figure 2.3 is the agreement among lattice determinations, and their agreement with the four-loop perturbative prediction, once a universal scaling analysis is carried out. This is true for [79] and this work. Previous pioneering determinations of the mass anomalous dimension, the

very first one in [117] and the ones in [19,101,13,80,176] were obtained through the analysis of specific H channels in the would-be hadron spectrum or the eigenvalues of the Dirac operator at some bare lattice coupling, without a systematic identification of the universal scaling contributions and violations thereof. Despite this, all determinations are contained in an interval that is well below $\gamma = 1$. This shows the stability of the prediction and the fact that the (lattice) system is not largely sensitive to deviations from the IRFP. Importantly, measurements can be done on both sides of the fixed point, being it the asymptotically free side or the QED-like side. In section 2.3.5 we futher discuss our determination of γ^* and the implications of the obtained value.

2.1.3 The Edinburgh plot

Besides conformal symmetry, one relevant ingredient characterizing the two-point functions in the conformal window is restored chiral symmetry. Everywhere in the asymptotically free and the QED-like phase, chiral Ward identities must be fulfilled by the renormalized correlation functions. There is no Goldstone boson, since chiral symmetry is not spontaneously broken, and all chiral partners, scalar and pseudoscalar, vector and axial, must be degenerate in the chiral limit[‖].

The Edinburgh plot, widely used in lattice QCD studies and suggested as a probe of the conformal window in [119], is constructed in terms of adimensional ratios of masses, and/or decay constants, and it traditionally offers a powerful way to combine results of lattice calculations performed at different lattice spacings and with different lattice actions. In this case, it also provides a clear visualisation of different mass regimes and distinguishes between QCD and theories inside the conformal window; we use it here to illustrate the behaviour of the $N_f = 12$ system, adopted as a prototype of theories inside the conformal window. Figure 2.4 shows the Edinburgh plot for the $N_f = 12$ infinite volume lattice results in table 2.1 for $am > 0.025$ and in table 2.5 for $am \leq 0.025$. The physical point of QCD (left of figure) corresponds to $m_\pi/m_\rho \simeq 0.18$ and $m_N/m_\rho \simeq 1.21$. At the other side of the figure a useful theoretical limit is the heavy quark mass limit, where all masses of the would-be hadrons are given by the sum of their valence quark masses so that $m_\pi/m_\rho = 1$ and $m_N/m_\rho = 3/2$. A QCD scenario would correspond to a curve in figure 2.4 that extrapolates to the QCD physical point for decreasing quark masses, i.e., it would join the two red points in figure 2.4. Instead, we

[‖]Exact chiral symmetry implies the degeneracy of the complete renormalized two-point functions in the channels that are chiral partners, and the degeneracy of the corresponding renormalized chiral susceptibilities — the integrals of the two-point functions.

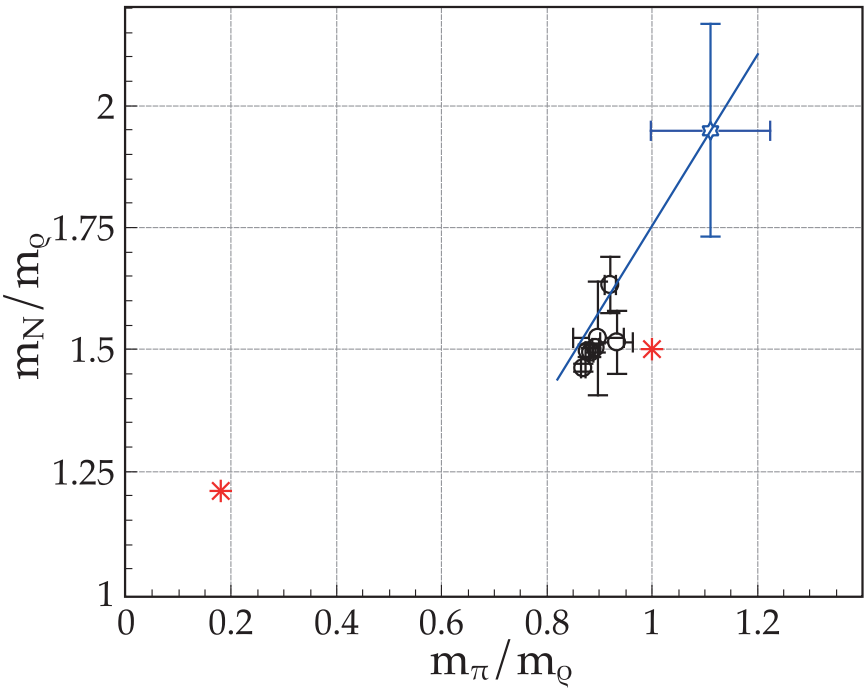

Figure 2.4: The $N_f = 12$ Edinburgh plot for the infinite volume lattice results in table 2.1 and 2.5 at $\beta_L = 3.9$: the ratio of the nucleon (N) and the vector (ρ) mass is shown as a function of the ratio of the pseudoscalar (π) and the vector mass. We show the scaling point (blue diamond) with coordinates $(x, y) = (c_\pi/c_\rho, c_N/c_\rho)$, with $c_{\pi,N}$ from Fit I in table 2.6 and c_ρ in table 2.8 (This work). The superimposed (blue solid) line $y = (c_N/c_\pi)x$ (error band not shown) entails the perturbative scaling violations derived in section 2.3. The coefficients c_H, $H = \pi, \rho, N$ are a priori β_L dependent, so that the solid (blue) line as well as the scaling point flow to their continuum value, as $\beta_L \to \infty$, cf. section 2.3.3. The QCD physical point (red star, leftmost) and the heavy quark limit (red star, rightmost) are also displayed.

observe that the two mass ratios are "stuck" at a tiny corner of the plot, away from the heavy-quark limit and the QCD physical point for a wide range of bare fermion masses $0.01 \leq am \leq 0.07$. This is to be expected inside the conformal window; would-be hadron masses scale as $m_H = c_H\, m^{\delta}$ at the IRFP, ideally producing one point in the Edinburgh plot. Moving away from the IRFP — in mass, coupling(s) and volume — produces some scattering of the data. A mild mass dependence of the infinite volume mass ratios is induced by perturbative scaling violations for $g \neq g^*$ and $m \neq 0$. Anticipating the results of section 2.3, these are represented by points distributed along the solid line that passes through the scaling point in figure 2.4. All scaling violations still obey the constraints implied by the underlying restored chiral symmetry.

2.2 Numerical setup

2.2.1 The action

We have generated configurations of an $SU(3)$ gauge theory with twelve degenerate flavours N_f of staggered fermions in the fundamental representation using a tree level Symanzik improved gauge action

$$S = -\frac{N_f}{4}\mathrm{Tr}\ln M(am, U) + \sum_{i=0,1}\beta_i(g^2)\sum_{\mathcal{C}\in\mathcal{S}_i}\mathrm{Re}(1 - U(\mathcal{C})) \tag{2.13}$$

where $U(\mathcal{C})$ are the traces of the ordered product of link variables along the closed paths $\mathcal{C}$ divided by the number of colours and $M(am, U)$ is the fermion matrix for the naive staggered fermion action for a single flavour with mass m. $\mathcal{S}_0$ and $\mathcal{S}_1$ contain all the 1×1 plaquettes and 1×2 and 2×1 rectangles, respectively. The $SU(3)$ lattice coupling of the unimproved action is given by $\beta = 6/g_L^2$ and the β_i are defined in terms of β as $\beta_0 = (5/3)\beta$ and $\beta_1 = -(1/12)\beta$. According to the way lattice simulations are performed and reported, we use $\beta_L (= \beta_0) = 10/g_L^2$ for the lattice results of this work, and $\beta = 6/g_L^2$ for some of the existing lattice results discussed in section 2.3.

Improvement is extended to the fermionic sector following the Naik prescription. The action of the fermionic sector can be written in terms of the one component staggered fermion field $\chi(x)$ as

$$
\begin{aligned}
S_F \quad &= a^4 \sum_{x;\mu} \eta_\mu(x)\bar{\chi}(x)\frac{1}{2a}\left\{c_1\left[U_\mu(x)\chi(x+\mu) - U^\dagger(x-\mu)\chi(x-\mu)\right]\right. \\
&+c_2\left[U_\mu(x)U_\mu(x+\mu)U_\mu(x+2\mu)\chi(x+3\mu)\right. \\
&\left.\left.-U^\dagger_\mu(x-\mu)U^\dagger_\mu(x-2\mu)U^\dagger_\mu(x-3\mu)\chi(x-3\mu)\right]\right\} \\
&+a^4 m \sum_x \bar{\chi}(x)\chi(x) \qquad (2.14)
\end{aligned}
$$

with the phase factor $\eta_\mu(x) = (-1)^{(x_0+x_1\ldots+x_{\mu-1})}$. Order a^2 accuracy at tree level is achieved by using the Naik choice $c_1 = 9/8$ and $c_2 = -1/24$.

This action is the same used in previous studies conducted by our group on $SU(3)$ with $N_f = 12$[117,114,96]. In particular, this action corresponds to the choice D of[114]. The theory under study exhibits a bulk transition separating a region at weak coupling where chiral symmetry is restored from a region at strong coupling where chiral symmetry is broken[117], as it is expected for all theories in the conformal window. For small enough bare fermion masses and with our choice of action, the competition induced by next-to-nearest neighbour interactions in eq. (2.14) causes the emergence of an intermediate phase at finite lattice spacing, just before chiral symmetry is broken, as one goes from weak to strong coupling[114], see also Fig. 2.1.

We generated configurations for a range of bare fermion masses going from $am = 0.01$ to $am = 0.07$ at fixed coupling $\beta_L = 10/g_L^2 = 3.9$. This choice guarantees that our simulations are carried in the chirally restored region, away from the bulk transition and the exotic phase induced by the improvement. For the heaviest bare masses $am = 0.06$ and $am = 0.07$ we simulated volumes $16^3 \times 24$ and 24^4. For bare masses $am = 0.05, 0.025$ and 0.020 we have simulated volumes 24^4 and 32^4. For bare masses $am = 0.01, 0.04$ we have simulated volumes $24^3 \times 32$ and 32^4. In addition, volume $16^3 \times 32$ was simulated for bare masses $am = 0.01, 0.02, 0.025$ in order to make it possible for us to obtain infinite volume estimates of the spectrum for these quark masses.

During the runs, the parameters for the acceptance rate have been tuned to yield a good acceptance while keeping a fixed trajectory length $l \approx 0.4$ for all ensembles. Configurations were saved every five simulated trajectories, so that saved configurations are separated by approximately two unit trajectory lengths. Measurements of observables such as the chiral condensate and the average plaquette were conducted on the fly, while the measurements of the particle spectrum were con-

ducted on the saved configurations following the strategy described in the next section.

2.2.2 Strategy for the spectrum measurements

We have measured the two-point functions with currents $J_M \sim \bar{q}\Gamma_M q$ in the scalar, pseudoscalar, vector and axial channels and the nucleon correlation function on the saved ensembles using corner-wall sources with fixed Coulomb gauge. The gauge fixing procedure in traditional QCD is known to reduce contamination from excited states and helps to better isolate the ground state of the system. In order to extract the lowest-lying masses we found it useful to construct the meson correlators from quark propagators with different combinations of temporal boundary conditions. This procedure was discussed in [276], it is extensively used in lattice QCD and, recently, it was explicitly implemented for $SU(3)$ with $N_f = 12$ in [13]. Some caveats are in order inside the conformal window, where the two-point function has the form in eqs. (2.7) and (2.8). We first summarize the strategy in the case of an exponentially decaying two-point function with constant coefficient, which is realized in all studied cases over a large time interval. Consider the quantity

$$\overline{C(t)} = \frac{1}{2}\left[C_{p.b.c.}(t) + C_{a.b.c.}(t)\right] \tag{2.15}$$

built from meson correlators with periodic ($C_{p.b.c.}$) and antiperiodic ($C_{a.b.c.}$) temporal boundary conditions on a lattice of temporal extent T. It can be shown that the resulting combined correlator $\overline{C(t)}$ has its lattice temporal extent effectively doubled and it can also be written as the periodic correlator $C_{p.b.c.}(t)$ with doubled period $2T$ [276]. In the case of the pseudoscalar meson, the staggered two-point function does not contain a staggered parity partner state. Taking into consideration a possible constant oscillation term that might appear as a consequence of the wrapping of a quark line around the antiperiodic time boundary, we can then write

$$\overline{C_{PS}(t)} = A\left(e^{-m_\pi t} + e^{-m_\pi(2T-t)}\right) + B(-1)^t \tag{2.16}$$

The constant oscillation term can be removed by using the combination

$$\tilde{C}_{PS}(2t) = \frac{\overline{C_{PS}(2t)}}{2} + \frac{\overline{C_{PS}(2t+1)}}{4} + \frac{\overline{C_{PS}(2t-1)}}{4} \tag{2.17}$$

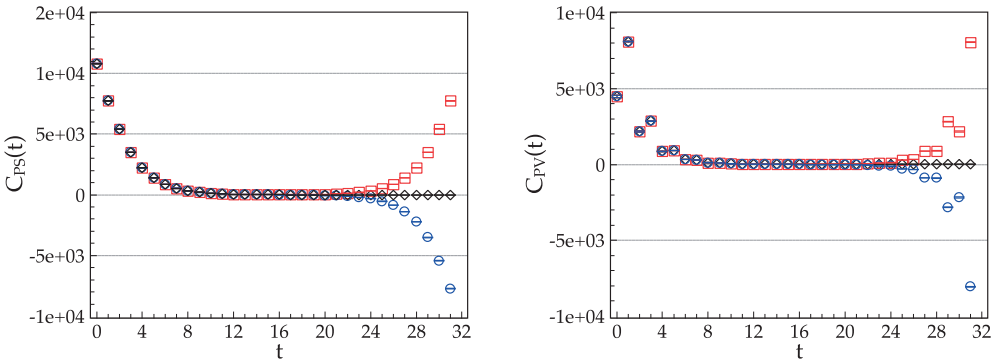

Figure 2.5: Examples of antiperiodic (blue circles), periodic (red squares) and combined (black diamonds) meson correlators from eq. (2.15), obtained from configurations generated with bare quark mass $am = 0.05$ at volume $V = 32^4$. (Left) The pseudoscalar correlator, (right) the pseudovector correlator.

so that the final correlator is

$$\tilde{C}_{PS}(2t) = A\left(e^{-m_\pi 2t} + e^{-m_\pi(2T-2t)}\right). \tag{2.18}$$

The effective doubling of the temporal extent allows to better isolate the first term in eq. (2.9) and enlarges the corresponding effective mass plateau.

A similar combination of meson correlators with different boundary conditions in the time direction can be performed for the other mesons. We use the PV correlator to extract the masses of the would-be ρ vector meson and the a_1 axial meson. The averaged PV correlator can be written in this case as

$$\overline{C_{PV}(t)} = A_\rho\left(e^{-m_\rho t} + e^{-m_\rho(2T-t)}\right) + A_{a_1}(-1)^t\left(e^{-m_{a_1} t} + e^{-m_{a_1}(2T-t)}\right) + B(-1)^t, \tag{2.19}$$

It is possible to proceed with a similar combination to that of eq. (2.17), so that

$$\tilde{C}_{PV}(2t) = \tilde{A}_{\rho 1}\left(e^{-m_\rho 2t} + e^{-m_\rho(2T-2t)}\right) + \tilde{A}_{\rho 2}\left(e^{-m_{a1} 2t} + e^{-m_{a1}(2T-2t)}\right). \tag{2.20}$$

In fact, such an approach has been followed in [13], where it was noted that, for the range of volumes and quark masses studied by the authors, $\tilde{A}_{\rho 1} \gg \tilde{A}_{\rho 2}$, and the resulting correlator is well approximated by a single exponential form with coefficient $\tilde{A}_{\rho 1}$

$$\tilde{C}_{PV}(2t) \simeq \tilde{A}_{\rho 1}\left(e^{-m_\rho 2t} + e^{-m_\rho(2T-2t)}\right). \tag{2.21}$$

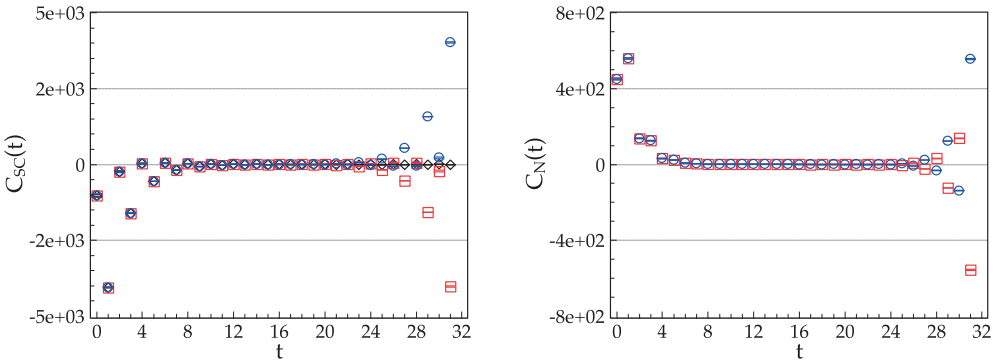

Figure 2.6: (Left) The periodic (red squares), antiperiodic (blue circles) and combined (black diamonds) scalar correlators, (right) the periodic (red squares) and antiperiodic (blue circles) nucleon correlator for a bare quark mass $am = 0.05$ and volume $V = 32^4$.

We have noticed that while the approximation (2.21) holds true for our heavier quark masses, it starts to break down for our lightest quark masses. In addition to that, we are also interested in studying the behaviour of the mass of the axial meson m_{a_1}. For these reasons, we fit the PV correlators obtained from our configurations to the complete functional form (2.19) in order to extract both m_ρ and m_{a1}. Examples of the initial correlators and the quality of the final combined correlators are shown in figure 2.5.

In similar fashion to eq. (2.19), we extract the mass m_σ of the scalar meson from the averaged S correlator

$$\overline{C_S(t)} = A_\sigma \left(e^{-m_\sigma t} + e^{-m_\sigma (2T-t)} \right) + B_\sigma (-1)^t \left(e^{-Mt} + e^{-M(2T-t)} \right) + B(-1)^t \,. \tag{2.22}$$

Lastly, we built the nucleon correlators from quark and antiquark propagators with antiperiodic boundary conditions in the temporal direction. These were then fitted with the usual expression for the lowest-lying states of a staggered baryon two-point function containing four parameters

$$C_N(t) = A_N \left(e^{-m_N t} - (-1)^t e^{-m_N (T-t)} \right) + B_N (-1)^t \left(e^{-Mt} - (-1)^t e^{-M(T-t)} \right) \tag{2.23}$$

with parity partner of mass M. Examples of these correlation functions are shown in figure 2.6.

2.3 Results

Table 2.1 collects all lattice measurements of this work. Simulations have been done at inverse lattice

coupling $\beta_L = 3.9$, located in the QED-like region of figure 2.1. The same coupling was also used in our first study[117]. The masses of all would-be hadrons have been measured for a range of bare fermion masses between $am = 0.01$ and $am = 0.07$, and volumes between $16^3 \times 24$ and 32^4. This section is organized as follows. After comparing the two-point functions with the ones of the free theory, and testing them against eqs. (2.7) and (2.8) in section 2.3.1, we provide in section 2.3.2 a tool to establish in which phase, QED-like or asymptotically free, the lattice system is. Section 2.3.3 is dedicated to the spectrum in a finite volume. It establishes the realization of universal scaling for the lattice results according to eq. (2.12) and provides a unified description of all available lattice data for the $N_f = 12$ system while identifying the pattern of scaling violations on both sides of the IRFP. Section 2.3.4 treats the extrapolation to infinite volume, needed for the lightest masses. Section 2.3.5 is dedicated to the spectrum at infinite volume, it established the realization of universal scaling for the lattice results according to eq. (2.10) and identifies the pattern of scaling violations, in particular, for the spin-1 states of this work and those in[13]. This analysis leads to the determination of γ^* that consistently describes all available lattice data for the spectrum of the $N_f = 12$ system at finite and infinite volume. Finally, section 2.3.6 is a brief discussion of mass ratios and degeneracies of chiral partners, probe of restored chiral symmetry.

2.3.1 Two-point functions

We have analyzed all two-point functions according to eq. (2.7) and its asymptotic forms in eq. (2.8). Our results are easily summarized. For the entire range of masses explored, the best fits to $\overline{C(t)}$ (with period $2T$) over the late time range are obtained for the form $a \exp(-mt)$, symmetrized on $2T$, with a constant and mass m. Time dependent corrections will increasingly be present at small times for decreasing masses, rendering more difficult the determination of the would-be hadron masses. The corrected form $a \exp(-mt) + b/t \exp(-nt)$, with $b > 0$ and $n > m$, ameliorates the fits at smaller times, as expected — for our lightest mass $am = 0.01$, such corrections start to become relevant when considering times $t < 10$ and requires $n \gtrsim m$.

In figure 2.7 we compare the two-point functions at $\beta_L = 3.9$ with the corresponding ones obtained in the free case, with the same lattice staggered action and the same bare fermion masses; this comparison is useful to clarify how far the studied regime is from the free limit. In fact, if the theory is deconfined one may expect a faster approach to the free limit than it is realised in the confined theory.

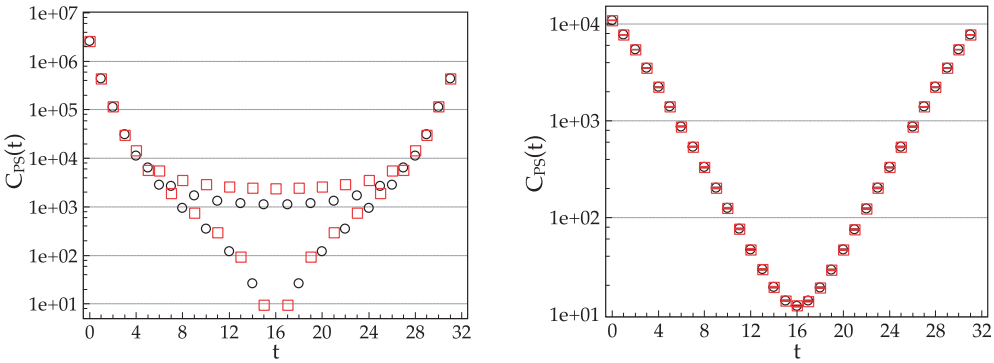

Figure 2.7: (Left) The pseudoscalar two-point function $C_{p.b.c.}$ (logarithmic scale) in the free case with $am = 0.05$, made of two free quark propagators with antiperiodic boundary conditions (red squares) and periodic boundary conditions (black circles) in the temporal direction. (Right) The same two-point function at $\beta_L = 3.9$. Vertical axes are rescaled to match.

One useful ingredient in the comparison is that two-point functions built with increasingly free quarks exhibit increasing sensitivity to the change of boundary conditions, both in the spatial and temporal direction. The zero-momentum free meson two-point functions reproduce the known analytical form for staggered correlators on even and odd temporal sites[64], and indeed figure 2.7 (left) shows the significant difference between the standard periodic meson two-point function built with periodic (P) and the one built with antiperiodic (A) temporal boundary conditions on the single free quark propagators. This difference is absent in the two-point functions at $\beta_L = 3.9$ in figure 2.7 (right), for the same bare fermion mass. Note also that exact point-by-point degeneracy of the scalar and pseudoscalar free meson correlators in the chiral limit is only realized at zero lattice spacing, since they involve a sum over the momenta of the fermion and antifermion propagators. In accordance with their analytical form[64], we find that pairs of chiral-partner free correlators are exactly degenerate at odd times and increasingly degenerate at even times towards the chiral limit. This comparison confirms that the two-point functions at $\beta_L = 3.9$ are significantly away from the free limit, and well described by an exponential with a constant coefficient A_H over a large time interval.

2.3.2 Would-be hadrons in the QED-like region

Figure 2.8 provides a tool to understand which phase of the $N_f = 12$ system we are looking at. It shows the mass ratio of the would-be pseudoscalar and vector mesons as a function of the bare fermion mass; these are the infinite volume lattice results in table 2.1 for $am > 0.025$ and in table 2.5

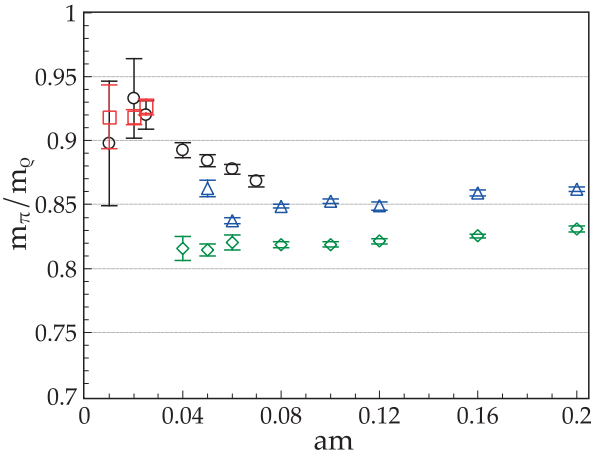

Figure 2.8: The pseudoscalar (π) to vector (ρ) mass ratio as a function of the bare fermion mass. Data at $\beta_L = 3.9$ (left of figure) are at the largest volumes from table 2.1 (black circles) and the infinite volume extrapolation from table 2.5 is shown for the three lightest points (red squares). Data at $\beta_L = 4.0$ would draw a line to the right of $\beta_L = 3.9$ [117]. Data from [13] (right of figure) are obtained with a HISQ staggered action, at $\beta = 6/g_L^2 = 3.7$ (green diamonds) and $\beta = 4.0$ (blue triangles), $am = 0.04$ to 0.2.

for $am \leq 0.025$. It also provides a direct comparison of our results with those of [13], the latter obtained with a HISQ staggered action at two lattice couplings. In our initial study [117], where more than one lattice coupling — including $\beta_L = 3.9$ and 4.0 — was considered, we could conclude that our results were located in the QED-like region of the theory, i.e. on the strong coupling and non asymptotically free side of the IRFP, with a positive β-function. The results in figure 2.8 update that study at lattice coupling $\beta_L = 3.9$; data for the ratio at $\beta_L = 4.0$ would be located on a curve with similar slope, to the right of $\beta_L = 3.9$. The analogous study in [13] led the authors conclude that their results are instead located on the weak coupling and asymptotically free side of the IRFP. The same can be inferred from figure 2.8, where the crucial ingredients are the slopes and the ordering of curves. A line of constant physics would lead to a constant ratio m_π/m_ρ; a realization of such a line occurs at the IRFP, where the β-function is zero and universal scaling holds with $m_{\pi,\rho} = c_{\pi,\rho} m^\delta$. Away from the fixed point, a family of curves at different lattice couplings as in figure 2.8 carries information about the sign of the β-function. For our data, the crossing of a line of constant ratio with the curves at fixed lattice coupling — $\beta_L = 3.9$ and an ideal line for $\beta_L = 4.0$ at its right — implies a positive sign of the β-function, where to first approximation we assume a constant physical mass between the intersections. The data of [13] have the opposite behaviour, and correspond instead to a negative sign of the β-function. At first sight, the reduced slope of the curves in the latter case would suggest

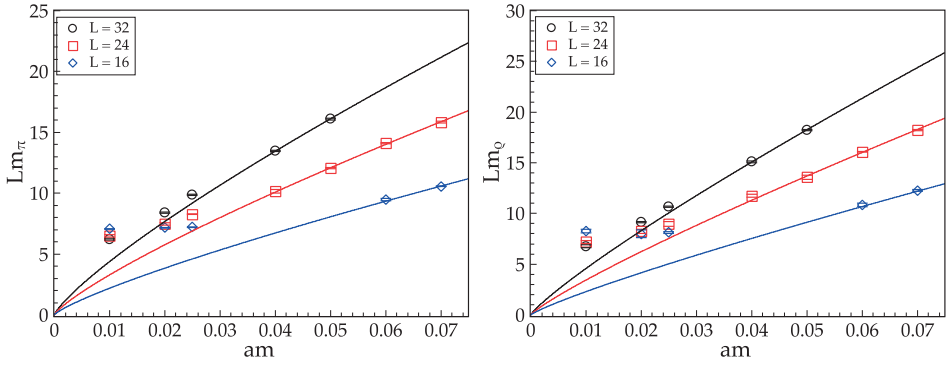

Figure 2.9: Lm_H for the pseudoscalar (left) and vector (right) would-be hadrons as a function of am and for varying L. For sufficiently large volumes and masses the points fall onto a curve (superimposed), which is the power-law best-fit curve obtained at infinite volume (table 2.6).

that the data of[13] are less affected by violations of scaling and plausibly closer to the IRFP. Another possibility, implied by the results in section 2.3.3 and in line with[79], is that different mass regimes are covered by the two sets of lattice measurements, both affected in different ways and to different degree by violations of universal scaling. Summarizing, the combined set of data in figure 2.8 nicely covers the region on both sides of the IRFP. This illustrates the fact that observables in this system are actually sensitive to the change of sign of the β-function and that some clever combination of these observables can be used to locate the IRFP; we are currently investigating a strategy along this line.

2.3.3 The spectrum in a box

Figure 2.9 illustrates the pseudoscalar and vector products Lm_H for each given L as a function of the bare fermion mass. It is clear that finite volume effects are present at the largest spatial volume for the three lightest bare masses $am = 0.01\,, 0.02$ and 0.025. At the same time, these data offer the interesting option of a finite size scaling study with the aim of identifying a universal scaling behaviour and define the functional form appropriate to extrapolate these data to infinite volume. Barring the emergence of new operators, we proceed to identify universal and nonuniversal behaviours in the space of couplings (g, m). A comparison with the superimposed best-fit curves obtained at infinite volume in section 2.3.5 helps locating the threshold where substantial deviations from a genuine power-law appear in the scaling of Lm_H, at fixed L. These deviations can a priori contain nonasymptotic contributions to the scaling function $f(x)$ of eq. (2.12), as well as genuine scaling violations not

described by $f(x)$. The following analysis is devised to identify these contributions at small and large x.

Anticipating the results of section 2.3.5, we note that the infinite volume best fit to eq. (2.10) for the pseudoscalar, scalar and nucleon masses gives a critical exponent $\delta = 0.81$, while the vector and axial states favour a slightly larger exponent $\delta = 0.86$, see table 2.6. While the difference in the values of δ for different H channels is in itself an indication of scaling violations, we note that universality appears to be realized in all but the vector channels and $\delta = 0.81$ gives a value of $\gamma^* = 1/\delta - 1$ in agreement, within uncertainties, with the best fit reported in [79] and, noticeably, with the four-loop perturbative prediction [304,305]; it is thus tempting to conclude that our data are in the universal scaling regime and provide a measure of the mass anomalous dimension at the IRFP. The study that follows supports this conclusion.

In figure 2.10 we vary the scaling variable x about the best-fit value for δ (central figures) and on the range $\delta = [0.5, 1]$ to study the x dependence of the ratio Lm_π/c_π (left) and Lm_ρ/c_ρ (right). For $x \gtrsim 1$, the data in the central figures align on a common curve. They increasingly scatter and deviate from it when δ is moved away from its best-fit value, over the range 0.5 to 1. Figure 2.11 reports all states for the reference value $\delta = 0.81$; we observe the universal behaviour of the pseudoscalar, scalar and nucleon states at $x \gtrsim 1$ and the displacement and slight change of slope of the vector and axial states. For $x \lesssim 1$, the asymptotic behaviour of the universal scaling function $f(x) \to const$ as $x \to 0$, is corrected by nonperturbative L-dependent scaling violations. These are discussed in the next section.

Inspired by recent work [79], we now attempt a unified description of the finite volume results of this work and the results obtained for the same system with other lattice actions, at a priori different bare lattice couplings and fermion masses. In particular, we consider the results at $\beta = 2.2$ in [134] and the results at $\beta = 3.7$ and $\beta = 4.0$ in [13]. We limit this analysis to the pseudoscalar channel, studied in all works, while later in section 2.3.5 we compare our results and those in [13] for the vector state. Figure 2.12 summarises this study, where we show the collapse on a common universal curve of data obtained with different lattice actions and lattice couplings, once perturbative corrections to the universal scaling are divided out. The general conclusions of this analysis are in good agreement with the study in [79], while our analysis differs from [79] in some details and interpretation of the parameters. We briefly highlight the relevant ingredients and results.

- Perturbative corrections to universal scaling are present whenever the system is close to, but

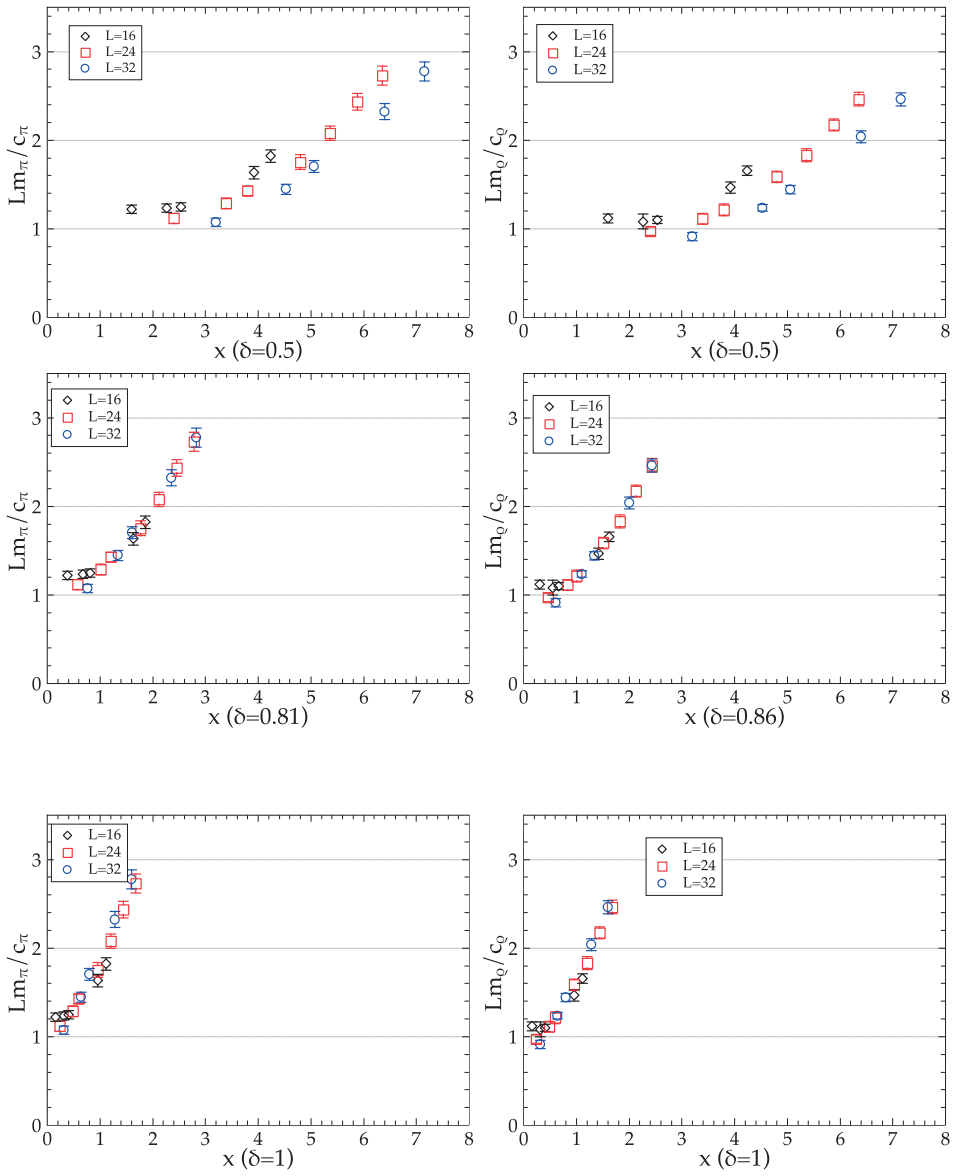

Figure 2.10: Ratios $Lm_H/c_H, c_H$ from table 2.6, for the pseudoscalar state (left) and the vector state (right) as a function of the scaling variable $x = Lm^\delta$ for varying δ on $[0.5, 1]$ and $L = 16, 24, 32$. The central figures display the data alignment for the best-fit values of δ in table 2.6.

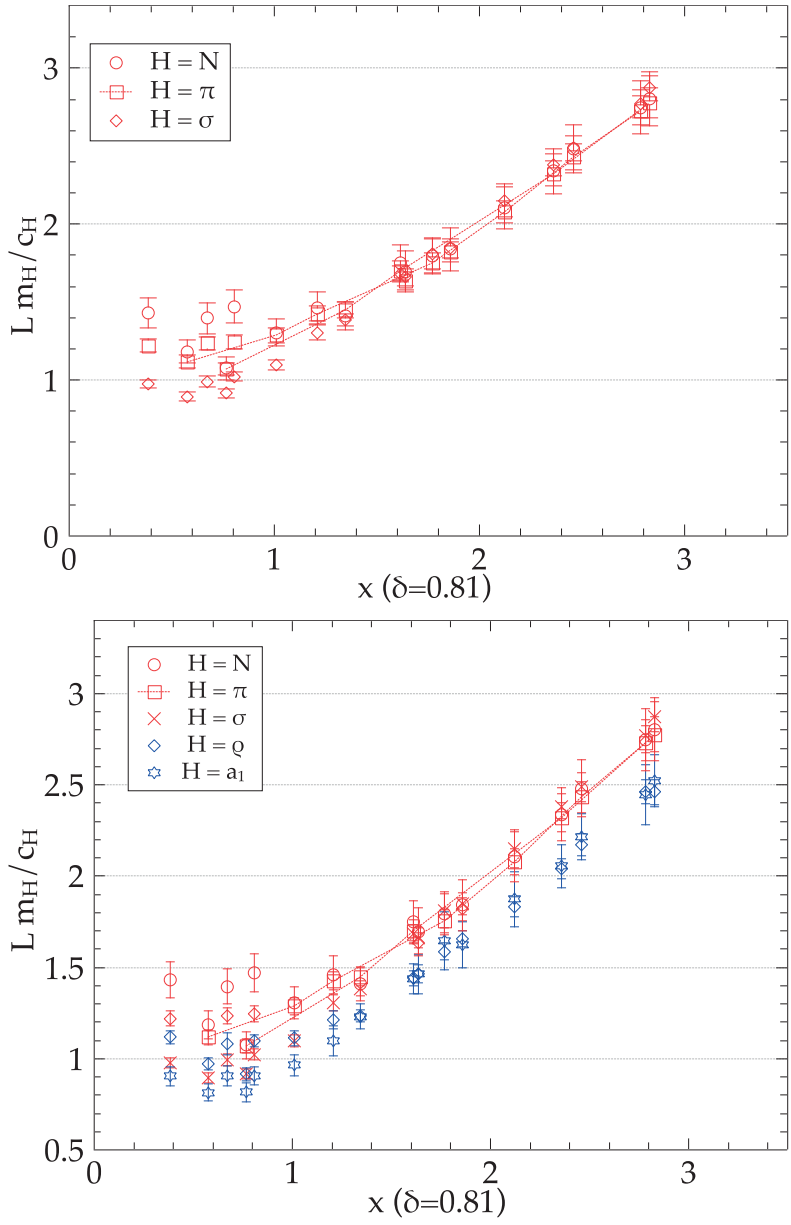

Figure 2.11: $Lm_H/c_H, c_H$ from table 2.6, as a function of $x = Lm^\delta$ with $\delta = 0.81$, excluding the vector and axial states (top) and including them (bottom).

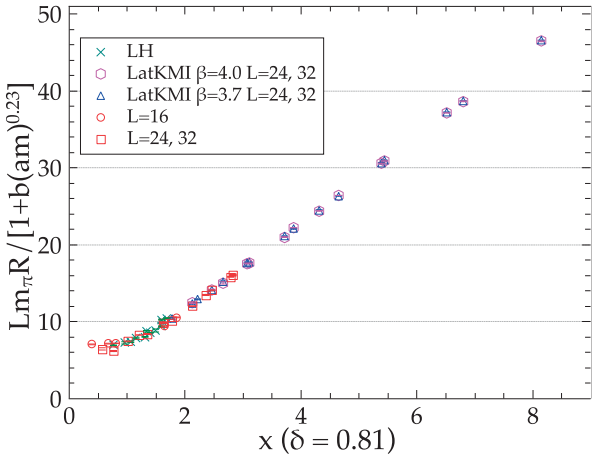

Figure 2.12: Collapse of curves for the rescaled pseudoscalar product $Lm_\pi R/(1+bm^\omega)$, with $\omega = 0.23$ from 4-loop perturbation theory and R, b in table 2.2, as a function of the universal scaling variable $x = Lm^\delta$ with $\delta = 0.81$ from this work. Data are from [134] at $\beta = 2.2$ (LH, green crosses), [13] at $\beta = 4.0$ (LatKMI, magenta hexagons) and $\beta = 3.7$ (LatKMI, blue triangles), and from this work for $L = 24, 32$ (red squares) and $L = 16$ (red circles).

not at the fixed point. As pointed out in [79], perturbative corrections due to $g \neq g^*$ and a finite fermion mass can explain the deviations from universal scaling of many results for the $N_f = 12$ system. As explained in section 2.1.1, these contributions can be parameterized to leading order as multiplicative corrections $1 + b\, m^\omega$, with universal exponent $\omega = \delta\gamma_g^*$.

- We find that our best-fits favour values of ω lower than $\omega = 0.41$ of [79], though we cannot perform a fully unconstrained fit. It is therefore appealing to consider the value $\omega = 0.23$ given by $\delta = 0.81$ — our central value in good agreement with the 4-loop prediction within uncertainties — and the 4-loop prediction $\gamma_g^* \simeq 0.283$.

- The values of b in table 2.2 and the analysis of the vector state in table 2.8 corroborate the interpretation of Δg in section 2.1. We observe that all data are sufficiently close to universal scaling. Our data are located in the QED-like phase of the system and do not show corrections to scaling at these light masses, thus $b = 0$. The data from [134] are close to our data, and again they seem not to be sensitive to corrections to scaling at the light masses they consider; the only difference is that their data are located away from the asymptotic linear form of $f(x)$ and we cannot clearly discriminate to which phase they pertain. The results from [13] are located on the other — i.e. asymptotically free — side of the fixed point, thus showing $b < 0$. We expect the data of [79] to be located between ours and the data from [13] on the asymptotically free side, with $b < 0$, in agreement with their analysis. In section 2.3.5 we provide an example

of a positive b for our system in the QED-like phase, needed to successfully describe perturbative corrections to scaling for the vector and axial states. Thus, the parameter b changes sign at the boundary between the two phases of the lattice system and we expect it to flow to zero in the continuum, i.e. $\beta_L \to \infty$, where the lattice system reaches the IRFP.

- An overall rescaling is the usual procedure to bring together sets of data that follow universal scaling. We perform a rescaling of Lm_π by the factor R in table 2.2. R is given by the ratio of the coefficients c_H entering the infinite volume functional form $m_H = c_H m^\delta (1 + b_H m^\omega)$ for each given data set and channel H. Such a rescaling is asymptotically equivalent to a rescaling of the variable x, as used in [79], provided it does not enter the corrections to the universal scaling function. The factor R for LatKMI is derived in section 2.3.5. R shows a monotonic dependence on the lattice bare coupling β_L, converging to its universal value as $\beta_L \to \infty$. This statement, as the previous one for b, assumes that the lattice system is in the basin of attraction of the IRFP.

- Once rescaled by R and once the perturbative mass corrections are divided out, the product Lm_π for all the lattice data in figure 2.12 is described by a universal curve $f(x)$ for all x values, except for the presence of nonperturbative violations of scaling for $L \lesssim \xi$ for some data of this work.

2.3.4 Extrapolation to infinite volume

For $am = 0.04$ to 0.07, no residual finite volume dependence is left within the estimated uncertainties; we thus take the result at the largest available volume as the infinite volume value for $am = 0.04$ to 0.07. For the three lightest bare fermion masses, $am = 0.01,\ 0.02,\ 0.025$ we have instead performed an extrapolation to infinite volume. Lüscher's formula [213] for particles in a box does in principle apply to any interacting quantum field theory, provided the scattering amplitude of the particles involved is known. The latter problem is perturbatively solved by chiral perturbation theory (χPT) for QCD-like theories in the chirally broken phase, predicting the leading order behaviour of the Goldstone boson mass to be [141,89] $m_\pi(L) = m_\pi + c \exp(-m_\pi L)/(m_\pi L)^{3/2}$ for $m_\pi L \gg 1$. The functional form to be used in our case is what describes the scaling violations at small x in figures 2.10 and 2.11.

The small x behaviour of the pseudoscalar would-be hadron is analyzed in figure 2.13, for $\delta =$

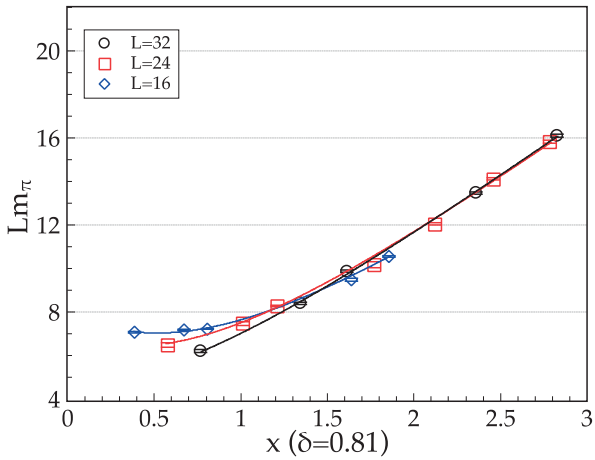

Figure 2.13: Lm_π as a function of the scaling variable $x = Lm^\delta$ with $\delta = 0.81$, for $L = 16,\ 24,\ 32$. The curves are the best fits to the functional form $F(x, L) = ax + c\exp(-kx)$, with a, c, k in table 2.3.

0.81. At the smallest values of x, Lm_π shows an L-dependent deviation from a common curve. L dependent deviations from scaling can be expected whenever the box size L becomes comparable to or smaller than the would-be hadron Compton wavelength $\sim \xi$. The entire range of x in figure 2.13 can be described in terms of the universal scaling function $f(x)$, with asymptotics $f(x) \sim x$ as $x \to \infty$ and $f(x) \to const$ as $x \to 0$, and a nonperturbative L-dependent violation of scaling at small x — note that perturbative corrections in L of the type $1 + \Delta g L^{-y_g}$ would instead multiply the entire scaling function $f(x)$ and modify its behaviour at all x. Hence, $F(x, L) = ax + g(L)\tilde{f}(x)$ should describe figure 2.13, except for the presence of nonlinear universal contributions to $f(x)$ at intermediate x. The coefficient a is nothing but c_H, $H = \pi$ of table 2.6, the function $g(L)$ increases for decreasing L according to figure 2.13, and $\tilde{f}(x) \to const$ as $x \to 0$. Figure 2.13 also displays the best-fit curves for the simplified ansatz $F(x, L) = ax + c\exp(-kx)$, with best-fit values of a, c, k in table 2.3. Rather than aiming at the optimal $\chi^2/d.o.f$, the purpose of this example is to illustrate the trend of small volume corrections through effective parameters c and k. The latter is quite stable for varying L, while, as expected, the parameter c increases with decreasing L; a polynomial $g(L) \sim (1 - bL)$ perfectly describes the data and provides a volume dependence milder than the universal scaling form $1/L\exp(-L/\xi)$ for $m_\pi(L)$ at small x. At the same time, the shift in the paramater a at $L = 16$, as compared to the larger volumes in table 2.3, should be attributed to the intermediate x contributions to $f(x)$ that are not captured by the simple ansatz for $F(x, L)$.

A volume dependence milder than QCD and milder than the universal scaling form can be traced

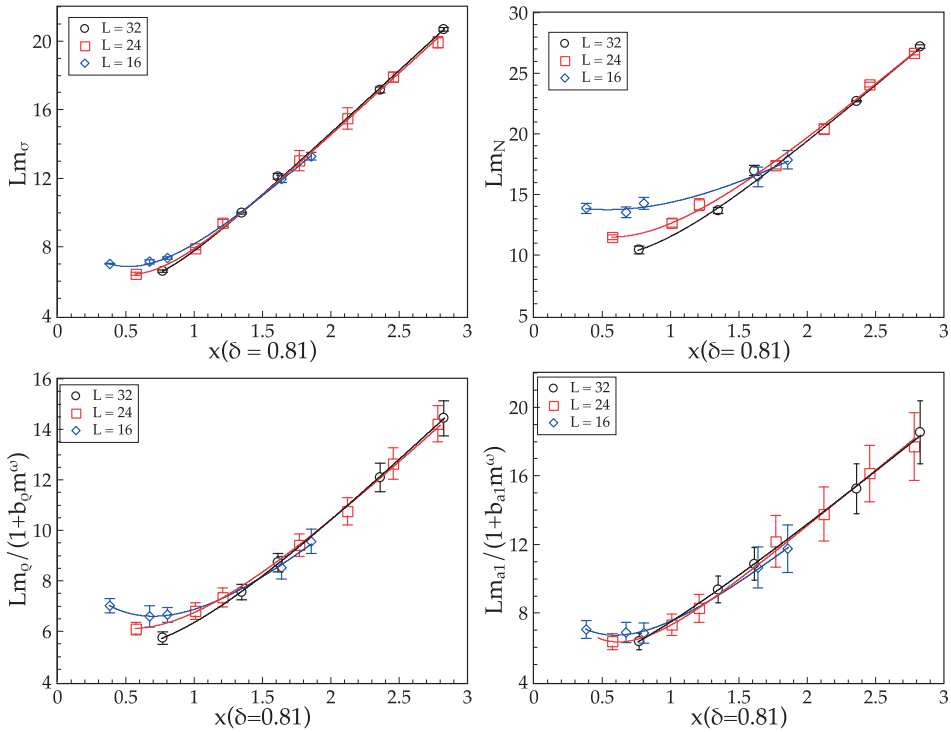

Figure 2.14: $Lm_H/(1+b_H m^{\omega})$ for $H = \sigma, N, \rho, a_1$ as a function of the scaling variable $x = Lm^{\delta}$ with $\delta = 0.81$, for $L = 16,\ 24,\ 32$. The coefficient $b_H = 0$ for $H = S, N, b_\rho = 0.52(12)$ and $b_{a_1} = 0.45(24)$. The curves are best fits to the functional form $F(x, L) = ax + c\exp(-kx)$, see table 2.4.

back to the Coulomb dynamics in the QED-like phase and the absence of a confining potential. It is favoured by the combination of data in figure 2.13, figure 2.15 and the infinite volume study of the heavier masses $am > 0.025$. Having only three volumes for each bare fermion mass, we have performed the extrapolation of the lightest would-be hadron masses to infinite volume with the simplest ansatz

$$m_H(L) = m_H + c\, e^{-\tilde{k} m_H L}, \qquad \text{H}=\pi, \sigma, \rho, a_1, N \tag{2.24}$$

with parameters c, $\tilde{k}$ and the infinite volume mass m_H for the channel H. The results of the extrapolation are summarized in Figure 2.15, Figure 2.16, and in table 2.5. In order to account for the uncertainty induced by the lack of a complete knowledge of the function $F(x, L)$ we add a second uncertainty to each extrapolated mass obtained as follows. The simple parameterization $g(L) = c(1-bL)$

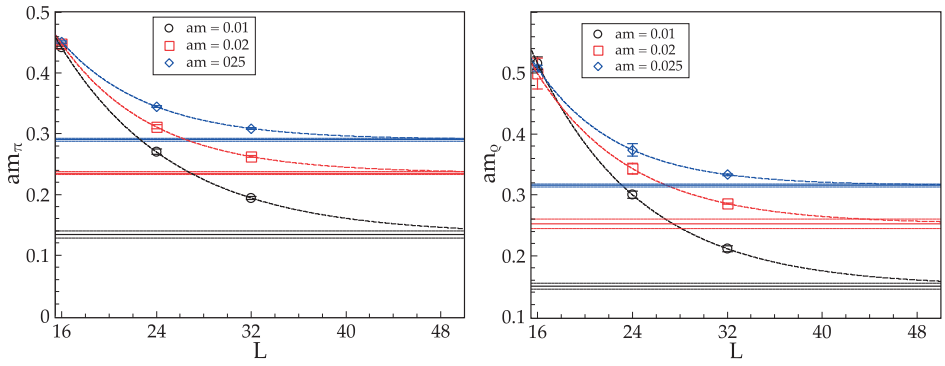

Figure 2.15: Spatial L dependence of the pseudoscalar mass (left) and the vector mass (right) and extrapolation to infinite volume according to eq. (2.24). From top to bottom, $am = 0.025$ (blue diamonds), $am = 0.02$ (red squares) and $am = 0.01$ (black circles). The extrapolated value and its uncertainty is indicated by the horizontal bands and reported in table 2.5.

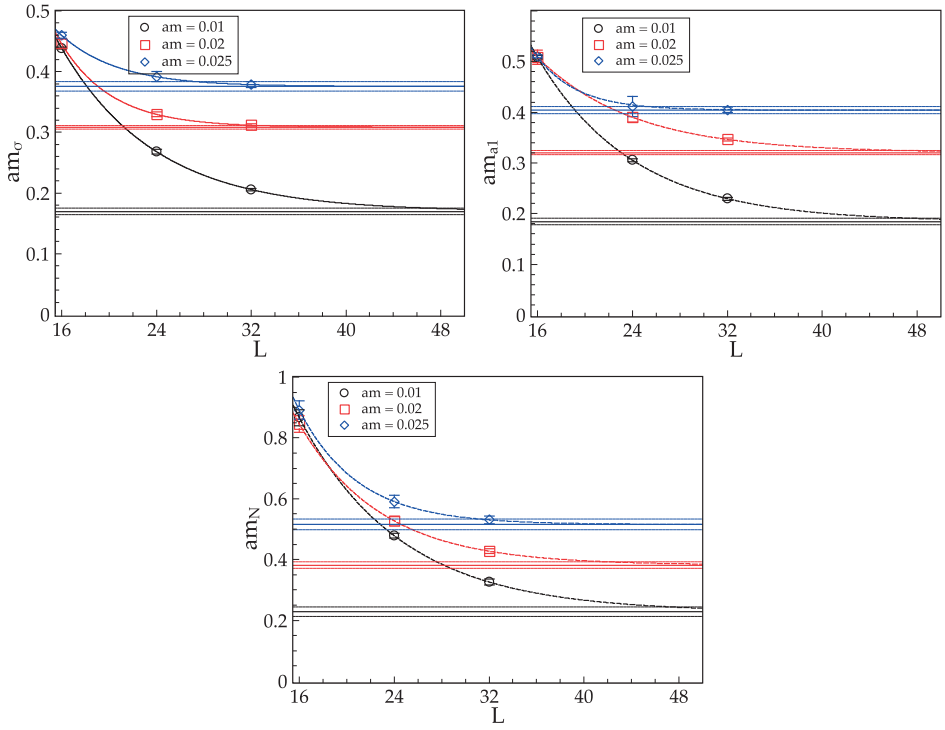

Figure 2.16: Spatial volume dependence and extrapolation to infinite volume with functional form eq. (2.24) for the masses of the scalar (top left), axial (top right) and the nucleon (bottom) states, and bare fermion masses $am = 0.01$, 0.02 and 0.025. The extrapolated value and its uncertainty is indicated by horizontal lines and can be read from table 2.5.

provides an explicit expression for $F(x, L)$, which in turn gives the volume dependence

$$m_H(L) = m_H + c\left(\frac{1}{L} - b\right) e^{-\frac{k}{c_H} m_H L} . \tag{2.25}$$

Here, we used $x = Lm^\delta$ and the infinite volume mass relation $m_H = c_H m^\delta$ inside $F(x, L)$, where c_H is nothing but the parameter a in the scaling study of figure 2.13 and table 2.3. For each channel H, the second asymmetric uncertainty on the infinite volume mass in table 2.5 has the $L = 32$ mass value as upper bound, and as a lower bound we take the infinite volume mass given by a fit to eq. (2.25), with free parameters c, b and m_H and fixed k/c_H equal to its $L = 24$ value in table 2.3 and table 2.4.

2.3.5 The spectrum at infinite volume

Figure 2.17 shows the bare fermion mass dependence of the would-be hadron masses at infinite volume, taken from tables 2.1 and 2.5. The results of a single power-law fit on the heavier mass range (Fit I), the full mass range (Fit II), and a linear fit with free intercept (Fit III) are summarized in table 2.6 and reproduced in figure 2.17. The linear fit turns out to be significantly worse than the power-law fits in all cases. This confirms, once again, that chiral symmetry is restored. Fit IIb, reported in table 2.7, is a single power-law fit on the full mass range where the symmetrized second uncertainty in table 2.5 has been added in quadrature to the first uncertainty. In almost all cases in table 2.7 we obtain a $\chi^2/dof \lesssim 1$, likely indicating that the uncertainties on the lightest points are in this case slightly overestimated. What is most interesting is the value of the exponent δ and its dependence, or lack thereof, on the different quantum numbers H. A value $\delta \neq 1/2$ for the pseudoscalar state says that it is not a Goldstone boson and chiral symmetry is exact. A value $\delta < 1$ says that we are away from the heavy quark limit where $m_H \sim m$. We observe a common $\delta = 0.81$ within errors in the channels $H = PS, S, N$ — a sign of universality — and a slightly larger value $\delta = 0.86$ within errors for the vector states $H = V, PV$; this could be attributed to the different pattern of spin-spin interactions for spin-1 and spin-0 or 1/2 states. Noticeably, the value $\delta = 0.81$ agrees with the four-loop prediction[304,305] at the IRFP and it agrees with the best-fit result of[79]. We conclude that the lattice results for the pseudoscalar, scalar and the nucleon states are in the universal scaling regime, i.e., at masses sufficiently light to be insensitive to perturbative mass corrections to universal scaling arising for $g \neq g^*$. For this reason, we take $\delta = 0.81$ and these results for the pseudoscalar (scalar and nucleon) state as reference in the combined analysis with other lattice results, i.e., $R = 1$ and

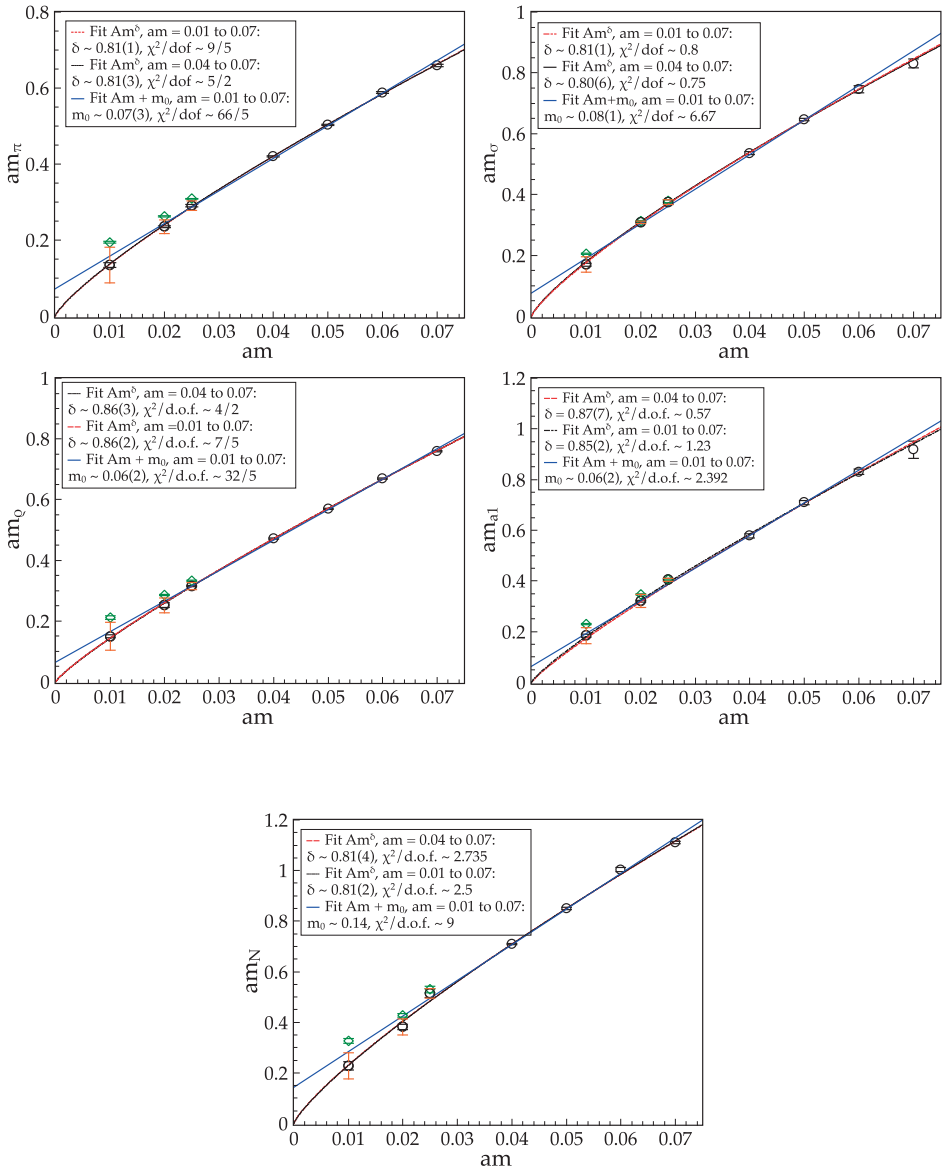

Figure 2.17: Would-be hadron masses at $L = \infty$ in the pseudoscalar (top left), scalar (top right), vector (centre left), axial (centre right) and the nucleon (bottom) channels as a function of the bare fermion masses. Three fits are shown: Fit I (solid black) is a power-law on the range $am = 0.04$ to 0.07, Fit II (dashed red) is a power-law on the range $am = 0.01$ to 0.07, and Fit III (solid blue) is a linear fit with free intercept on the range $am = 0.01$ to 0.07. The total uncertainty used in Fit IIb is shown (red bar) for $am = 0.01,\ 0.02,\ 0.025$. Largest volume data are also shown for the same points (green diamonds). Fit results are in table 2.6 and 2.7.

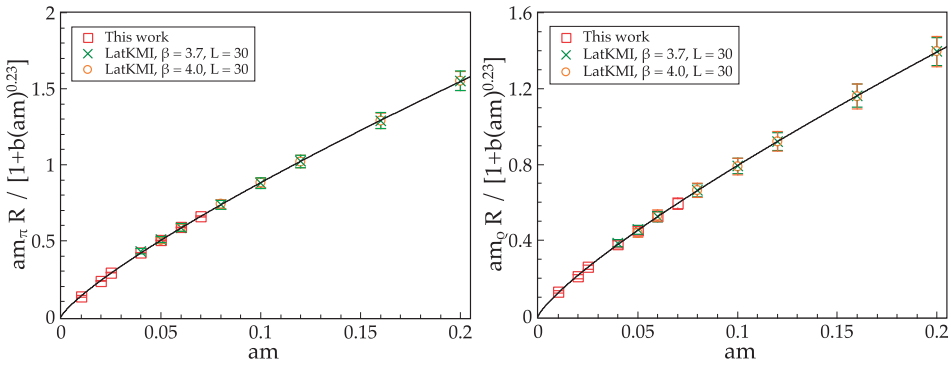

Figure 2.18: Collapse of the rescaled infinite volume masses $am_H R/(1+b_H(am)^{\omega})$, $\omega = 0.23$, for the pseudoscalar (π) and vector (ρ) states in this work (red squares), and in [13] at $\beta = 4.0$ (orange circles) and $\beta = 3.7$ (green crosses). The values of $R = c_H/c_H^{KMI}$ and $b_H, H = \pi, \rho$, are from table 2.8.

$b = 0$ in table 2.2.

Instead, $\delta = 0.86$ for the vector states suggests the presence of perturbative corrections to scaling. The results of a fit with two power laws, according to the parameterization of the perturbative corrections to scaling discussed in section 2.1.1

$$m_H = c_H\, m^{\delta}\,(1 + b_H m^{\omega}) \tag{2.26}$$

with $\delta = 0.81$ and $\omega = 0.23$ for the vector state are in table 2.8 (This work). Note that $b_\rho > 0$, as expected, consistently with the fact that our system is on the strong coupling side of the IRFP. To further corroborate this statement we combine the data for the vector and the pseudoscalar with those of [13], all at infinite volume within uncertainties. The best-fit values for eq. (2.26) are in table 2.8. While $b_H > 0$ on the strong coupling side of the IRFP (This work), $b_H < 0$ on the weak coupling side of the IRFP (LatKMI), and we expect $b_H \to 0$ for $\beta_L \to \infty$. Finally, figure 2.18 shows the collapse of the infinite volume pseudoscalar and vector states of this work and [13], after rescaling. The rescaling factor $R = c_H/c_H^{KMI}$ is the ratio of the leading power-law coefficients for the channel H in table 2.8. This analysis leads to the determination of the mass anomalous dimension γ^* at the IRFP. We quote the value obtained from Fit I in the pseudoscalar channel from table 2.6

$$\delta = 0.81(3), \qquad \gamma^* = 0.235(46) \tag{2.27}$$

This value is in agreement with the perturbative four-loop prediction, with the best-fit result of [79]

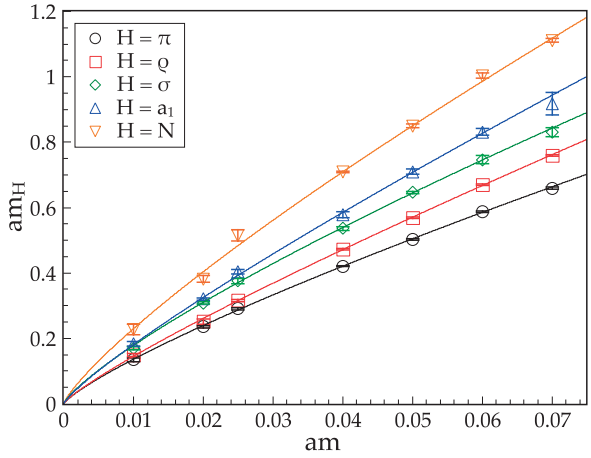

Figure 2.19: Ordering of the would-be hadrons in the QED-like phase of the $N_f = 12$ system. From bottom to top, the pseudoscalar (π), the vector (ρ), the scalar (σ), the axial (a_1) and the nucleon N.

and not far from the first lattice determination of the fermion mass anomalous dimension for the $N_f = 12$ system in [117], though the latter was affected by rather large uncertainties. The value of γ^* in eq. (2.27) suggests a rather weakly coupled $N_f = 12$ system at the IRFP, so that perturbation theory should be expected to hold. Conversely, four-loop perturbation theory seems to fail for $N_f \sim 8$, where it predicts an IRFP at rather strong coupling g^* and, even worse, a change of sign of the mass anomalous dimension for $g < g^*$, see end of section 2.1.2. This effect is not encountered at two loops. This reinforces the idea that nonperturbative dynamics, known to be chiral dynamics in this case, has to play a role at the opening of the conformal window, for $8 \lesssim N_f \lesssim 12$. Also, if $\gamma^* = 1$ has to be realized at the lower endpoint of the IRFP line, where the conformal window disappears, a rapid variation of the mass anomalous dimension for $N_f^c \lesssim N_f \lesssim 12$ should be expected in a lattice (or any nonperturbative) determination of the IRFP line, where nonperturbative dynamics is fully encompassed. The present study also corroborates the view that the IRFP of these theories is not associated to a physical singularity, no discontinuity happens there and estimates of physical observables including the anomalous dimensions can be attempted on either side of the fixed point.

We conclude this section with showing the ordering of the would-be hadrons in figure 2.19. To summarize, a universal power law with exponent $\delta = 0.81$ describes all would-be hadrons, with additional perturbative mass corrections of the type $1 + \Delta g m^{\delta \gamma_g^*}$ in the vector and axial channels. The pseudoscalar is the lightest state, but it is not a Goldstone boson. The vector, the scalar, the

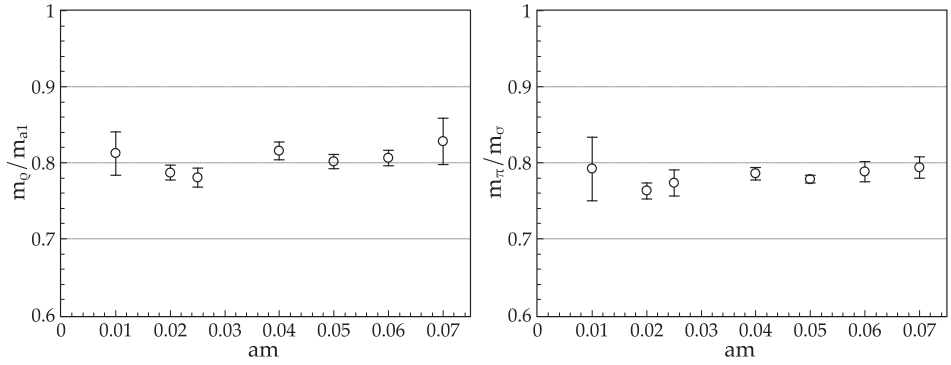

Figure 2.20: The ratio of the vector and axial masses (left) and the ratio of the pseudoscalar and scalar masses (right) as a function of the bare fermion mass.

axial, and finally the nucleon follow. It is worth noting that the scalar state[**] is heavier than the vector state. Their ordering becomes phenomenologically relevant when the theory is just below the conformal window — it remains, however, difficult to identify a broad scalar resonance, such as $f_0(500)$ of QCD[††], on the lattice.

2.3.6 Mass ratios and degeneracies

We conclude this work with some remarks on the interplay of conformal and chiral symmetry inside the conformal window. Ratios and degeneracies of would-be hadron masses are a combined probe of both symmetries, and, as shortly discussed below, the $U(1)$ axial symmetry. At the IRFP conformal symmetry implies exact chiral symmetry. Away from the IRFP, inside the conformal window, restored chiral symmetry implies the degeneracy of chiral partners in the chiral limit. Figure 2.20 shows the mass ratios pseudoscalar-scalar and vector-axial. The two ratios are essentially constant $\sim$ 0.8 over the explored mass range, as it can be deduced from the best-fit values for the power-law exponent δ. Due to the presence of perturbative corrections to universal scaling for the vector states, deviations from a constant ratio will instead be observed in all cases that mix the vector (or axial) channel with the other ones, one example is figure 2.8.

Before discussing the degeneracy patterns, it is important to recall that the scalar "σ" studied here is extracted from the quark-line connected piece of the scalar-isoscalar two-point function; for clarity, we then call this state σ_c in the following discussion and with σ we refer to the lowest-lying

[**] We remind the reader that σ of this work is the state extracted from the connected scalar two-point function.

[††] This state could in addition be an admixture of ordinary $\bar{q}q$ states and tetraquarks.

state of the complete (connected plus disconnected) scalar-isoscalar correlator. The pseudoscalar π and the scalar σ, not σ_c, belong to the same chiral multiplet of $SU(N_f)_L \times SU(N_f)_R$, and they must be degenerate in the chiral limit $m \to 0$ when chiral symmetry is not spontaneously broken.

The vector ρ and the axial a_1 are also chiral partners and show the same degeneracy pattern. In other words, the mass degeneracy of the chiral partners ρ and a_1, π and σ, can be used as an indicator of the restoration of chiral symmetry. What about the degeneracy of π and σ_c? For degenerate fermion masses, as in our case, the connected contribution to the scalar-isoscalar, σ_c, equals the connected contribution to the scalar-isovector δ — the latter has no disconnected contributions. The δ is the $U(1)_A$ partner of π. We should thus conclude that the degeneracy of π and σ_c is probing the effective restoration of $U(1)_A$, at least at the level of the two-point functions[‡‡] Figure 2.21 shows the mass difference and the ratio $(m_i - m_j)/(\overline{m_i + m_j})$ for the spin-0 $U(1)_A$ partners $\pi - \sigma_c$ and the spin-1 chiral partners $\rho - a_1$.

The degeneracies in the chiral limit are evident from the best-fit curves of the mass difference on the left of figure 2.21, thus confirming once again exact chiral symmetry and the effective restoration of $U(1)_A$. This also implies that the disconnected contributions to the scalar-isoscalar correlator are at least $O(m)$. We defer to future work the question to which degree $U(1)_A$ is exact inside the conformal window beyond the two-point functions and how its restoration pattern compares with high-temperature QCD. The approximately constant ratios on the right of figure 2.21 highlight, once again, the realisation of the scaling form $c_H\, m^{\delta}$, modulo small perturbative corrections $(1 + b_H m^{\omega})$ in the spin-1 case, with universal exponents δ and ω and mass independent nonuniversal coefficients c_H and b_H.

2.4 Conclusions

We have studied the $SU(3)$ gauge theory with twelve fundamental fermions as a prototype of theories inside the conformal window, with emphasis on the two-point functions and their properties when the IRFP is perturbed by a fermion mass. In order to disentangle the imprint of the IRFP in the dynamics of the system, we have analysed the complete would-be hadron spectrum, the would-be mesons and the nucleon, and performed a universal scaling study at finite and infinite volume. The identification of universal contributions dictated by the conformal invariance at the fixed point

[‡‡] A complete probe of $U(1)$ axial and chiral restoration obviously includes the direct observation of the disconnected contributions and the degeneracy patterns of all states, including η' and σ.

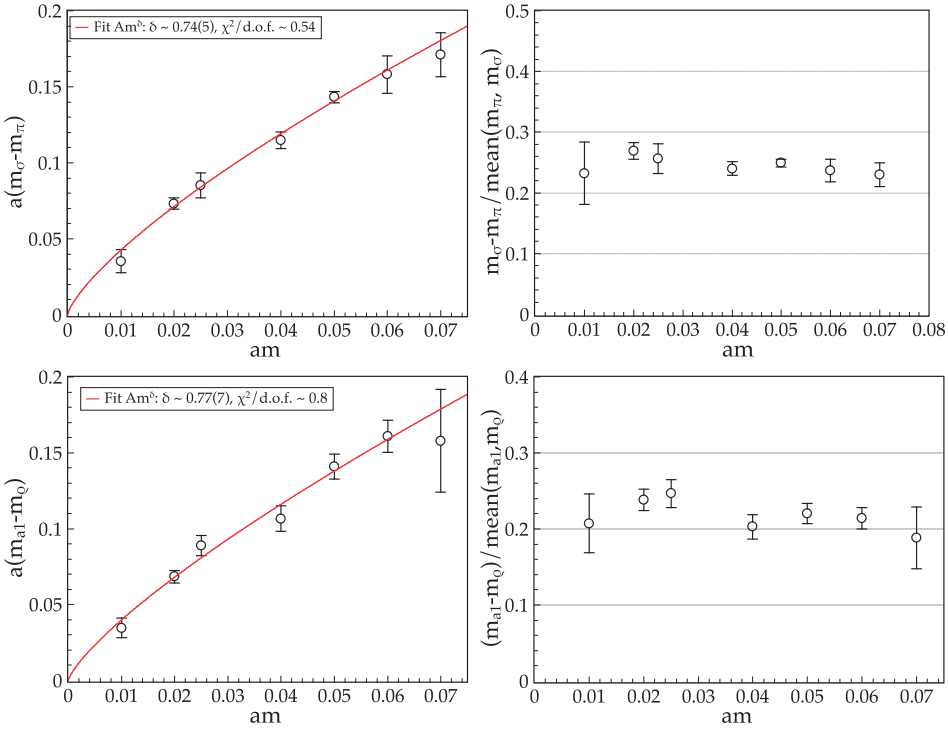

Figure 2.21: Degeneracy pattern and best-fit curve of the pseudoscalar π and the scalar σ_c (connected) (top left) states. The ratio of the mass difference to the mass average (top right). Analogous figures for the vector ρ and the axial a_1 states (bottom).

and deviations from universal scaling induced in the surroundings of the fixed point has allowed for the nonperturbative determination of the fermion mass anomalous dimension $\gamma^* = 0.235(46)$ and a unified description of all lattice results for the would-be hadron spectrum of the $N_f = 12$ theory.

This analysis shows that the lattice system retains all signatures of the underlying conformal symmetry of the fixed point, in addition to the restored chiral symmetry, that the pattern of symmetries can be followed across the IRFP and the critical exponents — or any other physical observable — can be determined on either side of the fixed point, be it the asymptotically free phase of the lattice system or the QED-like phase. In other words, one should conclude that no singularity is associated to such a fixed point.

The obtained nonperturbative value of γ^* hints at a rather weakly coupled $N_f = 12$ system at the IRFP. It is thus amusing, and perhaps not unexpected, to observe the agreement with the four-loop perturbative prediction at the fixed point. Based on this agreement, it is tempting to infer that the perturbative expansion is working well in this range of N_f, and that the missing nonperturbative contributions and the effects of a truncation of the perturbative series amount to a negligible correction for this system. It also reinforces the idea that nonperturbative dynamics, known to be chiral dynamics in this case, has to play a role at the opening of the conformal window.

According to previous literature, a lower edge above $N_f = 8$ was expected. The small value of γ_m for $N_f = 12$ actually suggests that the theory with $N_f = 12$ flavours is located well inside the conformal windows and the lower edge is significantly below, therefore most probably around $N_f = 8$. Next chapter will clarify this very important and for many years controversial point.

As a byproduct, we have confirmed the restoration of chiral symmetry through the degeneracy of chiral partners and the effective restoration of the $U(1)$ axial symmetry at the level of the two-point functions.

am	*Volume*	am_π	am_ρ	am_N	am_σ	am_{a_1}
0.01	$16^3 \times 32$	0.4421(17)	0.516(10)	0.867(26)	0.4388(15)	0.5086(36)
	$24^3 \times 32$	0.2701(44)	0.3002(61)	0.478(9)	0.2682(36)	0.305(30)
	32^4	0.1942(21)	0.2114(52)	0.326(10)	0.2057(22)	0.2295(31)
0.02	$16^3 \times 32$	0.4480(16)	0.499(25)	0.846(27)	0.446(8)	0.509(14)
	24^4	0.3112(34)	0.3432(85)	0.528(14)	0.3297(35)	0.3903(91)
	32^4	0.2624(13)	0.2857(11)	0.428(8)	0.3117(20)	0.3464(34)
0.025	$16^3 \times 32$	0.4511(16)	0.5081(46)	0.892(31)	0.4598(48)	0.5102(32)
	24^4	0.3447(12)	0.374(10)	0.591(21)	0.3916(82)	0.411(20)
	32^4	0.3087(13)	0.3332(16)	0.530(13)	0.3786(49)	0.4048(55)
0.04	$24^3 \times 32$	0.4236(57)	0.4890(60)	0.726(13)	0.543(24)	0.617(49)
	32^4	0.4210(16)	0.4717(23)	0.709(2)	0.5359(51)	0.5783(83)
0.05	24^4	0.5020(23)	0.5652(76)	0.851(17)	0.6452(26)	0.703(41)
	32^4	0.5031(21)	0.5689(17)	0.850(5)	0.6463(32)	0.7097(83)
0.06	$16^3 \times 24$	0.5921(48)	0.678(12)	1.028(49)	0.747(13)	0.823(40)
	24^4	0.5881(20)	0.6700(18)	1.003(8)	0.746(19)	0.831(10)
0.07	$16^3 \times 24$	0.6600(19)	0.7663(48)	1.116(47)	0.831(14)	0.914(48)
	24^4	0.6596(27)	0.7597(24)	1.111(6)	0.831(27)	0.918(34)

Table 2.1: Masses of the lowest-lying would-be hadrons, the pseudoscalar (π), the vector (ρ), the scalar (σ) — obtained from the quark-line connected part of the isoscalar correlator — the axial (a_1), and the nucleon (N) for bare quark masses $am = 0.01$ to 0.07 and lattice coupling $\beta_L = 3.9$. The volumes span from $16^3 \times 24$ to 32^4.

	R	b
This work	1	0
LH	1	0
LatKMI 3.7	1.054	−0.5435
LatKMI 4.0	1.193	−0.4926

Table 2.2: Values of R and b used in figure 2.12.

	$L=16$	$L=24$	$L=32$
a	5.21(20)	5.59(10)	5.63(20)
c	8.07(70)	7.1(2.0)	4.7(3.2)
k	1.20(20)	1.31(30)	1.22(70)
χ^2/dof	8.5	10	9

Table 2.3: Best-fit values of the parameters a, c, k and χ^2/dof for the fits of Lm_π to the functional form $F(x,L) = ax + c\exp(-kx)$, with $x = Lm^\delta$ and $\delta = 0.81$.

	$H=\sigma$			$H=N$		
	$L=16$	$L=24$	$L=32$	$L=16$	$L=24$	$L=32$
a	7.10(17)	7.25(10)	7.31(9)	7.8(1.4)	9.54(10)	9.56(19)
c	10.12(80)	12.2(3.4)	10.84(19.58)	14.83(2.26)	14.84(3.20)	13.49(21.02)
k	2.23(23)	2.93(48)	3.15(2.35)	0.82(41)	1.57(35)	1.93(1.84)
	$H=\rho$			$H=a_1$		
	$L=16$	$L=24$	$L=32$	$L=16$	$L=24$	$L=32$
a	4.77(17)	5.01(06)	5.08(06)	6.24(30)	6.53(12)	6.45(16)
c	9.077(76)	7.52(70)	6.1(1.1)	10.4(1.7)	13.3(5.0)	3.8(1.9)
k	1.46(20)	1.47(15)	1.57(25)	2.08(40)	2.84(66)	1.30(70)

Table 2.4: Best-fit values of the parameters a, c, k for the fits of $Lm_H, H = \sigma, N, \rho, a_1$ to the functional form $F(x,L) = ax + c\exp(-kx)$, with $x = Lm^\delta$ and $\delta = 0.81$.

am	am_π	am_ρ	am_N	am_σ	am_{a1}
0.01	$0.1343(58)(^{+599}_{-321})$	$0.1496(49)(^{+618}_{-277})$	$0.228(16)(^{+80}_{-17})$	$0.1696(51)(^{+361}_{-149})$	$0.1842(64)(^{+453}_{-176})$
0.02	$0.2353(26)(^{+271}_{-77})$	$0.2522(79)(^{+335}_{-136})$	$0.382(11)(^{+57}_{-3})$	$0.3084(27)(^{+32}_{-0})$	$0.3205(40)(^{+259}_{-0})$
0.025	$0.2903(27)(^{+184}_{-60})$	$0.3155(24)(^{+177}_{-55})$	$0.515(18)(^{+5}_{-0})$	$0.3755(76)(^{+30}_{-0})$	$0.4043(66)(^{+5}_{-0})$

Table 2.5: Values of the would-be hadron masses extrapolated to infinite volume for $am = 0.01,\ 0.02,\ 0.025$. The first uncertainty is given by the best-fit to eq. (2.24). The second uncertainty accounts for the lack of complete knowledge of $F(x,L)$, see text.

Ch.	Fit I	Fit II	Fit III
π	$\delta = 0.81(3), c_\pi = 5.7(5)$	$\delta = 0.81(1), c_\pi = 5.8(2)$	$m_0 = 0.07(3), c_\pi = 8.6(3)$
ρ	$\delta = 0.86(3), c_\rho = 7.5(6)$	$\delta = 0.86(2), c_\rho = 7.4(2)$	$m_0 = 0.06(2), c_\rho = 10.0(2)$
σ	$\delta = 0.80(6), c_\sigma = 7(1)$	$\delta = 0.81(1), c_\sigma = 7.2(2)$	$m_0 = 0.08(1), c_\sigma = 11.4(4)$
a1	$\delta = 0.87(7), c_{a1} = 10(2)$	$\delta = 0.85(2), c_{a1} = 9.0(5)$	$m_0 = 0.06(2), c_{a1} = 12.9(4)$
N	$\delta = 0.81(4), c_N = 10(1)$	$\delta = 0.81(2), c_N = 9.7(6)$	$m_0 = 0.14(3), c_N = 14.1(6)$

Table 2.6: Best-fit results for the fermion mass dependence of the would-be hadrons at $L = \infty$. Fit I is a power-law $c_H\, m^\delta$ on the range $am = 0.04$ to 0.07, Fit II is a power-law on the range $am = 0.01$ to 0.07 that includes only the first uncertainty for the three lightest masses, and Fit III is a linear fit with free intercept $m_0 + c_H m$ on the range $am = 0.01$ to 0.07. Values of the $\chi^2/d.o.f.$ are reported in the figures.

Ch.	Fit IIb		
π	$\delta = 0.81(1)$	$c_\pi = 5.71(19)$	$\chi^2/dof = 0.95$
ρ	$\delta = 0.86(1)$	$c_\rho = 7.47(23)$	$\chi^2/dof = 0.82$
σ	$\delta = 0.80(1)$	$c_\sigma = 7.08(24)$	$\chi^2/dof = 0.43$
a1	$\delta = 0.83(2)$	$c_{a1} = 8.43(57)$	$\chi^2/dof = 0.64$
N	$\delta = 0.81(2)$	$c_N = 9.58(46)$	$\chi^2/dof = 1.72$

Table 2.7: Fit IIb is Fit II of table 2.6 where the second (symmetrized) uncertainty for $am = 0.01, 0.02$ and 0.025 is added in quadrature to the first one in table 2.5.

	c_π	b_π	c_ρ	b_ρ
This work	5.7(5)	0	5.13(26)	0.52(12)
LatKMI 3.7	5.408(86)	−0.544(16)	6.899(68)	−0.594(10)
LatKMI 4.0	4.778(64)	−0.493(14)	5.96(11)	−0.560(18)

Table 2.8: Best-fit values for two power laws eq. (2.26) for the infinite volume pseudoscalar and vector masses from this work and [13]. The exponents are fixed to $\delta = 0.81$ and $\omega = 0.23$. The value of c_π from this work is from Fit I in table 2.6.

Often these highly quantitative, demanding computations will have to precede simpler qualitative analysis in order to be certain the many traps potentially awaiting any renormalization group analysis have been avoided.

Kenneth Wilson

3

Approaching Conformality

In this chapter we study the zero-temperature line of chiral symmetry breaking phase transitions in the conformal window of fundamental $SU(N_c = 3)$ for a varying number of flavours and compare it to the finite temperature chiral symmetry breaking transitions below the conformal window. We provide a theoretical argument that the behaviour of the line of bulk transitions is consistent with a lower edge of the conformal window between $N_f = 6$ and $N_f = 8$, remarkably in agreement with perturbation theory and recent large-N arguments.

In addition, we present a theoretical analysis of the behaviour of the anomalous dimension of the scalar glueball operator $G^a_{\mu\nu}G^a_{\mu\nu}$, a probe of confinement. Once the conformal window is entered and the theory deconfines, the vacuum expectation value of this operator vanishes at the fixed point and the two-point correlator of the scalar glueball operator acquires conformal scaling with nonzero anomalous dimension γ_G. We compare the results for γ_G from perturbation theory for $n = 2, 3, 4$

loops inside the conformal window with the Veneziano limit of large-N QCD [61]. We show that γ_G, for varying N_f along the line of infrared fixed points, carries information on the nature of the endpoint and the zero temperature pre-conformal phase. We show that its agreement with perturbation theory and large-N arguments would be sufficient to exclude an ultraviolet-infrared fixed-point merging as a mechanism for the loss of conformality, such as the one presented by Kaplan et al [187].

In Quantum Chromodynamics with massless fermions conformal symmetry is lost in a highly non trivial way. One single breaking phenomenon then manifests itself in two forms: asymptotic freedom and confinement [*]. One cannot exist without the other. This concept is clear in the recently proposed solution [60] for the scalar glueball two point function in the 't Hooft limit of large-N QCD.

It has become clear that a wide class of gauge field theories arising from applying present-day AdS/CFT correspondence are fundamentally different from QCD: they cannot become QCD through perturbation of the conformal field theory in the ultraviolet nor in the infrared. The family of theories called the conformal window falls into this category, living, in the continuum, at a non-trivial infrared fixed point (IRFP) and being separated from QCD or supersymmetric-QCD (SQCD) by a phase transition in the parameter N_f, where N_f varies on a continuum of values, whose nature has yet to be established.

We are likely to learn more about the deep differences between confining and conformal gauge theories and the applicability of the AdS/CFT correspondence by better understanding which mechanism(s) separate the conformal window from QCD and SQCD; as a byproduct, we may hope to shed light on the detailed consequences of removing supersymmetry.

The strategy of this study is motivated by the observation that most quantities will plausibly evolve in a nonsingular way from the conformal to the confining phase, rendering the determination of the endpoint numerically uncertain if not corroborated by the signature of a phase transition. We attempt to establish to what extent the emergence of the conformal window realises the predictions of perturbation theory or the implications of large-N arguments. We combine the use of observables sensitive to chiral symmetry and observables sensitive to confinement as a way to understand the interplay of confinement and chiral symmetry breaking at the lower edge of the conformal window. A numerical determination of the lower edge of the conformal window of QCD is also one way to establish how far large-N QCD or perturbation theory to a given loop order are from the complete

[*] which is understood, in this context, as the existence of a mass-gap, i.e., a non-zero glueball mass in quenched QCD

theory.

3.1 Numerical Setup

We have generated configurations of $SU(N_c = 3)$ gauge theories with $N_f = 4, 6, 7, 8, 9, 10, 11$ and 12 flavours of staggered fermions in the fundamental representation using the MILC code implementation of the tree level Symanzik improved gauge action and the Naik improved fermion action. This represents the same choice of gauge and fermion actions as in the work presented in the previous chapter, shown in Equation 2.13 and Equation 2.14. The simulations were conducted at a fixed quark bare mass $am = 0.01$. For $N_f = 7, 8, 9, 10, 11$, we have performed zero temperature simulations at volume $12^3 \times 24$. For $N_f = 4, 6, 7, 8$ zero temperature simulations were performed at volume $16^3 \times 32$. In addition, we have performed finite temperature simulations at volumes $24^3 \times 6$ and $24^3 \times 12$ for $N_f = 4, 6$ and 8. For $N_f = 4$, an extra finite temperature volume $24^3 \times 8$ was also simulated.

We are interested in exploring properties of the system related to chiral symmetry and confinement. The main observables for the study of chiral symmetry are the chiral condensate (its order parameter), the chiral susceptibilities and the chiral cumulant. These have been introduced in Section 1.2 of this thesis.

Another observable of interest in this study is the Polyakov Loop,

$$L = \frac{1}{N_c N_s^3} \sum_x \mathrm{Re} \left\langle \mathrm{Tr}_c \prod_{t=1}^{N_t} U_{4,tx} \right\rangle . \tag{3.1}$$

Here Tr_c is the trace in colour space and $U_{4,tx}$ is the temporal link variable. As explained in Section 0.1.3, the Polyakov Loop is a probe of confinement. Here we recall the caveat that the centre symmetry for dynamical fermions is only realised in an approximate way, and the Polyakov loop therefore is an approximate order parameter for the deconfinement transition.

For each set of N_f and volume, we have simulated the theory for a set of values of the coupling spanning the region where a (sharp) crossover of the chiral symmetry order parameter (the chiral condensate) takes place. As the time of writing of this volume, a finite size scaling study of the disconnected susceptibility and the other observables is ongoing to discriminate between a first order phase transition or a crossover at this mass, a study analogous to the one conducted for T_c of real

world QCD. We are also performing finite temperature simulations at increased aspect ratio N_s/N_t for $N_t = 12$ in order to obtain sharper transitions signals (see Discussion in Section 3.2).

3.2 Results

Now we present the results for the measured observables discussed above for the simulated ensembles with the various values of N_f under study. We start with a presentation of the finite temperature and zero temperature runs for the theories with $N_f = 4$ and $N_f = 6$. These are followed by the results for the $N_f = 8$ case. Finally, we present the results for the remaining values of N_f.

For the $N_f = 4$ and $N_f = 6$, we also show the absolute value of the numerical derivative of the chiral cumulant R_π, labelled in the figures as dR_π. These have been obtained by simple differences ratios and then smoothed by a locally weighted polynomial regression. The peak location of dR_π helps identifying the location of the chiral symmetry breaking transition (or crossover). In theories with fundamental fermions the chiral symmetry breaking and confining transition are intertwined. This, however, does not necessarily implies that the location of both transitions coincide. In our results, we have observed, in general, a good agreement between the peak of dR_π and the point where the Polyakov loop onsets. The ongoing finite size scaling study of the disconnected susceptibility might reveal new aspects of this observation.

3.2.1 Results for $N_f = 4$ and 6

We start this section reporting on the results for theories with $N_f = 4$ and $N_f = 6$. First, we show a summary of the results for the chiral condensate and the chiral cumulant for all the simulated volumes. This will be followed by a more detailed presentation of all the observables for each ensemble, separated in two parts: we start with a presentation of the finite temperature volumes $24 \times N_t$, for $N_t = 6, 8, 12$. These have been obtained through a study analogous in spirit to the work by Miura et al.[236]. This is followed by a discussion of the results for the zero temperature ensembles. We conclude with a 2−loop asymptotic scaling analysis.

Figure 3.1 summarises the results of the chiral condensate and the chiral connected cumulant, for $N_f = 4$. The chiral condensate (Figure 3.1, left) exhibits a clear sharp change of slope at the smallest N_t, and the signal becomes smoother as N_t is increased, as expected. The same observation holds true for the cumulant R_π (Figure 3.1, right), as it goes from zero, at strong coupling, to its unity saturation

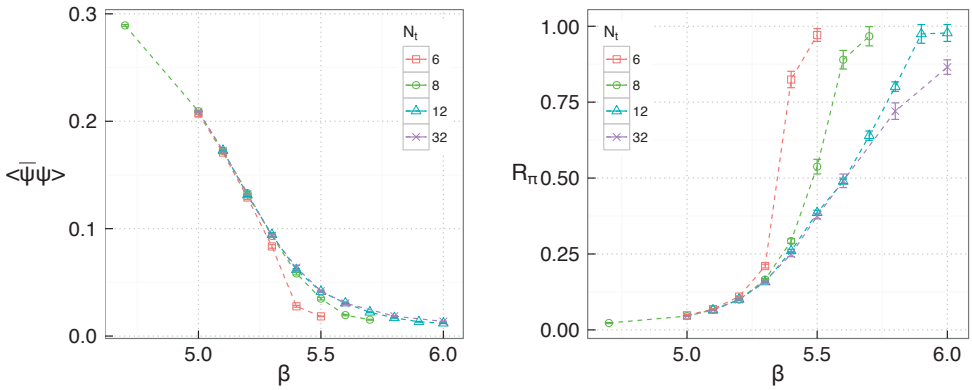

Figure 3.1: Summary of the results on the chiral condensate and the chiral connected cumulant measured on the $N_f = 4$ ensembles for four different volumes: $24^3 \times 6$ (red squares), $24^3 \times 8$ (green circles), $24^3 \times 12$ (blue triangles) and $16^3 \times 32$ (purple crosses).

value at weak couplings.

Let us now look in detail into the results at each volume in order to properly locate the transitions in each system. Figure 3.2 presents a more detailed view of the results for the $N_f = 4$ ensembles with volumes $24^3 \times N_t$, for $N_t = 6$ (top), 8 (centre), and 12 (bottom). The results for $N_f = 4$ with volume $24^3 \times 6$ possesses a series of clear signals related to the transition (or sharp crossover), all taking place between $\beta = 5.3$ and $\beta = 5.4$. First, in this region the chiral condensate has its largest, sharp, variation. Secondly, this region also marks the onset of the real part of the Polyakov loop (here understood as a drastic increase in its value). Finally, it contains a peak of the chiral connected susceptibility and the maximum variation of the chiral cumulant. The clear sharpness of the observed crossovers in the observables for coinciding β allows us to directly identify the critical coupling as the midpoint of the sharp crossovers: $\beta_c = 5.35 \pm 0.05$.

For increasing N_t with fixed N_s, the smaller aspect ratio N_s/N_t contributes to smoothing the signal of the transition, as it should be, making it harder to determine its location. For volume $24^3 \times 8$ it is hard to determine the location of the transition from the chiral condensate. The other observables, however, present clearer signals: the maximum variation of R_π is observed between $\beta = 5.5$ and $\beta = 5.6$, indicated by the peak in the derivative of R_π. The connected susceptibility has a peak at $\beta = 5.5$ and the onset of the real part of the Polyakov occurs place between $\beta = 5.4$ and $\beta = 5.6$. Combining this evidence, we estimate the transition to take place at $\beta = 5.5 \pm 0.1$, so that the region contains all three signals.

The signals are further smoothed at volume $24^3 \times 12$, especially the chiral condensate and chiral

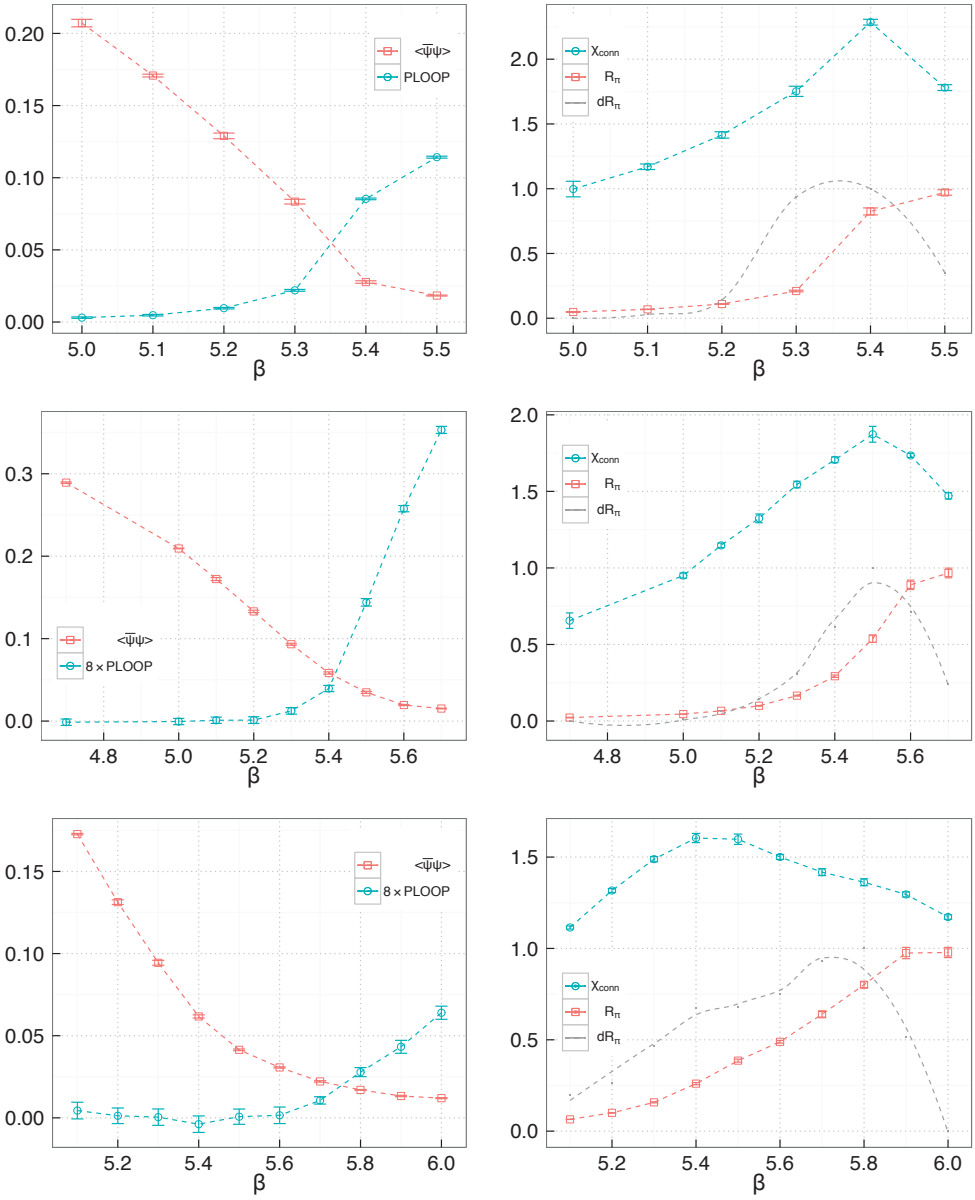

Figure 3.2: Measured observables for the $N_f = 4$ theory with $V = 24^3 \times 6$ (top), $24^3 \times 8$ (centre) and $24^3 \times 12$ (bottom): the chiral condensate and Polyakov Loop (left) and the connected susceptibility and associated chiral connected cumulant (right). The Polyakov loop has been rescaled in some cases in order to make the visualisation easier.

connected susceptibility. The maximum variation of the chiral cumulant happens between $\beta = 5.7$ and $\beta = 5.8$, as can be seen from the peak of its derivative. The real part of the Polyakov loop also onsets between $\beta = 5.7$ and $\beta = 5.8$. The connected susceptibility exhibits an odd behaviour, with a broad structure that resembles a peak at a smaller $\beta \sim 5.5$. The simulations being performed with larger N_s/N_t should help clarify this issue. Taking into consideration all of these uncertainties, we estimate the transition for this system to happen at $\beta = 5.75 \pm 0.15$.

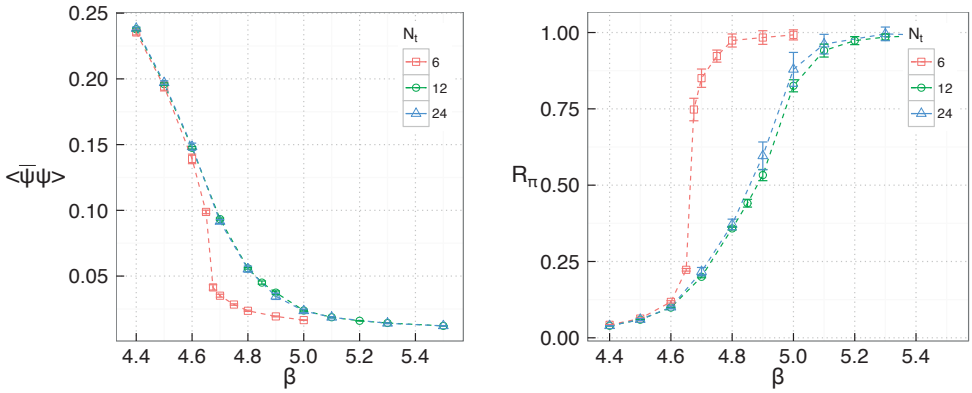

Figure 3.3: Summary of the results on the chiral condensate and the chiral connected cumulant measured on the $N_f = 6$ ensembles for three different volumes: $24^3 \times 6$ (red squares), $24^3 \times 12$ (green circles) and $12^3 \times 24$ (blue triangles).

Now, let us turn our attention to the theory with $N_f = 6$. Figure 3.3 shows a summary of the chiral condensate and of the chiral cumulant results for the three volumes simulated. Figure 3.4 contains the results for the four observables of interest and for all the finite temperature volumes simulated.

At volume $24^3 \times 6$ (Figure 3.4 top), the chiral condensate presents a clear sharp crossover between $\beta = 4.65$ and $\beta = 4.675$. This is the same location at which the onset of the real part of the Polyakov loop takes place, also via a sharp crossover. This is also the region where the chiral connected susceptibility has a (sharp) maximum and where the chiral cumulant has a clear sharp variation. In analogous fashion to that used in the $N_f = 4$ case with $N_t = 6$, we identify the location of the transition as the midpoint of the sharp crossovers: $\beta_c = 4.6625 \pm 0.0125$.

At volume 24×12 (Figure 3.4 bottom), the beta dependence of the chiral condensate is smoother with respect to the $N_t = 6$ case, for the same reasons already pointed out for $N_f = 4$. The chiral connected susceptibility has a broader maximum, and starts decreasing around $\beta = 5.0$. It is in the region between $\beta = 4.9$ and $\beta = 5.0$ that the chiral cumulant exhibits its largest derivative.

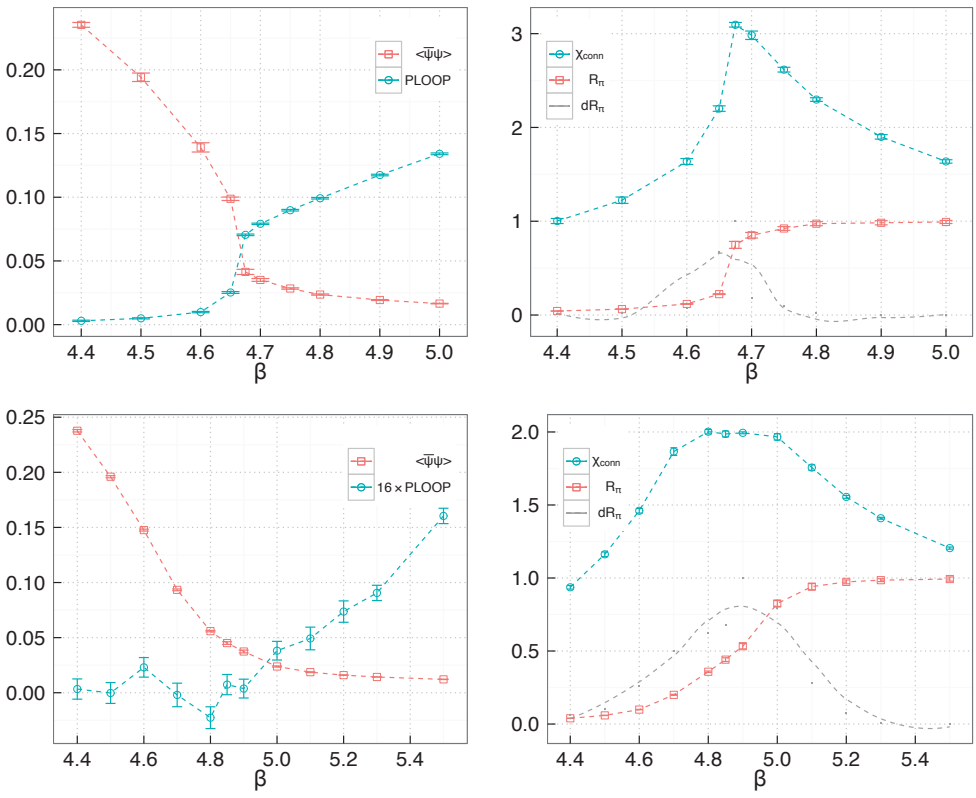

Figure 3.4: Measured observables for the $N_f = 6$ theory with $V = 24^3 \times 6$ (top), $V = 24^3 \times 12$ (bottom): the chiral condensate and Polyakov Loop (left) and the connected susceptibility and associated chiral connected cumulant (right). The Polyakov loop has been rescaled in some cases in order to make the visualisation easier.

This interval also marks the onset of the real part of the Polyakov Loop. Taking all these signals into consideration, we estimate the critical coupling at $\beta_c = 4.95 \pm 0.1$.

The results presented above suggest the occurrence of a thermal phase transition (or sharp crossover) in the $N_f = 4$ and $N_f = 6$ systems. In order to confirm this behaviour, we perform a $2-$loop asymptotic scaling analysis to verify that we are indeed measuring a critical temperature for the systems in the continuum. Integrating the beta function in Equation 24 up to $2-$loops, we obtain the well-known $2-$loop asymptotic scaling relation,

$$R(g_L) \equiv a(g_L)\Lambda_L = (\beta_0 g_L^2)^{\beta_1/(2\beta_0^2)} \exp\left[\frac{-1}{2\beta_0 g_L^2}\right], \tag{3.2}$$

where β_0 and β_1 are the universal one- and two-loop coefficients in Equation 25, Λ_L is the lattice Lambda-parameter and the coupling g_L is the coupling in the lattice regularisation, connected to the lattice parameter β through the relation $\beta = 10/g_L^2$. An improved coupling will be later considered inside the same asymptotic scaling formula in Equation 3.2.

The critical temperature of the transition is defined in terms of the lattice temporal extent N_t and the lattice spacing $a(g_L^c)$ as

$$T_c = \frac{1}{a(g_L^c)N_t}. \tag{3.3}$$

Inserting the definition of $R(g_L)$ of Equation 3.2 into Equation 3.3, we arrive at the relation,

$$R(g_L^c)\, N_t = \left(\frac{T_c}{\Lambda_L}\right)^{-1} = \text{constant}, \tag{3.4}$$

i.e., the critical coupling g_L^c rescales, so that simulations performed at different values of N_t yield the same physical critical temperature T_c, if such temperature exists. The left-hand side of Equation 3.4 can be obtained by plugging into $R(g_L)$ the critical coupling β_c measured from lattice simulations at one given N_t and numerically determines the value of $(T_c/\Lambda_L)^{-1}$. The β_c at different N_t should follow the asymptotic scaling curve $R(g)$ provided the lattice results are in the scaling region. However, due to the increasing presence of lattice artefacts as the lattice spacing grows, agreement with the asymptotic scaling relation to a given loop order in perturbation theory is expected to diminish for decreasing N_t.

With that in mind, for each value of N_f, we first insert into Equation 3.4 the critical coupling obtained at lattice volumes with the largest temporal extent, i.e., $N_t = 12$ and check for the agreement

between the resulting scaling curve and the measured values for smaller N_t. The results are presented in Figure 3.5 (blue points) and Figure 3.6 (blue curves), where it is possible to note a disagreement between the lattice data and the two-loop scaling curve. This does not come as a surprise. The bare lattice coupling is known to provide a poor expansion parameter for the perturbative asymptotic scaling relation. In addition, it is a priori not given, – especially close to the conformal window – that two-loop asymptotic scaling is all we need to describe the running coupling (in a given renormalisation group scheme).

There are two possible sources of corrections to the scaling in Equation 3.2: missing higher order contributions in perturbation theory and corrections due to the finiteness of the lattice spacing. Allton [11] presented a general form for the asymptotic scaling formula taking into consideration these corrections:

$$a^{-1}(g_L) = \frac{\Lambda_{RG}}{R(g^2_{RG})} \times \left(1 + \sum_{l=l_0} d_{l-1} g^{2l-4}_{RG}\right)^{-1} \times \left(1 + \sum_{n=1} c_n(g^2_{RG}) R^n(g^2_{RG})\right). \qquad (3.5)$$

Here, the coefficients d_i account for the corrections coming from perturbation theory and the c_i coefficients for the corrections due to the finite the lattice spacing. The coupling g_{RG} used in this formula (and its corresponding asymptotic scale Λ_{RG}) is defined in some renormalisation group scheme (not necessarily the coupling g_L in the lattice regularisation) and it should be appropriately related to the lattice coupling g_L. The aim of the improvement is to find a coupling for which the perturbative expansion has an improved convergence. As noted by Lepage and Mackenzie [205], the key problem is in the choice of the expansion parameter for the perturbation theory: g_L is typically a very poor choice, since it ignores the possibility of a large scale-dependent renormalisation of the bare coupling (see below). Therefore, in order to reconcile lattice results with perturbation theory, g_L should better be replaced by some renormalised coupling.

There are some possible strategy choices starting from Equation 3.5. One can set $d_i = 0$ while keeping the corrections due to the finite lattice spacing. This strategy is known as *lattice distorted perturbation theory*. The alternative with $c_n = 0$ relies on renormalised perturbation theory and neglects distortions due to the finiteness of the lattice spacing. In addition, one can consider non-zero d_i and c_i contributions.

It was also noted [205] that tadpole contributions coming from higher order terms in the expansion of the lattice link variables defined in Equation 42 spoil our intuition about the connection between

lattice operators and the continuum. The convergence of the perturbative expansion can then be improved by tadpole improving the lattice coupling, which amounts to replacing

$$g_L^2 \to \frac{g_L^2}{\langle (1/3)\,\mathrm{Tr}\, U_{\mathrm{Plaq}} \rangle} = \frac{g_L^2}{u_0^4}, \tag{3.6}$$

where the denominator uses the plaquette operator U_{Plaq} measured for the zero temperature system at g_L and defines the tadpole parameter u_0. A related strategy is to use the E-scheme coupling[226], defined by

$$g_E^{-2} = \frac{1/3}{1 - \langle (1/3)\,\mathrm{Tr}\, U_{\mathrm{Plaq}} \rangle}. \tag{3.7}$$

In the following, we examine our data following the prescription of lattice distorted perturbation theory, i.e., we set $d_i = 0$, keep R(g) to two loops, use the coupling of the lattice regularisation $g_{RG} = g_L$ and allow for non-zero c_i corrections. A study of the other possible strategies described above is ongoing and will be presented in future work.

Considering $d_i = 0$ in Equation 3.5, Equation 3.2 can be rewritten in terms of an improved function $R(\beta_L)$ as follows

$$R^{\mathrm{imp}}(\beta_L) = \Lambda_L^{\mathrm{imp}}\, a(\beta_L) \equiv \frac{R(\beta_L)}{1+h} \times \left[1 + h\,\frac{R^2(\beta_L)}{R^2(\beta_{\mathrm{ref}})}\right], \tag{3.8}$$

where the reference coupling β_{ref} can be arbitrarily set and the h parameter is adjusted to minimise scaling violations. The limit $h \to 0$ recovers the unimproved scaling relation in Equation 3.2.

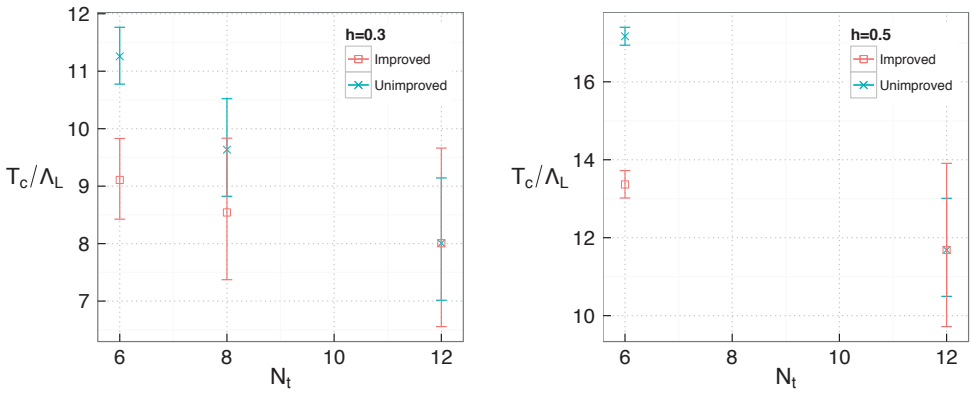

Figure 3.5: The ratio T_c/Λ_L in the lattice scheme for $N_f = 4$ (left) and $N_f = 6$ (right). Results are presented with (red squares) and without (blue diagonal crosses) improvement[11]. The improved results were obtained using the parameters $\beta_{\mathrm{ref}} = \beta_c(N_t = 12)$ and $h = 0.3$ for the $N_f = 4$ case and $h = 0.5$ for the $N_f = 6$ case.

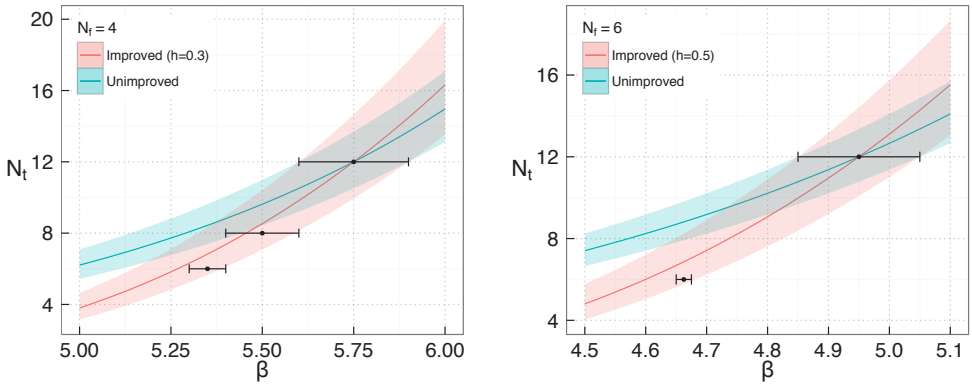

Figure 3.6: Perturbative 2—loop asymptotic scaling study for the $N_f = 4$ (left) and $N_f = 6$ (right) theories. In both cases, we have used the estimated critical couplings obtained for $N_t = 12$ and Equation 3.4 to predict the scaling curve (black and dashed line). The blue error band was estimated from the predicted scaling curves for the extreme values of the error for the critical couplings at $N_t = 12$. Agreement of the critical couplings with the predicted line is expected to increase as N_t grows and the lattice spacing diminishes.

In Figure 3.5 (red points) and Figure 3.6 (red curves), we present results for the improved scaling. The reference coupling β_{ref} was adjusted to match the results at $N_t = 12$. The improvement visibly ameliorates the agreement between lattice data and the scaling curves but, specially for the $N_f = 6$ case, requires a rather large value of the parameter h. The increase of h from $N_f = 4$ to $N_f = 6$ is, however, consistent with the fact that the latter theory has a lower critical temperature, implying larger lattice spacing corrections.

Two additional aspects must be taken into consideration: the first are finite mass effects. The asymptotic scaling as described above is valid in the massless limit. We have, however, used it to analyse results obtained with a finite bare quark mass $am = 0.01$. In doing so, we have assumed that the shift of the (pseudo) critical couplings by the non-zero mass is smaller than other errors. A verification of this assumption requires an extrapolation to the chiral limit in future works.

It is also very plausible that our data actually reflects the fact that contributions to the beta function beyond two loops become increasingly relevant at $N_f = 6$, close to the lower edge of the conformal window. In this case, the data would be better described by a four-loop asymptotic scaling relation. In Section 3.4 we will explore the differences in the zeros of the two-loop and four-loop beta functions.

We now turn to the analysis of the zero temperature volumes simulated for $N_f = 4$ and $N_f = 6$. The results are presented in Figure 3.7.

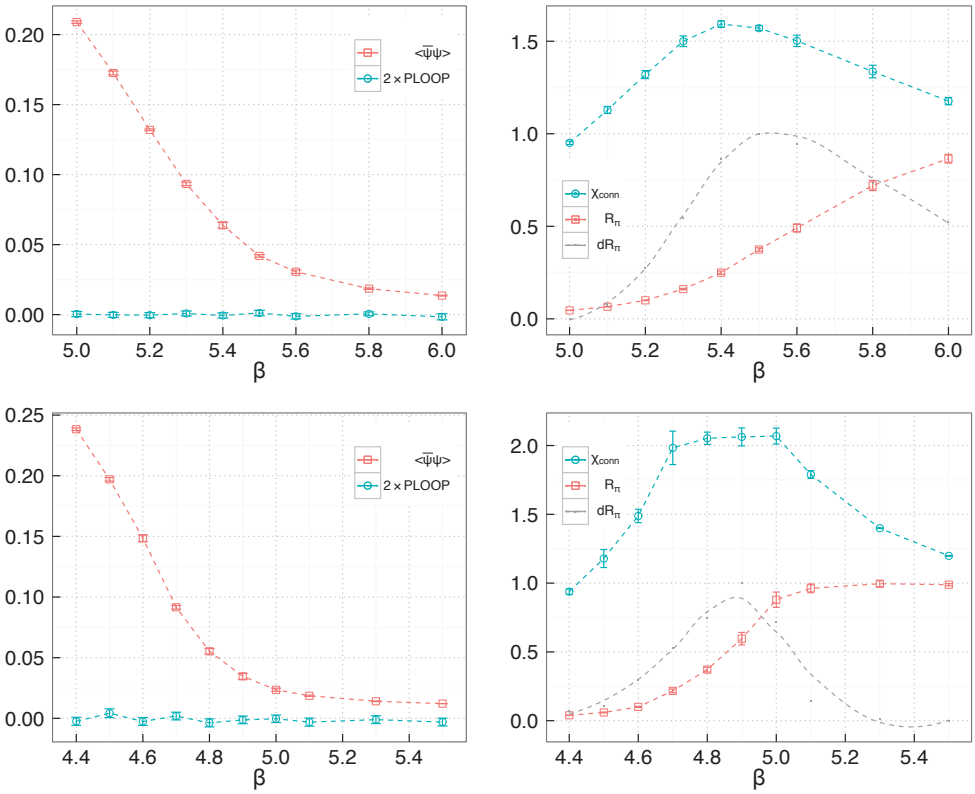

Figure 3.7: Measured observables for the $N_f = 4$ theory at $V = 16^3 \times 32$ (top) and the $N_f = 6$ theory at $V = 12^3 \times 24$ (bottom): the chiral condensate and Polyakov Loop (left) and the connected susceptibility and associated chiral connected cumulant (right). The Polyakov loop has been rescaled in some cases in order to make the visualisation easier.

It is clear from Figures 3.1, 3.3 and 3.7 that the chiral condensate and chiral cumulant results for the zero temperature volumes closely follow those of volumes $24^3 \times 12$ for the same N_f. One crucial difference, however, is expected between the two cases: at finite temperature, true chiral symmetry breaking and deconfining transitions should take place. These should be absent at zero temperature below the conformal window, where chiral symmetry is already broken and the system is already confined at zero temperature. This means that the decrease in the chiral condensate observed at the zero temperature volumes should not indicate a true transition. One strong evidence of this fact is provided by the behaviour of the Polyakov loop: while it has a clear onset at the transition at finite temperature, it remains zero all along the simulated range of couplings at the zero temperature volumes.

It is, however, a well known fact that the signal of the Polyakov loop tends to be statistically weak for a small number of measurements. One way to overcome this and gain a better understanding of its behaviour is by looking at its phase distribution: while it is symmetrically distributed on the interval $[-\pi/2, \pi/2]$ in the complex plane for confining configurations, if fermions are present in a deconfined system it will tend towards the real phase of its $Z(3)$ centre.

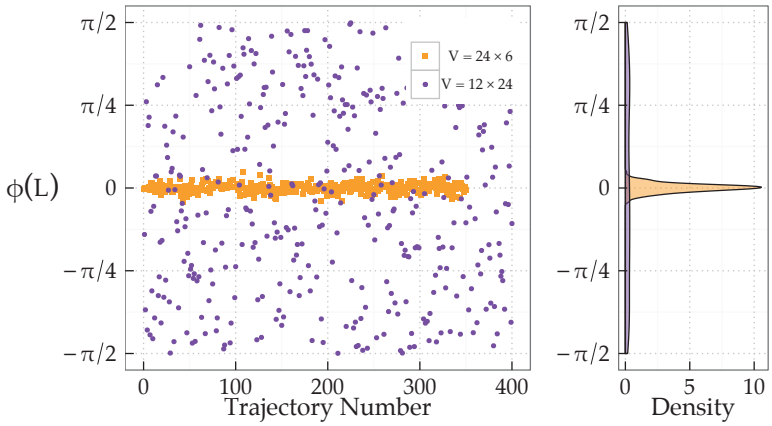

Figure 3.8: Monte Carlo history and its distribution for $N_f = 6$ with $V = 24^3 \times 6, \beta = 5.0$ (orange squares) and $V = 12^3 \times 24, \beta = 5.5$. These correspond to the weakest coupling ensembles at each volume for $N_f = 6$. The distribution flattens around zero for the finite temperature ensemble, where the system is deconfined, and is randomly distributed between $-\pi/2$ and $\pi/2$ in the zero temperature case, confined below the conformal window.

In Figure 3.8 we present the phase $\varphi(L)$ distribution for the $N_f = 6$ ensembles with $V = 24^3 \times 6$ (finite temperature) and $V = 12^3 \times 24$ (zero temperature). The observed behaviour is evidence that indeed the zero temperature ensembles remain confined at weak couplings: note the normal distri-

bution of the Polyakov loop phase around zero for the $V = 24^3 \times 6$ ensemble and the contrasting distribution between $-\pi/2$ and $\pi/2$ for the $V = 12^3 \times 24$ ensemble.

3.2.2 Results for $N_f = 8$

We now analyse the results for the $N_f = 8$ system. A summary of the results for the chiral condensate and the chiral connected cumulant is presented in Figure 3.9 and the results for the four observables of interest in Figure 3.10.

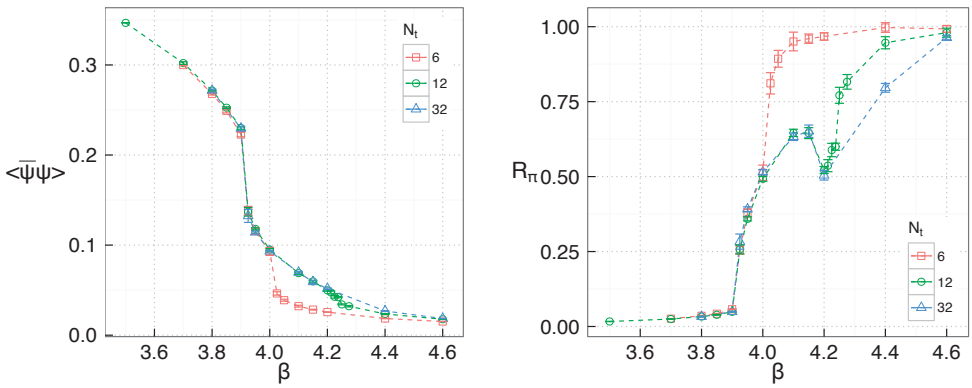

Figure 3.9: Summary of the results on the chiral condensate and the chiral connected cumulant measured on the $N_f = 8$ ensembles for three different volumes: $24^3 \times 6$ (red squares), $24^3 \times 12$ (green circles) and $16^3 \times 32$ (blue triangles).

Two striking differences are present in the results for this theory with respect to the $N_f = 4, 6$ theories discussed before: firstly, note the coincidence of the very sharp and larger crossovers in the chiral condensate evolution for all the volumes (and N_t values) simulated – i.e. finite and zero temperature results nicely overlap (N_t-independence); secondly, note the existence of a second, smaller and N_t-dependent up to a certain N_t, sharp crossover of the chiral condensate at weaker coupling. These evidences point to the existence of a true bulk transition at stronger coupling, followed by the emergence, at weaker coupling, of the exotic phase, the genuine lattice artefact previously observed for $N_f = 12$[114,83] and studied in detail in Chapter 1 of this thesis. In fact, the behaviour of the crossovers observed in Figure 3.10 (left) and detailed above match those observed for $N_f = 12$. Note, also, the existence of a *dip* in the chiral cumulant coinciding with the location of the weak coupling edge of the exotic phase, again in agreement with the observed behaviour for $N_f = 12$.

The results for the Polyakov loop and for the connected susceptibility are presented in Figure 3.10

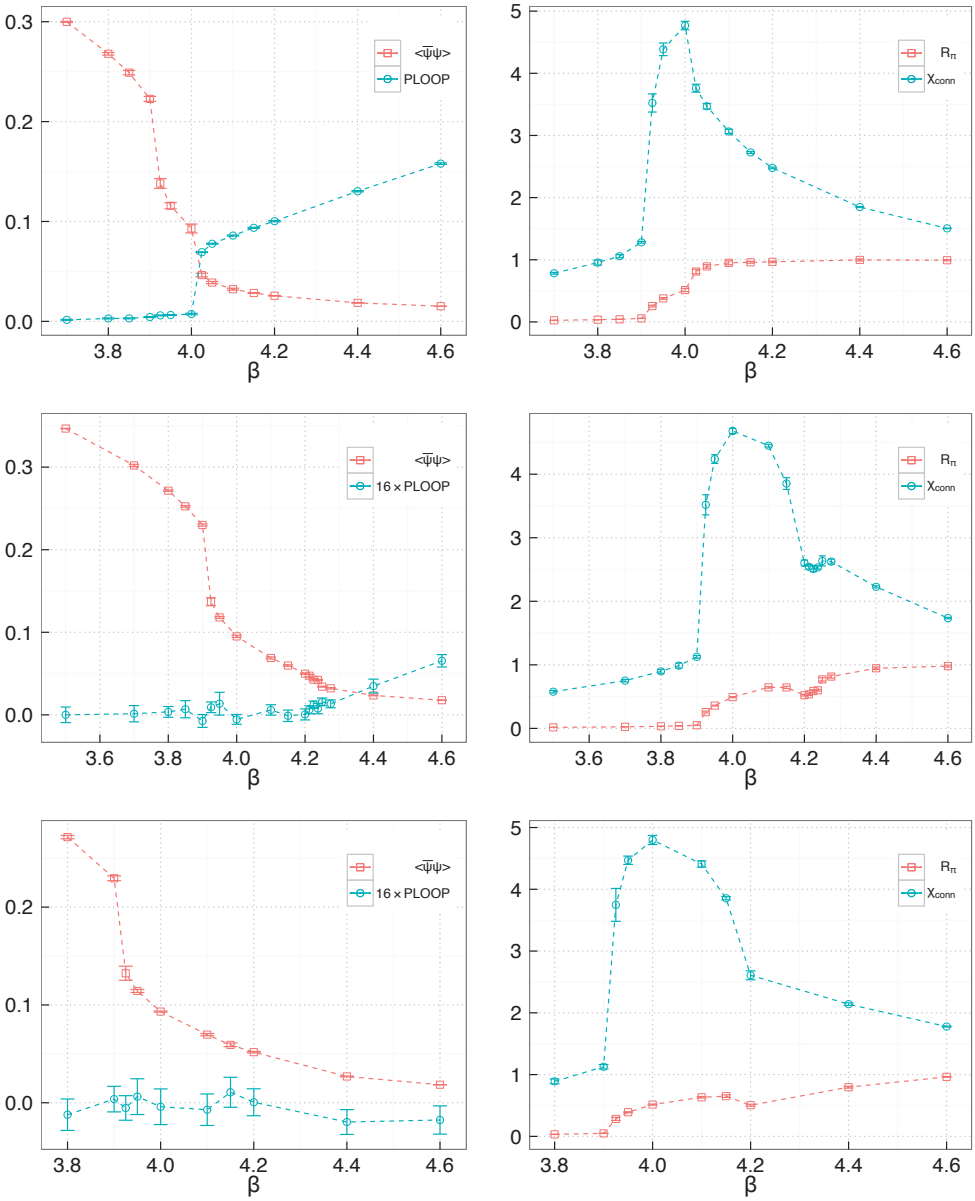

Figure 3.10: Measured observables for the $N_f = 8$ theory at $V = 24^3 \times 6$ (top), $V = 24^3 \times 12$ (centre) and $V = 16^3 \times 32$ (bottom): the chiral condensate and Polyakov Loop (left) and the connected susceptibility and associated chiral connected cumulant (right). The Polyakov loop has been rescaled in some cases in order to make the visualisation easier.

(right). The emergence of the real part of the Polyakov Loop coincides with the weak coupling crossover for the finite temperature volumes simulated. Contrary to our expectations, for the zero temperature volume the real part of the Polyakov Loop remains zero, analogously to the $N_f = 4$ and $N_f = 6$ cases. We attribute the lack of signal to the low statistics for this large volume. As of the time of writing of this thesis, we are also implementing a renormalisation group blocking of the Polyakov Loop in order to improve the signal. Note, also, that the exotic phase is present, and its lower edge for the volume $16^3 \times 32$ seems to be located at $\beta_c = 4.2$, as indicated by the chiral connected susceptibility and the chiral cumulant. However, this phase has not been fully mapped out at the time of writing.

To summarise, the $N_f = 4$ and $N_f = 6$ theories behave in a very similar fashion: no exotic phase is observed at strong coupling and the critical couplings associated with the breaking of chiral symmetry exhibit a clear N_t-dependence. In sharp contrast, for the $N_f = 8$ theory the critical coupling exhibits no N_t-dependence, indicating the bulk nature of the transition. In addition, we have observed the emergence of an exotic phase at strong coupling in this theory. The behaviour of the $N_f = 8$ theory matches the behaviour observed for $N_f = 12$ and discussed in Chapter 1.

3.2.3 Results for $N_f = 7, 9, 10$ and 11

In addition to the above mentioned results, we have also measured the chiral condensate evolution for theories with $N_f = 7, 9, 10$ and 11 on our zero temperature ensembles described in Section 3.1. These are presented in Figure 3.11, in conjunction with the corresponding results for $N_f = 8$ presented above and the $N_f = 12$ results presented in previous works[114] and in Chapter 1.

The figure illustrates the sequence of sharp crossovers that nicely align to form the critical bulk line, which is depicted in Figure 3.12. For $N_f = 12, 9$ and 8 we have also mapped the edge of the chirally symmetric exotic phase, which is observed to be N_t dependent up to some N_t and disappears in the massless limit consistently with exact chiral symmetry[114]. At nonzero mass, it is a useful discriminator on the lattice of theories inside and outside the conformal window.

We conclude this section by noting that throughout this study, we have not observed an anomalous behaviour that could hint at consequences of the fourth-root of the fermion determinant for staggered lattice fermions. Such anomalous behaviour would affect all N_f values not multiples of four, for which the fourth-root has to be taken.

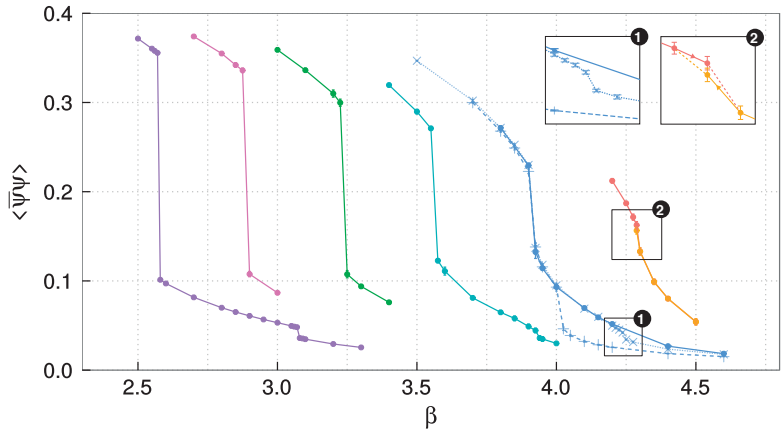

Figure 3.11: Sequence of sharp crossovers of the chiral condensate for $N_f = 12$ to 7 (left to right). Data for $N_f = 12$ from [114], $N_f = 11,\ 10,\ 9$ with volume $12^3 \times 24$, $N_f = 8$ with volumes $16^3 \times 32$ and $24^3 \times N_t = 6, 12$, and $N_f = 7$ with volume $16^3 \times 32$, all at bare lattice mass $am = 0.01$. Exotic phase displayed for $N_f = 12,\ 9$ and $N_f = 8$, $N_t = 6$. Enlarged view (top right) shows data for two branches of possible hysteresis loop for $N_f = 7$.

3.3 Discussion of the lattice results

The main result of this work is summarised in Figure 3.12: we have used the results presented above to numerically map the line of zero-temperature (bulk) chiral symmetry breaking phase transitions for $N_f \leq 12$, aiming to identify the critical number of flavors N_f^c that signals the disappearance of the conformal window. The best fit to the data for $N_f \geq 8$ is linear in β. An extrapolation of the line up to $N_f = 16$, obtaining $\beta_c \sim 1.2$ consistent with previous studies [114] and † carried out with different actions and heavier fermions.

The critical coupling g_c line as a function of N_f should manifest the fact that fermion screening is increasingly effective for increasing N_f. This N_f dependence is a leading order effect separating two phases with different symmetries for $N_f \geq N_f^c$, different in nature from the subleading N_f dependence carried by genuine lattice artefacts possibly occurring within the chirally broken phase at $N_f < N_f^c$ on coarse lattices. The critical bulk line should flatten at N_f^c in the massless limit, as sketched in Figure 3.12; this is its only possible fate if the conformal window exists and given its nature of phase transition separating a chirally broken and a chirally symmetric region in the plane $Nf{-}1/beta$. This line is the $N_t = 1/(aT) \to \infty$ limit of an N_t-finite family of thermal phase transitions that exists for all $N_f > 0$.

To illustrate this and provide a determination of N_f^c we also show in Figure 3.12 the location of

†The transition occurs at $\beta_c = 1.675 \pm 0.025$ at $am = 0.025$, same action (unpublished).

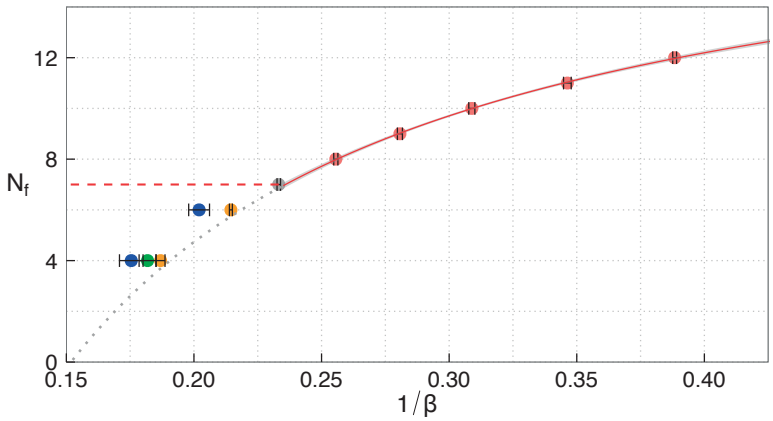

Figure 3.12: Lattice phase diagram $N_f - 1/\beta, \beta$ the inverse squared lattice coupling. Data points for $N_f = 7, \ldots, 12$ are midpoints of sharp crossovers in Figure 3.11. Best fit to data (solid red line) is linear in β and extrapolated down to $N_f = 4$ (dotted grey). Flattening of bulk line at endpoint is sketched (dashed red); chiral symmetry is broken below the line. Thermal transitions for $Nf = 4, 6$ occur away from the bulk line, at weaker coupling, with volumes $24^3 \times N_t$ for $N_t = 6$ (orange), 8 (green) and 12 (blue).

the thermal phase transitions for varying $N_t < N_l$, with spatial volume $L = aN_l$, for the $N_f = 6$ and $N_f = 4$ theories, as reported in the previous section. For theories below the conformal window, where chiral symmetry restoration occurs at a critical temperature T_c, the locations move to weaker coupling for increasing N_t.

Figure 3.12 also shows that already at the smallest $N_t = 6$ the transitions occur at a coupling weaker than the one predicted by the linear in β extrapolation of the bulk line. At the same time, no zero-temperature phase transition occurs for $N_f = 6,\ 4$ along the extrapolated line, nor it is observed at weaker coupling: the main discriminator between the finite-temperature $N_f = 4, 6$ systems with $N_t = 12$ and mass $am = 0.01$ and the same systems at zero temperature (volume $12^3 \times 24$) is the Polyakov loop; only the finite temperature system undergoes a change from zero of the real part of the Polyakov loop, signalling deconfinement. The quality of this signal should improve once we conclude the simulations at larger aspect ratio N_s/N_t for $N_t < N_s$ and the measurements of the disconnected susceptibility currently being performed as of the time of writing. The observed behaviour is consistent with the fact that chiral symmetry is all the way broken for these systems at zero temperature. The behaviour of the $N_f = 4, 6$ systems has to be contrasted with the one of the $N_f = 8$ system, for which we have carried out the same study.

Figure 3.13 displays the differences between the $N_f = 8$ and $N_f = 6$ systems. The chiral condensate, the connected chiral cumulant and the real part of the Polyakov loop are shown for the $N_t = 6$

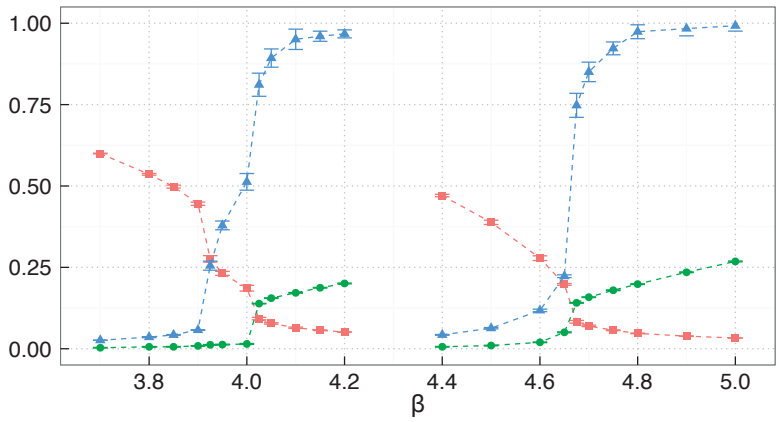

Figure 3.13: Chiral condensate, (connected) R_π and (rescaled) Polyakov loop for $N_f = 8$ and $N_f = 6, 24^3 \times 6$, $am = 0.01$. Points in Figure 3.12 correspond to the combined observation of the maximum derivative of the chiral condensate, of R_π and, when appropriate, of the Polyakov loop.

case. Notable differences are:

- $N_f = 6$ exhibits no exotic phase, while $N_f = 8$ does. The weak coupling edge of the exotic phase is signalled by a second jump in the chiral condensate and a dip in R_π, see also [114]
- The Polyakov loop becomes nonzero at the thermal transition for $N_f = 6$, signalling the onset of the high-temperature deconfined phase. For $N_f = 8$ it only becomes nonzero at the edge of the exotic phase, where the system is deconfined and chiral symmetry exact. Finally, $N_f = 6$ behaves as $N_f = 4$.

The most striking result of the study in this chapter is the extension of the bulk line in Figure 3.12, and therefore the conformal window, below $N_f = 8$. The fate of $N_f = 7$ is less certain at this stage: though we observe a reduced crossover, an almost closing gap, and signs of hysteresis in the interval $\beta = [4.275, 4.3]$ right on the bulk line a study analogous to $N_f = 8,\ 6$, possibly at a lighter fermion mass, is likely to clarify the situation. These results also clearly suggest that the $N_f = 6$ theory is located below the conformal window. The sharp crossovers in Figure 3.13 do not leave space for a behaviour analogous to $N_f = 8$ at a lower mass.

In Figure 3.14 we present the transition observed by Deuzeman et al. [116] for $N_f = 8$ — with a different improvement of the fermion action — for the cases $N_t = 6$ (left) and $N_t = 12$ (right). The authors have interpreted the scaling of the transition location as evidence that it was a genuine thermal transition. We suspect that it may instead be the edge of the exotic phase, later on discovered by

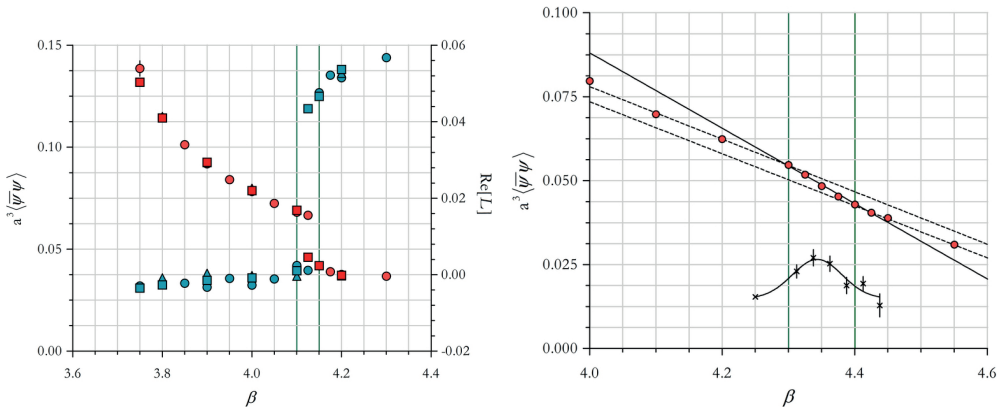

Figure 3.14: (left) Chiral condensate and Polyakov measured by Deuzeman et al. [116] for $N_f = 8$ with $N_t = 6$ and $N_s = 12$ (red circles), $N_s = 20$ (triangles) and $N_s = 24$ (squares). Results were obtained with a different improvement of the fermion action. (right) Chiral condensate presented in the same reference for $N_f = 8$ with $N_t = 12$ and $N_s = 24$.

the same authors and extensively studied [114,83,113]: note the resemblance between the results from the cited reference shown in Figure 3.14 and the exotic phase for the $N_f = 8$ theory presented in this current work in Figure 3.10 (top and centre). Note, also, that the chiral condensate in Figure 3.14 remain rather small on the strong coupling side of the crossover (both works use the same normalisation of the chiral condensate). This conclusion does not contradict the upper bounds on the chiral phase boundary in, e.g., [209,209], but it shows the delicacy of this study and how the gradual understanding of many aspects of the conformal window finally seems to lead to a consistent picture.

Interestingly, a lower edge below $N_f = 8$ and close to $N_f = 7$ is not far from the prediction of two-loop perturbation theory and intriguingly in good agreement with the large-N result $N_f/N = 5/2$, for $N = 3$ [61] and four-loop perturbation theory. It is also in agreement with the perturbatively small value of the fermion mass anomalous dimension for $N_f = 12$ [208,79], because $N_f = 12$ is not close to the lower edge of the conformal window.

3.4 The anomalous dimension of the scalar glueball operator in perturbation theory and large-N

In this section, we present a perturbative analysis of the behaviour of the anomalous dimension of the scalar glueball operator $G^a_{\mu\nu}G^a_{\mu\nu}$ across the lower edge of the conformal window. We also comment on the consequences of its behaviour for the UV-IR merging mechanism for the emergence of the conformal window proposed by Kaplan et al. [187].

It is well known that the anomalous dimension of the scalar glueball operator $G^a_{\mu\nu}G^a_{\mu\nu}$ is constrained by the trace anomaly, i.e., the nonzero contribution to the trace of the energy-momentum tensor. The trace anomaly of QCD that enters the matrix elements of renormalised gauge invariant operators is [‡]

$$T^\mu_\mu = \frac{\beta(\alpha)}{16\pi\alpha^2}\,\mathrm{Tr}(G^2) + \text{fermion mass contribution}\,, \tag{3.9}$$

with the beta-function

$$\beta(\alpha) \equiv \frac{d\alpha(\mu)}{d\ln\mu} \qquad \alpha \equiv \frac{g^2}{4\pi}\,. \tag{3.10}$$

The dimension of a quantum operator O is dictated by the scaling equation

$$\frac{dO}{d\ln\mu} = d_O O \qquad O(\mu) \sim \mu^{d_O}\,, \tag{3.11}$$

$d_O = d_c + \gamma_O$, with canonical dimension d_c and anomalous dimension γ_O. The nonrenormalisation of T^μ_μ implies that it scales classically, i.e., $d_{T^\mu_\mu} = 4$ in four dimensions, and the scaling equation (3.11) applied to Equation 3.9 gives for $\mathrm{Tr}(G^2)$

$$d_G = 4 - \beta'(\alpha) + \frac{2}{\alpha}\beta(\alpha)\,, \tag{3.12}$$

with $\beta'(\alpha)$ the derivative of the beta-function w.r.t. α. At a nontrivial stable IRFP, $\beta(\alpha_*) = 0$ and the anomalous dimension

$$\gamma_G = -\beta'(\alpha_*) \tag{3.13}$$

is a physical property of the system, renormalisation scheme independent. It is instructive to determine γ_G in perturbation theory to a given loop order inside the conformal window, and compare this result with the Veneziano limit of large-N QCD ($N \to \infty$, $N_f/N = \text{const}$)[61].

The beta function of the theory can be expressed as a series

$$\frac{d\alpha}{dt} = -2\alpha\sum_{l=1}^{\infty} b_l a^l = -2\alpha\sum_{l=1}^{\infty}\overline{b}_l\alpha^l. \tag{3.14}$$

[‡]Here we are not interested in the most general expression, which also involves gauge-fixing and EoM operators, see [24,8,93,8].

The quantity

$$a \equiv \frac{g^2}{16\pi^2} = \frac{\alpha}{4\pi} \tag{3.15}$$

is, times appropriate group invariants, the expansion parameter and l denotes the number of loops involved in the calculation of b_l and $\bar{b}_l = b_l/(4\pi)^l$.

As discussed in Chapter 0, the coefficients b_1 and b_2 in the expansion are universal[156,267,74,183] and given by

$$\begin{aligned} b_1 &= \frac{1}{3}(11C_A - 4T_f N_f) \\ b_2 &= \frac{1}{3}\left[34C_A^2 - 4(5C_A + 3C_f)T_f N_f\right]. \end{aligned} \tag{3.16}$$

Here they are written in terms of the quadratic Casimir invariants $C_f \equiv C_2(R)$ and $C_A \equiv C_2(G)$, for, respectively, the representation R to which the N_f fermions belong and the adjoint representation. The quantity $T_f \equiv T(R)$ is the trace invariant for the representation R.

Coefficients of higher order are scheme-dependent[155,154] and have been calculated up to four-loop order[302,203,304]. In Table 3.1 we list a subset of these values, for the $SU(N_c = 3)$ theory with $8 \leq N_f \leq 12$.

N_f	$\bar{b}_1$	$\bar{b}_2$	$\bar{b}_3$	$\bar{b}_4$
8	0.451	0.004	−0.213	0.015
9	0.398	−0.076	−0.303	0.025
10	0.345	−0.156	−0.386	0.072
11	0.292	−0.236	−0.463	0.154
12	0.239	−0.317	−0.534	0.273

Table 3.1: The l-loop beta function coefficients $\bar{b}_l$ defined in Equation 3.14 for the SU($N_c = 3$) gauge theory with N_f fundamental fermions.

The value α_* of the IRFP coupling can by obtained by solving $\beta_\alpha = 0$. The derivative β'_α can be expressed in terms of the coefficients b_l listed in Table 3.1 as:

$$\beta'_\alpha = -2\sum_{l=1}^{\infty}(l+1)\bar{b}_l\alpha^l \tag{3.17}$$

Adding the pieces of information above, it is then possible to calculate $\beta'_\alpha(\alpha_*)$. Note that the

N_f	$\alpha_{\mathrm{IR},2l}$	$\beta'_\alpha(\alpha_{\mathrm{IR},2l})$	$\alpha_{\mathrm{IR},3l}$	$\beta'_\alpha(\alpha_{\mathrm{IR},3l})$	$\alpha_{\mathrm{IR},4l}$	$\beta'_\alpha(\alpha_{\mathrm{IR},4l})$	$\alpha_{4l,u}$
6	–	–	12.992	84.646	–	–	–
7	–	–	2.453	5.956	–	–	–
8	–	–	1.464	2.654	1.552	1.784	14.0282
9	5.237	4.169	1.027	1.472	1.07	1.460	12.262
10	2.21	1.522	0.764	0.869	0.815	0.851	5.62
11	1.23	0.706	0.578	0.513	0.626	0.496	3.29
12	0.754	0.360	0.435	0.296	0.470	0.281	2.295

Table 3.2: The infrared zeros in α of the SU($N_c = 3$) beta function with N_f fundamental fermions at n-loop order are listed as $\alpha_{\mathrm{IR},n\,l}$ following the convention in [274]. The four-loop beta function is a cubic equation which has three zeros, one of which is negative and not listed here. The one closest to the origin is listed as$\alpha_{IR,4l}$, and the third zero, which is positive but farther from the origin, is listed as $\alpha_{4l,u}$.

zero of the beta-function is in general a necessary, but not sufficient condition for the existence of a stable IRFP. At two loops $\alpha_{\mathrm{IR},2} = -b_1/b_2$ and$\beta'(\alpha_{\mathrm{IR},2}) = -b_1^2/b_2$. The four-loop beta-function is a cubic equation with three zeros, one of which is negative [274]. The results are summarised in Table 3.2 and agree with those listed on works by Shrock [288,289] .

In all cases, the derivative $\beta'(\alpha_*)$ is positive and increases along the IRFP line for decreasing N_f. The disappearance of the zero occurs for $N_f > 8$ at two loops, while it shifts to lower N_f at three and four loops, suggesting a lower endpoint of the conformal window in the range $7 < N_f < 8$ at four loops — provided the zero can be taken as sufficient condition. At two loops the disappearance of the zero is determined by the change of sign of b_2, implying that the fixed point disappears at infinite coupling $\alpha_{\mathrm{IR},2} \to \infty$. This behaviour, however, is likely to be an artefact of the truncated perturbative expansion; the same singularity occurs in $\beta'(\alpha_{\mathrm{IR},2})$.

It is most interesting to compare these results with the implications of the exact beta-function of large-N QCD in the Veneziano limit derived by Bochicchio [61], which manifests salient analogies and differences with the exact beta-function of SQCD [249,250,286]. Writing in short the large-N QCD beta-function for the canonical 't Hooft coupling as

$$\beta(g) = \frac{g^3\, c(g)}{1 - \frac{4}{(4\pi)^2} g^2}\,, \tag{3.18}$$

the absence of supersymmetry generates a new anomalous dimension contribution, not present in SQCD, in $c(g)$. The fate of a fixed point will depends on the numerator and denominator of Equation 3.18: the pole generates a cusp in the flow of g, unless the numerator has a zero before the pole is hit — and a zero associated to an IRFP inside the conformal window must be shown to be renormalisation scheme independent. Remarkably, this has been shown to be true [61] for the large-N QCD beta-function in the Veneziano limit at the lower edge of the conformal window, identified at $N_f/N = 5/2$ where the stability of the glueball kinetic term is lost.

Below the conformal window, zeroes of the beta-function may still occur. One example is the saturation of the coupling g_{phys} entering the static inter-quark potential in large-N Yang-Mills

$$V(r) = \sigma r - \frac{g^2_{phys}(1/r)}{4\pi r}\,, \tag{3.19}$$

with nonzero string tension σ. The effective charge g_{phys} in the Coulomb potential is observed to saturate to a constant at large distances in lattice $SU(3)$ Yang-Mills [219] and provides agreement with the effective bosonic string theory prediction and open-close string duality [220]. In other words: the beta function of g_{phys} develops a zero, while conformal symmetry remains broken due to the linear confining contribution to the potential (non-zero string tension) dominating the large distance behaviour.

In [59] a renormalisation scheme for the large-N Yang-Mills exact beta-function was constructed, where the canonical 't Hooft coupling coincides with the physical effective charge entering the static inter-quark potential in Equation 3.19, and it develops a zero at the Landau pole of the Wilsonian coupling, at $r^{-1} = \Lambda_W$. Hence, it actually predicts that for $r > \Lambda_W^{-1}$ the effective charge g_{phys} saturates to a constant.

If the same behaviour is realised beyond large-N in the presence of $N_f < N_f^c$ massless fundamental flavors, then the QCD beta-function below the conformal window in a given renormalisation scheme can develop zeros without implying conformal symmetry. The only probes of the absence of conformal symmetry remain the n-point functions that involve the string-tension term of the inter-quark potential, the observables sensitive to chiral symmetry breaking and, importantly, topological quantities.

A fundamental difference between SQCD and QCD is the presence in SQCD of a phase just below the lower edge, for $N_c + 2 \leq N_f \leq 3N_c/2$, where the only description that makes physical

sense is in terms of the dual variables that describe the free non-Abelian magnetic phase [281]; this property is consistent with the occurrence of the cusp in the flow just below the conformal window for SQCD. The absence of this phase in QCD calls instead for a differentiable flow, thus without cusps, across and below the lower edge of the conformal window. It is rewarding that the beta-function of large-N QCD can realise this property [61]. It also supports that the lower edge singularity for $b_2 = 0$ at two loops arises as an artefact of n-loop perturbation theory.

Finally, since the large-N beta-function reproduces the two-loop one up to $O(1/N^2)$ contributions [61], the predicted γ_G also reproduces the two-loop result up to $O(1/N^2)$; however, it is expected to remove the singularity for $b_2 = 0$ at the lower edge of the conformal window.

Perturbation theory, as well as the large-N solution thus predict an increasing anomalous dimension $|\gamma_G|$ ($|\beta'(\alpha_*|)$) for $N_f \searrow N_f^c$.

This behaviour is precisely the opposite to the one implied by an UV-IR fixed-point merging phenomenon at N_f^c. In this scenario, we can assume without loss of generality, that, close to N_f^c where the merging would occur, we have [188]:

$$\beta(\alpha, N_f) = (N_f - N_f^c) - (g - g^c)^2. \tag{3.20}$$

The beta function has roots at $g_\pm = g^c \pm \sqrt{N_f - N_f^c}$ and develops a local maximum at $N_f = N_f^c$, i.e., $\beta'(g^c) = 0$, with decreasing $|\beta'|$ along the IRFP line $N_f \searrow N_f^c$. For $N_f < N_f^c$, both roots $\alpha_\pm$ acquire an imaginary component. This behaviour is illustrated in Figure 3.15 (left).

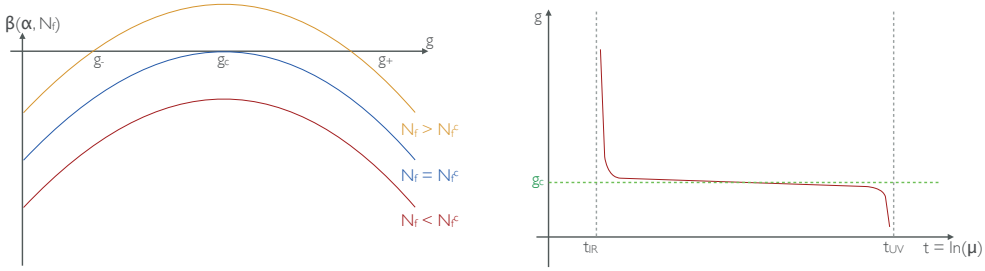

Figure 3.15: (left) Depiction of the prototyped beta function in Equation 3.20: For N_f^c there are fixed points at $g_\pm$ which are attractors in the infrared (g_-) and ultraviolet (g_+); for $Nf = N_f^c$, these fixed points merge at g_c; for $N_f < N_f^c$, they disappear. (right) The renormalisation group flow of the coupling g as a function of the variable $t = \ln \mu$ for a theory in the pre-conformal region $N_f \nearrow N_f^c$.

This mechanism is actually a realisation of Miransky/Berezinsky-Kosterlitz-Thouless [199,231,234,188] scaling of observables in the just below the conformal window for $N_f \nearrow N_f^c$. It is phenomeno-

logically interesting because it is the simplest framework in which the walking scenario discussed in Chapter 0 can be realised in the preconformal region of the phase diagram. If $N_f \lessapprox N_f^c$, and the coupling has an initial value g_{UV} at the UV scale μ_{UV}, as the theory flows to the IR, the coupling will grow. In the region where the beta function is small, the coupling will grow very slowly ("walk") before quickly blowing up, at which point it defines the infrared scale Λ_{IR} that characterises the longest correlation length in the theory, see Figure 3.15 (right). This scale can be computed by the integral

$$\frac{\Lambda_{IR}}{\Lambda_{UV}} = \exp\left[t_{IR} - t_{UV}\right] = \exp\left[\int_{g_{UV}}^{g_{IR}} \frac{dg}{\beta(g, N_f)}\right] \approx \exp\left[-\frac{\pi}{\sqrt{(N_f^c - N_f)}}\right]. \tag{3.21}$$

The approximation in the last step is valid under the assumption that $|g_{IR,UV} - g_c| \gg |N_f - N_f^c|$.

A nonperturbative measurement of γ_G for varying N_f inside the conformal window and in agreement with perturbation theory and large-N would exclude therefore this mechanism for the conformal window of QCD.

3.5 Conclusion

We have numerically studied the order parameters of chiral symmetry breaking and related quantities and also probes of deconfinement for $SU(N_c = 3)$ theories with a large number of flavours. The results presented here point at a lower edge of the conformal window for QCD below $N_f = 8$ and close to $N_f = 7$, in agreement with perturbation theory calculations and large-N arguments, the latter based on the behaviour of glueball operators sensitive to confinement.

We have also presented a study of the behaviour of the scalar glueball operator, a probe of confinement, across the opening of the conformal window. We showed that it carries information on the nature of the endpoint and the zero temperature pre-conformal phase. The agreement with perturbation theory and large-N arguments would be sufficient to exclude an ultraviolet-infrared fixed-point merging as a mechanism for the loss of conformality, such as the one presented by Kaplan et al[187].

A lattice determination of the anomalous dimension of the scalar glueball operator at the conformal IRFP is therefore desirable. We also recognise that the Wilson flow proposed in [214,242] can be a useful tool in this context, in order to discriminate between a conformal and a confining behaviour in the theory formulated on a lattice[258].

Finally, a conformal window for non-supersymmetric QCD extending to flavors as low as $N_f = 7$ would make these theories more appealing for phenomenology beyond the standard model, realising the emergence of conformal symmetry right above QCD at the electroweak symmetry breaking scale.

If the fixed-point merging turns out not to occur in QCD, it becomes interesting to understand from a renormalisation group point of view if preconformal scaling can at all be realised with a single IRFP, and if it can reproduce the trend of the anomalous dimensions implied by perturbation theory and large-N arguments.

We shall not cease from exploration, and the end of all our exploring will be to arrive where we started and know the place for the first time.

T.S. Eliot

4

Concluding Remarks

We conclude this thesis with a summary of the results presented throughout the chapters and a critical discussion in light of the recent results that appeared in literature. We also elaborate on possible paths for future extensions of these studies.

By the time we started the project contained in this thesis, in late 2010, the challenge of understanding the phase diagram for QCD-like theories, i.e., $SU(N = 3)$ with N_f fundamental flavours, had various missing ingredients, which made it difficult to form a coherent picture. With the work performed by many groups since then, we seem to be arriving at a point where important pieces have finally appeared and it all starts to fit together. We feel that the work presented in this volume has made important contributions to this effort.

Chapter 1 verses about the role played by the improvement of field theory actions formulated on a spacetime lattice in the emergence of an exotic phase between the chirally broken strongly coupled

regime and the more weakly coupled Coulomb (QED-like) phase of theories inside the conformal window. The original motivation of the work was to determine the order of the bulk transition for the $N_f = 12$ theory and check whether it would allow for the UV-IR fixed point merging mechanism for the disappearance of the conformal window proposed by Kaplan et al.[187] to be realised in QCD-like theories. We were initially surprised by the observation of two independent sharp crossovers of the chiral condensate at a non-zero fermion mass, which definitely required a better understanding.

The simulations later performed with different combinations of gauge and fermion actions support the theoretical conclusion that such an exotic phase emerges as a result of the competition, at strong coupling, between the nearest-neighbour terms and the next-to-nearest neighbour interactions introduced by the Naik improvement of the fermion action. This competition allows for a nontrivial realisation of baryon number conservation when the underlying chiral symmetry is not spontaneously broken. Such an explanation for the emergence of the exotic phase is a rather general feature of improvement, also consistent with the breaking of shift symmetry and would identify the exotic phase discussed in this work with the ϕ^4 phase observed by Cheng et al.[82] using a different action. It would be interesting in future works to investigate more quantitatively the connection between the poles in the quark propagator - as emerging from the non-Hermiticity of the transfer matrix with Symanzik improvement and the detailed structure of the two-point meson correlation functions in the intermediate phase.

Returning to the main Physics goal of the study, we have also presented very strong evidence that the bulk transition occurring inside the conformal window at sufficiently strong coupling is of first order: the presence of metastability at small volumes, the presence of hysteresis at larger volumes and a linear scaling of the transition location with the bare quark mass all favour a first order phase transition. This result was favouring the absence of a UV fixed point at strong coupling inside the conformal window, while it could still emerge as the endpoint of the line of first order bulk phase transitions. This picture would still make it possible for the UV-IR merging mechanism to be realised. One caveat in this analysis concerns the role of higher dimensional operators in the QCD action at strong coupling. The analysis is limited to the QCD action with one gauge coupling g. Additional operators, such as four-fermion operators, have not been added by hand in the theory and it remains to be clarified if the lattice formulation of the QCD action can capture the complete renormalisation group flow of the theory in the strong coupling regime. The fixed point structure of theories with more complex operators may be more complicated and should certainly be analysed in

the enlarged space of couplings. Note, however, that all these effective field theory operators should guarantee exact conformal symmetry if a infrared or ultraviolet fixed point is there.

An important result of this work was to make evident that improvement may generally affect any lattice system at strong coupling, be it graphene or non abelian gauge theories inside or slightly below the conformal window. In fact, the way improvement acts at sufficiently strong coupling can be considered analogous to the way the physics of nearest-neighbour spin systems is modified by the presence of non-nearest neighbour interactions. The simplest and instructive example is the Ising spin chain (1D) with a next-to-nearest neighbour term. In general, the competition of local and less-local interactions in the theory can generate new phases in the system, as known for the axial next-to-nearest neighbour Ising (ANNNI) model[282]. The Symanzik improvement procedure for a gauge or a fermion lattice action is in this respect fully analogous to spin systems, in which case the new phases are physical, as it could be the case for graphene, or the same reasoning could lead to interesting properties of known and new materials in different regimes of their interactions.

When performing the analysis of lattice configurations of theories inside the conformal window at a fixed coupling, it is mandatory to verify in which region of the parameter space the system lies, since improvement can introduce lattice artefacts that might spoil results if not checked for. Such an observation, for example, was of vital importance to the spectrum study presented in Chapter 2 and to the work presented in Chapter 3.

The study of the $N_f = 12$ theory was marked by a initial period of confusion, with different groups finding contradictory results. This demonstrated how complicated this type of study is and how many subtle nuances must be taken into consideration in order to achieve trustworthy results. Fortunately, as the studies matured and we acquired a better comprehension of the subtleties in the several strategies explored, most recent studies started to align and indicate that this theory indeed exhibits a conformal behaviour.

The results we present in Chapter 2 also point in this direction, as well as the very first study by our group in 2009[112]. We presented the results from our study of the spectrum of the $SU(N = 3)$ theory with $N_f = 12$ fundamental flavours as a prototype of theories inside the conformal window. We have analysed the would-be hadron spectrum, the would-be mesons and the nucleon, and performed a universal scaling study at finite and infinite volumes. We also performed a nonperturbative estimation of the fermion mass anomalous dimension taking into account deviations from universal scaling. We have also confirmed the restoration of chiral symmetry through the degeneracy of

chiral partners and the effective restoration of the U(1) axial symmetry at the level of the two-point functions.

Our estimated value of the fermion mass anomalous dimension $\gamma_m = 0.235(46)$ is in very good agreement with the value obtained by Cheng et al.[79] from finite size scaling $\gamma_m = 0.235(15)$. Results obtained independently from the Dirac eigenmodes spectrum by the Cheng et al.[80] and also by Itou[177], while disagreeing on the exact value, also point at a small anomalous dimension. Surprisingly, these results are also in agreement with the prediction from four-loop perturbation theory in the $\overline{MS}$ scheme, $\gamma_m \approx 0.25$[304,305] . A recent analysis by Gracey and Simms[152] in the momentum subtraction (MOM) scheme has estimated the exponent as $0.263 - 0.268$ (recall that γ_m at the fixed point is a scheme independent quantity).

The small value of γ_m measured in these different studies came as a bit of a surprise initially, since there was a consensus in the field that the $N_f = 8$ theory exhibited chiral symmetry breaking and the $N_f = 12$ was believed to be located close to the lower edge of the conformal window. As noted in our original reference on the matter[208], this scenario would require a very rapid variation of the mass anomalous dimension between N_f^c and $N_f = 12$ in order to realise $\gamma_m \approx 1$ at the lower endpoint of the IRFP line. The other alternative would be that the lower endpoint should actually be located at a considerably lower number of flavours than twelve. This alternative is strongly favoured by the results we present in Chapter 3.

A possible place for improvement in the work of Chapter 2 would be to perform the simulations of the ensembles with the lightest bare quark masses at larger lattice volumes. In our study of the spectrum at infinite volume, we have used extrapolations of the would-be hadron masses to their infinite volumes. Ideally, one would desire to replace these by results obtained from the lattice in the infinite volume limit. We have shown, however, the stability of the fits with respect to the fitting range and the effectiveness of the combined analysis considering also the data obtained by the LatKMI collaboration[13]. Thus, we have strong evidence that our results are solid. Moreover, these results indicate that the underlying patterns of symmetry can be followed across the IRFP, and the critical exponent can be determined on both sides of the IRFP. This conclusion also contradicts scenarios in which a singularity in the order parameters or their derivatives is associated to the IRFP.

The combination of the results above strongly supports that the $SU(3)$ theory with $N_f = 12$ is inside the conformal window.

In Chapter 3 we presented strong evidences supporting the scenario in which the $N_f = 8$ theory

is also conformal in the infrared. We consider this an important and somewhat conclusive step in the understanding of the phase diagram of non-Abelian gauge theories with fundamental fermions. We have performed a numerical study of the chiral symmetry order parameter and probes of confinement for QCD-like theories with a varying number of flavours and presented the evidence that N_f^c, the critical number of flavours that marks the lower edge of the conformal window, is located between $N_f = 6$ and $N_f = 8$, in agreement with perturbation theory calculations and very recent large-N arguments.

In the case of the $N_f = 8$ theory, we have argued that the crossover identified in Deuzeman et al.[116] as the finite temperature transition of a spontaneously chirally broken theory is most definitely actually the weak coupling edge of the exotic phase we studied in Chapter 1. A chiral symmetry breaking transition actually takes place at a stronger coupling for the zero temperature system.

The numerical results presented in Chapter 3 are being expanded with ongoing simulations at larger volumes and new analysis strategies aiming at better understanding the nature of the finite temperature transition with an improved asymptotic scaling analysis and at clarifying the behaviour of the Polyakov Loop for the zero temperature simulations. The results will appear in an upcoming work. While these can provide insight into new aspects of the systems under study, they are not expected to change our main conclusions on the matter. The deviation of the (pseudo) critical couplings for the $N_f = 4$ and $N_f = 6$ theories from the line of bulk transitions is definitive, though a study at lower masses, and eventually in the chiral limit would certainly be welcome. The underlying pattern of symmetries that result in the emergence of the exotic phase is not present in theories for which chiral symmetry is spontaneously broken. The sharpness of the crossovers observed in the $N_f = 8$ theory does not leave space for a change of behaviour at a lower mass.

Many groups are already studying the $N_f = 8$ theory, also using a different fermion discretisation than the staggered formulation typically used for this type of studies. More definitive results from these collaborations should appear soon and it will be interesting to see how do they play out.

In the second part of Chapter 3, we presented a theoretical analysis on the scalar glueball operator, which is a probe of confinement. We showed that information on the nature of the endpoint and the zero temperature pre-conformal phase is encoded in the behaviour of the glueball operator. The perturbative behaviour is shown to be in agreement with the solution in the Veneziano limit of large-N QCD and contrary to what is expected in case the UV-IR fixed point merging mechanism is realised. This mechanism is the simplest way to produce Miransky/BKT scaling.

These perturbative results beg for a nonperturbative confirmation, given their theoretical and phenomenological implications. If nonperturbative results are in agreement with perturbation theory and with the large-N results, the emergence of the conformal window for QCD-like theories can not be explained through UV-IR annihilation and walking behaviour would have to be realised through a different mechanism.

A nonperturbative measurement of the anomalous dimensions can be performed from the calculation of the two-point correlation function of the scalar glueball operator on the lattice. Another interesting possibility has been raised by Pallante [258] and consists in studying the Wilson flow of the vacuum expectation value of of the scalar glueball operator with an appropriately devised evolution kernel. Lattice results on this matter can not come soon enough.

In summary, the picture that emerges in light of recent results is that the $SU(N = 3)$ theory with $N_f = 12$ fundamental flavours lives inside the conformal window and can be studied as a prototype of a conformal theory at the IRFP. Deviating from what was thought for some time recently, the lower edge of the conformal windows does not seem to occur close to $N_f = 12$, but rather seems to be located between $N_f = 6$ and $N_f = 8$, explaining the small mass anomalous dimension measured in different lattice studies for the $N_f = 12$ theory and in agreement with the $\gamma_m \sim 1$ value measured by the LSD collaboration for the theory with $N_f = 8$ [20].

From the phenomenological point of view, the scenario above could turn $SU(N = 3)$ theories with fermions in the fundamental representation more attractive, since conformality can be achieved for a considerably lower number of flavours than what was initially believed. In fact, the pre-conformal region of the phase diagram would lie right above the number of flavours of QCD with all six active flavours in the Standard Model around the electroweak symmetry breaking scale.

Some questions, on the other hand, remain open: in addition to a more precise determination of N_f^c, the exact shape of the chiral phase boundary below the conformal window as a function of N_f and the underlying dynamics close to N_f^c still need to be further explored. If UV-IR merging mechanism is indeed excluded, can walking be realised in the preconformal region? How? These are some of the questions to be answered in the coming years, as simulations become computationally cheaper and new actions, algorithms and, above all, ideas, come into scene. Other non-perturbative methods, as, for example, the conformal bootstrap [269,129,272], can also provide new insights into these questions.

The effort and computational resources dedicated by researchers in lattice field theory into understanding the phase diagram of gauge theories have provided us not only with a greater understanding

of the topic, building an important framework for models of BSM Physics, but is has also equipped lattice theorists with the tools, the computational strategies and the experience to tackle many new problems in the field.

The experiments at the LHC have reached one of the greatest feats in the history of mankind with the discovery of the Higgs boson. Many questions, however, remain unanswered, the absence of a smoking gun signal of new Physics making the challenge all the more interesting. The Standard Model is successful in modelling electroweak symmetry breaking, but still provides no explanation for it, nor a solution to the naturalness issue. It also provides no explanation to neutrino oscillations. The composite nature of the discovered Higgs has not been established nor excluded so far. The nature of dark matter is still unknown. The existence of Supersymmetry in nature is still a question not confirmed nor excluded by experiments. A number of lattice works studying specific Standard Model extensions addressing these issues have emerged in recent years, marking a shift from the more fundamental studies to more phenomenologically driven ones, but clearly profiting from the expertise developed by them.

Looking at the years ahead of us, the still relatively young BSM lattice community is in a privileged position to give a decisive contribution on fundamental questions on BSM Physics. There was certainly never a more exciting time to be a part of it.

A

Samenvatting

De mensheid heeft, tot nog toe, vier fundamentele interacties geformuleerd: de zwaartekracht, de elektromagnetische kracht, de zwakke kernkracht en de sterke kernkracht. Het gedrag van de laatste drie interacties wordt beschreven in een model genaamd het "standaard model van de deeltjes fysica". Volgens dit model is alle materie opgebouwd uit zes quarks (up, down, strange, charm, bottom en top) die elk in drie kleuren voorkomen, zes leptonen (het elektron, de muon, de tau en hun respectievelijke neutrino's). De interacties worden verder overgedragen door deeltjes genaamd vector bosonen: acht gluonen voor de sterke kernkracht, de $W^{\pm}$ en Z bosonen voor de zwakke kernkracht en het foton voor de elektromagnetische kracht.

Deze thesis is gewijd aan een dieper begrip van de sterke kernkracht, die beschreven wordt door een ijktheorie genaamd de kwantumchromodynamica (QCD), aangezien het interacties beschrijft van deeltjes met een kleurlading: quarks en gluonen. QCD is een ijktheorie, hetgeen betekend dat

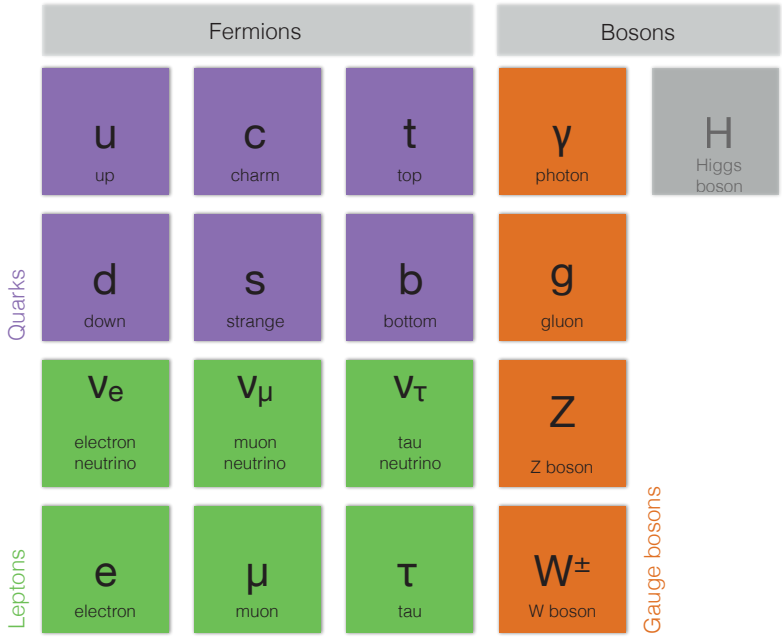

Figure A.1: De elementaire deeltjes der materie.

er een continue groep van transformaties bestaat die fysisch relevante grootheden onveranderd laat. Deze groep van transformaties wordt een ijkgroep genoemd en is in het geval van QCD de speciale unitaire groep, of in het kort $SU(3)$. Waar de 3 staat voor het aantal verschillende kleur ladingen in de theorie. Quarks kunnen bestaan in verschillende smaken en in de natuur komen er zes smaken voor: *up, down, strange, charm, bottom and top*. Deze informatie is samengevat in figuur A.1.

Experimenteel is het standaardmodel met een zeer grote precisie getest. Echter sommige vraagstukken hebben in dit raamwerk nog steeds geen oplossing en fysici zoeken naar oplossingen in extensies van het standaard model, een onderzoeksrichting genaamd *de natuurkunde voorbij het standaard model*. Dit proefschrift onderzoekt een aantal van deze vraagstukken. Meer specifiek is het doel om een beter begrip te krijgen van de fasediagram van de materie die interacties vertoont met de sterke kernkracht (en de ijktheorie die dit beschrijft) en het ontstaan van conformiteit.

Een belangrijke eigenschap van QCD in deze studie is de chirale symmetrie: QCD is op hoge temperatuur en met massaloze velden invariant onder onafhankelijke rotaties van de links- en rechtshandige velden. Deze symmetrie is expliciet gebroken door de massa term in de theorie. Bovendien kan het ook spontaan gebroken zijn door een condensaat van quarkvelden die een verwachtingswaarde ontwikkeld ongelijk aan nul door een herverdeling van het vacuüm van de theorie, zoals

in QCD met een temperatuur gelijk aan nul. Met dit condensaat is het verschil tussen twee verschillende fases van de theorie te onderscheiden: in de ene fase bestaat het condensaat niet — oftewel de verwachtingswaarde is nul — en is de symmetrie niet spontaan gebroken, terwijl in de andere fase de verwachtingswaarde voor het condensaat niet nul is en is de theorie in de chiraal gebroken fase. Een grootheid met een dergelijk gedrag dat het mogelijk maakt om het verschil tussen verschillende fases van een systeem te onderscheiden heet een orde parameter.

Een ander belangrijke — en in zekere zin een definiërende — eigenschap van QCD is het gedrag van de "veranderende Koppelingsconstante", dat is gerelateerd aan de fenomenen asymptotische vrijheid en quark opsluiting. De kracht van de sterke interactie wordt gereguleerd door een grootheid genaamd de koppelingsconstante, die feitelijk niet constant is maar veranderd (vloeit) met de energieschaal op welke de theorie wordt beschreven. Politzer, Gross en Wilczek en 't Hooft hebben aangetoond dat de koppelingsconstante van QCD monotoon naar nul daalt als de energie schaal van de theorie groeit, wat betekend dat op hoge energie de theorie zwak gekoppeld is. Dit concept is bekend onder de naam asymptotische vrijheid, en in 2004 kregen Politzer, Gross en Wilczek een nobelprijs voor deze ontdekking in QCD.

Aan de andere kant van asymptotische vrijheid is er quark opsluiting: deeltjes die kleurlading bevatten (zoals quarks) zijn, als de temperatuur en dichtheid nul is, in de natuur nooit geïsoleerd waargenomen, maar als combinaties zonder kleurlading, genaamd *hadronen*. Het rigoureus bewijzen van kleuropsluiting is nog steeds een open vraagstuk en blijft dus slechts een aanname dat consistent is met experimentele waarnemingen. Het bewijzen van quark opsluiting is een van de millennium problemen van het Clay Institute.

Op hoge temperatuur, zoals op temperaturen kort na het ontstaan van het universum 10^{-4} seconden na de big bang, zijn de composiete toestanden gebroken en is de theorie in een fase met vrije quarks genaamd het quark-gluon plasma (QGP). Hoewel er dus nog geen rigoureus bewijs is voor quark opsluiting heeft Polyakov een grootheid gevonden — genaamd de Polyakovlus — dat als orde parameter kan fungeren voor deze faseovergang naar vrije quarks op hoge temperaturen.

Chirale symmetrie en quark opsluiting spelen een belangrijke rol in het fasediagram van ijktheorieën. Een ander belangrijk ingrediënt is de verschijning van conformiteit. Zoals al eerder gezegd veranderd de grootte, het vloeien, van de QCD koppelingsparameter met de energieschaal van de theorie. Dit vloeien wordt meestal beschreven met de zogenaamde bèta functie, die feitelijk de "snelheid" van het vloeien van de koppelingsconstante met het energieniveau beschrijft. De observatie dat

de QCD koppelingsconstante monotoon naar nul vloeit is equivalent aan de uitspraak dat de QCD bèta functie altijd negatief is en een nulpunt heeft als de koppelingsconstante nul is. Een punt waar de bèta functie nul is heet een "dekpunt " en, in dit scenario, wordt het eerdergenoemde nulpunt ook wel het triviale dekpunt genoemd.

Als het aantal smaken wordt vergroot zal de bèta functie een niet-triviaal infrarood dekpunt ontwikkelen op $N_f = N_f^c$. Als vervolgens het aantal smaken verder wordt vergroot boven $N_f = N_f^{AF}$ zal de bèta functie overal positief worden waardoor asymptotische vrijheid verloren gaat. Op het dekpunt zal de theorie schaalonafhankelijk worden, wat betekend dat de koppelingsconstante onafhankelijk wordt van de energieschaal en de conforme theorie hersteld wordt.

Een mogelijk scenario dat het herstel van conforme symmetrie verklaard in niet-Abelse ijktheorieën is het zogenaamde "conforme venster" scenario. In dit scenario bestaat er een familie van theorieën tussen N_f^c en N_f^{AF} die bevrijd zijn en zelfs op het thermodynamische nulpunt een exacte chirale symmetrie hebben. Elk van deze theorieën heeft een niet-triviaal dekpunt op een zekere waarde van de koppelingsconstante.

De afgelopen jaren is er veel onderzoek gedaan naar de vorm van het fasediagram, voornamelijk naar de opening van de conforme raamwerk scenario, om zo het punt te vinden waar deze zich opent en om begrip te krijgen over de pre-conforme regio. Deze vragen zijn theoretisch gezien interessant voor velden theorieën, omdat ze nieuwe informatie geven over ijktheorieën die fundamentele interacties beschrijven. Ze kunnen ook belangrijke consequenties hebben voor de ijkveld-zwaartekracht dualiteit en voor de connectie tussen theorieën met en zonder supersymmetrie. Ze zijn ook interessant voor rooster theoreten, omdat nieuwe algoritmen en technieken worden ontwikkeld en getest, die in verschillende onderzoeksgebieden gebruikt kunnen worden. Tenslotte, uit het oogpunt van fenomenologie zijn deze vragen ook relevant: de bijna-conforme regio van het fasediagram kan voorbereidende effecten van conformiteit vertonen die relevant zijn voor fenomenologie en het bouwen van modellen, die een basis vormen voor de groep van elektrozwakke theorieën bekend zijn als "walking technicolor" modellen.

Het breken van de elektrozwakke symmetrie is een fenomeen dat gerelateerd is aan de basis van de massa's in het standaard model door middel van het Higgs mechanisme. De ontdekking van het Higgs boson in de Large Hadron Collider (LHC) is één van de grootste prestaties in de geschiedenis. Helaas bied het Higgs mechanisme geen extra inzicht in de structuur van het Higgs deeltje zelf. Technicolour modellen zijn een poging om deze vraagstukken te beantwoorden en zij genereren een

dynamische verklaring voor de breking van de elektrozwakke symmetrie binnen het stelsel van de effectieve veldentheorieën, waarin veldentheorieën niet compleet zijn tot op arbitrair hoge energieën, maar slechts tot een zekere waarde.

Al in 1980 werd opgemerkt dat de originele technicolour modellen niet goed functioneerden, hetgeen beschreven zal worden in Hoofdstuk 0, en niet bruikbaar zijn voor het beschrijven van de smaak sector van het standaardmodel. In walking modellen veranderd de koppelingsconstante slechts een klein beetje als de energie veranderd, vandaar de naam. Dit gedrag van de koppelingsconstante verbeterd een aantal problemen van de oorspronkelijke technicolour theorieën, en maakt deze theorieën weer aantrekkelijk. De huidige activiteiten van de LHC zijn grotendeels gedaan uit interesse voor dit onderwerp, waardoor het werk van deze promotie een zeer actief onderzoeksveld is.

Een groot deel van het onderzoek in dit proefschrift is gebaseerd op rooster-ijkveldtheorie methoden die het mogelijk maken om op een niet-perturbatieve numerieke manier ijktheorieën te beschrijven. Het algemene idee van deze methoden is om ruimtetijd te discretiseren, dus om de continuë ruimtetijd te vervangen door een discreet vierdimensionaal rooster. De gediscretiseerde versie van de theorie die hier onderzocht gaat worden kan dan numeriek gesimuleerd worden op computers met behulp van Monte Carlo methoden en fysisch interessante observabelen kunnen worden berekend.

Het inleidende hoofdstuk van dit proefschrift geeft de lezer kennis van de achtergrond van de theoretische aspecten en de niet-perturbatieve roostertechnieken die gebruikt worden in dit werk. Deze informatie zal voldoende moeten zijn om de rest van dit proefschrift te kunnen begrijpen.

Het eerste hoofdstuk van dit proefschrift zal gericht zijn op het gedrag van $SU(3)$ ijktheorieën met twaalf smaken in de fundamentele representatie op hoge koppelingsconstante. Wij zullen de transitie beschouwen waar de chirale symmetrie gebroken wordt op hoge waarden voor de koppelingsconstante en het ontstaan van een nieuwe exotische fase als de koppelingsconstante wordt vergroot, voordat chirale symmetrie is gebroken. Wij zullen de orde parameter van de chirale symmetrieovergang, het chirale condensaat, beschrijven samen met gerelateerde grootheden. We zullen de chirale faseovergang lokaliseren en zijn natuur van een eerste orde faseovergang bepalen. Ook zullen wij aantonen hoe het ontstaan van deze exotische fase is gerelateerd aan een verbetering in de roosteractie en de onderliggende symmetrieën binnen het conforme venster.

In hoofdstuk twee presenteren wij een studie naar het "would-be" hadron spectrum van de $SU(3)$ theorie met twaalf fundamentele smaken. Geleid door het patroon van onderliggende symmetrieën, chiraal en conform, presenteren we de tweepunt-functies zowel theoretisch als op het rooster en

bepalen we de eindige-roosterlengte schaling en de oneindig-volume fermion massa afhankelijkheid van de "would-be ''hadron massa's. We tonen aan dat het gedrag van het spectrum beschreven kan worden in de context van een universele schaling analyse en we geven een niet-perturbatieve bepaling van de van de fermion massa anomale dimensie op het infrarode fixed point. De gemeten waarde $\gamma* = 0.235(46)$ is klein, en komt overeen met andere studies en is consistent met het scenario waar de theorie binnen het conforme venster is.

Hoofdstuk drie is gewijd aan de studie van $SU(3)$ theorieën met meerdere smaken fermionen boven de ondergrens van het conforme venster. Wij presenteren een roosterstudie van de N_f afhankelijkheid van de bulk transities van deze theorieën op nul temperatuur, consistent met het openen van het conforme venster tussen $6 < N_f < 8$. Wij presenteren ook een theoretische analyse naar de anomale dimensie van de scalaire lijmbal operator, welke de vrije quark transitie kan vaststellen, en zijn consequenties voor een samengevoegd mechanisme waarin het verlies van conformiteit het resultaat is van het annihileren van het infrarood dekpunt en het ultraviolet dekpunt. Zo een mechanisme is het simpelste raamwerk waarbinnen het walking scenario gerealiseerd kan worden in het pre-conforme regio van het fase-diagram.

Dit proefschrift besluit met een kritische discussie van de hier gepresenteerde resultaten en een vooruitblik.

B

Acknowledgments

The completion of a PhD degree marks the last steps of a long walk that started many years before the PhD defence date in the life of the candidate. I certainly would not be able to reach the end of this road without all of the support I have received from many people during all these years, and for which I'm deeply grateful. I would like to thank all of these people.

Em primeiro lugar, eu gostaria de agradecer à minha família por ter sempre dado à minha educação a importância e a prioridade que ela merece. Serei eternamente grato por todo o apoio e todo o esforço que fizeram para me prover, desde muito pequeno, educação do melhor nível possível, e por sempre estimularem minha curiosidade e meu desenvolvimento intelectual. Não possuo palavras para expressar o quanto eu os admiro por isso. Agradeço, também, por todo o apoio e liberdade que sempre me deram na escolha de meus caminhos profissionais. Se hoje concluo essa caminhada do meu doutoramento é porque vocês estiveram segurado minhas mãos em meus primeiros passos.

I would also like to thank my supervisor, Prof. Elisabetta Pallante for all the scientific guidance, all the discussions, all the words of encouragement (and wake-up calls when required) and for her friendship. I do not know of many people who are as passionate and dedicated to science as Elisabetta. I certainly learned a lot from her broad scientific expertise in these years. But I also must note that I learned a lot from her about how to be a good scientist. I promise to take these lessons with me and follow her example.

Maria Paola, it has also been an enormous pleasure to collaborate with you during these years. I have greatly benefited from your scientific expertise in our discussions throughout the various projects we have worked on together. We have also been together presenting the works of our collaboration in conference around the world and I'm grateful for the support you gave me during those moments.

Albert Deuzeman and Kohtaroh Miura, you were the other two elements of our small collaboration, briefly named CAPSICO, and briefly the holder of the coolest logo of any scientific collaboration I know of: a dancing pepper. It has been a pleasure to work with both of you. Thank you for all the scientific discussions, the much appreciated help in my first years in the group and the nice moments in conferences around the world.

The Field Theory and Particle Physics group in Groningen was also composed by people that, while not necessarily collaborating directly with me, always provided nice discussions and a great work environment. For that, I am thankful to Siebren Reker, Joyce Myers, Avihay Kadosh, and my "junior" collaborators Dries Conne, Nestor Subirón, Vincent Thiery and Lasse Roebroek.

I was very fortunate to have many inspiring teachers and professors through the years, who lit the fire of science inside me and helped keeping it burning through all of these years. I want to thank my school teachers Vera (the first person to say I would become a scientist), Welson Klein, Ana Paula, Maria de Jesus, Luiz Carlos, Marcelo and my professors at the Physics Department at UFPE Mauro Copelli, Flavio Aguiar, Giovani Lopes, Ernesto Raposo and José Tabosa for that. I specially thank professors Marcelo Leite and Bruno Carneiro da Cunha, my undergraduate and Masters project supervisors, for introducing me to the wonderful world of theoretical Physics and for their great contribution to my scientific formation.

I want to thank all the Professors who made the Centre for Theoretical Physics always an interesting and stimulating environment for research: Daniel Boer, Diederik Roest, Eric Bergshoeff, Kyriakos Papadodimas, Maxim Mostovoy, Mees de Roo, Rob Timmermans, and Thomas Jansen. I

also want to thank the secretaries of the Centre For Theoretical Physics, Iris de Roo-Kwant and Annelien Blanksma for all the help in navigating all the bureaucratic issues that emerged during these years.

Moving across the ocean can be a bit scary at first glance. I have been extremely fortunate to meet amazing people from my very first day in Groningen, who made the entire process much easier.

Siebren Reker, you were the first person I met when I arrived in Groningen, at Centraal Station. We have also shared the office and kicked each others feet under the table during the first years of my PhD. We also had very interesting discussions and trips to conferences together. You very quickly became a friend and I had the honour of being your paranymph in your PhD defence. You have also introduced me to one of my greatest addictions in my free time: StarCraft 2 (and let's say Patricia is not very happy about that). I could not have asked for a better cicerone to the Dutch world.

Next, I want to thank all the people who shared the place at Vindicatstraat 26 during these years with me: the "Dejan Petrovic and Primoz Pirih continuum" (I was actually only sharing the apartment with Dejan, but it is impossible to separate them both), Victor Caldas, Aline Ramos and Evgenyia Salamatova. In my first months in the city, when I was still a bit scared of the brave new world that was Groningen, Dejan and Primoz took me under their wings and introduced me to the city and to many interesting people. I owe to you the discovery of many interesting places in the city: how else would I find a Balkanic pub in the middle of Groningen called "New York"? Victor shares many common interests with me. He quickly became a friend of mine and a companion for several activities, ranging from volleyball to salsa. He also became, even quicker, a couple with Aline. It is very easy to realise how good of a couple you are together and I wish you both success in the coming years together. It is also remarkable that we met our better halves practically at the same time, and I can never thank Aline enough for that. Evgenyia, we spent the shortest time sharing the house, but you were always very nice and polite to me. I am thankful to all of you.

I would like to thank all the fellow PhD students and postdocs at the CTN who made it a pleasure to work there: Aditya, Adolfo, Ana, Andrea, Andrés, Anna Stradomska, Blaise, Dennis, Dries, Gideon, Giuseppe, Gökhan, Hamid, Irene, Ivonne, Jacob, Jan, Job, Jordy, Julian, Keri, Lorena, Luca, Lucia, Marco, Marija, Mario, Mayer, Niels, Remko, Ricardo, Roel Andringa, Roel Tempelaar, Sophie, Sjoerd, Souvik, Thomas, Victor and Luci, Wout, Wouter, and Yihao.

In addtion to Siebren, Lorena, Dries and Julian were also my officemates, and I am thankful for the nice discussions we had during the period and the nice atmosphere you always brought to our

office. I also thank Lorena, Ana and Marija for being so nice office neighbours and an infinite source of chocolate.

I have also spent some great evenings with Adolfo, Ana, Andrea, Jacob, Jordy, Julian, Keri, Lorena, Marija, Mayer, Sophie, Thomas, Victor, Luci and Wout either parting in the city, cooking and enjoying some nice dinners or just playing games. I am grateful for the moments shared with you. I must specially thank Lorena for teaching me so nicely how to cook Mexican food (another addiction I have acquired in Groningen).

I have also spent memorable times in the city with friends I met outside of the CNT: Gustaw and Anne Floor, Laura Giurge, Jesús, Thamy, Isa, Dani Torchia, Brenda, Anu, Femke, Irina, Susan, Robert, Anna Katinka, Olga, Walter, Brenda, Cyntia, Aysa and Visnja. I thank you the great moments together and hope we can repeat them, someday, somewhere.

The Dutch Research School of Theoretical Physics always organised interesting activities and made it possible to meet colleagues from other institutes within the country. I want to thank señor Pablo Ortiz, Chiara Toldo, Thijs van der Broek, Giuseppe d'Ambrosi, Alessandro Sfondrini, Rob Knegjens, Jan Weenink and Sander Mooij for making all these events and visits to NIKHEF very enjoyable.

I also want to thank the members of the Kroton volleyball club in Groningen, where I player for 3 seasons and managed to conquer a third class championship in my last year, specially the members and trainers of my team: Daniel, Jannes, Roelof, Rutger, Gerben, Andrey, Alexey, Olexander, Michiel, Jens and Hanne. Thank you all for the great times.

I also spent a short stint practicing Brazilian Jiu Jitsu at Gracie Barra Groningen, until my knee decided I needed a break. I met some great people there, and I want to thank them for all the lessons and the time spent on the mat, specially Ying Hao, Orlando, Robert, Amir, Xi-En, Bram, Niels and Marco.

A long time away from home makes you miss many important moments with friends you love. But when a friendship is true, this love stays. I am grateful to my Brazilian friends, whose friendship I value more at each passing day for enduring through all these years of distance (but not absence): Mariah, Rebecca, Emerenciano and Marcela, you are the best friends I could ever ask for. We can miss each other, but with your friendship, I know I'll never be (and let you be) alone.

I also want to thank everybody from "Baga□a Sportclub" for making it possible for me to stay in touch with the Brazilian daily discussions and providing me with a good dose of much needed

comic relief.

I want to thank my paranymphs, Oana and Jan-Willem, for being so good friends and for accepting the task at hand. I had the pleasure of Oana's company in a trip to a conference to California, after which we became very good friends. I admire how knowledgeable and sweet she is, making her the perfect company for a coffee over a conversation on any topic, even organising pubquizes. Jan is known and liked by entire CTN, and it is easy to see why with the big heart he has. A cup of coffee with him can lighten the mood of even the most stressful day. I'm happy and honoured to have you both my side on the day of my defence.

At last, but definitely not least, I must thank the most incredible woman I have met in my entire life, and the best gift the city of Groningen has given to me: Patrícia. You not only make me feel whole every day I spend with you, but you taught me the meaning of a true, irresistible love. Thank you for always believing in this feeling and for never letting go of my hand even at the most difficult and uncertain moments. What we have built in these years is so much bigger than the sum of two. It makes me happy to know that we will build much more in our future together.

References

[mil] The Clay Institute Millenium Problems. http://www.claymath.org/millennium-problems. [Online; accessed 7-October-2015].

[nob] The Nobel Prize in Physics 2008. http://www.nobelprize.org/nobel_prizes/physics/laureates/2008/. [Online; accessed 7-October-2015].

[3] (2013). Search for top partners with charge 5e/3 in the same-sign dilepton final state.

[4] Aad, G. et al. (2012). Observation of a new particle in the search for the Standard Model Higgs boson with the ATLAS detector at the LHC. *Phys. Lett.*, B716:1–29.

[5] Aad, G. et al. (2015). Combined Measurement of the Higgs Boson Mass in *pp* Collisions at $\sqrt{s} = 7$ and 8 TeV with the ATLAS and CMS Experiments. *Phys. Rev. Lett.*, 114:191803.

[6] Adams, J. et al. (2005). Experimental and theoretical challenges in the search for the quark gluon plasma: The STAR Collaboration's critical assessment of the evidence from RHIC collisions. *Nucl. Phys.*, A757:102–183.

[7] Adcox, K. et al. (2005). Formation of dense partonic matter in relativistic nucleus-nucleus collisions at RHIC: Experimental evaluation by the PHENIX collaboration. *Nucl. Phys.*, A757:184–283.

[8] Adler, S. L., Collins, J. C., and Duncan, A. (1977). Energy-momentum-tensor trace anomaly in spin-1/2 quantum electrodynamics. *Phys. Rev.*, D15:1712–1721.

[9] Agashe, K., Contino, R., and Pomarol, A. (2005). The Minimal composite Higgs model. *Nucl. Phys.*, B719:165–187.

[10] Akiba, T. and Yanagida, T. (1986). Hierarchic Chiral Condensate. *Phys.Lett.*, B169:432.

[11] Allton, C. R. (1996). Lattice Monte Carlo data versus perturbation theory.

[12] Andersen, J. R. et al. (2011). Discovering Technicolor. *Eur. Phys. J. Plus*, 126:81.

[13] Aoki, Y., Aoyama, T., Kurachi, M., Maskawa, T., Nagai, K.-i., Ohki, H., Shibata, A., Yamawaki, K., and Yamazaki, T. (2012). Lattice study of conformality in twelve-flavor qcd. *Phys. Rev. D*, 86:054506.

[14] Aoki, Y., Borsanyi, S., Durr, S., Fodor, Z., Katz, S. D., Krieg, S., and Szabo, K. K. (2009). The QCD transition temperature: results with physical masses in the continuum limit II. *JHEP*, 06:088.

[15] Aoki, Y., Endrodi, G., Fodor, Z., Katz, S. D., and Szabo, K. K. (2006a). The Order of the quantum chromodynamics transition predicted by the standard model of particle physics. *Nature*, 443:675–678.

[16] Aoki, Y. et al. (2013). Walking signals in $N_f = 8$ QCD on the lattice. *Phys.Rev.*, D87(9):094511.

[17] Aoki, Y. et al. (2014). Light composite scalar in eight-flavor QCD on the lattice. *Phys.Rev.*, D89:111502.

[18] Aoki, Y., Fodor, Z., Katz, S. D., and Szabo, K. K. (2006b). The QCD transition temperature: Results with physical masses in the continuum limit. *Phys. Lett.*, B643:46–54.

[19] Appelquist, T., Babich, R., Brower, R. C., Cheng, M., Clark, M. A., Cohen, S. D., Fleming, G. T., Kiskis, J., Lin, M. F., Neil, E. T., Osborn, J. C., Rebbi, C., Schaich, D., and Vranas, P. M. (2011). Parity doubling and the *s* parameter below the conformal window. *Phys. Rev. Lett.*, 106:231601.

[20] Appelquist, T. et al. (2014). Lattice simulations with eight flavors of domain wall fermions in SU(3) gauge theory. *Phys.Rev.*, D90(11):114502.

[21] Appelquist, T., Fleming, G., and Neil, E. (2008a). Lattice Study of the Conformal Window in QCD-like Theories. *Physical Review Letters*, 100(17):1–4.

[22] Appelquist, T., Fleming, G., and Neil, E. (2009). Lattice study of conformal behavior in SU(3) Yang-Mills theories. *Physical Review D*, 79(7):1–16.

[23] Appelquist, T., Fleming, G. T., and Neil, E. T. (2008b). Lattice study of the conformal window in qcd-like theories. *Phys. Rev. Lett.*, 100:171607.

[24] Appelquist, T., Lane, K., and Mahanta, U. (1988a). Ladder approximation for spontaneous chiral-symmetry breaking. *Phys. Rev. Lett.*, 61:1553–1556.

[25] Appelquist, T. and Nash, D. (1990). Critical behavior in (2+1)-dimensional qcd. *Phys. Rev. Lett.*, 64:721–724.

[26] Appelquist, T., Nash, D., and Wijewardhana, L. C. R. (1988b). Critical behavior in (2+1)-dimensional qed. *Phys. Rev. Lett.*, 60:2575–2578.

[27] Appelquist, T., Ratnaweera, A., Terning, J., and Wijewardhana, L. C. R. (1998). Phase structure of an SU(n) gauge theory with N_f flavors. *Phys. Rev. D*, 58:105017.

[28] Appelquist, T., Rodrigues da Silva, P. S., and Sannino, F. (1999). Enhanced global symmetries and the chiral phase transition. *Phys. Rev.*, D60:116007.

[29] Appelquist, T., Terning, J., and Wijewardhana, L. (1996a). Zero Temperature Chiral Phase Transition in SU(N) Gauge Theories. *Physical review letters*, 77(7):1214–1217.

[30] Appelquist, T., Terning, J., and Wijewardhana, L. C. R. (1995). $(2+1)$-dimensional qed and a novel phase transition. *Phys. Rev. Lett.*, 75:2081–2084.

[31] Appelquist, T., Terning, J., and Wijewardhana, L. C. R. (1996b). Zero temperature chiral phase transition in su(N) gauge theories. *Phys. Rev. Lett.*, 77:1214–1217.

[32] Appelquist, T. and Wijewardhana, L. (1987a). Chiral Hierarchies from Slowly Running Couplings in Technicolor Theories. *Phys.Rev.*, D36:568.

[33] Appelquist, T. and Wijewardhana, L. C. R. (1987b). Chiral hierarchies and chiral perturbations in technicolor theories. *Phys. Rev. D*, 35:774–777.

[34] Appelquist, T. W., Karabali, D., and Wijewardhana, L. (1986). Chiral Hierarchies and the Flavor Changing Neutral Current Problem in Technicolor. *Phys.Rev.Lett.*, 57:957.

[35] Arisue, H. and Fujiwara, T. (1984). Analytic property of lattice theories with improved action. *Progress of Theoretical Physics*, 71(5):1026–1035.

[36] Arkani-Hamed, N., Cohen, A. G., and Georgi, H. (2001). (De)constructing dimensions. *Phys. Rev. Lett.*, 86:4757–4761.

[37] Arsene, I. et al. (2005). Quark gluon plasma and color glass condensate at RHIC? The Perspective from the BRAHMS experiment. *Nucl. Phys.*, A757:1–27.

[38] Arthur, R., Drach, V., Hansen, M., Hietanen, A., Lewis, R., et al. (2014). Composite (Goldstone) Higgs Dynamics on the Lattice: Spectrum of SU(2) Gauge Theory with two Fundamental Fermions. *PoS*, LATTICE2014:249.

[39] Aubin, C., Bernard, C., DeTar, C. E., Osborn, J., Gottlieb, S., Gregory, E. B., Toussaint, D., Heller, U. M., Hetrick, J. E., and Sugar, R. (2004). Light pseudoscalar decay constants, quark masses, and low energy constants from three-flavor lattice QCD. *Phys. Rev.*, D70:114501.

[40] Baak, M., C□th, J., Haller, J., Hoecker, A., Kogler, R., M□nig, K., Schott, M., and Stelzer, J. (2014). The global electroweak fit at nnlo and prospects for the lhc and ilc. *The European Physical Journal C*, 74(9).

[41] Back, B. B. et al. (2005). The PHOBOS perspective on discoveries at RHIC. *Nucl. Phys.*, A757:28–101.

[42] Banks, T., Susskind, L., and Kogut, J. B. (1976). Strong Coupling Calculations of Lattice Gauge Theories: (1+1)-Dimensional Exercises. *Phys. Rev.*, D13:1043.

[43] Banks, T. and Zaks, A. (1982). On the phase structure of vector-like gauge theories with massless fermions. *Nuclear Physics B*, 196(2):189 – 204.

[44] Bardeen, W. A., Hill, C. T., and Lindner, M. (1990). Minimal Dynamical Symmetry Breaking of the Standard Model. *Phys. Rev.*, D41:1647.

[45] Barranco, A., Pallante, E., and Russo, J. G. (2011). N=1 SQCD-like theories with Nf massive flavors from AdS/CFT and beta functions. *JHEP*, 1109:086.

[46] Bazavov, A. (2013). An overview of (selected) recent results in finite-temperature lattice QCD. *J.Phys.Conf.Ser.*, 446:012011.

[47] Bazavov, A. (2015). Lattice QCD at Non-Zero Temperature. In *Proceedings, 32nd International Symposium on Lattice Field Theory (Lattice 2014)*.

[48] Bazavov, A. et al. (2010). Nonperturbative QCD simulations with 2+1 flavors of improved staggered quarks. *Rev. Mod. Phys.*, 82:1349–1417.

[49] Bazavov, A. et al. (2012). The chiral and deconfinement aspects of the QCD transition. *Phys. Rev.*, D85:054503.

[50] Bellazzini, B., Csaki, C., Hubisz, J., Serra, J., and Terning, J. (2013). A Higgslike Dilaton. *Eur. Phys. J.*, C73(2):2333.

[51] Bernard, C. (2006). Staggered chiral perturbation theory and the fourth-root trick. *Phys. Rev.*, D73:114503.

[52] Bernard, C., Burch, T., Orginos, K., Toussaint, D., DeGrand, T. A., DeTar, C., Datta, S., Gottlieb, S., Heller, U. M., and Sugar, R. (2001). Qcd spectrum with three quark flavors. *Phys. Rev. D*, 64:054506.

[53] Bernard, C., DeTar, C. E., Levkova, L., Gottlieb, S., Heller, U. M., Hetrick, J. E., Osborn, J., Renner, D. B., Toussaint, D., and Sugar, R. (2007a). Status of the MILC light pseudoscalar meson project. *PoS*, LAT2007:090.

[54] Bernard, C., Golterman, M., and Shamir, Y. (2007b). Effective field theories for rooted staggered fermions. *PoS*, LAT2007:263.

[55] Bernard, C. W., Blum, T., DeTar, C. E., Gottlieb, S. A., Heller, U. M., Hetrick, J., Rummukainen, K., Sugar, R., Toussaint, D., and Wingate, M. (1995). Two flavor staggered fermion thermodynamics at N(t) = 12. [Nucl. Phys. Proc. Suppl.47,499(1996)].

[56] Bernard, C. W., Duncan, A., LoSecco, J., and Weinberg, S. (1975). Exact Spectral Function Sum Rules. *Phys. Rev.*, D12:792.

[57] Bernard, C. W. et al. (1998). Quenched hadron spectroscopy with improved staggered quark action. *Phys.Rev.*, D58:014503.

[58] Bludman, S. A. and Klein, A. (1963). Broken symmetries and massless particles. *Phys. Rev.*, 131:2364–2372.

[59] Bochicchio, M. (2009). Quasi BPS Wilson loops, localization of loop equation by homology and exact beta function in the large N limit of SU(N) Yang-Mills theory. *JHEP*, 0905:116.

[60] Bochicchio, M. (2013a). Glueball and meson propagators of any spin in large-n {QCD}. *Nuclear Physics B*, 875(3):621 – 649.

[61] Bochicchio, M. (2013b). Yang-Mills mass gap, Floer homology, glueball spectrum, and conformal window in large-N QCD.

[62] Bochicchio, M. (2014). An asymptotic solution of large-*N QCD*, and of large-$N\mathcal{N} = 1$ *SUSY YM*.

[63] Borsanyi, S., Fodor, Z., Hoelbling, C., Katz, S. D., Krieg, S., Ratti, C., and Szabo, K. K. (2010). Is there still any T_c mystery in lattice QCD? Results with physical masses in the continuum limit III. *JHEP*, 09:073.

[64] Boyd, G., Gupta, S., Karsch, F., and Laermann, E. (1994). Spatial and temporal hadron correlators below and above the chiral phase transition. *Zeitschrift f□r Physik C Particles and Fields*, 64(2):331–338.

[65] Braun, J., Fischer, C. S., and Gies, H. (2011). Beyond Miransky Scaling. *Phys.Rev.*, D84:034045.

[66] Braun, J. and Gies, H. (2006). Chiral phase boundary of QCD at finite temperature. *JHEP*, 0606:024.

[67] Braun, J. and Gies, H. (2010). Scaling laws near the conformal window of many-flavor QCD. *JHEP*, 1005:060.

[68] Brown, F. R., Chen, H., Christ, N. H., Dong, Z., Mawhinney, R. D., Schaffer, W., and Vaccarino, A. (1992). Lattice QCD with eight light quark flavors. *Phys. Rev.*, D46:5655–5670.

[69] Burdman, G. and Evans, N. J. (1999). Flavor universal dynamical electroweak symmetry breaking. *Phys. Rev.*, D59:115005.

[70] Bursa, F., Del Debbio, L., Keegan, L., Pica, C., and Pickup, T. (2010). Mass anomalous dimension in SU(2) with two adjoint fermions. *Phys.Rev.*, D81:014505.

[71] B□nisch, R. (1991). Deriving the top mode standard model interaction from gauge theory. *Physics Letters B*, 268(3?4):394 – 400.

[72] Cacciapaglia, G., Csaki, C., Grojean, C., and Terning, J. (2004). Oblique corrections from Higgsless models in warped space. *Phys. Rev.*, D70:075014.

[73] Callan, C. G. (1970). Broken scale invariance in scalar field theory. *Phys. Rev. D*, 2:1541–1547.

[74] Caswell, W. (1974a). Asymptotic Behavior of Non-Abelian Gauge Theories to Two-Loop Order. *Physical Review Letters*, 33(4):244–246.

[75] Caswell, W. E. (1974b). Asymptotic behavior of non-abelian gauge theories to two-loop order. *Phys. Rev. Lett.*, 33:244–246.

[76] Catterall, S., Giedt, J., Sannino, F., and Schneible, J. (2009). Probes of nearly conformal behavior in lattice simulations of minimal walking technicolor.

[77] Chatrchyan, S. et al. (2012). Observation of a new boson at a mass of 125 GeV with the CMS experiment at the LHC. *Phys. Lett.*, B716:30–61.

[78] Chen, Y. et al. (2006). Glueball spectrum and matrix elements on anisotropic lattices. *Phys. Rev.*, D73:014516.

[79] Cheng, A., Hasenfratz, A., Liu, Y., Petropoulos, G., and Schaich, D. (2014). Finite size scaling of conformal theories in the presence of a near-marginal operator. *Phys. Rev. D*, 90:014509.

[80] Cheng, A., Hasenfratz, A., Petropoulos, G., and Schaich, D. (2013). Scale-dependent mass anomalous dimension from dirac eigenmodes. *Journal of High Energy Physics*, 2013(7).

[81] Cheng, A., Hasenfratz, A., and Schaich, D. (2011). Novel phase in SU(3) lattice gauge theory with 12 light fermions. *Arxiv preprint arXiv:1111.2317*, (November):4.

[82] Cheng, A., Hasenfratz, A., and Schaich, D. (2012a). Novel phase in su(3) lattice gauge theory with 12 light fermions. *Phys. Rev. D*, 85:094509.

[83] Cheng, A., Hasenfratz, A., and Schaich, D. (2012b). Novel phase in su(3) lattice gauge theory with 12 light fermions. *Phys. Rev. D*, 85:094509.

[84] Chivukula, R. S. (1998). Models of electroweak symmetry breaking: Course. In *Towards the millennium in astrophysics: Problems and prospects. Proceedings, 10th Course of the International School of Cosmic Ray Astrophysics, Erice, Italy, June 16-23, 1996*, pages 1339–1407. [,1339(1998)].

[85] Chivukula, R. S., Dobrescu, B. A., Georgi, H., and Hill, C. T. (1999). Top quark seesaw theory of electroweak symmetry breaking. *Phys. Rev.*, D59:075003.

[86] Clark, M., Babich, R., Barros, K., Brower, R., and Rebbi, C. (2010). Solving Lattice QCD systems of equations using mixed precision solvers on GPUs. *Comput.Phys.Commun.*, 181:1517–1528.

[87] Cleymans, J., Gavai, R., and Suhonen, E. (1986). Quarks and gluons at high temperatures and densities. *Physics Reports*, 130(4):217 – 292.

[88] Cohen, A. and Georgi, H. (1989). Walking beyond the rainbow. *Nuclear Physics B*, 314(1):7 – 24.

[89] Colangelo, G., Durr, S., and Sommer, R. (2003). Finite size effects on M(pi) in QCD from chiral perturbation theory. *Nucl.Phys.Proc.Suppl.*, 119:254–256.

[90] Collaboration, C. (2013). Search for Anomalous Top Quark Pair Production in the Boosted All-Hadronic Final State using pp Collisions at sqrt(s) = 8 TeV.

[91] collaboration, T. A. (2013a). A search for $t\bar{t}$ resonances in the lepton plus jets final state with ATLAS using 14 fb$^{?1}$ of pp collisions at $\sqrt{s} = 8$ TeV.

[92] collaboration, T. A. (2013b). Search for pair production of heavy top-like quarks decaying to a high-p_{T} W boson and a b quark in the lepton plus jets final state in pp collisions at $\sqrt{s} = 8$ TeV with the ATLAS detector.

[93] Collins, J. C., Duncan, A., and Joglekar, S. D. (1977). Trace and dilatation anomalies in gauge theories. *Phys. Rev.*, D16:438–449.

[94] Creutz, M. (2007). Chiral anomalies and rooted staggered fermions. *Physics Letters B*, 649(2?3):230 – 234.

[95] Csaki, C., Grojean, C., Murayama, H., Pilo, L., and Terning, J. (2004). Gauge theories on an interval: Unitarity without a Higgs. *Phys. Rev.*, D69:055006.

[96] da Silva, T. N. and Pallante, E. (2012). The strong coupling regime of twelve flavors QCD. *PoS*, LATTICE2012:052.

[97] Damgaard, P., Heller, U., Krasnitz, A., and Olesen, P. (1997). Lattice qcd with many flavours. *Physics Letters B*, 400(1–2):169 – 175.

[98] Damgaard, P. H., Heller, U. M., Niclasen, R., and Svetitsky, B. (2002). Patterns of spontaneous chiral symmetry breaking in vector - like gauge theories. *Nucl. Phys.*, B633:97–113.

[99] Davies, C. T. H., Follana, E., Gray, A., Lepage, G. P., Mason, Q., Nobes, M., Shigemitsu, J., Trottier, H. D., Wingate, M., Aubin, C., Bernard, C., Burch, T., DeTar, C., Gottlieb, S., Gregory, E. B., Heller, U. M., Hetrick, J. E., Osborn, J., Sugar, R., Toussaint, D., Pierro, M. D., El-Khadra, A., Kronfeld, A. S., Mackenzie, P. B., Menscher, D., and Simone, J. (2004). High-precision lattice qcd confronts experiment. *Phys. Rev. Lett.*, 92:022001.

[100] de Forcrand, P., Kim, S., and Unger, W. (2013). Conformality in many-flavour lattice QCD at strong coupling. *JHEP*, 1302:051.

[101] DeGrand, T. (2011). Finite-size scaling tests for spectra in su(3) lattice gauge theory coupled to 12 fundamental flavor fermions. *Phys. Rev. D*, 84:116901.

[102] DeGrand, T., Shamir, Y., and Svetitsky, B. (2009). Phase structure of su(3) gauge theory with two flavors of symmetric-representation fermions. *Phys. Rev. D*, 79:034501.

[103] DeGrand, T., Shamir, Y., and Svetitsky, B. (2010). Running coupling and mass anomalous dimension of su(3) gauge theory with two flavors of symmetric-representation fermions. *Phys. Rev. D*, 82:054503.

[104] DeGrand, T., Shamir, Y., and Svetitsky, B. (2011). Infrared fixed point in SU(2) gauge theory with adjoint fermions. *Phys.Rev.*, D83:074507.

[105] DeGrand, T., Shamir, Y., and Svetitsky, B. (2012). SU(4) lattice gauge theory with decuplet fermions: Schrodinger functional analysis. *Phys.Rev.*, D85:074506.

[106] DeGrand, T., Shamir, Y., and Svetitsky, B. (2013). Mass anomalous dimension in sextet QCD. *Phys.Rev.*, D87:074507.

[107] Del Debbio, L., Lucini, B., Patella, A., Pica, C., and Rago, A. (2009). Conformal versus confining scenario in SU(2) with adjoint fermions. *Phys.Rev.*, D80:074507.

[108] Del Debbio, L., Lucini, B., Patella, A., Pica, C., and Rago, A. (2010a). Mesonic spectroscopy of Minimal Walking Technicolor. *Phys.Rev.*, D82:014509.

[109] Del Debbio, L., Lucini, B., Patella, A., Pica, C., and Rago, A. (2010b). The infrared dynamics of Minimal Walking Technicolor. *Phys.Rev.*, D82:014510.

[110] Del Debbio, L., Lucini, B., Pica, C., Patella, A., Rago, A., and Roman, S. (2013). Large-volume results in SU(2) with adjoint fermions. In *Proceedings, 31st International Symposium on Lattice Field Theory (Lattice 2013)*.

[111] Del Debbio, L. and Zwicky, R. (2010). Hyperscaling relations in mass-deformed conformal gauge theories. *Phys. Rev. D*, 82:014502.

[112] Deuzeman, A., Lombardo, M., and Pallante, E. (2010a). Evidence for a conformal phase in SU(N) gauge theories. *Physical Review D*, 82(7):11.

[113] Deuzeman, A., Lombardo, M. P., da Silva, T. N., and Pallante, E. (2011a). Bulk transitions of twelve flavor QCD and $U_A(1)$ symmetry. *PoS*, LATTICE2011:321.

[114] Deuzeman, A., Lombardo, M. P., Nunes Da Silva, T., and Pallante, E. (2013). The bulk transition of QCD with twelve flavors and the role of improvement. *Phys.Lett.*, B720:358–365.

[115] Deuzeman, A., Lombardo, M. P., and Pallante, E. (2008a). The physics of eight flavours. *Physics Letters B*, 670(1):19.

[116] Deuzeman, A., Lombardo, M. P., and Pallante, E. (2008b). The Physics of eight flavours. *Phys. Lett.*, B670:41–48.

[117] Deuzeman, A., Lombardo, M. P., and Pallante, E. (2010b). Evidence for a conformal phase in SU(n) gauge theories. *Phys. Rev. D*, 82:074503.

[118] Deuzeman, A., Lombardo, M. P., and Pallante, E. (2010c). The bulk transition of many-flavour QCD and the search for a UVFP at strong coupling. *Arxiv preprint arXiv:1012.5971*, page 7.

[119] Deuzeman, A., Lombardo, M. P., and Pallante, E. (2011b). On the spectrum of QCD-like theories and the conformal window. *PoS*, LATTICE2011:083.

[120] Deuzeman, A., Pallante, E., and Lombardo, M. P. (2010d). The Bulk transition of many-flavour QCD and the search for a UVFP at strong coupling. *PoS*, LATTICE2010:067.

[121] Dietrich, D. D. and Sannino, F. (2007). Conformal window of SU(N) gauge theories with fermions in higher dimensional representations. *Phys.Rev.*, D75:085018.

[122] Dietrich, D. D., Sannino, F., and Tuominen, K. (2005). Light composite Higgs from higher representations versus electroweak precision measurements: Predictions for CERN LHC. *Phys.Rev.*, D72:055001.

[123] Dimopoulos, S. and Susskind, L. (1979). Mass Without Scalars. *Nucl.Phys.*, B155:237–252.

[124] Dobrescu, B. A. and Hill, C. T. (1998). Electroweak symmetry breaking via top condensation seesaw. *Phys. Rev. Lett.*, 81:2634–2637.

[125] Drut, J. E. and Nicholson, A. N. (2013). Lattice methods for strongly interacting many-body systems. *Journal of Physics G: Nuclear and Particle Physics*, 40(4):043101.

[126] Durr, S. (2006). Theoretical issues with staggered fermion simulations. *PoS*, LAT2005:021.

[127] Eichten, E. and Lane, K. D. (1980). Dynamical Breaking of Weak Interaction Symmetries. *Phys.Lett.*, B90:125–130.

[128] Ferrara, S., Gatto, R., and Grillo, A. (1974). Positivity restriction on anomalous dimensions. *Phys. Rev. D*, 9:3564–3565.

[129] Ferrara, S., Grillo, A. F., and Gatto, R. (1973). Tensor representations of conformal algebra and conformally covariant operator product expansion. *Annals Phys.*, 76:161–188.

[130] Fodor, Z., Holland, K., Kuti, J., Mondal, S., Nogradi, D., et al. (2015a). Baryon spectrum in the composite sextet model. *PoS*, LATTICE2014:270.

[131] Fodor, Z., Holland, K., Kuti, J., Mondal, S., Nogradi, D., et al. (2015b). The running coupling of 8 flavors and 3 colors. *JHEP*, 1506:019.

[132] Fodor, Z., Holland, K., Kuti, J., Mondal, S., Nogradi, D., et al. (2015c). Toward the minimal realization of a light composite Higgs. *PoS*, LATTICE2014:244.

[133] Fodor, Z., Holland, K., Kuti, J., Nogradi, D., and Schroeder, C. (2009). Chiral properties of SU(3) sextet fermions. *JHEP*, 0911:103.

[134] Fodor, Z., Holland, K., Kuti, J., Nogradi, D., Schroeder, C., et al. (2011). Twelve massless flavors and three colors below the conformal window. *Phys.Lett.*, B703:348–358.

[135] Fodor, Z., Holland, K., Kuti, J., Nogradi, D., Schroeder, C., et al. (2012). Can the nearly conformal sextet gauge model hide the Higgs impostor? *Phys.Lett.*, B718:657–666.

[136] Frezzotti, R., Grassi, P. A., Sint, S., and Weisz, P. (2000). A Local formulation of lattice QCD without unphysical fermion zero modes. *Nucl. Phys. Proc. Suppl.*, 83:941–946.

[137] Frezzotti, R., Grassi, P. A., Sint, S., and Weisz, P. (2001a). Lattice QCD with a chirally twisted mass term. *JHEP*, 08:058.

[138] Frezzotti, R., Sint, S., and Weisz, P. (2001b). O(a) improved twisted mass lattice QCD. *JHEP*, 07:048.

[139] Fukugita, M., Ohta, S., and Ukawa, A. (1988). Finite-temperature phase transitions in lattice qcd for a general number of flavors. *Phys. Rev. Lett.*, 60:178–181.

[140] Gangopadhyaya, M. (1981). *Indian atomism: History and sources (Bagchi indological series)*. Humanities Press.

[141] Gasser, J. and Leutwyler, H. (1988). Spontaneously broken symmetries: Effective lagrangians at finite volume. *Nuclear Physics B*, 307(4):763 – 778.

[142] Gavai, R. V. (2003). Improving the quark number susceptibilities for staggered fermions. *Nucl.Phys.Proc.Suppl.*, 119:529–531.

[143] Gell-Mann, M. (1961). The Eightfold Way: A Theory of strong interaction symmetry.

[144] Gell-Mann, M. (1962). Symmetries of baryons and mesons. *Phys. Rev.*, 125:1067–1084.

[145] Gell-Mann, M. (1964). A Schematic Model of Baryons and Mesons. *Phys. Lett.*, 8:214–215.

[146] Georgi, H. (2005). Fun with Higgsless theories. *Phys. Rev.*, D71:015016.

[147] Ginsparg, P. H. and Wilson, K. G. (1982). A remnant of chiral symmetry on the lattice. *Phys. Rev. D*, 25:2649–2657.

[148] Goldstone, J. (1961). Field theories with « superconductor » solutions. *Il Nuovo Cimento (1955-1965)*, 19(1):154–164.

[149] Goldstone, J., Salam, A., and Weinberg, S. (1962). Broken symmetries. *Phys. Rev.*, 127:965–970.

[150] Golterman, M. (2008). QCD with rooted staggered fermions. *PoS*, CONFINEMENT8:014.

[151] Gracey, J. (1996). The QCD Beta function at O(1/N(f)). *Phys.Lett.*, B373:178–184.

[152] Gracey, J. A. and Simms, R. M. (2015). Banks-Zaks fixed point analysis in momentum subtraction schemes. *Phys. Rev.*, D91(8):085037.

[153] Gregory, E., Irving, A., Lucini, B., McNeile, C., Rago, A., Richards, C., and Rinaldi, E. (2012). Towards the glueball spectrum from unquenched lattice QCD. *JHEP*, 10:170.

[154] Gross, D. J., Balian, R., and Zinn-Justin, J. (1976). *Methods in Field Theory, Les Houches 1975*. North Holland.

[155] Gross, D. J. and Wilczek, F. (1973a). Asymptotically free gauge theories. i. *Phys. Rev. D*, 8:3633–3652.

[156] Gross, D. J. and Wilczek, F. (1973b). Ultraviolet Behavior of Nonabelian Gauge Theories. *Phys.Rev.Lett.*, 30:1343–1346.

[157] Hasenfratz, A. (2009a). Investigating the critical properties of beyond-QCD theories using Monte Carlo Renormalization Group matching. *Phys.Rev.*, D80:034505.

[158] Hasenfratz, A. (2009b). Scaling properties of many-fermion systems from MCRG studies. *PoS*, LAT2009:052.

[159] Hasenfratz, A. (2015). Improved gradient flow for step scaling function and scale setting. *PoS*, LATTICE2014:257.

[160] Hasenfratz, A., Schaich, D., and Veernala, A. (2014). Nonperturbative beta function of eight-flavor SU(3) gauge theory.

[161] Hasenfratz, P. (1998). Prospects for perfect actions. *Nucl. Phys. Proc. Suppl.*, 63:53–58.

[162] Hasenfratz, P. and Karsch, F. (1983). Chemical Potential on the Lattice. *Phys.Lett.*, B125:308.

[163] He, H.-J., Hill, C. T., and Tait, T. M. P. (2002). Top quark seesaw, vacuum structure and electroweak precision constraints. *Phys. Rev.*, D65:055006.

[164] Hietanen, A., Lewis, R., Pica, C., and Sannino, F. (2014a). Fundamental Composite Higgs Dynamics on the Lattice: SU(2) with Two Flavors. *JHEP*, 1407:116.

[165] Hietanen, A., Pica, C., Sannino, F., and S□ndergaard, U. (2014b). Predictions for LHC from SO(4) MWT. *PoS*, LATTICE2013:105.

[166] Hietanen, A. J., Rummukainen, K., and Tuominen, K. (2009). Evolution of the coupling constant in SU(2) lattice gauge theory with two adjoint fermions. *Phys.Rev.*, D80:094504.

[167] Hill, C. T. (1991). Topcolor: top quark condensation in a gauge extension of the standard model. *Physics Letters B*, 266(3):419 – 424.

[168] Hill, C. T. (1995). Topcolor assisted technicolor. *Physics Letters B*, 345(4):483 – 489.

[169] Hill, C. T., Kennedy, D. C., Onogi, T., and Yu, H.-L. (1993). Spontaneously broken technicolor and the dynamics of virtual vector technimesons. *Phys. Rev. D*, 47:2940–2948.

[170] Hill, C. T., Pokorski, S., and Wang, J. (2001). Gauge invariant effective Lagrangian for Kaluza-Klein modes. *Phys. Rev.*, D64:105005.

[171] Hill, C. T. and Simmons, E. H. (2003). Strong dynamics and electroweak symmetry breaking. *Phys.Rept.*, 381:235–402.

[172] Holdom, B. (1981). Raising the Sideways Scale. *Phys.Rev.*, D24:1441.

[173] Holdom, B. (1985). Techniodor. *Phys.Lett.*, B150:301.

[174] Holdom, B. (2010). Large N flavor beta-functions: a recap. *Phys.Lett.*, B694:74–79.

[175] Ishikawa, K.-I., Iwasaki, Y., Nakayama, Y., and Yoshie, T. (2014). Global structure of conformal theories in the $su(3)$ gauge theory. *Phys. Rev. D*, 89:114503.

[176] Itou, E. (2015). A novel scheme for the wave function renormalization of the composite operators. *PTEP*, 2015(4):043B08.

[177] Itou, E. and Tomiya, A. (2014). Determination of the mass anomalous dimension for $N_f = 12$ and $N_f = 9$ SU(3) gauge theories. *PoS*, LATTICE2014:252.

[178] Iwasaki, Y., Kanaya, K., Kaya, S., Sakai, S., and Yoshie, T. (1998). Quantum chromodynamics with many flavors. *Prog. Theor. Phys. Suppl.*, 131:415–426.

[179] Iwasaki, Y., Kanaya, K., Sakai, S., and Yoshié, T. (1992). Quark confinement and number of flavors in strong coupling lattice qcd. *Phys. Rev. Lett.*, 69:21–24.

[180] Jin, X.-Y. and Mawhinney, R. D. (2008). Lattice QCD with Eight Degenerate Quark Flavors. *PoS*, LATTICE2008:059.

[181] Jin, X.-y. and Mawhinney, R. D. (2009). Lattice QCD with 8 and 12 degenerate quark flavors. *Arxiv preprint arXiv:0910.3216*, page 7.

[182] Jin, X.-Y. and Mawhinney, R. D. (2010). Evidence for a First Order, Finite Temperature Phase Transition in 8 Flavor QCD. *PoS*, LATTICE2010:055.

[183] Jones, D. (1974). Two-loop diagrams in yang-mills theory. *Nucl. Phys.*, B75(3):531 – 538.

[184] Kaplan, D. B. (1992). A Method for simulating chiral fermions on the lattice. *Phys. Lett.*, B288:342–347.

[185] Kaplan, D. B. and Georgi, H. (1984). SU(2) x U(1) Breaking by Vacuum Misalignment. *Phys. Lett.*, B136:183.

[186] Kaplan, D. B., Georgi, H., and Dimopoulos, S. (1984). Composite Higgs Scalars. *Phys. Lett.*, B136:187.

[187] Kaplan, D. B., Lee, J.-W., Son, D. T., and Stephanov, M. A. (2009a). Conformality lost. *Phys. Rev. D*, 80:125005.

[188] Kaplan, D. B., Lee, J.-W., Son, D. T., and Stephanov, M. A. (2009b). Conformality Lost. *Phys. Rev.*, D80:125005.

[189] Karsch, F. (1998). Deconfinement and chiral symmetry restoration in QCD with fundamental and adjoint fermions. [PoScorfu98,008(1998)].

[190] Karsch, F. (2007). Recent lattice results on finite temperature and density QCD. Part I. *PoS*, CPOD07:026.

[191] Kocic, A., Kogut, J. B., and Lombardo, M.-P. (1993). Universal properties of chiral symmetry breaking. *Nucl. Phys.*, B398:376–404.

[192] Kogut, J., Lagae, J., and Sinclair, D. (1998). Topology, fermionic zero modes and flavor singlet correlators in finite temperature QCD. *Phys.Rev.*, D58:054504.

[193] Kogut, J. and Sinclair, D. (2011). Thermodynamics of lattice QCD with 2 sextet quarks on N_t=8 lattices. *Phys.Rev.*, D84:074504.

[194] Kogut, J. and Sinclair, D. (2014). Thermodynamics of lattice QCD with 3 flavours of colour-sextet quarks II. $N_t = 6$ and $N_t = 8$. *Phys.Rev.*, D90(1):014506.

[195] Kogut, J. and Susskind, L. (1975). Hamiltonian formulation of wilson's lattice gauge theories. *Phys. Rev. D*, 11:395–408.

[196] Kogut, J. B., Matsuoka, H., Stone, M., Wyld, H., Shenker, S. H., et al. (1983). Chiral Symmetry Restoration in Baryon Rich Environments. *Nucl.Phys.*, B225:93.

[197] Kogut, J. B., Polonyi, J., Wyld, H. W., and Sinclair, D. K. (1985). Simulations and speculations on gauge theories with many fermions. *Phys. Rev. Lett.*, 54:1475–1478.

[198] Kogut, J. B. and Sinclair, D. K. (1988). SU(2) and SU(3) Lattice Gauge Theories With Many Fermions. *Nucl. Phys.*, B295:465.

[199] Kosterlitz, J. M. (1974). The critical properties of the two-dimensional xy model. *Journal of Physics C: Solid State Physics*, 7(6):1046.

[200] Kronfeld, A. S. (2007). Lattice gauge theory with staggered fermions: How, where, and why (not). *PoS*, LAT2007:016.

[201] Kurachi, M. and Shrock, R. (2006). Behavior of the S Parameter in the Crossover Region Between Walking and QCD-Like Regimes of an SU(N) Gauge Theory. *Phys. Rev.*, D74:056003.

[202] Kurachi, M. and Shrock, R. (2007). Study of the change from walking to non-walking behavior in a vectorial gauge theory as a function of N(f). In *The origin of mass and strong coupling gauge theories. Proceedings, 5th International Workshop, SCGT'06, Nagoya, Japan November 21-24, 2006*, pages 285–291.

[203] Larin, S. and Vermaseren, J. (1993). The Three loop QCD Beta function and anomalous dimensions. *Phys.Lett.*, B303:334–336.

[204] Lepage, G. P. (1998). Lattice QCD for novices. In *Strong interactions at low and intermediate energies. Proceedings, 13th Annual Hampton University Graduate Studies, HUGS'98, Newport News, USA, May 26-June 12, 1998*, pages 49–90.

[205] Lepage, G. P. and Mackenzie, P. B. (1993). On the viability of lattice perturbation theory. *Phys. Rev.*, D48:2250–2264.

[206] Lin, C. J. D., Ogawa, K., Ohki, H., Ramos, A., and Shintani, E. (2014). SU(3) gauge theory with 12 flavours in a twisted box. *PoS*, LATTICE2014:259.

[207] Lindner, M. and Ross, D. (1992). Top condensation from very massive strongly coupled gauge bosons. *Nuclear Physics B*, 370(1):30 – 50.

[208] Lombardo, M., Miura, K., da Silva, T. J. N., and Pallante, E. (2014a). On the particle spectrum and the conformal window. *JHEP*, 1412:183.

[209] Lombardo, M. P., Miura, K., da Silva, T. N., and Pallante, E. (2014b). Approaching Conformality. *PoS*, LATTICE2014:242.

[210] Lucini, B. (2010). Strongly Interacting Dynamics beyond the Standard Model on a Spacetime Lattice. *Phil. Trans. Roy. Soc. Lond.*, A368:3657–3670.

[211] Lucini, B. (2013). Glueballs from the Lattice. *PoS*, QCD-TNT-III:023.

[212] Lucini, B. and Panero, M. (2014). Introductory lectures to large-N QCD phenomenology and lattice results. *Prog. Part. Nucl. Phys.*, 75:1–40.

[213] Lüscher, M. (1986). Volume dependence of the energy spectrum in massive quantum field theories. *Communications in Mathematical Physics*, 105(2):153–188.

[214] Lüscher, M. (2010a). Properties and uses of the Wilson flow in lattice QCD. *JHEP*, 1008:071.

[215] Lüscher, M. (2010b). Trivializing maps, the Wilson flow and the HMC algorithm. *Commun.Math.Phys.*, 293:899–919.

[216] Lüscher, M., Narayanan, R., Weisz, P., and Wolff, U. (1992). The Schrodinger functional: A Renormalizable probe for nonAbelian gauge theories. *Nucl.Phys.*, B384:168–228.

[217] Lüscher, M., Sommer, R., Weisz, P., and Wolff, U. (1994). A Precise determination of the running coupling in the SU(3) Yang-Mills theory. *Nucl.Phys.*, B413:481–502.

[218] Lüscher, M. and Weisz, P. (1984). Definition and general properties of the transfer matrix in continuum limit improved lattice gauge theories. *Nuclear Physics B*, 240(3):349 – 361.

[219] Lüscher, M. and Weisz, P. (2002). Quark confinement and the bosonic string. *JHEP*, 2002(07):049.

[220] Lüscher, M. and Weisz, P. (2004). String excitation energies in su(n) gauge theories beyond the free-string approximation. *JHEP*, 2004(07):014.

[221] Lüscher, M., Weisz, P., and Wolff, U. (1991). A Numerical method to compute the running coupling in asymptotically free theories. *Nucl.Phys.*, B359:221–243.

[222] Mack, G. (1977). All unitary ray representations of the conformal group su(2,2) with positive energy. *Communications in Mathematical Physics*, 55(1):1–28.

[223] Marciano, W. J. (1989). Heavy top-quark mass predictions. *Phys. Rev. Lett.*, 62:2793–2796.

[224] Martin, S. P. (1992). Renormalizable top quark condensate models. *Phys. Rev.*, D45:4283–4293.

[225] Martin, S. P. (1993). Self-breaking technicolor. *Nuclear Physics B*, 398(2):359 – 375.

[226] Martinelli, G., Parisi, G., and Petronzio, R. (1981). Monte Carlo Simulations for the Two-dimensional O(3) Nonlinear σ Model. *Phys. Lett.*, B100:485.

[227] Matsuzaki, S. and Yamawaki, K. (2012). Holographic techni-dilaton at 125 GeV. *Phys. Rev.*, D86:115004.

[228] McEvilley, T. (2001). *The Shape of Ancient Thought: Comparative Studies in Greek and Indian Philosophies*. Allworth Press.

[229] McNeile, C. (2009). Lattice status of gluonia/glueballs. *Nucl. Phys. Proc. Suppl.*, 186:264–267.

[230] Meyer, H. B. and Teper, M. J. (2005). Glueball Regge trajectories and the pomeron: A Lattice study. *Phys. Lett.*, B605:344–354.

[231] Miransky, V. (1985). Dynamics of spontaneous chiral symmetry breaking and the continuum limit in quantum electrodynamics. *Il Nuovo Cimento A (1965-1970)*, 90(2):149–170.

[232] Miransky, V. (1999). Dynamics in the conformal window in QCD like theories. *Phys.Rev.*, D59:105003.

[233] MIRANSKY, V., TANABASHI, M., and YAMAWAKI, K. (1989). Is the t quark responsible for the mass of w and z bosons? *Modern Physics Letters A*, 04(11):1043–1053.

[234] Miransky, V. A. (1997). Conformal phase transition in gauge theories. *Physical Review D*, 55(8):5051–5066.

[235] Miransky, V. A., Tanabashi, M., and Yamawaki, K. (1989). Dynamical Electroweak Symmetry Breaking with Large Anomalous Dimension and t Quark Condensate. *Phys. Lett.*, B221:177.

[236] Miura, K. and Lombardo, M. P. (2013). Lattice Monte-Carlo study of pre-conformal dynamics in strongly flavoured QCD in the light of the chiral phase transition at finite temperature. *Nucl. Phys.*, B871:52–81.

[237] Miura, K., Lombardo, M. P., and Pallante, E. (2012). Chiral phase transition at finite temperature and conformal dynamics in large Nf QCD. *Phys.Lett.*, B710:676–682.

[238] Morningstar, C. J. and Peardon, M. J. (1999). The Glueball spectrum from an anisotropic lattice study. *Phys. Rev.*, D60:034509.

[239] Naik, S. (1989). On-shell Improved Lattice Action for QCD with Susskind Fermions and Asymptotic Freedom Scale. *Nucl.Phys.*, B316:238.

[240] Nambu, Y. (1989). Enrico Fermi Institute Report No. 89-08. (unplubished).

[241] Nambu, Y. and Jona-Lasinio, G. (1961). Dynamical model of elementary particles based on an analogy with superconductivity. i. *Phys. Rev.*, 122:345–358.

[242] Narayanan, R. and Neuberger, H. (2006). Infinite N phase transitions in continuum Wilson loop operators. *JHEP*, 0603:064.

[243] Nash, D. (1989). Higher-order corrections in (2+1)-dimensional qed. *Phys. Rev. Lett.*, 62:3024–3026.

[244] Ne'eman, Y. (1961). Derivation of strong interactions from a gauge invariance. *Nucl. Phys.*, 26:222–229.

[245] Neuberger, H. (1998a). Exactly massless quarks on the lattice. *Phys. Lett.*, B417:141–144.

[246] Neuberger, H. (1998b). More about exactly massless quarks on the lattice. *Phys. Lett.*, B427:353–355.

[247] Nielsen, H. and Ninomiya, M. (1981). A no-go theorem for regularizing chiral fermions. *Physics Letters B*, 105(2-3):219 – 223.

[248] Nielsen, N. (1977). The Energy Momentum Tensor in a Nonabelian Quark Gluon Theory. *Nucl. Phys.*, B120:212–220.

[249] Novikov, V., Shifman, M., Vainshtein, A., and Zakharov, V. (1983a). Exact gell-mann-low function of supersymmetric yang-mills theories from instanton calculus. *Nucl. Phys.*, B229(2):381 – 393.

[250] Novikov, V., Shifman, M., Vainshtein, A., and Zakharov, V. (1986). The beta function in supersymmetric gauge theories. instantons versus traditional approach. *Phys. Lett.*, B166(3):329 – 333.

[251] Novikov, V. A., Shifman, M. A., Vainshtein, A. I., and Zakharov, V. I. (1983b). Instanton Effects in Supersymmetric Theories. *Nucl. Phys.*, B229:407.

[252] Ochs, W. (2013). The Status of Glueballs. *J. Phys.*, G40:043001.

[253] Ohta, S. and Kim, S. (1991). Finite-temperature phase structure of lattice qcd for 8 and 17 flavors. *Phys. Rev. D*, 44:504–512.

[254] Olive, K. et al. (2014). Review of Particle Physics. *Chin.Phys.*, C38:090001.

[255] Olive, K. and Group, P. D. (2014). Review of particle physics. *Chinese Physics C*, 38(9):090001.

[256] Pagels, H. and Stokar, S. (1979). Pion decay constant, electromagnetic form factor, and quark electromagnetic self-energy in quantum chromodynamics. *Phys. Rev. D*, 20:2947–2952.

[257] Pallante, E. (2009). Strongly and slightly flavored gauge theories. *PoS*, LAT2009:015.

[258] Pallante, E. (2015). Topology, the meson spectrum and the scalar glueball: three probes of conformality and the way it is lost. In *Sakata Memorial KMI Workshop on Origin of Mass and Strong Coupling Gauge Theories (SCGT15) Nagoya, Japan, March 3-6, 2015*.

[259] Patella, A. (2012). A precise determination of the psibar-psi anomalous dimension in conformal gauge theories. *Phys. Rev.*, D86:025006.

[260] Peskin, M. E. and Takeuchi, T. (1992). Estimation of oblique electroweak corrections. *Phys. Rev. D*, 46:381–409.

[261] Pica, C. and Sannino, F. (2011). Ultraviolet and infrared zeros of gauge theories at the four-loop order and beyond. *Phys. Rev. D*, 83:035013.

[262] Pich, A. (2013). The Physics of the Higgs-like Boson. *EPJ Web Conf.*, 60:02006.

[263] Pich, A., Rosell, I., and Sanz-Cillero, J. J. (2012). One-Loop Calculation of the Oblique S Parameter in Higgsless Electroweak Models. *JHEP*, 08:106.

[264] Pich, A., Rosell, I., and Sanz-Cillero, J. J. (2013a). Strongly Coupled Models with a Higgs-like Boson. *EPJ Web Conf.*, 60:19009.

[265] Pich, A., Rosell, I., and Sanz-Cillero, J. J. (2013b). Viability of strongly-coupled scenarios with a light Higgs-like boson. *Phys. Rev. Lett.*, 110:181801.

[266] Pich, A., Rosell, I., and Sanz-Cillero, J. J. (2014). Oblique S and T Constraints on Electroweak Strongly-Coupled Models with a Light Higgs. *JHEP*, 01:157.

[267] Politzer, H. D. (1973). Reliable perturbative results for strong interactions? *Phys. Rev. Lett.*, 30:1346–1349.

[268] Polyakov, A. (1978). Thermal properties of gauge fields and quark liberation. *Physics Letters B*, 72(4):477 – 480.

[269] Polyakov, A. M. (1974). Non-Hamiltonian approach to conformal quantum field theory. *Soviet Journal of Experimental and Theoretical Physics*, 39:10.

[270] Randall, L. and Sundrum, R. (1999). A Large mass hierarchy from a small extra dimension. *Phys. Rev. Lett.*, 83:3370–3373.

[271] Rantaharju, J., Karavirta, T., Leino, V., Rantalaiho, T., Rummukainen, K., et al. (2014). The gradient flow running coupling in SU2 with 8 flavors. *PoS*, LATTICE2014:258.

[272] Rattazzi, R., Rychkov, V. S., Tonni, E., and Vichi, A. (2008). Bounding scalar operator dimensions in 4D CFT. *JHEP*, 12:031.

[273] Ryttov, T. A. and Sannino, F. (2008). Supersymmetry inspired qcd beta function. *Phys. Rev. D*, 78:065001.

[274] Ryttov, T. A. and Shrock, R. (2011). Higher-loop corrections to the infrared evolution of a gauge theory with fermions. *Phys. Rev. D*, 83:056011.

[275] Ryttov, T. A. and Shrock, R. (2012). Scheme transformations in the vicinity of an infrared fixed point. *Phys. Rev. D*, 86:065032.

[276] Sasaki, K. and Sasaki, S. (2005). Excited baryon spectroscopy from lattice qcd: Finite size effect and hyperfine mass splitting. *Phys. Rev. D*, 72:034502.

[277] Schaefer, S. (2011). Algorithms for lattice QCD: progress and challenges. *AIP Conf.Proc.*, 1343:93–98.

[278] Schaich, D. (2014). Eight light flavors on large lattice volumes. *PoS*, LATTICE2013:072.

[279] Schaich, D., Cheng, A., Hasenfratz, A., and Petropoulos, G. (2012). Bulk and finite-temperature transitions in SU(3) gauge theories with many light fermions. *PoS*, LATTICE2012:028.

[280] Schaich, D., Hasenfratz, A., and Rinaldi, E. (2015). Finite-temperature study of eight-flavor SU(3) gauge theory. In *Sakata Memorial KMI Workshop on Origin of Mass and Strong Coupling Gauge Theories (SCGT15) Nagoya, Japan, March 3-6, 2015*.

[281] Seiberg, N. (1995). Electric - magnetic duality in supersymmetric nonAbelian gauge theories. *Nucl. Phys.*, B435.

[282] Selke, W. (1988). The annni model - theoretical analysis and experimental application. *Physics Reports*, 170(4):213 – 264.

[283] Shamir, Y. (2005). Locality of the fourth root of the staggered-fermion determinant: Renormalization-group approach. *Phys. Rev.*, D71:034509.

[284] Shamir, Y., Svetitsky, B., and DeGrand, T. (2008). Zero of the discrete beta function in SU(3) lattice gauge theory with color sextet fermions. *Phys.Rev.*, D78:031502.

[285] Sharpe, S. R. (2006). Discretization errors in the spectrum of the hermitian wilson-dirac operator. *Phys. Rev. D*, 74:014512.

[286] Shifman, M. and Vainshtein, A. (1986a). Solution of the anomaly puzzle in {SUSY} gauge theories and the wilson operator expansion. *Nucl. Phys.*, B277(0):456 – 486.

[287] Shifman, M. A. and Vainshtein, A. I. (1986b). Solution of the Anomaly Puzzle in SUSY Gauge Theories and the Wilson Operator Expansion. *Nucl. Phys.*, B277:456. [Zh. Eksp. Teor. Fiz.91,723(1986)].

[288] Shrock, R. (2013a). Higher-loop calculations of the ultraviolet to infrared evolution of a vectorial gauge theory in the limit $N_c \to \infty, N_f \to \infty$ with N_f/N_c fixed. *Phys. Rev.*, D87:116007.

[289] Shrock, R. (2013b). Higher-loop structural properties of the β function in asymptotically free vectorial gauge theories. *Phys. Rev.*, D87(10):105005.

[290] Shrock, R. (2014). Generalized scheme transformations for the elimination of higher-loop terms in the beta function of a gauge theory. *Phys. Rev. D*, 90:045011.

[291] Shuryak, E. (2009). Physics of Strongly coupled Quark-Gluon Plasma. *Prog. Part. Nucl. Phys.*, 62:48–101.

[292] Smilga, A. V. (1997). Physics of thermal QCD. *Phys. Rept.*, 291:1–106.

[293] Sommer, R. (1994). A New way to set the energy scale in lattice gauge theories and its applications to the static force and alpha-s in SU(2) Yang-Mills theory. *Nucl. Phys.*, B411:839–854.

[294] Susskind, L. (1977). Lattice fermions. *Phys. Rev. D*, 16:3031–3039.

[295] Susskind, L. (1979a). Dynamics of Spontaneous Symmetry Breaking in the Weinberg-Salam Theory. *Phys.Rev.*, D20:2619–2625.

[296] Susskind, L. (1979b). Lattice models of quark confinement at high temperature. *Phys. Rev. D*, 20:2610–2618.

[297] Svetitsky, B. (1986). Symmetry aspects of finite-temperature confinement transitions. *Physics Reports*, 132(1):1 – 53.

[298] Symanzik, K. (1970). Small distance behaviour in field theory and power counting. *Communications in Mathematical Physics*, 18(3):227–246.

[299] Symanzik, K. (1971). Small distance behavior analysis and Wilson expansion. *Commun.Math.Phys.*, 23:49–86.

[300] Szabo, K. (2014). QCD at non-zero temperature and magnetic field. *PoS*, LATTICE2013:014.

[301] 't Hooft, G. (1979). A Property of Electric and Magnetic Flux in Nonabelian Gauge Theories. *Nucl. Phys.*, B153:141.

[302] Tarasov, O., Vladimirov, A., and Zharkov, A. Y. (1980). The Gell-Mann-Low Function of QCD in the Three Loop Approximation. *Phys.Lett.*, B93:429–432.

[303] Teper, M. (2009). Large N and confining flux tubes as strings - a view from the lattice. *Acta Phys.Polon.*, B40:3249–3320.

[304] van Ritbergen, T., Vermaseren, J., and Larin, S. (1997). The Four loop beta function in quantum chromodynamics. *Phys.Lett.*, B400:379–384.

[305] Vermaseren, J. A. M., Larin, S. A., and van Ritbergen, T. (1997). The four loop quark mass anomalous dimension and the invariant quark mass. *Phys. Lett.*, B405:327–333.

[306] Weinberg, S. (1976). Implications of Dynamical Symmetry Breaking. *Phys.Rev.*, D13:974–996.

[307] Wilson, K. G. (1974). Confinement of quarks. *Phys. Rev. D*, 10:2445–2459.

[308] Wilson, K. G. (1975). Quarks and Strings on a Lattice. In *Boston Conf. 1975:99, Erice Subnucl.Phys.1975:0069*, page 99. [,0069(1975)].

[309] Winter, F., Clark, M., Edwards, R., and Jo□, B. (2014). A Framework for Lattice QCD Calculations on GPUs.

[310] Yamawaki, K., Bando, M., and Matumoto, K.-i. (1986). Scale Invariant Technicolor Model and a Technidilaton. *Phys.Rev.Lett.*, 56:1335.

[311] Yang, C. N. and Mills, R. L. (1954). Conservation of isotopic spin and isotopic gauge invariance. *Phys. Rev.*, 96:191–195.

This thesis was typeset using LaTeX, originally developed by Leslie Lamport and based on Donald Knuth's TeX. The body text is set in 11 point Egenolff-Berner Garamond, a revival of Claude Garamont's humanist typeface. The above illustration, "Science Experiment 02", was created by Ben Schlitter and released under CC BY-NC-ND 3.0. A template that can be used to format a PhD thesis with this look and feel has been released under the permissive MIT (XII) license, and can be found online at github.com/suchow/Dissertate or from its author, Jordan Suchow, at suchow@post.harvard.edu.